The Pennsylvania State University

The Graduate School

Department of Mechanical and Nuclear Engineering

OPTIMAL ACTUATOR PLACEMENT AND ACTIVE STRUCTURE DESIGN FOR CONTROL OF HELICOPTER AIRFRAME VIBRATIONS

A Thesis in

Mechanical Engineering

by

David E. Heverly II

Submitted in Partial Fulfillment
of the Requirements
for the Degree of

Doctor of Philosophy

August 2002

We approve the thesis of David E. Heverly II.

Date of Signature

Kon-Well Wang
William E. Diefenderfer Chaired Professor in
Mechanical Engineering
Thesis Co-Advisor
Co-Chair of Committee

Edward C. Smith
Associate Professor of Aerospace Engineering
Thesis Co-Advisor
Co-Chair of Committee

Farhan Gandhi
Associate Professor of Aerospace Engineering

Panagiotis Michaleris
Assistant Professor of Mechanical Engineering

Richard C. Benson
Professor and Head
Department of Mechanical and Nuclear Engineering

ABSTRACT

A comprehensive research program on active control of rotorcraft airframe vibration is detailed in this thesis. A systematic design methodology, to realize an active vibration control system, is proposed and studied. The methodology is a four-part design cycle and relies heavily on numerical computation, modeling, and analysis. The various analytical tools, models, and processes required to execute the methodology are described. Two dynamic models of the helicopter airframe and an optimization procedure for actuator placement are utilized within the methodology. The optimization procedure simultaneously determines the type of actuation, the locations to apply actuation, and the corresponding active control actions.

A feasibility study is conducted to examine the effectiveness of helicopter vibration control by distributing actuators at optimal locations within the airframe, rather than confining actuation to a centralized region. Results indicate that distributed actuation is capable of greater vibration suppression and requires less control effort than a centralized actuation configuration.

An analytical and experimental investigation is conducted on a scaled model of a helicopter tailboom. The scaled tailboom model is used to study the actuation design and realization issues associated with integrating dual-point actuation into a semi-monocoque airframe structure. A piezoelectric stack actuator configuration is designed and installed

within the tailboom model. Experimental tests indicate the stack actuator configuration is able to produce a bending moment within the structure to suppress vibration without causing excessive localized stress in the structure.

TABLE OF CONTENTS

LIST OF FIGURES

LIST OF TABLES

ACKNOWLEDGMENTS

I wish to express sincere appreciation to my thesis advisors, Dr. Kon-Well Wang and Dr. Edward Smith, for their support, encouragement, guidance, and genuine commitment to this research project. I am also grateful to Dr. Farhan Gandhi and Dr. Panagiotis Michaleris for serving on my committee and providing insightful guidance.

Support for this research by the National Rotorcraft Technology Center and Dr. Yung Yu, Technical Monitor, is gratefully acknowledged. Thank you to The Boeing Company for providing helicopter airframe models. In addition, I would like to thank engineers Dr. M. Toossi, Dr. M. Meyyappa, and Dr. V. Anand of Boeing Mesa for providing data, technical assistance, and valuable guidance for this project.

A special thanks goes out to my fellow students at the Penn State Structural Dynamics and Controls Laboratory for their friendship, and support. In addition, I would like to thank American Piezo Ceramics for their technical assistance.

Finally, I would like to most sincerely thank my wife, Maria, for her patience, understanding, encouragement, and unconditional support throughout this program. I am also grateful to my parents and family for their encouragement and support.

Chapter 1

INTRODUCTION

1.1 Background

Helicopter fuselage vibration has been a long-standing problem from the earliest days of rotorcraft development. Oscillatory motion of the airframe is a serious concern from many viewpoints [1]. The oscillatory strains of the airframe necessitate consideration for the fatigue of structural components. Airframe vibrations influence production costs and maintenance costs. Vibrations constitute a hostile environment for all kinds of equipment. Instruments are difficult to read, sights hard to point, weapons hard to point, and vibrations add to the fatigue of pilots, crew, and passengers [1].

Understandably, helicopter vibration is a serious concern and numerous control approaches have been devised to help alleviate vibration. The principal sources and nature of helicopter airframe vibration are explained in the following to provide insight and understanding of the various vibration control approaches. Then, many of the vibration control approaches are summarized, highlighting the advantages and disadvantages.

1.1.1 Helicopter Vibration Sources

Airframe vibrations are caused by several important excitation sources, but the more prominent sources are the main rotor hub forces and moments [2, 3]. In steady-state forward flight, the main rotor blades experience an asymmetric airflow. There is a larger velocity of airflow on the advancing side of the rotor as compared to the retreating side, which results in a periodic variation of air loads on the rotor blades. The air load variations cause periodic motion of the rotor blades, which in turn, generate periodic forces and moments at the root of each rotor blade. These blade loads are transmitted to the main rotor hub, and the net effects are periodic hub loads that excite the helicopter airframe. If all rotor blades are identical, the main rotor system acts as a filter and transmits only pN/rev harmonics to the airframe, where p is an integer and N is the number of blades, and all other harmonics cancel at the rotor hub. The most dominant hub loads occur at the $N\Omega$ frequency, where Ω is the main rotor speed. Thus, helicopter fuselage vibration is primarily characterized by harmonic excitation from the main rotor hub at N/rev. Another excitation at the hub can result from small dissimilarities in structural and aerodynamic properties of the rotor blades, which produce 1/rev periodic hub forces and moments.

The helicopter fuselage is also excited by sources entering the airframe through load paths other than the main rotor hub. Important excitations result from the aerodynamic interaction between the main rotor wake and the airframe surfaces [3]. Main rotor vortices interact with the horizontal and vertical tail surfaces creating pN/rev

excitation at the tail of the aircraft. The airframe is also excited by *pN*/rev pressure pulses resulting from the rotor blades passing within close proximity to the upper fuselage surfaces. In addition, *pN*/rev harmonic loads enter the airframe through the primary flight control system. Airframe excitations are created by the engines, transmission, tail rotor, and tail rotor shafting, however, these excitations typically occur at frequencies much higher than ***NΩ.*** The principal airframe excitation sources and the areas at which they enter the airframe are displayed in *Figure 1.1* [3].

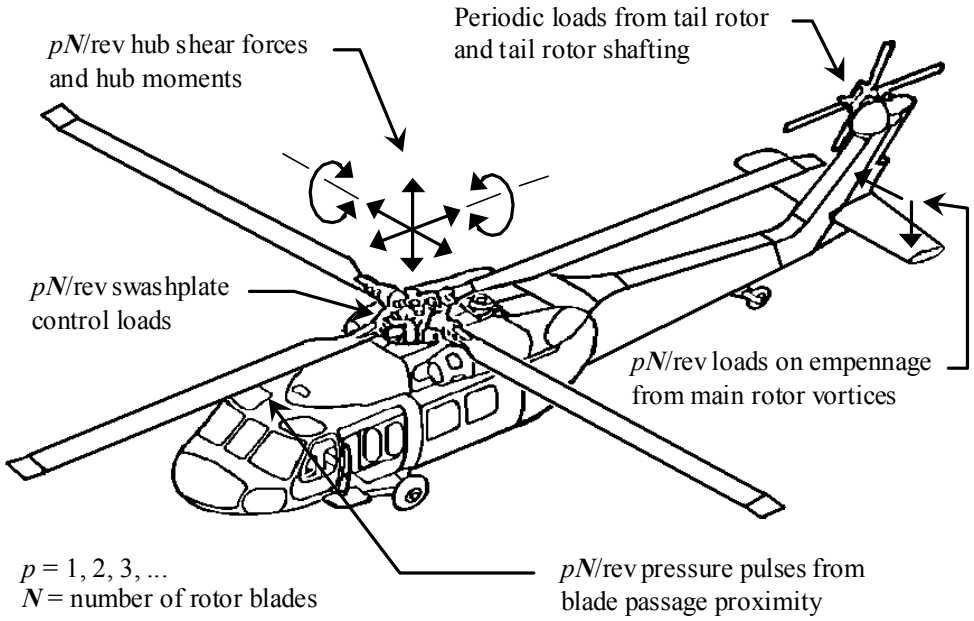

Figure 1.1: Principal sources of airframe excitation. [3]

Airframe vibration is generally low in hover and increases with forward flight speed to highest vibration levels at the maximum forward speed of the aircraft [2]. Increased

vibration levels also occur in transition from hover to forward flight, because of the main rotor wake influence on the rotor blade loading, *Figure 1.2*.

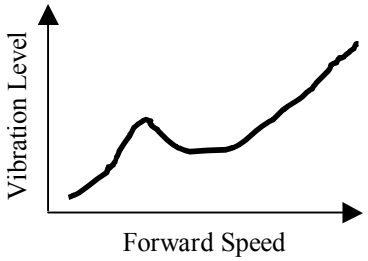

Figure 1.2: Vibration levels in forward flight

1.1.2 Vibration Control Methods

Considerable progress has been made over the years in designing helicopters, which have lower vibration levels. However, the trends of increased forward speed, prolonged mission duration, greater passenger comfort, and increased component life result in ever more stringent vibration specifications. Thus, the helicopter vibration problem is not likely to be solved in an absolute sense, and there will be continued efforts to strive for more effective vibration control measures with reduced penalties in terms of weight, complexity, and reliability.

Helicopter vibration control devices can be broadly categorized as either passive or active devices. Isolation systems, dynamic absorbers, and pendulum absorbers are examples of passive vibration control devices that do not require an external energy source. Actively tunable dynamic absorbers, Higher Harmonic Control (HHC), Individual Blade Control (IBC), Trailing Edge Flap (TEF) control, and Active Control of Structural

Response (ACSR) are active vibration control devices or methods that require an external energy source. Passive vibration control methods are summarized in the next section and active control methods in the following section.

1.1.2.1 Passive Control Methods

In a passive isolation system, the isolated object is mounted on a structure through springs that are tuned to minimize the transmission of loads. Isolation has been used for seats, equipment, cargo floors, and the main rotor. A number of rotor isolation systems have been successfully flown on a variety of helicopters [1]. Systems have been designed to isolate the rotor from the fuselage at the ***N***/rev frequency in all directions of excitation except yaw, and the motions that could affect control and drive system components have been kept to acceptable levels [1]. One difficulty with rotor isolation is that steady state loads and loads resulting from maneuvers and wind gusts must be carried over the same load path along which isolation is desired.

A dynamic absorber is composed of a small mass on a spring with the natural frequency tuned to the excitation frequency. The dynamic absorber vibrates in resonance and generates an opposing force to reduce vibration amplitudes at a particular point in the structure. One successful application of the dynamic absorber, which reduces vibration at the pilot seat, is to use a battery located under the pilot seat as the absorber mass [1]. One

drawback of the dynamic absorber is the tuned natural frequency is fixed and must match the excitation frequency for optimum effectiveness.

Another common dynamic absorber on helicopters is the pendulum absorber. A typical pendulum absorber is a small cantilever beam with a tip mass, and the absorber can be mounted on the hub or each rotor blade. Hub mounted pendulum absorbers are capable, in theory, of generating forces and moments in all directions and all harmonics. However, in practice the absorber is mostly used to generate forces in the plane of rotation at the blade passage frequency [1]. Blade mounted pendulum absorbers produce forces that are transmitted to the hub at the blade root, and the ideal absorber causes the net force at the blade root to be zero. Blade mounted absorbers are difficult to design because analytical blade root load predictions are not highly accurate [1]. One advantage of pendulum absorbers is their natural frequencies are proportional to the rotor speed; therefore, they tend to remain properly tuned regardless of rotor speed. An undesirable aspect of pendulum absorbers is the added physical volume that increases the aerodynamic drag of the rotor hub.

Passive vibration control devices have demonstrated a significant degree of vibration suppression, which is why most production rotorcraft are equipped with one or more passive devices [1]. Passive control methods are based on fundamental concepts and straightforward to design, but they are not immune to problems. Some passive devises are tuned for a particular frequency and unable to adapt to frequency variations

that may result from changes in flight condition or payload. Typically, there is a weight penalty associated with passive devices because components are added to the helicopter. Both isolation systems and dynamic absorbers must have low friction and displacement amplitudes must remain small to stay in the linear range of the mounting springs. Pendulum absorbers can become detuned when oscillation amplitudes are excessive and the added physical volume increases aerodynamic drag [1].

1.1.2.2 Active Control Methods

The active vibration control methods (HHC, IBC, TEF, and ACSR) can be further divided into two distinct categories. The first category applies control actions on the main rotor system and is designated a rotor-based approach. This approach involves modification of the unsteady loads being generated by the main rotor system and reduces the vibratory loads transmitted through the hub to the airframe. Higher Harmonic Control (HHC), Individual Blade Control (IBC), and Trailing Edge Flap (TEF) control are rotor-based approaches that reduce airframe vibrations by reducing the dominant excitation source. The second category, designated as airframe-based, applies control actions directly on the airframe. Airframe-based approaches do not attempt to alleviate the excitation sources; instead, the vibration caused by external sources is cancelled by superposition of an actuator induced airframe response. Actively tunable dynamic absorbers and Active Control of Structural Response (ACSR) are airframe-based approaches.

The Higher Harmonic Control (HHC) method actuates the swashplate to superimpose small perturbations at ***N***-1/rev, ***N***/rev, and ***N***+1/rev with the 1/rev cyclic pitch control. The higher harmonic perturbations are commanded to alter the blade aerodynamics such that the periodic hub loads are reduced. A significant amount of research has been devoted to HHC over the past two decades. HHC feasibility and effectiveness has been demonstrated analytically, in the wind tunnel, and by flight tests; however, it has yet to be implemented on a production aircraft [4]. The HHC control method has demonstrated an 80% to 90% reduction of airframe cockpit vibrations. Some drawbacks that hinder HHC implementation are: degraded rotor performance, airworthiness issues associated with modifying the primary flight control system, reduced effectiveness for stiff hingeless rotors, and the large power requirements approaching 0.2% to 1.4% of the total rotor power [4].

Individual Blade Control (IBC) operates on similar aerodynamic principles as HHC; however, each blade is actuated individually rather than actuating the swashplate to achieve periodic blade pitch perturbations. Independent control of each rotor blade provides greater flexibility, and IBC can be used to alleviate undesirable dynamic phenomena that go beyond vibration reduction [4]. IBC research and development has not reached the same level of maturity as HHC. Implementation of IBC on a production helicopter may require the replacement of the conventional swashplate by an electronic equivalent [4].

Trailing Edge Flap (TEF) control also alters the blade aerodynamics to reduce the oscillatory hub loads. A small flap device located on the trailing edge of each rotor blade alters the blade aerodynamics. The flap is actuated to produce small oscillatory flap deflections at integer harmonics of the blade passage frequency. Advantages of this approach are lower power consumption and enhanced airworthiness, as compared to HHC or IBC. Trailing Edge Flap control feasibility and effectiveness has been demonstrated analytically and experimentally. Friedmann and Millott have analytically studied the TEF, and predicted an 80% reduction in the ***N***/rev hub loads and predicted the power consumption to be 10 to 20 times less than conventional IBC. One of the major obstacles to TEF control is the flap actuation. A significant amount of research is currently being devoted to the development of a small, lightweight, and energy efficient blade mounted actuating device to produce the flap deflections [4].

The actively tunable dynamic absorber generates an opposing force to reduce vibration amplitudes at a particular frequency at a particular point in the structure. An oscillating spring/mass assembly with an active natural frequency tuning mechanism generates the absorber force, or possibly a pair of counter-rotating eccentric weights generates the absorber force. Such active dynamic absorbers have the advantage that their frequency can be keyed to the main rotor speed to maintain proper tuning [1]. An actively controlled dynamic absorber has been successfully demonstrated on a CH-47D Chinook helicopter [5]. A self-tuning vibration absorber was placed under the pilot's seat to reduce

vibration at the aircraft's blade passage frequency. Ground shake testing and closed loop control revealed an average vibration reduction of 93.6 percent at four cockpit locations.

The Active Control of Structural Response (ACSR) principle consists of a number of actuators between points in the airframe, control system hardware, and an active control algorithm [6]. The actuators apply forces to the airframe structure, and the magnitude and phase of the applied loads are chosen to minimize vibration at a number of locations in the fuselage. The ACSR method has been demonstrated on a Westland 30 helicopter. Flight tests demonstrated an average vibration reduction of 80% at 10 sensor locations. The principle advantages of ACSR over HHC are improved performance, lower power requirements, ease of installation, and minimal airworthiness impact [7]. Additional details and results of the ACSR method will be presented in the literature review section.

1.2 Problem Statement and Research Objectives

Airframe-based active vibration control approaches are being seriously considered and investigated because they have advantages over the rotor-based approaches. Study and flight-testing of airframe-based approaches have demonstrated enough promise to begin appearing on production rotorcraft, such as the EH-101 [7] and the Sikorsky S-92 [8]. Unlike rotor-based approaches, the airframe-based schemes should have minimal

impact on the airworthiness of the helicopter, since the main rotor system and primary flight control system are not being altered directly. Airframe-based systems could also avoid the complexities associated with transmitting data or control actions from the fixed-frame (airframe) to the rotating-frame (rotor). System installation is greatly simplified as compared to installing a rotor-based system. Power consumption of airframe-based systems has been estimated to be an order of magnitude lower than HHC systems [9]. Rotor-based active control methods reduce the oscillatory hub loads, but may not be capable or efficient at controlling excitations that do not enter the airframe through the main rotor hub. That is, the airframe would continue to be excited by other harmonic sources, even if the vibratory hub loads are completely eliminated. Therefore, some type of airframe-based control system is required, unless all problematic excitation sources can be eliminated.

Even though current airframe-based active control approaches are effective, the system performance can be greatly improved with technological advances and design innovations. The characteristics and limitations of present systems are summarized as follows. The current control strategies tend to focus on disturbances coming from the main rotor, or they target localized areas for vibration suppression. In general, the actuators are centrally located in the cockpit area or near the main rotor gearbox. Actuator placement is based largely upon engineering experience and limitations imposed by retrofitting the existing airframe structure. The helicopter airframe is a complex structure, and it has a complex dynamic response; therefore, determining the best actuator

locations is not a simple task. A systematic and comprehensive design approach is needed to explore the vast multitude of potential active control configurations and determine which is best. It is not clear that actuators centralized near the main rotor gearbox will be effective at suppressing vibration over a broad area or effectively address disturbance sources away from the main rotor hub. The current systems also require substantial control effort and use relatively heavy actuators.

To overcome the limitations of present systems and advance the state-of-the-art, a new actuator placement and active structure design methodology is proposed and explored in this research. There are two overall goals of this investigation. First, develop a systematic and comprehensive design methodology for realizing an airframe-based active vibration control system. This design methodology is termed the Optimally Distributed Actuation Realization Methodology (ODARM). The methodology is a four-part design cycle and relies heavily on numerical computation, modeling, and analysis. The second overall goal is to examine the feasibility and effectiveness of helicopter vibration control by distributing actuators at optimal locations within the airframe. An optimization procedure is developed that simultaneously determines the type of actuation, location of actuation, and the corresponding active control actions. System analysis and comparison studies are performed to provide insight and evaluate the merits of distributing actuation throughout the airframe.

With optimized actuator locations and active structure designs, the following benefits may be obtained. The multiple excitations, which occur throughout the airframe, could be more effectively controlled by an appropriate distribution of actuator locations. Optimally distributed actuators could be more effective at reducing vibration throughout the entire airframe or in localized areas. With optimized actuator locations, the proposed system could also require significantly less control effort to achieve similar or better vibration reduction than present systems. Because control effort requirements are reduced, smaller and lighter actuators can be used. Thus, the weight penalty and control power of the active system can be reduced. Also, with reduced control effort requirements, smart material-based actuator technology may become suitable for designing an active airframe structure.

1.3 Literature Review

A literature survey is conducted that focuses primarily on three topics relevant to this research study. The first topic is helicopter airframe structural dynamic models to determine what types of model have been generated and how the models have been used. The second topic is the state-of-the-art in airframe-based active vibration control methods. The intent is to acquire an understanding of the state-of-the-art configurations, their vibration control effectiveness, and their limitations. The third topic of the literature survey is actuator placement methods for active structural control. Actuator placement methods are reviewed to gain an understanding of what techniques have been used and to investigate the influence of actuator placement on active vibration control.

1.3.1 Helicopter Airframe Dynamic Models

A literature review of helicopter structural dynamic models was conducted and a primary source was the Design Analysis Methods for VIBrationS (DAMVIBS) program. DAMVIBS was a ten-year joint government and industry research program to develop a technology base for advanced finite element dynamic analysis [10, 11, 12, 13, 14]. Contracts were awarded to the four major helicopter airframe manufacturers, Bell, Boeing, McDonnell Douglas, and Sikorsky. Several finite element models, with up to 25000 degrees-of-freedom, were developed by the companies for various helicopter airframes. Correlation studies were conducted comparing vibration shake tests to the finite element model predictions of frequency response. In general, all airframes studied indicated good agreement up through 10 Hz, partially satisfactory agreement from 10–20 Hz, and generally unsatisfactory agreement above 20 Hz. The DAMVIBS program showed that considerably improved correlation could be obtained if modeling details, which have been historically regarded as secondary in importance, are taken into account. Several areas were identified to improve the finite element model predictions; such as, modeling of secondary structural panels, sealed canopy glass, nonproportional structural damping, nonlinear effects of elastomeric mounts, and modeling of the suspension system for shake testing.

Reduced order models and model reduction techniques also resulted from the DAMVIBS program. The reduced order airframe models are appealing for optimization applications, because the efficiency of numerical computation is greatly improved.

Structural optimization has been applied, utilizing a reduced order airframe model, to tune the natural frequencies and modes of a helicopter airframe [15]. Two dynamic models of the helicopter airframe are utilized in this study, and the details of each model are covered in later chapters.

1.3.2 Active Vibration Control of Helicopter Airframe

Friedmann, Chiu, and Cribbs have analytically studied the ACSR approach with a coupled rotor/fuselage aeroelastic response model [16, 17, 18]. The rotor model represented a hingeless rotor with each blade undergoing coupled flap-lag-torsion elastic deformation. The researchers created a three-dimensional flexible fuselage model with 966 global degrees of freedom. The fuselage model, which resembles a MBB BO-105 helicopter, was assembled from Euler-Bernoulli beam, truss, and non-structural mass elements. The ACSR system modeled a rigid rectangular plate, four linear spring elements, and four high force/small displacement actuators. The ACSR system was configured by mounting the rotor system on the rigid plate and connecting the plate to the fuselage at each corner with a spring element in parallel with an actuator. Chiu and Friedmann developed the coupled rotor/fuselage model. Cribbs added a free wake model and rotor/fuselage interactional aerodynamic effects. The ACSR control scheme was capable of reducing vertical and longitudinal vibrations at the pilot seat by at least 45% for advance ratios ranging from 0.15 to 0.4. ACSR was not as effective at reducing vibration in the lateral direction. The actuator tip displacement was small, below 0.00022

inches, but the actuator control forces were quite large with maximums near 12000 lb. ACSR actuator power was estimated to be 1% to 1.5% of the total rotor power.

Hanagud and Babu have analytically investigated the feasibility of using piezoceramic sensors and actuators for vibration reduction in the helicopter airframe [19]. A simple beam finite-element-model with concentrated masses was used to model the airframe. The single-axis beam model consisted of 10 elements, 11 nodes, and 33 degrees-of-freedom. The beam model was excited with harmonic loads at a location representing the rotor hub. Using a collocated piezoceramic actuator and sensor, along with an H-infinity controller, vibration in the vertical direction was reduced 60% at the sensor location. They concluded that future work should include a more sophisticated airframe and actuator model.

The Active Control of Structural Response (ACSR) system, developed by King and Staple at Westland, actively controls the airframe by the superposition of an actuator-induced response with the response due to oscillatory hub loads [6]. The ACSR system consists of airframe mounted accelerometers, a digital control computer, and a set of electro-hydraulic force actuators mounted across the airframe/main transmission interface. An Independent Modal Space Control algorithm and a Frequency Domain Control algorithm were investigated for the ACSR implementation. Through extensive simulation, the frequency domain control algorithm was selected because it proved to be robust, simple to realize, and produced better vibration reduction. The Frequency Domain

Control algorithm can be expressed as the minimization of a quadratic performance index, comprising the weighted sum of the vibration measurements and the weighted sum of the actuator efforts. Simulation studies were conducted utilizing a NASTRAN finite element model of a Westland 30 airframe. Ten sensor locations in the main cabin were targeted for vibration suppression, and simulations were conducted for forward flight speeds ranging from 100 to 140 knots. The simulations predicted a 90% vibration reduction in the cabin, and the maximum actuator control loads were 2250 lbs.

Ground vibration shake tests and flight tests have also been conducted on a Westland 30 helicopter equipped with an Active Control of Structural Response system [7]. The ACSR control unit received airframe vibration signals from 24 accelerometers located around the airframe, 17 in the cabin and cockpit areas, 4 on the engines, and 3 on the tail rotor gearbox. The control algorithm to compute the actuator commands used only 10 accelerometer signals from the 24 available. On the Westland 30 helicopter, the main rotor and gearbox are mounted on a rectangular raft that is attached to the airframe at each corner with an elastomeric mount. Four electro-hydraulic actuators were incorporated into the gearbox/fuselage interface at the four elastomeric mount locations, see *Figure 1.3*. The actuation devices were designed to produce a maximum of +/- 2023

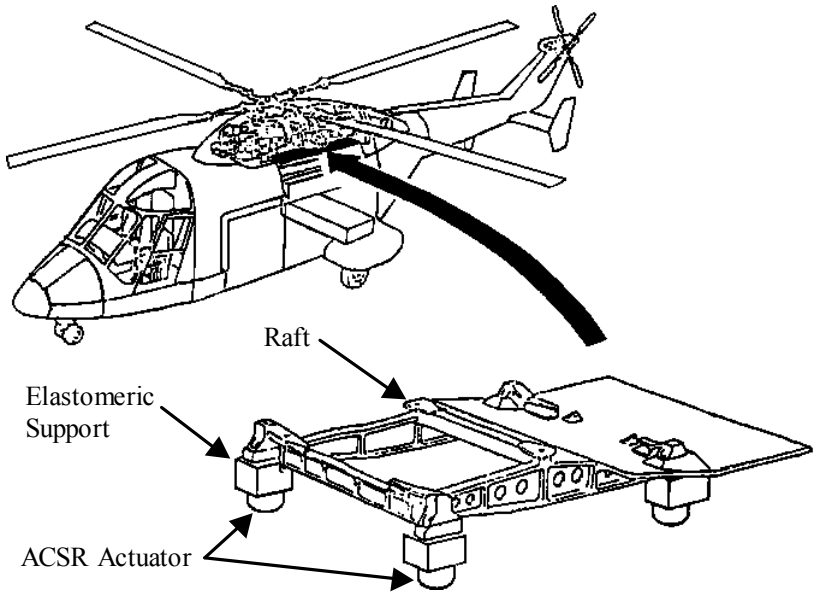

Figure 1.3: ACSR actuator installation on Westland 30 helicopter. [7]

lbs at the blade passage frequency (22 Hz) with a maximum displacement of 0.01 inches. The shake test was conducted on a demonstration aircraft with a standard flight configuration. The aircraft was suspended by soft springs through a dummy rotor head, and ***N***/rev loads representative of the flight environment were applied to the rotor head through electro-magnetic shakers. Results from the shake tests indicated an average vibration reduction of 80% at the 10 control sensor locations. Average vibration reduction at all 24 sensor locations was 67% from 0.12 g to 0.04 g.

Flight tests were also conducted on the Westland 30 Helicopter for two aircraft loading conditions: the baseline aircraft loading at 11800 lbs take-off weight, and a higher loading of 12800 lbs [7]. Flight trials were conducted to evaluate ACSR under steady flight conditions at forward speeds from 40 to 124 knots, and flight trials were

conducted for various maneuver conditions. The flight trials of the baseline aircraft loading at steady forward speeds indicated an average vibration reduction of at least 80% at the 10 control sensor locations, and average reductions between 55% and 60% for all 24 sensor locations. The robustness of the ACSR control approach to changes in aircraft loading was demonstrated. When the aircraft take-off weight was increased to 12800 lbs, the uncontrolled vibration levels increased by 25%; however, ACSR reduced vibrations to levels very near the controlled vibrations of the 11800 lbs aircraft. Throughout the complete range of flight trials incorporating various maneuvers, the ACSR system provided substantial vibration reductions. From an airframe vibration perspective, the transition to hover maneuver is one of the most severe cases. Results from the transition to hover maneuver indicated that ACSR maintained vibrations below 0.45 g throughout the entire maneuver, while the uncontrolled vibration levels were at least 0.2 g greater and peaked at 1.6 g. The weight penalty of any vibration control system is always a concern. On the Westland 30 helicopter, it was estimated that a production ACSR installation would weigh approximately 80 lbs, as compared to 122 lbs for the passive rotor mounted absorber currently fitted on the aircraft. An added benefit of ACSR reported by the pilot and flight crew was the pronounced reduction of interior noise levels.

The Active Control of Structural Response approach has also been demonstrated on a Sikorsky S-76B helicopter [9]. The main rotor gearbox attachments were modified to incorporate six electro-hydraulic actuators in parallel with four stiff spring mounts, as

shown in *Figure 1.4*. Accelerometers were distributed throughout the airframe to monitor sixty sensor signals. The ACSR controller accommodated up to ten accelerometer signals and up to four control actuators. Ground shake testing was conducted with the aircraft suspended from soft springs at the main and tail rotor hubs. To evaluate ACSR effectiveness in suppressing multi-harmonic response, the aircraft was subjected to hub loads composed of representative 1/rev, ***N***-1/rev, ***N***/rev, and 2***N***/rev loads. The ACSR system was optimized for the Aeronautical Design Standard 27 (ADS-27) vibration requirements that have been adopted by the U.S. Army. ADS-27 vibration requirements are more stringent than previous requirements, and ADS-27 uses an intrusion index as the

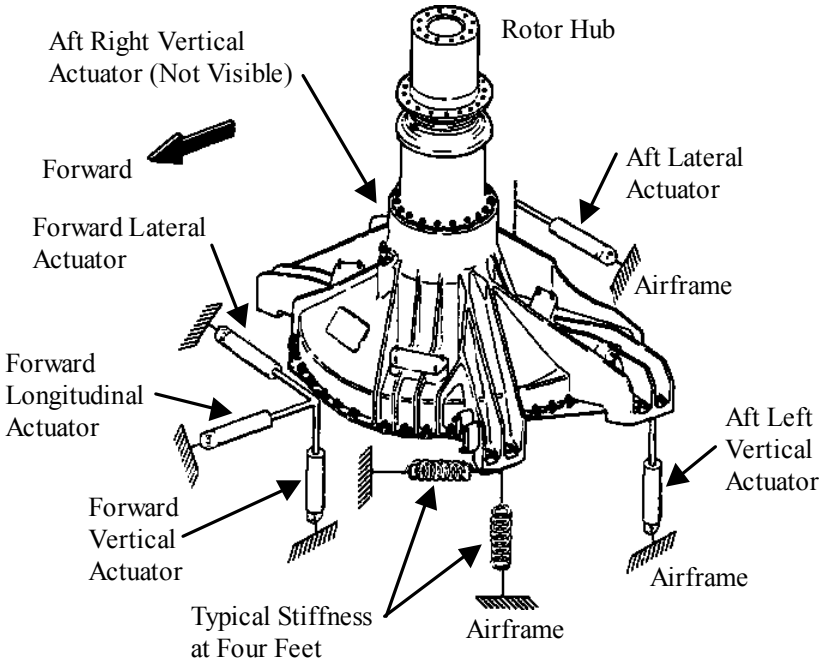

Figure 1.4: S-76 helicopter main gearbox supports and ACSR actuator locations [9]

performance metric [9, 20, 21]. The intrusion index is a weighted sum of the four largest vibration harmonics at specific locations in the helicopter. Ground shake testing indicated that ***N***/rev cockpit vibration could be reduced by 86% and 50% reductions were realized for the ***N***-1/rev and 2***N***/rev responses. Closed loop tests were examined for simulated flight at forward speeds from 60 to 162 knots. Throughout the entire speed range the ACSR control system effectively suppressed vibration at the pilot and copilot stations and kept the intrusion index well below the ADS-27 limit. Simulated in-flight actuator loads and power were predicted. The maximum actuator load range was from 2000 lbs to 3200 lbs over the forward speed range. A maximum power of 9.5 horsepower was required to operate four actuators.

Welsh and others demonstrated an ACSR like active vibration control system on a Sikorsky UH-60 Black Hawk helicopter [22]. The adaptive vibration control system consisted of ten accelerometer sensors, a control computer, and two inertial force generating units. Four of the accelerometer sensors were located in the cockpit area near the copilot and pilot seats. The six remaining sensors were located in the forward, middle, and rear of the helicopter cabin area. The control computer used a common frequency domain algorithm to compute actuator commands that cancel vibration at the *N*/rev frequency. Actuators of the control system are inertial-type force generators that apply control forces at a single point of the fuselage. The inertial force generator, shown in *Figure 1.5*, is a hybrid resonant device that integrates the UH-60 passive vibration absorber with a hydraulic servo actuator and internal feedback sensors.

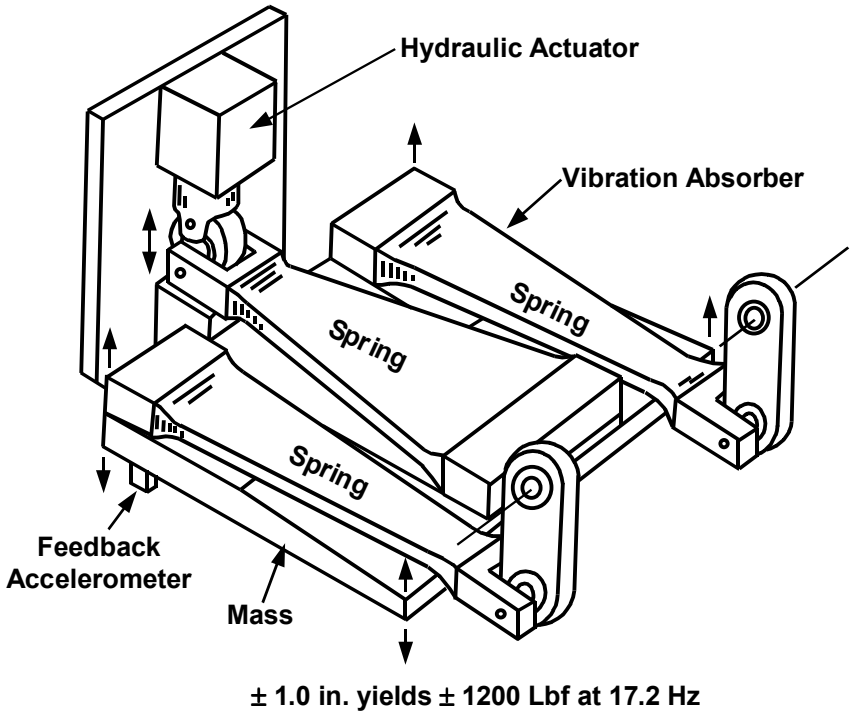

Figure 1.5: Sikorsky UH-60 Servo Inertial Force Generator (SIFG) [22]

Thus, the force generator could be used in a passive mode like the original equipment vibration absorber, or in an active mode to generate commanded actuation forces. The inertial mass of each force generator weighed 40 lbs and had a maximum travel distance of 2.0 inches. Each force generator was capable of producing a 1200 lb force at the *N*/rev frequency of 17.2 Hz. The actuators were installed on the left and right side of the cabin overhead just forward of the main rotor gearbox, which correspond to the original equipment locations of the UH-60 passive vibration absorbers. Vibration data was collected and compared for a baseline no vibration control configuration, a passive vibration absorber configuration, and the active vibration control configuration. All three

configurations were evaluated for various flight conditions; steady level flight at increasing forward speeds, variations of nominal rotor speed, and a transient approach to hover maneuver. The active vibration control system achieved significant vibration suppression at most of the sensor locations; however, small vibration increases were observed at some of the sensor locations. The active system consistently outperformed the passive vibration control system at all forward speeds. At a forward speed of 145 knots, the active vibration control system suppressed vibration by 65% as compared to 45% for the passive system. Unlike the passive system, the active control system was insensitive to rotor speed variations. Maximum hydraulic power required to operate the two force generators was in the 1.0 to 8.0 horsepower range, depending upon the flight condition and main rotor speed. Vibration comparisons for the transition to hover maneuver were not impressive, and the authors concluded that the active system performance was limited by the quasi-steady assumption of the controller algorithm. Two additional conclusions of the authors are related to actuator location and actuator size. The installed force generator locations were near a nodal point and unable to effectively control a torsional mode of the helicopter airframe. Therefore, other actuator locations may yield a more effective active vibration control system. They also concluded that a larger number of small force generators may be more effective than a fewer number of large force generating units. Thus, smaller actuator devices could be placed at more locations in the airframe and avoid the unfortunate circumstance of placing all actuators near modal nodes.

Sikorsky Aircraft Corporation has designed and flight-tested an active vibration control system for the S-92 helicopter [8]. The Active Vibration Control (AVC) system acquires vibration measurements at 10 sensor locations in the cockpit and cabin, and a control computer provides commands to inertial force generating devices mounted on the airframe. The control computer uses a common frequency domain algorithm to compute actuator commands. Actuators are single point devices that generate controlled vibratory loads to reduce fuselage vibration at the *N*/rev frequency. Each inertial force generator is able to produce a 1000 lb sinusoidal force from a pair of counter-rotating eccentric disks. A finite element model of the S-92 airframe was utilized for an extensive parameter study to determine the appropriate number of force generator devices and their airframe attachment locations. Actuator locations were restricted to 15 candidate airframe locations in the cockpit and cabin areas with each location having three possible force directions. Three actuators combined with 45 candidate location/direction sets resulted in 14190 control configurations to be evaluated. The first flight test of a S-92 prototype aircraft with the AVC system took place in December of 1998. The AVC system demonstrated substantial vibration suppression over a broad range of flight conditions and ballast configurations. Average cockpit and cabin vibration was reduced by at least 50% (below 0.15 g) from hover to forward speeds of 150 knots.

The Total Vibration Reduction (TVR) system is an active vibration control system developed by Kawasaki Heavy Industries of Japan to reduce helicopter vibrations at 1/rev, ***N***/rev, and 2***N***/rev [23, 24]. The complete TVR system consists of two separate

and independent active control systems. One system (Automatic Adjustable Pitch Link – AAPL) incorporates actively adjustable pitch links for automatic tracking and balancing of the main rotor by adjusting the length of pitch links to reduce 1/rev vibrations. The other active system (Active Vibration Reduction – AVR) is an ACSR like system that incorporates hydraulic actuators in parallel with the main gearbox mounts to reduce vibrations at N/rev and 2N/rev. Stiffness of the main gearbox mounts was optimized for maximum AVR effectiveness. The AVR system was put into series production on the Kawasaki BK117 helicopter in 1997. Both active control systems use a frequency domain control algorithm and feedback sensors located in the cockpit and cabin of the aircraft. Flight tests of the TVR system on a series production model BK117 helicopter were conducted to evaluate the concept at forward speeds from hover to 150 knots. The AAPL system reduced 1/rev vertical vibrations at the pilot seat below 0.01 g throughout the entire forward speed range and achieved a 50% reduction at 150 knots. The AVS system reduced N/rev and 2N/rev vertical vibrations at the pilot seat below 0.1 g throughout the entire forward speed range and achieved at least a 45% reduction of N/rev vibrations at all forward speeds.

The Multipoint Adaptive Vibration Suppression System (MAVSS), developed by Bell Helicopter, is an active control system to reduce rotor-induced vibrations over a broad area of the airframe [25]. In general, the MAVSS system consists of airframe mounted sensors, a digital control computer, and a set of force actuators. MAVSS uses the property of superposition of vibratory responses to reduce or cancel vibration. The

control algorithm computes the actuator commands by minimizing a performance index, which is a weighted sum of the measured response data and the weighted actuator commands. Aircraft structural dynamics are self-identified by sending known signals to the control actuator and measuring the resulting change in the system vibrations produced by each actuator. The MAVSS system has been laboratory tested on a lumped-mass bench-top stick model of the Cobra helicopter, and a non-flying Model 412 Bell helicopter. Ground shake testing of the Model 412 was conducted with four hydraulic control actuators placed in parallel with elastomeric gearbox mounts. Testing of the MAVSS system on the Model 412 helicopter demonstrated an average vibration reduction of 94% at six sensor locations. MAVSS has also been tested on a V-22 0.2-scale aeroelastic semispan tiltrotor model. The testing revealed an aerodynamic control surface (aileron) could produce the forces required for vibration suppression. This testing also revealed the limitations of utilizing only one actuator (aileron) for the control of multiple responses. It was demonstrated that three vibratory moments (wing bending, chord bending, and wing torsion) at the wing root could be suppressed individually; however, all three vibratory moments could not be reduced simultaneously.

Boeing Helicopter's Active Vibration Suppression (AVS) uses electromagnetic resonant actuators placed in the cockpit to cancel vibration at N/rev and $2N$/rev [5]. The AVS system consists of electromechanical actuators, a digital controller, multiple accelerometers, and a rotor RPM sensor. The AVS control system is synchronized with the rotor RPM, and the actuators produce structural forces to attenuate vibration at the

sensor locations. Each actuator unit contains a pair of electromagnetically controlled spring/mass assemblies that are tuned to the ***N***/rev and 2***N***/rev frequencies. Actuator commands were computed using a frequency domain control algorithm. The AVS system, with one ***N***/rev actuator under the pilot seat, was installed on a CH-47D helicopter, and ground shake testing demonstrated a 97% reduction of ***N***/rev vibrations at the pilot seat. Peak actuator force outputs were 2600 lbs at ***N***/rev and 1500 lbs at 2***N***/rev.

In summary, the airframe-based active vibration control systems effectively suppressed vibration throughout the entire forward speed range. Most of the systems were able to reduce cabin vibrations by at least 50 percent. Dual point actuation systems utilized hydraulic actuators located at the interface of the airframe and the main rotor support structure. Control forces of the single point actuation systems were generated by inertial devices. The maximum control loads were between 1000 and 3200 pounds. The weight of a production ACSR system installed on a Sikorsky S-76 was estimated to be less than a hub mounted pendulum absorber. On the Sikorsky S-76 system 9.5 horsepower was required to operate four actuators. A maximum of 8.0 horsepower was required to operate two inertial force generators in the UH-60 active vibration control system. Friedmann analytically predicted the ACSR control power to be 1% to 1.5% of the total rotor power.

1.3.3 Actuator Placement Methods

Various placement techniques have been formulated to determine actuator locations for the control of flexible structures. The actuator placement problem is typically solved by an optimization technique to maximize or minimize a cost function. The optimization problem has been solved with gradient-based techniques and non-gradient techniques. Various performance metrics have been formulated for the optimization cost function, such as; metrics based on the entries of the actuator influence matrix, metrics formed from the controllability grammian, metrics to maximize the energy dissipation, and metrics to minimize the system energy. An extensive review has been conducted on this topic; however, only a representative sampling of the various approaches will be presented.

Lim at the NASA Langley Research Center devised an optimal actuator and sensor placement method for large flexible structures [26]. The method is based on the combined degree of controllability and observability of each structural mode to be controlled. A set of actuator and sensor locations was deemed most suitable if the set was capable of simultaneously controlling and observing all significant structural modes to a high degree. The structure's dynamic model was transformed to a state space representation using a set of significant structural modes that are to be controlled. The controllability grammian was computed and the controllable subspace for each actuator location was derived. The observability grammian was also calculated and the observable subspace for each sensor location was determined. An intersection subspace was formed

from the controllable and observable subspaces of each actuator/sensor pair. The optimization cost function was based on the weighted projection of structural modes into the intersection subspaces. The problem reduced to choosing for each structural mode a pair of actuator and sensor locations that maximize the cost function. The design method was computationally efficient because the problem size and design space are proportional to the number of actuators, unlike other methods where the design space is factorially related to the number of actuators. The optimization cost functional did not incorporate closed-loop control; therefore, any control method could be applied after the actuator positions are determined. One disadvantage of the method is that a priori knowledge of which modes are to be controlled is required.

Xu, Warnitchai, and Igusa developed an optimal actuator placement method that uses a performance function including both the structural response and the control effort [27]. Their method was an extension of an energy dissipation method developed by Schultz and Heimbold [28]. The optimization problem was solved by a gradient-based nonlinear programming technique. A direct output velocity feedback control law was used. A quadratic cost function was formulated that includes both the structural response and the control effort. To avoid dependence on initial conditions for the disturbances, the trace of the cost function was used. The resulting cost function was an average over all initial conditions that can be represented by a unit vector in the state space. Thus, the method is useful for structures that may have a wide variety of external disturbances, but it may not be appropriate for structures with specific disturbances. Analytical expressions

were derived for the gradients of the cost function. The computational effort required to evaluate the analytical gradient expressions is far less than that required in finite differences. The actuator placement methodology was demonstrated on a two-dimensional membrane structure. The cost function had multiple local minima; therefore, randomly generated initial actuator locations were used to obtain a set of solutions.

DeLorenzo devised a sensor and actuator selection algorithm for regulation of large-scale, linear, stochastic systems [29]. The algorithm uses an LQG controller and an efficient selection technique, based upon successive approximation, for determining the LQG weighting matrices. Metrics were developed to identify the individual effectiveness of each sensor and actuator in the presence of LQG control. The first step of DeLorenzo's algorithm is solving the LQG control configuration with actuators and sensors located at all candidate locations on the structure. Next, effectiveness metrics were computed for each actuator and sensor position, and the metrics were ranked according to their algebraic values. Then, elimination of the lowest ranking actuators and sensors produced a modified control configuration. LQG control was computed for the modified actuator/sensor configuration, and the process was repeated until the final actuator/sensor configuration enabled the closed-loop system to meet output specifications with minimal power. The algorithm does not involve complex gradient calculations and has proven numerically tractable for large linear models. One advantageous feature of the algorithm is that the solution sequence provides the controls engineer with information for actuator sizing and optimal number.

Choe and Baruh devised an actuator placement method for structural control problems [30]. The method utilizes a modal space representation of the structure to be controlled. Four actuator types, a point force, a piecewise continuous force, a point torque, and a piecewise continuous torque, were analyzed in the study. Optimization studies were conducted to minimize objective functions based on the entries of the actuator influence matrix, which give general measures of controllability. Two objective functions were formulated with the assumption that specific modes of the structure are to be controlled, and the objective functions could be used in conjunction with any control law. Two additional objective functions were formulated for modal control laws. The study analyzed a pinned-pinned beam structure for actuator placement and control. Their study indicated that relatively even distributions of actuators gave satisfactory performance, whereas very closely spaced actuators lead to excessive energy use. As the number of actuators was increased, the actuators became less sensitive to their placement. The performance of the torque actuators was more sensitive to placement than force actuators.

Singiresu and Tzong-Shii solved the actuator placement problem using Genetic Algorithms [31]. The discrete optimal actuator location selection problem in actively controlled structures was cast in the framework of a zero-one optimization problem. A Linear Quadratic Regulator (LQR) control approach was used. The dissipation energy of the active controller was used as the objective function for maximization by the

optimizer. A two-bay planar truss structure was analyzed for the placement of three actuators. Several cases were run using different probability function values in the Genetic algorithm. Most of the optimization runs found the global optimal solution, and a small number found the second optimal solution.

Kirby, Matic, and Lindner examined the use of Genetic algorithms to place and size piezoceramic actuators for active damping of a vibrating cantilevered beam [32]. Optimal solutions were determined for centralized (global) control and decentralized (local) control. The effects of actuator mass and stiffening were considered and compared with optimization solutions for which the actuator mass and stiffening was negligible. State variable feedback and Linear Quadratic Regulator (LQR) design were used for the centralized control. Collocated negative rate feedback was used for the local control studies. The optimization objective functions minimized the kinetic and potential energy of the system for centralized control, and maximized the dissipation energy for decentralized control. Their optimization results showed that significant actuator mass and localized stiffening alters the optimal size and placement of bonded piezoceramic actuators. The type of control law, global or local, influenced the optimal actuator locations. Genetic algorithms were effective tools for determining actuator size and location and effective for locating near optimal solutions from solution spaces that contain multiple numbers of local maximums. With the guidance of genetic algorithms, it was possible to obtain a nearly optimal solution by evaluating less than 0.5% of the total solution space.

Sepulveda, Jin, and Schmit presented a methodology for a combined passive structural design and active control synthesis in which the optimal location of active members was treated as (0, 1) variables [33]. The passive structural member sizes, active control gains, and (0, 1) placement variables were treated simultaneously as design variables. The optimization problem was formulated as a mixed nonlinear mathematical programming problem involving both continuous and discrete (0, 1) variables. A direct output feedback control law was adopted for the voltage applied to active members, and displacement and velocity gains for each active member were treated as design variables. The combinatorial aspects of the mixed discrete and continuous optimization problem were dealt with using a strategy that combines approximation concepts and a branch and bound technique. An eighteen bar truss structure was analyzed to test the proposed synthesis methodology. Their results demonstrated the effectiveness of the design methodology, as well as, the computational efficiency of the branch and bound technique combined with approximation concepts. The final designs were obtained with relatively small number of iterations; however, the presence of local minima presented some difficulty and clearly indicated the need for improvements in the design method to deal with nonconvexity.

Maghami and Joshi developed an optimization approach for sensor and actuator placement in the control of flexible space structures [34]. The approach reduces the sensor/actuator positioning problem to a solution of a nonlinear programming problem.

The discrete control forces and discrete output measurements are approximated by spatially continuous functions in order to avoid discontinuity problems. The space structure was divided into sections with each section allocated a fixed number of actuators and sensors. A nonlinear programming problem, with the actuator/sensor locations as design variables, was posed to minimize a performance metric. Two different criteria were chosen for the performance metric. The first performance metric was formulated from the transmission zeros of the system such that the transmission zeros are moved farther to the left of the imaginary axis by the optimization process. In the second criterion, a performance metric related to the singular values of the Hankel matrix was formulated. The optimization process places actuators and sensors such that the singular values of the Hankel matrix increase in value. The Hankel matrix includes both measures of controllability and observability; therefore, the second criterion was maximizing the controllability and observability of the system. The effect of actuator dynamics on the actuator/sensor placement was also investigated. It was shown that actuator dynamics could have considerable influence on the optimal actuator/sensor locations, particularly when the actuator bandwidth is near the operational closed-loop bandwidth.

Lindberg and Longman developed a new design technique, based on Independent Modal Space Control (IMSC), for actuator placement and controller design [35]. The IMSC method determines the optimal control action by minimizing a quadratic cost functional comprised of the system states and the generalized control forces. A primary advantage of IMSC for large systems is the significant reduction of computational effort.

The standard IMSC approach requires the solution of n decoupled 2x2 Riccati equations, rather than a single ($2n$ x $2n$) Riccati equation, where n is the number of structural modes used in the modal reduction. However, in order to implement the standard IMSC method, one actuator must be used for each structural mode to be controlled. Lindberg and Longman developed a new formulation of Independent Modal Space Control (IMSC), which relaxes the restriction on the number of actuators by synthesizing an approximation to the optimal feedback. Their approximation allows one to reduce the number of actuators required by the IMSC method and maintains computational efficiency, but compromises other features of the IMSC method. The quadratic cost functional no longer contains the usual adjustable parameters, which have a one-to-one correspondence to each actuator's control effort. The state penalty in the quadratic cost functional does not directly dictate the state performance. These two characteristics of the new formulation complicate the cost functional tuning to generate the desired system performance. A third limitation is that closed-loop system stability is not assured and system stability must be checked after obtaining the optimized design.

Venkatesan and Udayasankar devised a method for selecting sensor locations to be used for active vibration control of helicopter fuselages [36]. Their procedure uses the Fisher information matrix and the Effective Independence Distribution Vector (EIDV) to sequentially eliminate the redundant sensor locations from an initial set of many candidate locations. Within their procedure, the system equations of motion are transformed to a modal representation. A potentially limiting feature of the method is that

the minimum number of required sensors is equal to the number of modes used in the modal transformation. Venkatesan applied the sensor placement method to a simplified model of a helicopter fuselage. The optimal sensor location results were then utilized in an active vibration control study. He concluded that vibration control using measurements from the optimal sensor locations yields maximum vibration suppression, as compared to vibration control using measurements from a non-optimal sensor set. Although the proposed method was not devised for actuator placement, it is included here because the approach has a number of similarities with the reviewed actuator placement methods. In addition, this study indicates that sensor location can have a significant impact on active vibration control effectiveness.

The majority of present day helicopter airframes are of semi-monocoque construction; therefore, actuator placement within an airframe is most likely relegated to a finite number of distinct locations. Unlike simple continuous beam or plate structures, the actuator placement in helicopter airframes is discrete in nature, and non-gradient optimization algorithms are well suited for the discrete actuator placement problem. In addition, the non-gradient approaches are less likely to converge to a local minimum solution. Most of the approaches incorporating simultaneous controller design are designing the active system to address excitations over a broad frequency range, rather than discrete known excitation frequencies. Some of the approaches attempted to control specific structural modes; however, such an approach requires a priori knowledge of which modes are significant or which modes are to be controlled. Other approaches

solved the problem without consideration of the active control law, but researchers have demonstrated the influence of control laws and performance objectives on the actuator placement. Drawing on the knowledge acquired from previous research, a systematic actuator placement methodology will be formulated for the unique characteristics of helicopter airframe vibration control.

1.4 Summary and Thesis Outline

Reducing helicopter airframe vibrations has numerous payoffs with regard to passenger comfort, weapons sighting, structural fatigue, production costs, and maintenance costs. Airframe vibrations are caused by several important excitation sources; however, the dominant sources are the main rotor hub forces and moments. Historically, helicopter vibrations have been addressed with passive control methods, and considerable progress has been made in designing rotorcraft with lower vibration levels. However, vibration specifications continue to be ever more stringent, and there will be continued efforts to strive for more effective vibration control measures. Thus, active vibration control methods are receiving considerable attention and study. One of the more promising airframe-based active control approaches is commonly referred to as Active Control of Structural Response (ACSR). In general terms, an ACSR system consists of airframe mounted sensors, a control computer, and a set of force actuators mounted on the airframe. Vibration control is achieved by the superposition of an actuator-induced airframe response with the response caused by external loads. Numerous analytical and experimental studies have been conducted on variations of the ACSR control approach.

Study and flight-testing of airframe-based approaches have demonstrated significant vibration suppression and enough promise to begin appearing on production rotorcraft. Actuator placement, in the airframe-based systems, is based largely upon engineering experience and limitations imposed by retrofitting an existing airframe structure. Some researchers have concluded that actuator locations, different from their selected locations, may yield a more effective active vibration control system. They also concluded that a larger number of small actuators may be more effective than a fewer number of large actuator devices. Thus, smaller actuators could be placed at more locations in the airframe and avoid the unfortunate circumstance of placing all actuators near modal nodes. The helicopter airframe is a complex structure, and it has a complex dynamic response; therefore, determining the best actuator locations is not a simple task. Distributing actuators at optimal locations in the airframe needs to be studied to investigate feasibility and examine the potential for improving vibration suppression. The design and realization issues associated with integrating actuation into a semi-monocoque airframe structure needs to be investigated. In addition, a need exists for a formal design methodology and optimization procedure to realize an active airframe with optimally distributed actuators. The main objectives of this research project are to address these needs, and advance the state-of-the-art of airframe-based active vibration control systems.

Chapter 1 summarized the helicopter vibration problem, vibration control methods, problem statement, research objectives, and the results of a literature review. In Chapter 2, a comprehensive design methodology is proposed and detailed for actuator

placement, active structure design, and realization of a helicopter active vibration control system. Chapter 3 presents the helicopter airframe models and excitation loads used in this study. Also presented in Chapter 3 is the hybrid optimization process for determining actuator placement and computing the active control actions. Chapter 4 presents the optimal actuator placement results and compares with a state-of-the-art active control configuration. Analytical results are presented to illustrate the benefit of applying the proposed design methodology, and results are presented to provide physical insight into the optimally distributed actuator placement. Chapter 5 describes an in-depth analytical study of optimally distributed actuation realization issues. A high fidelity helicopter airframe model is utilized to assess active structure designs, vibration control system effectiveness, and control system influences on airframe structural integrity. Chapter 6 presents an analysis and experimental demonstration of one particular active structure design concept applied to a scaled model of a semi-monocoque airframe structure. The scaled model structure design and fabrication is described along with the corresponding analytical models. Installation of piezoelectric stack actuation devices for vibration control is presented. Vibration control is studied analytically, and a physical demonstration is illustrated. Chapter 7 contains a summary and conclusions of the research project. In addition, recommendations for future research activities are presented.

Chapter 2

OPTIMALLY DISTRIBUTED ACTUATION REALIZATION METHODOLOGY

2.1 Introduction

Airframe-based active vibration control approaches are being seriously considered and investigated because they have advantages over the rotor-based approaches. Rotor-based active control methods reduce the oscillatory hub loads, but may not be capable or efficient at controlling excitations that do not enter the airframe through the main rotor hub. Until all problematic excitation sources are eliminated, some type of airframe-based control system is required to meet more stringent vibration specifications. Even though current airframe-based active control approaches have demonstrated substantial vibration reductions, the system performance can be greatly improved with technological advances and design innovations. An extensive literature search was conducted and the limitations of the current airframe-based active control approaches were identified. A systematic and comprehensive design approach is needed to explore the vast multitude of potential active control configurations and determine which is best. To overcome the limitations of present systems and advance the state-of-the-art, a new actuator placement and active structure design methodology is proposed and explored in this research. The design methodology, presented in this chapter, is termed the Optimally Distributed Actuation

Realization Methodology. This methodology is a four-part design cycle and each part of the method is explained in detail. The various analytical tools, models, and processes required to execute the methodology are described.

2.2 Optimally Distributed Actuation Realization Methodology

The Optimally Distributed Actuation Realization Methodology (ODARM), illustrated in *Figure 2.1*, is versatile enough to be applied to any rotorcraft. The methodology is a four-part design cycle. The first step is to create a detailed numerical (Finite Element, FE) model of the helicopter airframe. Creation of a detailed finite element model is an arduous and lengthy process, however, finite element models are part of the customary rotorcraft development process. These models are typically used for static and dynamic analysis of the airframe, and the very same models can be used in the ODARM for realizing a distributed actuator vibration control system. Thus, the first step of the methodology may simply be an adaptation of existing airframe models. The size and detail of typical airframe FE models range from 2000 to 25,000 degrees-of-freedom [10]. The necessary level of detail is dependent upon the intended use of the model. A general guideline, for selecting the degree of detail in the FE model for the ODARM, is to select enough detail in order to adequately capture localized dynamics in the vicinity of potential actuator locations. In other words, a high level of model detail is not required in areas of the airframe where actuator installation is not possible or practical.

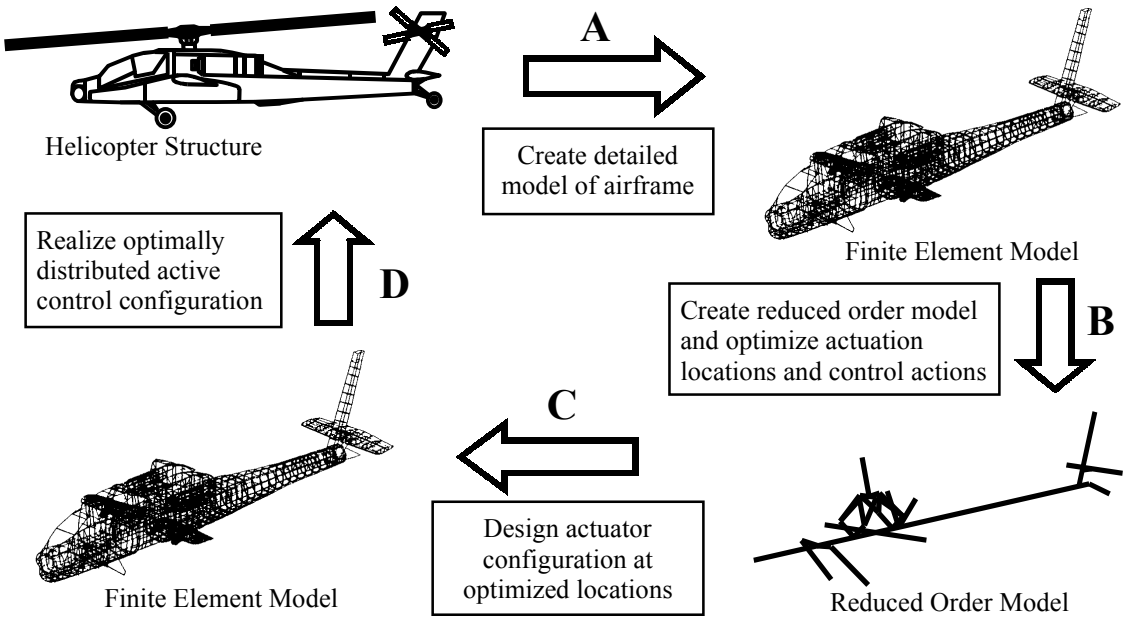

Figure 2.1: Optimally Distributed Actuation Realization Methodology (ODARM)

The second step of the ODARM is to create a reduced order model of the airframe, which is utilized in the optimization procedure to determine actuation locations and control actions. The recommended airframe model reduction method and optimization procedure are detailed in later chapters. Model reduction is an essential part of the ODARM in order to condense the optimization problem to a manageable size by reducing the size of the design space. There are literally thousands of potential actuator locations within the actual helicopter airframe, as well as within the detailed FE airframe model. Utilizing the detailed FE model and incorporating all potential actuator locations into the optimization problem expands the design space immensely and greatly increases the computation time to find a solution. To illustrate this point, consider a detailed FE model that has one thousand (n = 1000) candidate actuator locations and a set of eight (k = 8) actuators are to be distributed throughout the airframe. According to statistics and

probability counting techniques, there are 2.4115×10^{19} combinations (equation 2.1) of actuator configurations that define the design space [37]. Thus, conducting a parameter study to examine each of the potential actuator configurations or applying an optimization procedure to such a large design space is not practical or advisable.

$$C_{k,n} = \frac{n!}{k!(n-k)!} = \frac{1000!}{8!(1000-8)!} = 2.4115\times10^{19} \qquad (2.1)$$

Applying the optimization procedure to a reduced order model is more efficient from a computational viewpoint, because the number of potential actuator locations can be constrained considerable. For instance, consider a reduced order airframe model with one hundred (n = 100) candidate actuator locations, equation 2.2. The number of possible actuator configurations (1.8609×10^{11}) remains large, but the number of possibilities is reduced by eight orders of magnitude. Examination of each possible actuator configuration is not practical, but applying an optimization procedure to the reduced design space is significantly more efficient.

$$C_{k,n} = \frac{n!}{k!(n-k)!} = \frac{100!}{8!(100-8)!} = 1.8609\times10^{11} \qquad (2.2)$$

The third step of the ODARM is to utilize the optimization results and design a detailed actuator configuration that produces the desired control actions. The optimization procedure, which uses the reduced order airframe model, produces results

that indicate the actuation locations, type of actuation, and the necessary control effort. Actuation locations indicate the geometric regions of the airframe where active control is to be applied. Actuation type indicates the type of control action: single point force, dual point forces, or dual point bending moments. Actuation type definitions and descriptions are covered in a later section. Control effort is determined by an optimal control formulation and indicates the required active control input magnitude and phase. Actuation inputs to the reduced order model are not specific to a particular actuator device; but instead, they are conceptual force and moment inputs. Therefore, in the third step of the ODARM, design and analysis is applied to the high fidelity airframe model. Specific actuator configurations are analyzed using the detailed airframe FE model. At this point in the methodology, specific actuators (electromagnetic, hydraulic, piezoelectric, et al) are modeled and incorporated into the detailed airframe FE model. Various actuator configurations, that produce the control actions indicated by the optimization procedure, are designed and analyzed to refine the active control system. Structural modifications of the airframe to install the actuators are evaluated by using the detailed airframe model. In addition, the detailed airframe model can be used to evaluate localized structural dynamics. Localized structural integrity of the airframe near the actuator installation is evaluated with the detailed FE model. The final designs are evaluated for sufficient control authority and vibration suppression.

The fourth and final step of the Optimally Distributed Actuation Realization Methodology is to utilize the analytical knowledge acquired in the previous steps to

install the hardware and realize the active vibration control system in the actual helicopter structure. System specifications are defined by analyses of the previous steps and are used to purchase, install, and configure the necessary hardware and software. At the discretion of the designer, steps three and four may be reiterated multiple times to refine the final active vibration control system design.

A framework for realizing a distributed actuation control system has been formulated and explained. It should be noted; this research study has focused on demonstrating and validating steps two and three of the ODARM. Step one, creation of a detailed finite element model, is not covered because this subject is well established and well documented. Execution of step one was not necessary because pre-existing helicopter airframe models were generously provided by Boeing Company in Mesa, Arizona. Installing a distributed actuation control system in an actual helicopter, step four, is not economically feasible or within the scope of this research program.

Chapter 3

AIRFRAME MODEL, EXCITATION LOADS, AND OPTIMIZATION PROCESS

3.1 Airframe Structural Dynamic Model

Two dynamic models of the helicopter airframe are utilized within the ODARM methodology. One of the airframe models is a large degree-of-freedom finite element model that is detailed in a later chapter. The other is a reduced order model of the airframe, upon which the optimization procedure is applied for actuator placement. The reduced airframe model should not be overly complex nor require substantial numerical computations. However, the airframe model should be sophisticated enough to capture the global dynamic characteristics of a helicopter airframe. The selected model should have the flexibility to easily incorporate actuation loads and excitations at different locations. Airframe model reduction is an essential part of the ODARM methodology in order to reduce the optimization problem to a manageable size. Numerous model reduction techniques exist, however, one particular reduction method is recommended for the proposed design methodology. The recommended reduction procedure, developed by engineers at McDonnell Douglas, was found in the DAMVIBS literature [15]. This model reduction procedure creates the mass and stiffness matrices of a reduced order elastic line model representation from the mass and stiffness matrices of a much larger Finite

Element (FE) model of the helicopter airframe [15]. The reduced mass and stiffness matrices are produced by separate static condensation routines. Determination of the reduced mass matrix is based on a redistribution of the large FE model mass characteristics. A mass lumping volume is defined around each of the reduced model grid points, and a weighted distribution of each FE model mass item contained within the lumping volume is assigned to the reduced model grid point. The reduced order model stiffness matrix is created by application of a static influence coefficient method to the larger FE model stiffness matrix. The reduced mass and reduced stiffness matrices, along with an abridged set of model grid points, are the resultant representation of a reduced order elastic line airframe model. The reduction procedure is only summarized, because an airframe model in reduced form was directly obtained from McDonnell Douglas, and execution of the procedure was not necessary. A more detailed description of the reduction procedure can be found in reference 15.

The McDonnell Douglas model reduction technique is recommended because the method and resulting model have features that are beneficial to the ODARM. Most importantly, the reduced order model representation preserves the global dynamic characteristics of the larger FE model. *Table 3.1* lists the results of a correlation study done by McDonnell Douglas that compares a large FE airframe model with the corresponding reduced order model representation [15]. Some of the localized airframe vibration modes are lost in the reduction process, but the global vibration modes retain a high degree of correlation. Another unique feature of the procedure and the resulting

model is the capability to apply actuation loads directly on the Reduced Order Model (ROM). This feature eliminates the need to reapply the reduction process for a new actuator location, which greatly reduces computational effort. Unlike modal based reduction techniques, this method retains a geometric relationship between the large FE model and the ROM. Each node point of the reduced order elastic line model geometrically corresponds to one particular node point of the large finite element model. Therefore, an actuator location in the ROM is easily translated to a geometric region in the large FE model. This geometric feature could provide valuable guidance when realizing the optimized actuator distribution in a large finite element model or in the actual airframe structure.

Table 3.1: Modal correlation of large FEM versus Reduced Order Model. [15]

MODE	Frequency (Hz) Large FEM	Frequency (Hz) Reduced Order	Mode Shape Correlation
Tailboom Torsion	5.45	5.62	0.92
1st Vert. Bending	6.00	6.15	0.93
1st Lateral Bending	10.70	9.76	0.84
Engine Yaw & Pitch	11.44	11.67	0.90
Tail Long. Bending	11.97	12.31	0.91
Mast Long. Bending	13.41	14.33	0.87
Antisym. Engine Yaw	14.16	16.43	0.70
Stabilator Yaw	20.63	19.60	0.81
			1.0 = Perfect Correlation 0.0 = No Correlation

The Reduced Order Model (ROM) test bed selected for this study is an elastic line model of the Apache helicopter with 94 nodes and 564 degrees-of-freedom. The reduced order model and the larger finite element model that it was created from are shown in *Figure 3.1*. The mass and stiffness matrices of the ROM were generously supplied by Boeing Helicopters in Mesa, Arizona (formerly McDonnell Douglas). The ROM contains 94 node points and each node has six degrees-of-freedom, three translational and three rotational. Node point numbering for the model is displayed in *Figure 3.2*. Additional details of the reduced order model, geometry, natural frequencies, and mode shapes, are listed in *Appendix A*.

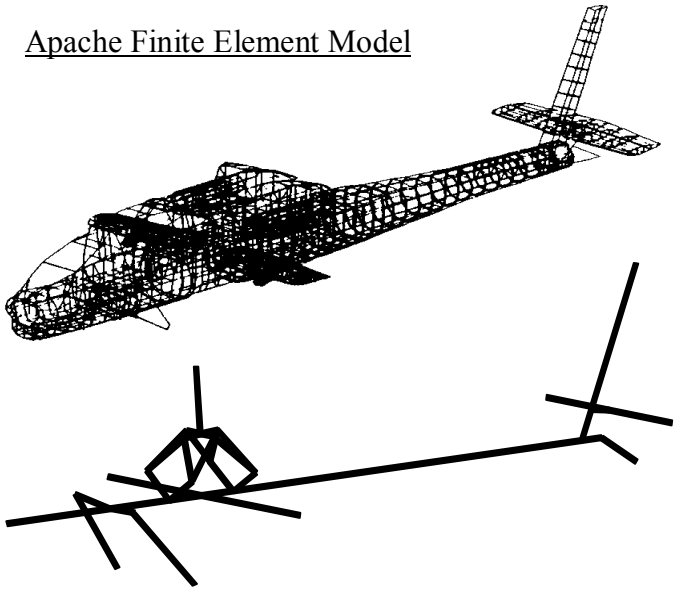

Figure 3.1: Apache AH-64 Reduced Order Elastic Line Model.

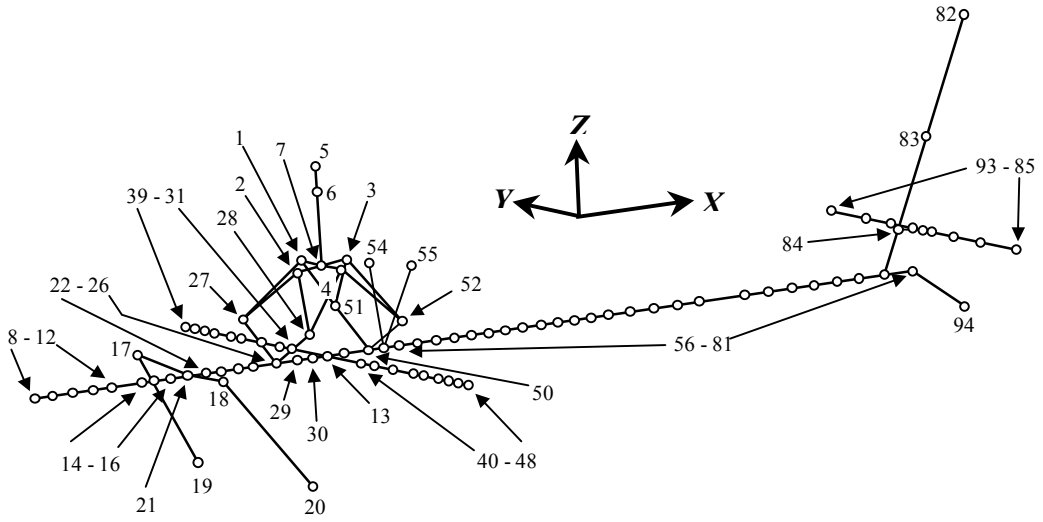

Figure 3.2: Reduced order airframe model node numbering.

3.2 Excitation Loads

The Apache helicopter has a four-bladed main rotor; therefore, the primary airframe excitation frequency (4/rev) is four times the rotor speed of 289 rpm. Two sets of 4/rev loads are formulated to excite the airframe model, one set at the main rotor hub (3 shear and 2 moment), and a second set at the horizontal tail (1 vertical shear and 2 moment), shown in *Figure 3.3*.

The hub loads were obtained from Boeing Mesa for a steady level flight condition at 0.3 advance ratio. The unsteady hub loads were derived from in-flight vibration measurements, rotor models, and airframe structural dynamic models. The hub loads used in this study are not necessarily equivalent to unsteady loads measured on a production

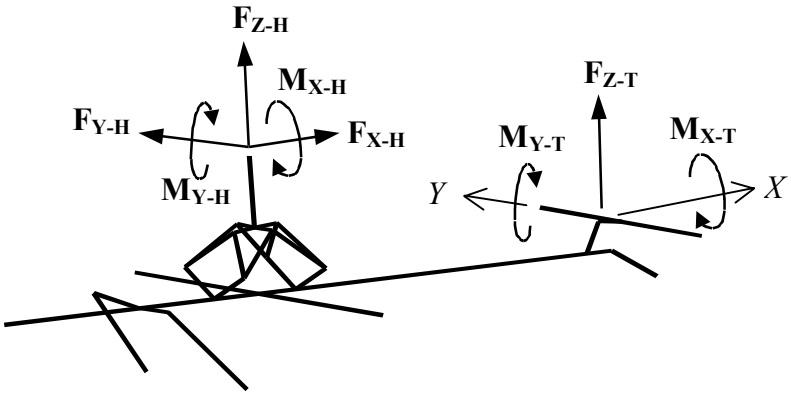

Figure 3.3: Airframe model excitations.

aircraft; however, the hub loads do excite the reduced order model to produce vibration levels consistent with in-flight vibration measurements on a production aircraft.

The unsteady tail loads are estimated using a method developed by Gangwani [37]. This method determines the unsteady vibratory airloads produced by the interaction of the main rotor wake with the helicopter empennage. While this approach is a simplified treatment of a complex interactional aerodynamic environment, it is useful in the context of the present fundamental investigation. Listed in *Table 3.2* are the applied loads. The load magnitude and phase is listed, and the airframe model node number where the load is applied.

Table 3.2: Airframe model 4/rev excitation loads			
Load Label	Magnitude [lb] or [in-lb]	Phase [deg]	Model Node Number
$\mathbf{F}_{X\text{-}H}$	185	0	5
$\mathbf{F}_{Y\text{-}H}$	185	90	5
$\mathbf{F}_{Z\text{-}H}$	920	90	5
$\mathbf{M}_{X\text{-}H}$	920	90	5
$\mathbf{M}_{Y\text{-}H}$	920	180	5
$\mathbf{F}_{Z\text{-}T}$	250	-90	89
$\mathbf{M}_{X\text{-}T}$	5400	195	89
$\mathbf{M}_{Y\text{-}T}$	1300	130	89

A rotor model is not incorporated into this study; therefore, the rotor loads are treated as inputs to the airframe model. Other researchers have demonstrated the coupled interaction of rotor and fuselage models [18, 38]. They have also demonstrated increased fuselage vibration levels with coupled rotor/fuselage models. The proposed optimization methodology could easily incorporate coupled rotor/fuselage models, but the additional complexity of coupled models was deemed unnecessary for synthesis of the methodology and a distributed actuation feasibility study. An important feature of our analysis is; the loads used to excite the airframe model do produce vibration levels that are consistent with measured in-flight vibrations.

3.3 Actuation Modeling

Three types of actuation are integrated with the airframe model. The first actuation type, designated Centralized Actuation (CA), emulates a state-of-the-art ACSR

type actuator configuration, where dual-point actuators are placed between the main rotor support assembly and the airframe. The Apache helicopter's main rotor mast and gearbox are supported and attached to the airframe by eight strut members, as shown in *Figure 3.4*. Centralized Actuation (CA) is formulated to simulate a configuration with longitudinal force actuators in parallel with each support strut. Since each actuator is in parallel with a support strut, they are not required to carry static loads. The Centralized Actuation is incorporated into the airframe model at nodes 1,2,3,4 on the mast base and nodes 27, 28, 51, 52 on the airframe.

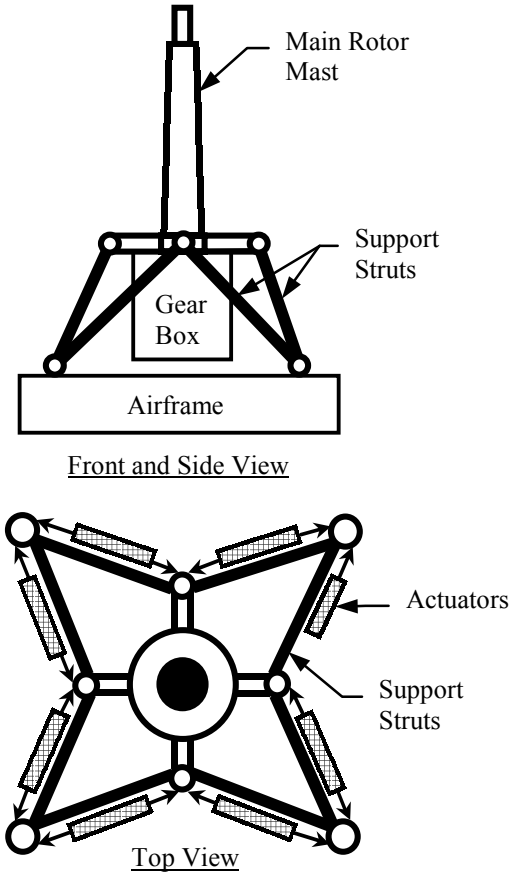

Figure 3.4: Centralized Actuation Configuration (CAC).

The second actuation type, designated a Force Actuation Unit (FAU), applies forces between adjacent nodes of the airframe model, *Figure 3.5*. The applied forces are equal in magnitude, but in opposite directions. The force direction is aligned with the

elastic segment joining the model nodes. Each Force Actuation Unit is conceptualized as two parallel dual-point force actuators that are equidistant from the model elastic segment. The two actuators of each FAU are commanded in-phase to produce a pure extension or contraction between model nodes.

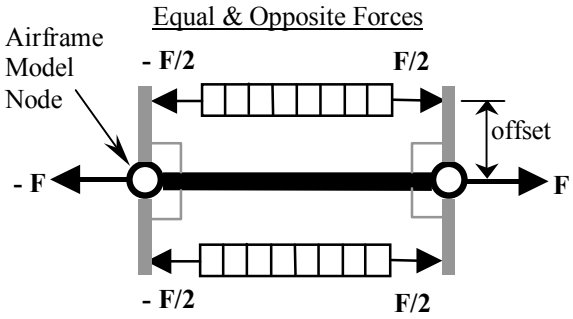

Figure 3.5: Force Actuation Unit (FAU).

The third actuation type, designated a Moment Actuation Unit (MAU), applies moments to adjacent nodes of the model, *Figure 3.6*. The applied moments are equal in magnitude, but in opposite directions. Each Moment Actuation Unit is conceptualized as two parallel force actuators that are equidistant from the model elastic segment. The actuator offset from the elastic segment is dependent upon the actual airframe geometry at the node location. The two actuators of each MAU are commanded 180 degrees out-of-phase to produce pure bending between model nodes. The MAU can produce transverse or lateral bending between model nodes. The direction of bending depends upon the

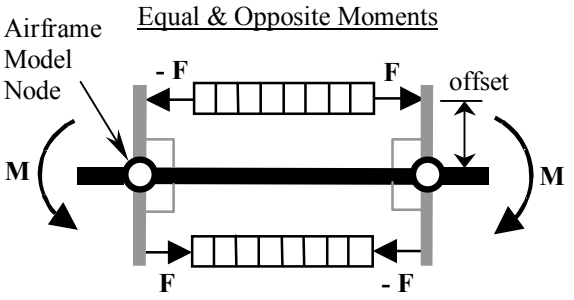

Figure 3.6: Moment Actuation Unit (MAU).

MAU orientation with respect to the elastic segment. Transverse bending is in the airframe global *X*-*Z* coordinate plane and lateral bending is in the global *X*-*Y* plane.

All actuation types (CA, FAU, MAU) produce a resultant pair of forces or moments that are applied to adjacent nodes of the airframe model. The actuation types are formulated such that loads applied to the airframe model can be resolved into equivalent FAU, MAU, or CA actuator forces. Thus, different control configurations can be objectively compared using a single unit of measure, since all control actions are expressed as individual actuator forces. The CA configuration will be used as a baseline for comparison of optimally distributed actuation configurations. A table of Actuation Unit definitions is listed in *Appendix A*.

Single-point inertial actuation is not defined or included in the actuation modeling, but single-point actuation could easily be incorporated if so desired. A conceivable single-point actuation concept consistent with the above formulation is illustrated in *Figure 3.7*. Single point actuation is not included because of the expected weight penalty associated with inertial force generating devices. In addition,

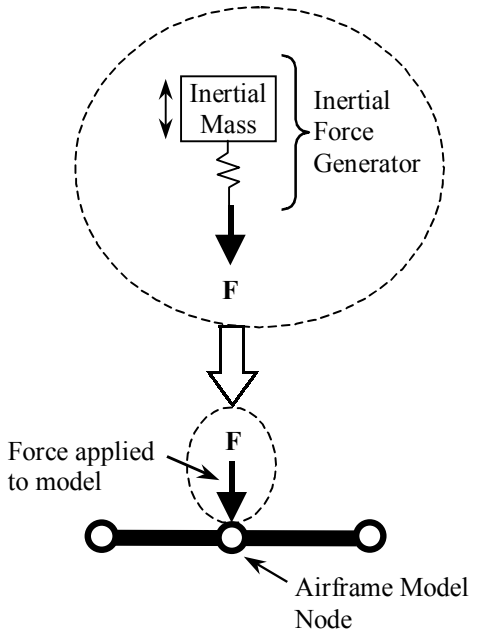

Figure 3.7: Single-point actuation concept

single-point actuation may introduce excessive localized structural stresses at their attachment location. Inertial force generators produce an output force (F) by oscillating a mass (m) through a displacement (x) at a specific frequency (ω), shown in equation 3.1.

$$F = m\,x\,\omega^2 \qquad (3.1)$$

The weight of the moving mass in an inertial force generator is related to the output force, mass displacement, and oscillation frequency according to equation 3.2.

$$W = m\,g = \frac{F\,g}{x\,\omega^2} \qquad (3.2)$$

Consider an inertial force generator that produces 1000 pounds with a 1.0 inch mass displacement and an oscillation frequency of 121 rad/sec (Apache 4/rev). Not including the actuator housing and other components, the inertial mass alone weighs 26.4 pounds. In contrast, a commercially available dual-point hydraulic actuator weighing 4.8 pounds can produce a 1020 pound force with an operating pressure of 3000 psi. The specification sheet, listed in *Appendix A*, indicates the hydraulic actuator stroke is 1.13 inches, which is larger than required for active vibration control. A custom-made hydraulic actuator with smaller stroke would weigh even less. The weight penalty associated with an active vibration control system incorporating single-point actuators may be quite significant. Thus, in this research study, actuation is restricted to dual-point concepts (CA, FAU, MAU).

3.4 System Modeling

The airframe dynamic model, actuation loads, and airframe excitations described in the previous sections need to be cast in a compatible form for analysis. Since the airframe model is excited at a discrete frequency of 4/rev, the forced airframe vibration response of interest is also at 4/rev. The discrete frequency nature of the helicopter vibration problem is well posed for a frequency domain analysis; therefore, a frequency domain transfer function model of the airframe is formulated. Starting with the discretized equation of motion expressed as:

$$[M]\{\ddot{x}\}+[K]\{x\}=\{v\}+[E]\{u\} \qquad (3.3)$$

where $\{x\}$ is the global displacement vector (3 translations and 3 rotations) in coordinates X,Y,Z for each node of the model. $[M]$ and $[K]$ are the respective mass and stiffness matrices of the reduced order elastic line model. $\{v\}$ is the vector of external excitations. $[E]$ is the actuation influence matrix and $\{u\}$ is the vector of actuation forces. The system is transformed to modal space via:

$$\{x\}=[\Phi]\{q\} \qquad (3.4)$$

where $[\Phi]$ is the eigenvector matrix and $\{q\}$ is the modal coordinate. When normalized with respect to the mass matrix $[M]$, the equation of motion becomes:

$$[\Phi]^T[M][\Phi]\{\ddot{q}\}+[\Phi]^T[K][\Phi]\{q\}=[\Phi]^T\{v\}+[\Phi]^T[E]\{u\} \qquad (3.5)$$

where $[\Phi]^T [M][\Phi]=[I]$ the identity matrix. In modal space, 0.2% proportional damping is added to the equations of motion to account for structural damping:

$$[D] = 2\zeta [\omega_n] \qquad (3.6)$$

where ζ = 0.002 is the damping factor and $[\omega_n]$ is a diagonal matrix of natural frequencies. The modal space equation of motion is transformed to a state space representation by defining the state vector as:

$$\{z\} = \begin{Bmatrix} q \\ \dot{q} \end{Bmatrix} \qquad (3.7)$$

$$\{\dot{z}\} = [A]\{z\} + [B_1]\{v\} + [B_2]\{u\} \qquad (3.8)$$

$$\{y\} = [C]\{z\} \qquad (3.9)$$

where $[A]$ is the state matrix, $[B_1]$ is the excitation input matrix, $[B_2]$ is the actuator input matrix, and $[C]$ is the output matrix of the state space representation.

$$[A] = \begin{bmatrix} [0] & [I] \\ -[\Phi]^T [K][\Phi] & -[D] \end{bmatrix} \qquad (3.10)$$

$$[B_1] = \begin{bmatrix} [0] \\ [\Phi]^T \end{bmatrix} \qquad (3.11)$$

$$[B_2] = \begin{bmatrix} [0] \\ [\Phi]^T [E] \end{bmatrix} \qquad (3.12)$$

$$[C] = [\,[\Psi] \quad [0]\,] \qquad (3.13)$$

The output equation of the state space model is formulated such that the output vector $\{y\}$ contains the translational acceleration response (in the *X,Y,Z* directions) for each node of the model. The matrix $[\Psi]$ is composed from the rows of $[\Phi]$ corresponding to the *X,Y,Z* translational degrees-of-freedom.

Two complex transfer function models are formulated, one for the external excitation inputs and another for the actuation inputs.

$$\{y_1(s)\} = [G_1(s)]\{v(s)\} = \left([C](s*[I] - [A])^{-1}[B_1]\right)\{v(s)\} \quad (3.14)$$

$$\{y_2(s)\} = [G_2(s)]\{u(s)\} = \left([C](s*[I] - [A])^{-1}[B_2]\right)\{u(s)\} \quad (3.15)$$

$$\{y_3(s)\} = \{y_1(s)\} + \{y_2(s)\} = [G_1(s)]\{v(s)\} + [G_2(s)]\{u(s)\} \quad (3.16)$$

The hub and tail loads are 4/rev oscillatory inputs to the excitation transfer function model $[G_1(s)]$, and the actuation loads are 4/rev oscillatory inputs to the actuation transfer function model $[G_2(s)]$. The output of both transfer function models is a vibration response vector of complex numbers, representing the magnitude and phase. The airframe response due to external excitation $\{y_1\}$ is summed with the response due to actuation $\{y_2\}$ to produce the controlled vibration response $\{y_3\}$.

Custom computer analysis codes are written in the MATLAB programming language to create the model formulation described above. A listing of the MATLAB source codes is found in *Appendix A*.

3.5 Hybrid Active/Passive Optimization Process

3.5.1 Active Control Law

The control law is an optimal control formulation that was devised by Johnson [39] and has been used frequently for helicopter vibration control applications. The control formulation assumes a linear relationship between the output (vibrations) and the oscillatory load inputs (excitation or actuators).

$$\{y_3\} = \{y_1\} + [G_2]\{u\} \qquad (3.17)$$

The vector $\{y_3\}$ is the controlled vibration response, while $\{y_1\}$ is the uncontrolled vibration response due to external excitation inputs. Matrix $[G_2]$ is the complex transfer function between the oscillatory actuation inputs $\{u\}$ and the airframe vibration response. The control scheme is open loop, where the active action is based upon the uncontrolled response due to external excitation. For a given set of Actuation Unit (AU) locations, the control action is computed based on optimal control theory, which minimizes a quadratic cost function [39]. The cost function J is a weighted sum of the output (vibration) and the input (control effort). Defined as:

$$J = \{y_3\}^T [W_y]\{y_3\} + \{u\}^T [W_u]\{u\} \qquad (3.18)$$

where $[W_y]$ and $[W_u]$ are diagonal matrices of weighting factors. The weighting matrices $[W_y]$ and $[W_u]$ can be tailored to emphasize vibration reduction over control effort

reduction or vice versa. Also, $[W_y]$ and $[W_u]$ can be tailored to put more emphasis on certain elements of $\{y_3\}$ or $\{u\}$ respectively. By minimizing the cost function J, the optimal control law is simultaneously achieving the greatest vibration reduction with the least control effort. Minimization of the cost function $(\partial J/\partial\{u\}=0)$ yields the following optimal control effort formulation:

$$\{u\} = -\left([G_2]^T [W_y][G_2] + [W_u]\right)^{-1} * \left([G_2]^T [W_y]\{y_1\}\right) \qquad (3.19)$$

3.5.2 Simultaneous Controller Design and Actuator Placement Method

The optimal actuator placement is not intuitive due to the complexity of the airframe structure, the numerous possible locations of the actuators, and the multiple excitation sources. A systematic methodology is developed to simultaneously determine the optimal Actuation Unit locations and the corresponding optimal control action. As presented in the literature survey of chapter one, methodologies similar to the proposed approach have been applied to generic structures for attitude control, shape control, and disturbance rejection. However, application of such a methodology on a helicopter poses some unique characteristics. The airframe structure is more complex, the excitation occurs at known discrete frequencies (integer multiples of the blade passage frequency), and the weight penalty of the control system is extremely important.

The proposed optimization procedure is a hybrid approach that couples a control law and an optimization routine for actuator placement. The procedure is formulated as a constrained minimization problem that can be stated as follows [40]:

Minimize: $J = f(\{y\},\{u\},\{p\})$

$$J = \{y_3\}^T [W_y]\{y_3\} + \{u\}^T [W_u]\{u\} + \{p\}^T [W_p]\{p\} \qquad (3.20)$$

Such that:

$$u_i \le 4000 \quad i = 1 \ldots Na \qquad (3.21)$$

$$x_i \in \{1,2,3,\ldots\} \quad i = 1 \ldots Na \qquad (3.22)$$

$$p_i = \max(0, (\hat{y}_i - \hat{p}_i)) \qquad (3.23)$$

$[W_y]$, $[W_u]$ and $[W_p]$ are diagonal weighting matrices. Vector $\{y_3\}$ is the vibration response of the model nodes targeted for vibration reduction. Vector $\{u\}$ is the control force for a given set of actuation locations defined by $\{x\}$, a vector of integer values. Each potential actuation type and location is assigned an integer value between 1 and 155, shown in *Appendix A*. The objective function is implicitly a function of $\{x\}$ since the control effort $\{u\}$ is directly dependent upon the actuation locations. Vector $\{\hat{y}\}$ is the vibration response at airframe model nodes not targeted for vibration reduction, and $\{\hat{p}\}$ is the vector of corresponding vibration constraint values not to be exceeded. Vibration constraints at non-target nodes are enforced by an external penalty function, $\{p\}^T [W_p]\{p\}$. In other words, the last term of equation (3.20) is only effective when constraints (3.23) are violated. It is also worth noting that equation (3.20) is equal to

(3.18) within the feasible region (i.e. no constraint violation). The proposed optimization procedure searches for the best actuation types and locations that will achieve the greatest vibration reduction with the least amount of control effort.

The optimization process to be coupled with the control law is called "Simulated Annealing" [40 - 42]. The Simulated Annealing algorithm is a stochastic technique to find a global minimizer for continuous, discrete, or integer non-linear programming problems. The basic idea of the method is to randomly generate feasible designs within the design space and evaluate the problem's objective function. Initially, the user provides a feasible design, and the corresponding objective function is computed and saved as the current best value. The inner most loop of the algorithm randomly generates new feasible designs by sequentially changing one design variable (Actuation Unit location) at a time, see *Figure 3.8*. One Cycle is defined as *n* executions of the inner most loop, where *n* is the number of design variables. The objective function value is computed for each new feasible design. If the new objective function value is less than the current best value, then the new design is accepted and the record for the best value is updated. If the new objective function value is greater than the current best value, then the new design is sometimes accepted and sometimes rejected. The acceptance is based on the value of a probability function and the relative size of the change in objective function value. Initially, the probability function value is large to permit acceptance of larger objective function values and permits the algorithm to escape local minima. As the algorithm progresses, the probability function's value decreases toward zero, thus in the final stages the worse designs are rejected.

The generation of new designs is not a pure random search, because each design variable change is constrained by a step size parameter. In the early stages of the process, the step size parameter is large to permit new designs far from the current. An initially large step size helps speed up the search process, and avoids being trapped at a local minimum. The step size parameter for each design variable is periodically adjusted within the algorithm to maintain a 50% acceptance rate for new feasible designs. This variable step size helps accelerate the convergence rate of the algorithm. If the number of accepted designs is large (greater than 60% of the total) then the step size is too small and will be increased. If the number of accepted designs is too small (less than 40% of the total), the step size will be decreased.

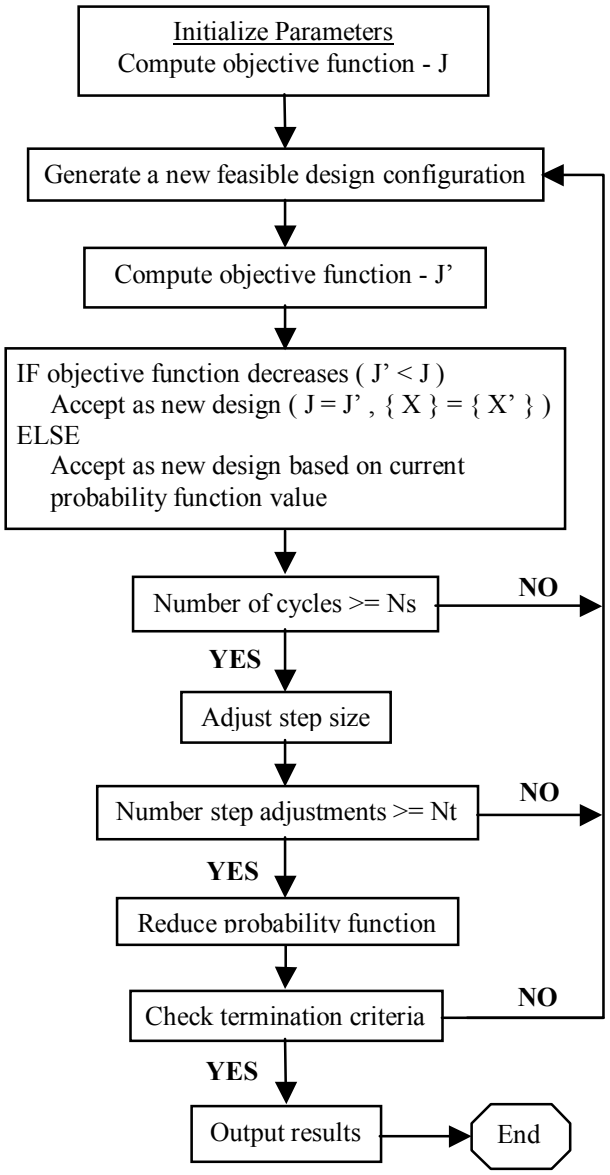

Figure 3.8: Simulated annealing optimization algorithm.

Convergence of the Simulated Annealing algorithm occurs when all new designs produce objective functions larger than the current best value, and larger values are no longer accepted because the probability function value is very small.

The Simulated Annealing algorithm is selected to search for optimal actuator locations, because it is compatible with certain features of the design problem. The Actuation Unit locations are the passive design variables. The AU locations are confined to discrete positions at model nodes; therefore, the passive design variable is discontinuous. Secondly, the objective function is discontinuous, because the passive design variable is discrete and discontinuous. These two aspects precluded the use of gradient-based optimization routines, since gradients cannot be computed. In addition, our analysis revealed that the objective function contains multiple local minima. The Simulated Annealing routine is capable of escaping local minima and more likely to find the global minimum. A standard Simulated Annealing algorithm is modified to incorporate the optimal control effort calculation into the iteration loop. For this active-passive hybrid optimization approach, the active design variables are the control gains of each Actuation Unit. The optimization process generates new AU locations, and the corresponding control action is updated as well. A flow chart of the coupled optimal control-optimization algorithm is shown in *Figure 3.9*.

Custom computer analysis codes are written in the MATLAB [43, 44] programming language to create the active-passive hybrid optimization routine. A listing of the MATLAB source codes is found in *Appendix A*.

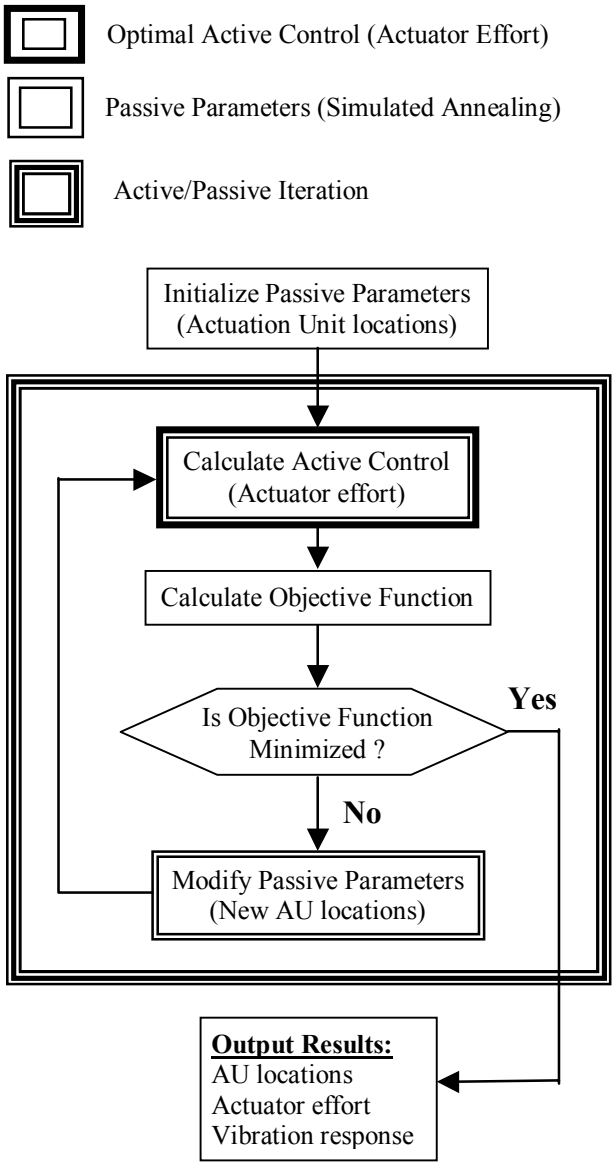

Figure 3.9: Hybrid active/passive optimization process.

Chapter 4

OPTIMAL ACTUATION PLACEMENT RESULTS

4.1 Introduction

The results of numerous analytical studies are summarized. The reduced order airframe model vibration response to external loading is examined. A state-of-the-art (centralized) active vibration control configuration is studied and used as a baseline for comparison. The formulated optimization procedure is applied to determine a number of optimally distributed actuation configurations. Distributed actuation is compared and contrasted with the baseline, centralized, configuration. Studies are conducted to acquire physical insight into the rational of the optimized distributions. The influences of actuation mass and actuation stiffness effects are examined. A parametric study on the appropriate number of Actuation Units is presented.

4.2 Uncontrolled Airframe Response

The uncontrolled airframe response is examined to determine which airframe modes are excited by the external disturbances. Results are examined for two loading conditions, external loading at the main rotor hub only, and external loading at both the hub and the horizontal tail simultaneously. The ten most prominently excited modes for

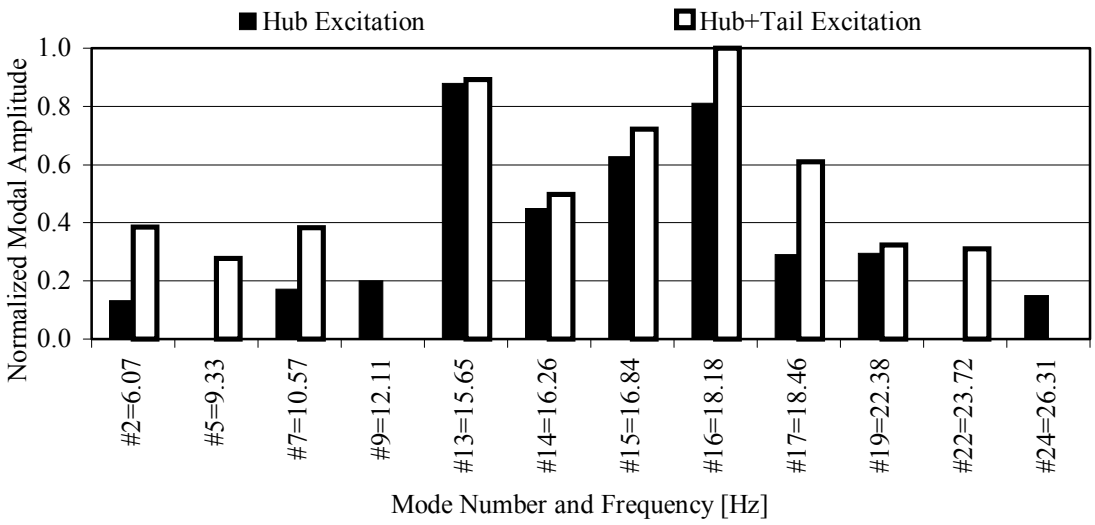

Figure 4.1: Modal participation of uncontrolled response to external excitation.

each loading condition are displayed in *Figure 4.1*. The oscillatory hub loads most prominently excite mode number 13. Mode number 13 is comprised of vertical airframe bending and fore-aft deflection of the main rotor mast. Oscillatory hub and tail loads most prominently excite mode number 16, which is primarily a lateral airframe-bending mode. Both loading conditions excite modes near the 4/rev frequency of 19.3 Hz; however, the tail loads clearly excite additional lower frequency modes (#2, #5, #7).

The area targeted for vibration reduction may be localized or spread throughout the airframe. In this study, the airframe nodes selected for vibration suppression are nodes [8,11,13,14,21,24,26,53,59,62,68], which are shown in *Figure 4.2*. The selected nodes are distributed along the centerline of the fuselage from the front into the forward tailboom section. The nodes are selected to target vibration suppression at the copilot station, pilot station, and avionics bays. The uncontrolled vibration response of the airframe model is displayed in *Figure 4.3*. The displayed vibration magnitude is a vector

sum of vibration amplitudes in the *X*, *Y*, and *Z* directions. The uncontrolled vibration response is in-line with the measured values reported by Boeing Mesa. The in-flight vibration levels of the Apache helicopter were 0.1-0.2g in the pilot area and 1.0-2.0g in the tail section, which correspond respectively to nodes 11-25 and nodes 80-93 shown in *Figure 4.3*.

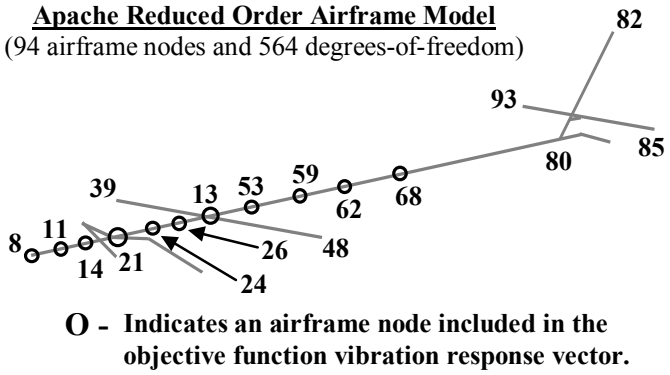

Figure 4.2: Nodes selected for vibration suppression

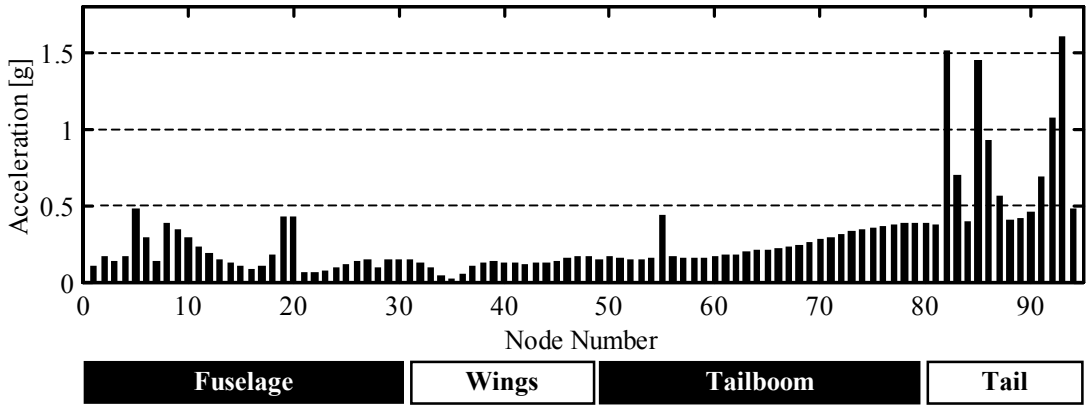

Figure 4.3: Uncontrolled airframe response to hub and tail excitation

The UTTAS/AAH development program [20] required vibration levels at the blade passage frequency to be 0.05g or less at the pilot, copilot, and passenger stations.

Although the 0.05g vibration requirement has been replaced by an intrusion index of Aeronautical Design Standard 27 (ADS-27) [21], the 0.05g level puts into perspective the desirable vibration requirement of the cockpit area. *Figure 4.4* displays the uncontrolled vibration response at the nodes targeted for vibration suppression. The 0.05 g level is exceeded at both the copilot (node 14) and pilot (node 24) stations.

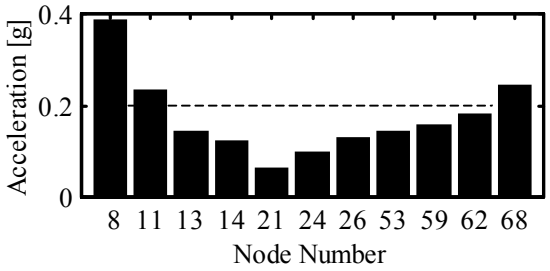

Figure 4.4: Uncontrolled vibration at target nodes

4.3 Baseline Active Control

The baseline active control configuration emulates a state-of-the-art ACSR type actuator configuration, where actuators are placed between the main rotor gearbox support assembly and the airframe. The Centralized Actuation Configuration (CAC) will be used as a baseline for comparison of optimally distributed actuation configurations. Control actions for the CAC are computed using the optimal control law, with the control weighting matrix $[W_u]$ chosen to yield a maximum control effort of 4000 lbs. The vibration response, in the *X*, *Y*, *Z* directions, at each target node will comprise the vector $\{y_3\}$ in the control law and $[W_y]=[I]$ so that all elements of $\{y_3\}$ are weighted equally. The CAC controlled vibration response is displayed in *Figure 4.5*. Vibration suppression was

achieved at the target nodes, however, a small vibration increase is observed for some of the non-target nodes. This observed vibration increase at non-target nodes was part of the motivation for including a penalty function in the hybrid optimization objective function. *Figure 4.6* displays the CAC controlled vibration response at the nodes targeted for vibration suppression. When compared to the uncontrolled response (*Figure 4.4*), the CAC achieved significant vibration suppression at all target nodes. At the copilot (node 14) and pilot (node 24) stations, vibration is suppressed below 0.08 g.

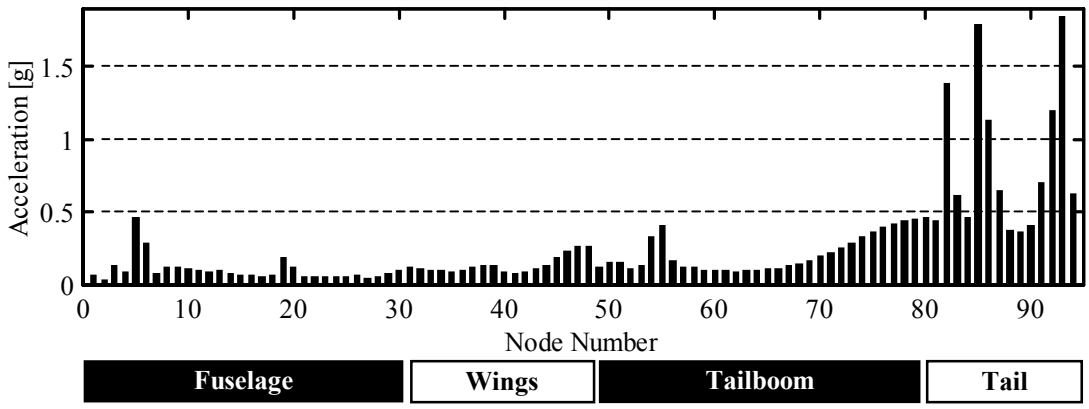

Figure 4.5: CAC controlled airframe response to hub and tail excitation.

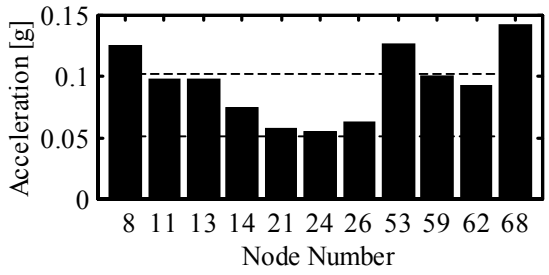

Figure 4.6: CAC controlled vibration at target nodes.

4.4 Active Control with Optimally Placed Actuation

Two types of actuation are formulated for distribution throughout the airframe model, the Force Actuation Unit (FAU), and the Moment Actuation Unit (MAU). The optimization methodology presented in chapter 3 is used to synthesize a distributed actuation configuration. The centralized configuration is formulated with eight Actuation Units; therefore, a distribution of eight Actuation Units is used to enable a fair comparison with the CAC. The actuation configuration produced by the hybrid optimization process is designated the Distributed Actuation Unit Configuration (DAUC). The optimization process determines the optimal AU locations, as well as the type of Actuation Unit (FAU or MAU). In the optimization objective function, the diagonal weighting matrices, $[W_y]$ and $[W_u]$, are defined such that all elements of $\{y_3\}$, the vibration response at target nodes, are weighted equally, and all elements of $\{u\}$, the actuation forces, are weighted equally. MATLAB software code to execute the optimization process is run on a desktop personal computer with a Pentium II 400 MHz processor and 128 MB of RAM. Total execution time for one optimization run is dependent upon the Simulated Annealing convergence criteria; the probability function's rate of change toward zero, the design variable step size parameter, and the objective function's change of value. Typical execution time for one optimization run is found to be between 105 and 135 minutes, which requires between 18,000 and 23,000 objective function evaluations. The CAC configuration is used as the initial design (Actuation Unit locations) for all optimization runs.

An optimization procedure is executed to emphasize vibration reduction and limit the control effort to less than 4000 pounds. The controlled vibration response at all airframe model nodes, for the resulting optimized DAUC, is displayed in *Figure 4.7*. The corresponding response at the target nodes is shown in *Figure 4.8*. The optimized DAUC achieves vibration suppression at nearly all airframe nodes from nose to tail. Vibration is reduced below 0.015g at all target nodes and below 0.005 g at the pilot stations. When compared to CAC (*Figure 4.6*), the DAUC achieved significantly better vibration reduction at all targeted nodes.

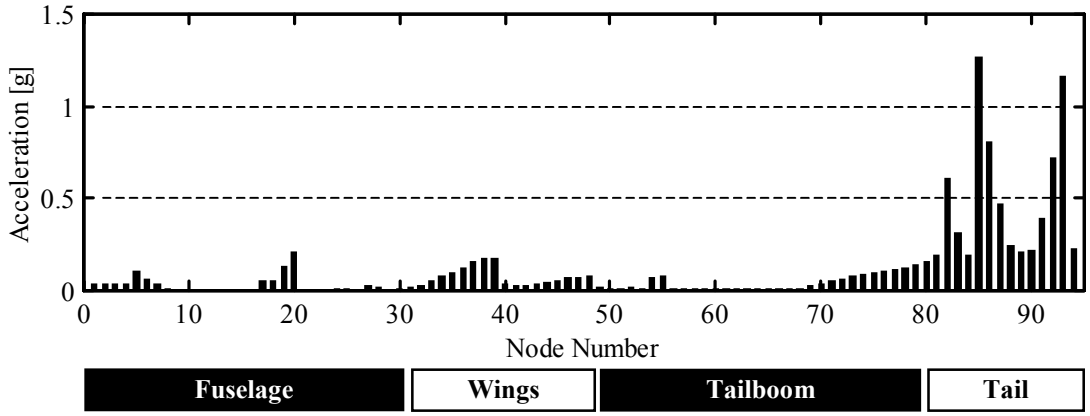

Figure 4.7: DAUC controlled airframe response to hub and tail excitation.

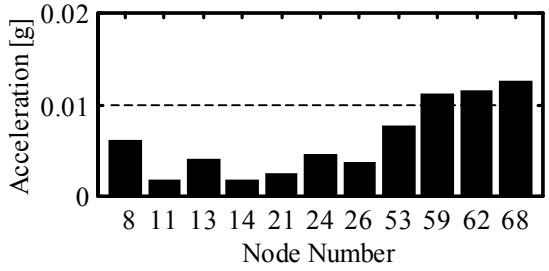

Figure 4.8: DAUC controlled vibration at target nodes.

In order to further evaluate the optimally distributed actuation concept and compare with the Centralized Actuation Configuration, three indices are defined.

1. The Vibration Index (V_{index}) is defined as the Root-Mean-Square value of the vibration response vector $\{y_3\}$, and m is the number of elements in vector $\{y_3\}$.

$$V_{index} = \sqrt{\{y_3\}^T \{y_3\}/m} \qquad (4.1)$$

2. The Control Index (C_{index}) is defined as the RMS value of the actuation effort vector, and n is the number of elements in vector $\{u\}$.

$$C_{index} = \sqrt{\{u\}^T \{u\}/n} \qquad (4.2)$$

3. The Maximum Control Effort (U_{max}) is defined as the maximum actuation effort, or the maximum element of the control effort vector $\{u\}$.

$$U_{\max} = \max\{|u_1|, |u_2|, \ldots, |u_n|\} \qquad (4.3)$$

The indices for the CAC are used as a baseline for comparison of the distributed actuation configurations. Shown in *Table 4.1* are the indices for the uncontrolled condition and the Centralized Actuation Configuration (CAC) for two excitation conditions. The control effort weighting matrix $[W_u]$ of the control law is selected such that the maximum control effort equals 4000 lb.

Table 4.1: Centralized Actuation Configuration indices.				
Airframe Excitation Condition	Uncontrolled V_{index} [g]	CAC V_{index} [g]	CAC C_{index} [lb.]	CAC U_{max} [lb.]
Hub Only	0.089	0.027	2304	4000
Hub & Tail	0.111	0.057	2521	4000

Based upon the vibration index, the centralized configuration is less effective when the airframe is excited by hub and tail loads simultaneously. The centralized configuration reduced the vibration index by 70% for the hub only excitation condition and reduced the vibration by 49% for the hub and tail excitation. For the hub only excitation condition, the centralized actuators do not completely eliminate airframe vibration, even though; the actuators are located between the hub and airframe. This apparent deficiency in vibration suppression can be explained. A broad area at eleven airframe nodes is targeted for vibration suppression. Secondly, the control weighting matrix has been selected to limit the maximum control effort to 4000 lb. If the control weighting is relaxed, the maximum control effort increases to 18,000 lb. and the vibration index is reduced to 0.0069. In addition, the centralized actuators are mounted parallel to the support struts, and a portion of the actuator effort must overcome the strut stiffness. With respect to the global coordinate frame, a centralized actuator produces longitudinal, lateral, and vertical components of force, because the actuator is oriented at an angle. One component of the actuator force may be counteracting a hub load, but the other two components may be exciting the airframe.

Vibration reduction or control effort reduction may be emphasized within the optimization process by adjusting the weighting matrices of the objective function. Optimizations are performed to produce three scenarios, a DAUC emphasizing vibration reduction, a DAUC emphasizing control effort reduction, and a DAUC producing intermediate reductions in both vibration and control effort. *Figure 4.9* through *Figure 4.11* display the evaluation indices for each scenario. Each figure displays the uncontrolled vibration index, the CAC indices, and the DAUC indices. The vibration indices are shown as a percentage of the uncontrolled vibration index. The control index and maximum control effort, for the DAUC, are shown as a percentage of the respective CAC indices.

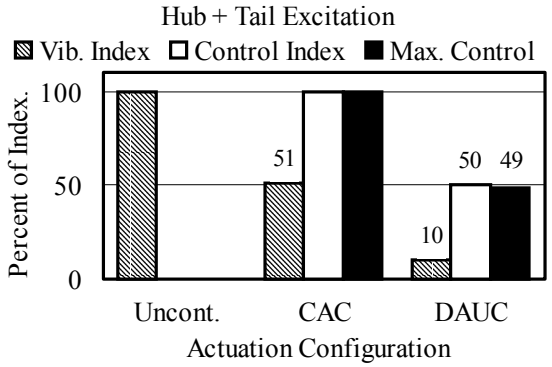

Figure 4.11: Optimized DAUC emphasizing both control effort and vibration reduction.

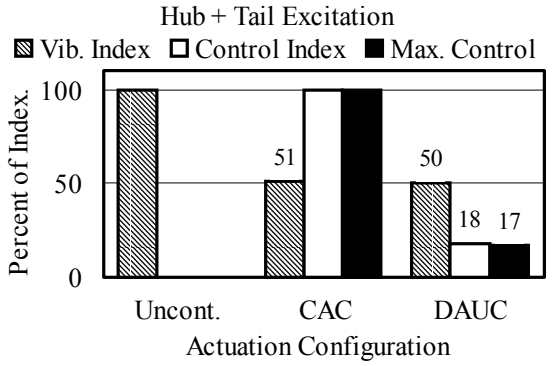

Figure 4.10: Optimized DAUC emphasizing control effort reduction.

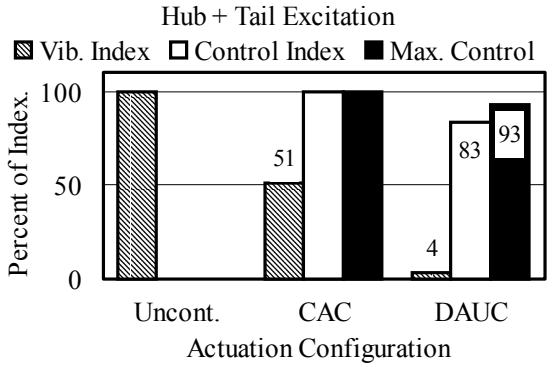

Figure 4.9: Optimized DAUC emphasizing vibration reduction.

For the results displayed in *Figure 4.9*, the weighting matrices are adjusted to emphasize vibration reduction, but also achieved a small reduction in control effort. When compared to the CAC baseline, the DAUC reduced vibration an additional 47 percent. The results displayed in *Figure 4.10* correspond to optimizations with weighting matrices adjusted to emphasize control effort reduction. When compared to the CAC baseline, the distributed configuration achieves similar vibration reduction, but requires 82% less control effort. Since the control system's effectiveness should be evaluated on both vibration reduction and control effort requirement, a more balanced weighting condition is considered with the outcome shown in *Figure 4.11*. Displayed in the figure are the results for a DAUC that achieves a 50% control effort reduction and another 41% reduction of vibration beyond the CAC.

All results presented thus far have been for a simultaneous hub and tail excitation condition. The hub only excitation condition was also examined, and the results are contained in *Appendix B*. To avoid repetition, hub excitation results are not presented here, because similar vibration and control effort reduction trends are exhibited by the DAUC.

The hybrid optimal control and optimization procedure determines the best Actuation Unit locations and actuation types to minimize the objective function. The optimized AU locations and types are displayed in *Table 4.2* and *Table 4.3*. Column one

of each table lists the number assigned to each Actuation Unit. The AU numbering starts at 1 and increases consecutively to 155. Number assignment is based upon the location of the applied actuation loads. Actuation Unit number 1 is located at the front of the airframe and applies loads to airframe nodes eight and nine.

Table 4.2: Actuation Unit locations for hub and tail excitation, emphasizing vibration reduction.

Actuation Unit Number	Location: Airframe Nodes	Applied Load
8	10-11	Pitch Moment
38	25-26	Pitch Moment
45	29-30	Yaw Moment
47	30-13	Pitch Moment
129	76-77	Yaw Moment
152	2-28	Axial Force
154	4-52	Axial Force
155	3-52	Axial Force

Bold Italic indicates a centralized Actuation Unit location

Table 4.3: Actuation Unit locations for hub excitation, emphasizing vibration reduction.

Actuation Unit Number	Location: Airframe Nodes	Applied Load
8	10-11	Pitch Moment
41	26-29	Pitch Moment
45	29-30	Yaw Moment
47	31-13	Pitch Moment
149	1-51	Axial Force
150	1-27	Axial Force
151	2-27	Axial Force
152	2-28	Axial Force

Bold Italic indicates a centralized Actuation Unit location

Number assignment for Actuation Unit definitions increases toward the tail section of the airframe. Thus, AU numbers 1 to 39 are located in the forward fuselage and AU numbers 130 to 147 are located in the tail section. In addition, Actuation Unit numbers 148 through 155 are assigned to centralized actuator locations at the main rotor mast base. Column two of each table lists the airframe node pair where each AU applies loads. The airframe node numbering begins with 8 at the front of the fuselage and continues sequentially to 94 in the tail section. Column three lists the type of loads applied to adjacent nodes of the model. The Force Actuation Unit (FAU) applies an axial force along the elastic segment joining the node pair. A Moment Actuation Unit (MAU) applies opposing moments to the model nodes listed in column two. The moments in column three are with respect to the global coordinate system of the airframe. The rolling moments are about the global *X*-axis, pitching moments are about the global *Y*-axis, and yawing moments are about the global *Z*-axis.

When the model is excited with hub and tail loads, the optimization process places four Actuation Units in the forward fuselage, one in the rear tailboom section, and three at centralized locations, (*Table 4.2*). When excited by hub loads only, the optimization places four AU in the forward fuselage and four at centralized locations, (*Table 4.3*). These results indicate that some AU in the centralized locations are necessary, but AU at all eight centralized locations are apparently redundant. Actuation in the forward fuselage greatly enhances the vibration reduction capabilities of the three or

four centralized AU. At least one Actuation Unit near the tail section is beneficial when the airframe is subject to oscillatory tail loading.

The preceding results indicate that vibration reduction can be greatly improved by applying the optimization procedure to determine the actuation locations. The optimal actuation set is composed of AU in centralized locations and actuation in the fuselage. Additional analysis has been done to provide some insight and physical understanding why the optimization process selected certain locations, and why the coupled active/passive optimization procedure is necessary.

The external disturbances excite a certain set of airframe modes, as shown in *Figure 4.1*. In order to control vibration, the actuation needs to effectively control the dominant airframe modes. Given the knowledge of which modes are being excited, a natural question is which actuation positions effectively control a particular mode. To acquire some insight, an analysis is conducted to examine which actuation locations have the greatest authority to control a single airframe structural mode. First, a new transfer function model is generated using a single airframe structural mode in the modal transformation. Therefore, a single mode contributes to the vibration response, rather than a sum of multiple airframe modes. A single Actuation Unit excites the new transfer function model, and the resulting vibration response is observed at the target nodes. The process is repeated for each prominent airframe mode shown in *Figure 4.1* and each

candidate actuation location. The Actuation Unit that excites the airframe and maximizes the vibration index indicates maximum control authority over a particular airframe mode.

The results of this analysis are summarized in *Table 4.4*. Column 1 lists the prominent airframe mode. Columns 2 through 6 list the Actuation Unit numbers in descending order of control authority. Actuation Unit numbers corresponding to centralized locations are highlighted with bold and italic text. Centralized actuation locations have the greatest control authority over airframe mode number 13, which is one of the largest modal contributors to the vibration response. This strongly supports the optimization results that placed some actuators in centralized locations. Interestingly, the other airframe modes are not controlled well by the centralized actuation, thus certain modes are controlled better by actuation in the fuselage or tailboom. Although a single mode analysis is insightful, an effective control system must control all of the dominant modes simultaneously and each AU must perform in conjunction with the others. The potential exists for AU to produce conflicting responses that superimpose to amplify the vibration response, rather than suppress vibration.

Table 4.4: Top five AU authorities to control a single airframe structural mode.

	Actuation Unit Number				
Airframe Mode No.	1st	2nd	3rd	4th	5th
2	38	142	8	59	128
5	142	59	49	143	56
7	142	8	147	38	143
9	***154***	142	***149***	48	147
13	***152***	***155***	***151***	***148***	***154***
14	57	48	***154***	***149***	***150***
15	8	38	147	41	56
16	48	57	147	142	33
17	48	57	147	142	***150***
22	142	***149***	114	120	***152***
24	142	8	153	41	***148***

Bold Italic indicates a centralized Actuation Unit location

4.5 Actuation Mass and Stiffness Effects

The analytical airframe model and optimization process are formulated without including actuation mass and stiffness in the dynamic airframe model. Actuation is idealized as control force generators, which have no mass and no stiffness. This type of actuation formulation is selected to simplify the analysis procedure, streamline the optimization process, and to maintain a generic actuation method without restricting the analysis to a specific actuation device. Inclusion of actuation mass and stiffness into the reduced order airframe model is not straightforward and open to numerous formulations. Actuation in this analysis is restricted to extenders and benders, applied to the ROM,

which can be realized by one, two, or multiple actuation devices in a semi-monocoque helicopter airframe structure. Thus, detailed actuation formulation to produce a net force or bending moment within a certain airframe region is an open design issue. Without restricting oneself to a specific actuation device and detailed device configuration, it is difficult to determine the appropriate amount of mass and stiffness to be added to the reduced order airframe model. In addition, inclusion of actuation mass and stiffness into the ROM will result in significantly more numerical computations and prolong the optimization process. The current formulation computes the airframe model's response transfer function one time and stores the transfer function for the optimization routine to access. However, inclusion of actuation mass and stiffness changes the airframe dynamic model, and requires the response transfer function to be re-computed for each new set of actuation locations generated by the optimization routine.

Adding actuation mass and stiffness to the airframe ROM will alter the structural dynamic response and require greater control forces from the actuation system. In general, these two effects are applicable to any actuation configuration, whether it is centralized or distributed. Optimization results, which neglected actuation mass and stiffness, indicate distributed actuation is superior to centralized actuation; however, the performance advantages of distributed actuation may or may not be compromised by taking actuation mass and stiffness into consideration. To investigate the effects of actuation mass and stiffness two case studies are conducted. Actuation mass and stiffness is added to the airframe ROM at locations corresponding to centralized actuation.

Stiffness and mass is also added to a previously determined distributed actuation configuration that achieved reductions in both the vibration response and the control effort. For these case studies, a piezoelectric stack actuator is selected as the force-generating device. Stack actuator sizing is based upon the maximum force (4000 lb.) and displacement (1.24×10^{-3} in.) requirements of the actuation systems. Two stack actuators are utilized for each Actuation Unit definition, and each stack actuator is considered to have a mass of 4.35×10^{-3} lb-s^2/in and a stiffness of 3.25×10^{6} lb/in.

Actuation mass and stiffness is added to the ROM at centralized locations and analyzed to compare with the baseline airframe model. Natural frequencies for both airframe models are computed and compared. Natural frequencies below 15 Hz are not altered significantly; however, adding actuation mass and stiffness altered a number of natural frequencies near 4/rev at 19.3 Hz. Thus, the uncontrolled vibration response, induce by external hub and tail loads, is also changed. With the addition of actuation mass and stiffness, the uncontrolled vibration index increases by 71 percent, from 0.111 to 0.190. For the baseline airframe model, centralized actuation is capable of suppressing the vibration index from 0.111 to 0.057, and the corresponding control index is 2521 pounds. With actuation mass and stiffness added to the baseline airframe model, centralized actuation is capable of suppressing the vibration index from 0.190 to 0.089, and the corresponding control index is 4726 pounds. Hence, centralized actuation is able to suppress vibration by 53 percent; however, the required control effort increases by 87 percent. In other words, adding actuation mass and stiffness to the centralized

configuration shifts airframe natural frequencies, increases vibration levels, and requires greater control effort to suppress vibration.

In a second case study, actuation mass and stiffness is added to the airframe ROM for an optimized distribution of actuation locations and analyzed to compare with the baseline airframe model. Again, the natural frequencies below 15 Hz are not altered significantly; however, adding actuation mass and stiffness altered a number of natural frequencies near 4/rev. The addition of actuation mass and stiffness increased the uncontrolled vibration levels at the target nodes. An increase in the vibration index of 23 percent is observed, escalating from 0.111 to 0.136. For the baseline airframe model, distributed actuation is capable of suppressing the vibration index from 0.111 to 0.046, and the corresponding control index is 1250 pounds. With actuation mass and stiffness added to the baseline airframe model, distributed actuation is capable of suppressing the vibration index from 0.136 to 0.058, and the corresponding control index is 7735 pounds. Thus, the distributed actuation case is able to suppress vibration by 57 percent; however, the required control effort increases by 6.2 times. The increase of control effort is quite remarkable, but the actuation locations are optimized for the baseline airframe model. Adding actuation mass and stiffness after the optimization procedure alters the airframe dynamic response; therefore, the actuation distribution is no longer optimal.

The two case studies indicate that inclusion of actuation mass and stiffness can have a profound effect on the active control system performance. Therefore, actuation

mass and stiffness should be considered within the optimization problem formulation or should be considered in the detailed actuation design following the optimization procedure. Including mass and stiffness into the optimization formulation is feasible; however, additional constraints are imposed on the optimization problem, and computational efficiency may be sacrificed. Another approach is to neglect the actuation mass and stiffness within the optimization procedure, then consider the actuation parameters afterwards. Such an approach would most likely involve a redesign of the passive airframe structure in the regions of actuation, such that, the airframe dynamic response is not altered by the actuation installation. This second approach has been followed throughout the research study and has been demonstrated experimentally on a scaled helicopter tailboom model, which is presented in chapter six.

4.6 Multi-objective Optimization Analysis

The data in *Table 4.2* and *Table 4.3* indicate that the optimization process selected some different actuation locations, when the airframe is subject to different loading conditions. One desirable feature of an active control system is to perform effectively for a variety of excitation conditions. The optimization methodology can be utilized to search for an actuation configuration that is robust with respect to multiple excitation conditions. To demonstrate how the optimization methodology can be applied for multiple excitations, a case study is presented. In order to find one set of actuation locations that performs effectively for two excitation conditions, a multi-objective optimization is

formulated. A composite objective function is formulated for the multi-objective optimization methodology.

$$\text{Multi-Objective Function: } J = J_1 + J_2 \qquad (4.4)$$

Hub only loading condition:

$$J_1 = \{y_1\}^T [W_{y1}]\{y_1\} + \{u_1\}^T [W_{u1}]\{u_1\} + \{p_1\}^T [W_{p1}]\{p_1\} \qquad (4.5)$$

Hub and tail loading condition:

$$J_2 = \{y_2\}^T [W_{y2}]\{y_2\} + \{u_2\}^T [W_{u2}]\{u_2\} + \{p_2\}^T [W_{p2}]\{p_2\} \qquad (4.6)$$

The multi-objective function is the sum of two scalar objective functions, one for each loading condition. J_1 is the objective function for the hub only loading condition, and J_2 is the objective function for the simultaneous hub and tail loading. The multi-objective optimization produced the AU locations and types listed in *Table 4.5*. The effectiveness of the multi-objective optimized actuation is compared to the centralized configuration and is illustrated in *Figure 4.12* and *Figure 4.13*. Both figures display the DAUC effectiveness to control each loading condition independently. This actuation configuration reduced the vibration index by 84% for hub only excitation and 71% for simultaneous hub and tail loading. In addition, this multi-objective optimized configuration requires less control effort than centralized actuation, 59% less for hub only excitation and 57% less control effort for the simultaneous hub and tail loading.

Table 4.5: Actuator locations for multi-objective optimization.		
Actuation Unit Number	Location: Airframe Nodes	Applied Load
8	10-11	Pitch Moment
38	25-26	Pitch Moment
39	25-26	Yaw Moment
42	26-29	Yaw Moment
47	31-13	Pitch Moment
126	75-76	Yaw Moment
149	1-51	Axial Force
151	2-27	Axial Force

Bold Italic indicates a centralized Actuation Unit location

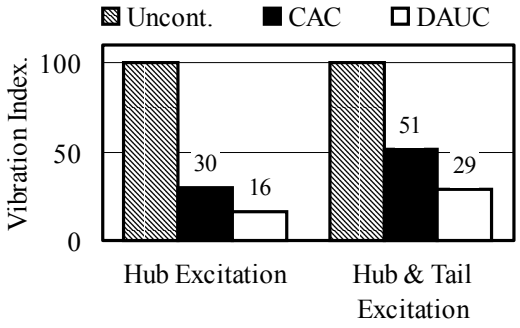

Figure 4.12: Vibration reduction of multi-objective optimized DAUC.

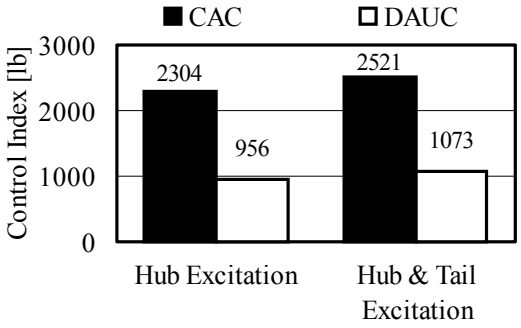

Figure 4.13: Control effort reduction of multi-objective optimized DAUC.

One point worth noting is that the multi-objective optimized DAUC sacrifices some vibration reduction, but still outperforms the centralized configuration. Examining vibration results displayed in *Figure 4.12* with *Figure 4.11*, it can be observed that the multi-objective optimized DAUC sacrificed about 19% in vibration suppression, as

compared to an actuator distribution optimized for one loading condition (simultaneous hub and tail excitation).

4.7 Simplified Actuator Placement Method

The hybrid optimization process produces actuator locations that effectively suppress vibration. For the purpose of evaluation, a simpler method is used to determine actuation locations, and the resulting AU configuration is compared to the hybrid optimized actuation configuration. This simpler method for selecting actuation locations mimics an experimental laboratory type method. A single Actuation Unit is used to excite the airframe, and the resulting vibration response is measured. The process is repeated for all candidate actuation locations to determine which locations produce the greatest response. This type of simple design process is simulated numerically with the airframe and actuation models. The first twenty-five airframe structural modes are used in the modal transformation. There is 155 candidate AU locations and the vibration response at all target nodes are the response parameters to be maximized. The vibration index at target nodes is used as the performance metric to determine the maximum control authority. The top eight AU locations from the simple design process are listed in *Table 4.6*. This set of Actuation Units is designated the Sequential Actuation Configuration (SAC). Four of the eight Actuation Units are in centralized locations and highlighted in bold italic text.

Table 4.6: Top eight Actuation Units for the Sequential design method.	
Actuation Unit Number	Vibration index [g]
48	0.296
57	0.263
148	0.184
153	0.168
155	0.159
142	0.156
150	0.152
147	0.128

Bold Italic indicates a centralized Actuation Unit location

In order to evaluate the simple actuator placement method, all eight AU of the SAC set are used simultaneously, and the optimal control law is applied to determine the control actions. The vibration response for the Sequential Actuation Configuration is computed to compare with the centralized and hybrid optimized actuation configurations. The SAC evaluation indices relative to the CAC and DAUC are illustrated in *Figure 4.14*. The Sequential Actuation Configuration (SAC) does not suppress vibration as well as the CAC or the DAUC. In addition, the SAC increased vibration in the tail section from 1.5g to 2.6g. This example highlights the need for multiple actuators to work in conjunction with each other to achieve vibration suppression. Each SAC actuator exhibits substantial individual control authority; however, the vibration reduction is not impressive when all eight AU are used simultaneously. Apparently, some of the SAC Actuation Units are combating others and producing conflicting responses. The DAUC actuators may not have the greatest individual control authorities, but their collaborative

effect produces substantial vibration reduction. Thus, the simultaneous optimal control and optimization methodology is required to search for actuation locations.

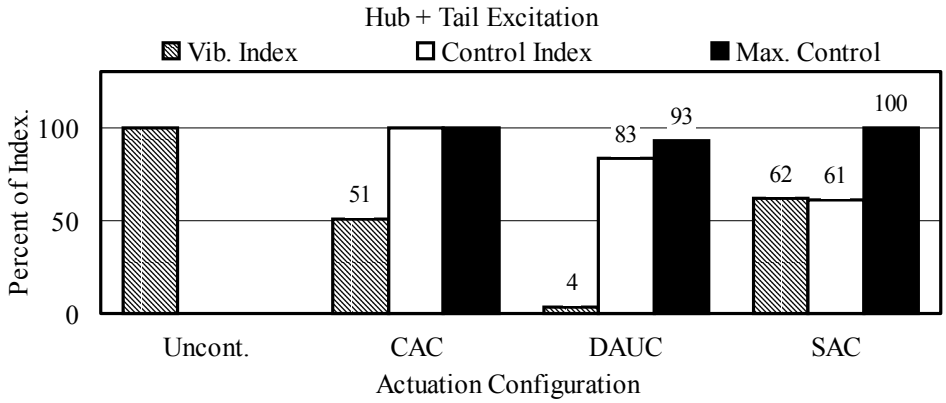

Figure 4.14: Evaluation indices for various actuation configurations.

4.8 Parametric Study on Number of Actuators

All of the prior analyses have involved eight Actuation Units, but eight AU may not be necessary for substantial vibration suppression. A fewer number of actuators would result in a simpler and lighter control system. A parametric study is conducted to determine an adequate number of Actuation Units that achieve vibration and control effort reductions. Eight different optimization runs are conducted to distribute actuation for a fixed number of AU in each run. In the first optimization run, the location of one AU is determined, and the eighth optimization run distributed eight Actuation Units. The analysis results indicate that increasing the number of AU beyond four, yielded relatively small incremental improvement in vibration suppression. Displayed in *Figure 4.15* are

the results, showing the objective function value and vibration index versus the number of Actuation Units. The evaluation indices for the four-AU set are shown in *Figure 4.16*. Actuation Unit numbers 38, 142, 151, and 154 are the set selected by the optimization process. The objective function weighting matrices are selected to achieve a good balance between vibration and control effort reductions. One item worth noting is that four distributed Actuation Units are more effective than eight centralized Actuation Units: four AU can achieve a 59% reduction of the vibration index and required 41% less control effort.

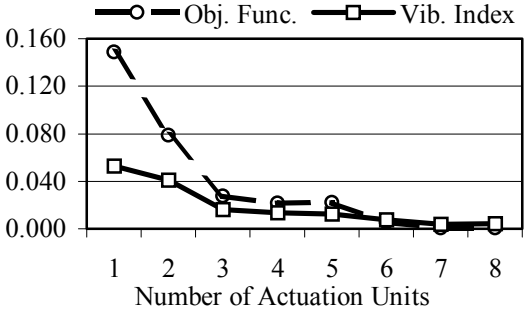

Figure 4.15: Optimization objective function and vibration index versus number of Actuation Units.

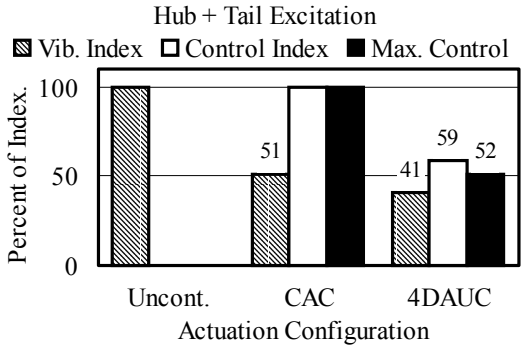

Figure 4.16: Evaluation indices of CAC and 4 optimally distributed Actuation Unit configuration.

4.9 Summary and Conclusions

A new approach has been formulated to examine the feasibility and effectiveness of optimal actuation placement for active control of helicopter vibrations. An airframe model was selected and prepared for analytical study. A systematic procedure was formulated to simultaneously determine the optimal actuation locations and optimal

control actions. An analysis was performed comparing distributed configurations to a representative state-of-the-art centralized actuation configuration. The following observations can be made with regard to the investigation results.

1. The optimally distributed actuator configurations are significantly more effective than centralized actuators in controlling vibration. A case study shows the CAC reduced vibration by 49% and the DAUC achieved a 96% reduction with similar control effort.

2. The control effort of the distributed configurations can be greatly reduced while maintaining substantial vibration suppression. One case study shows the DAUC can reduce vibration to the same level as the CAC system but with 88% less control effort.

3. The optimization procedure can be tailored to emphasize both vibration and control effort reductions. In this study, the distributed actuation configuration achieves a 90% reduction of vibration and requires 50% less control effort than the centralized configuration.

4. By including a penalty parameter in the objective function of the optimization process, an actuator configuration can be found to suppress vibration at target

areas and prevent vibration increases at non-target areas, for instance, the tail section in this study.

5. Individual actuator control authority on a single airframe structural mode was examined. Actuators in centralized locations have the greatest control authority over structural mode 13, however, actuation located in the airframe more effectively controls the other nine dominant structural modes excited by the external loadings.

6. Two sets of external loads, one at the main rotor hub and another at the horizontal tail excited the airframe model. Both sets of loads excite airframe modes near the 4/rev frequency; however, the tail loads excite additional lower frequency modes. Actuation located in the airframe more effectively controls the lower frequency modes excited by the tail loads.

7. The hybrid optimization process produces a more effective actuation configuration than a simple selection process (the Sequential Actuation Configuration) based on individual AU control authority. Each Actuation Unit of the Sequential Actuation Configuration (SAC) possesses large individual control authority, but the SAC does not suppress vibration as well as the CAC or the DAUC. In this study, the SAC reduced vibration by 38% as compared to 49% for

the centralized and 96% for the DAUC configurations with all three control configurations applying similar levels of maximum control effort.

8. The optimization procedure and a multi-objective function can be utilized to search for an actuation configuration that performs effectively for multiple excitation conditions. A case study demonstrated that the multi-objective optimized DAUC sacrifices some vibration suppression as compared to a configuration optimized for one loading condition. However, the multi-objective optimized DAUC outperforms the centralized configuration for each excitation condition.

9. The optimization process can be applied to determine the minimum number of actuators for adequate vibration suppression. In the scenario studied, it is found that four optimally distributed Actuation Units are more effective than eight centralized AU. The four distributed AU configuration achieves 10% more vibration reduction and requires 41% less control effort relative to the centralized configuration.

Chapter 5

ANALYTICAL REALIZATION OF DISTRIBUTED ACTUATION

5.1 Introduction

The purpose of the analytical realization study is to investigate actuation concepts and active structure designs that produce the desired forces and moments within the airframe. Another consideration is to illustrate the Optimally Distributed Actuation Realization Methodology (ODARM) in greater detail and to provide supporting analysis that substantiates the methodology.

The third step of the ODARM is to utilize the optimization results and design a detailed actuator configuration that produces the desired control actions. The optimization procedure, which utilized the reduced order airframe model, produces results that indicate the actuation locations, type of actuation, and the necessary control effort. The reduced order model optimization results are used to guide the analytical study of actuation concepts in a larger and more detailed helicopter airframe model. The contents of Chapter 5 are summarized as follows. The large NASTRAN model of the Apache helicopter airframe is presented and described. A model comparison study is presented that compares the uncontrolled vibration responses of the Reduced Order Model (ROM) and the larger NASTRAN Finite Element (FE) model. The NASTRAN FE

model is utilized to study an actuation concept that produces a net force or moment at specific airframe cross-sections. Controlled vibration responses of both Apache airframe models are examined, and the benefits of distributed actuation are assessed. Finally, dynamic stresses induced by external loads and active control loads are examined.

5.2 NASTRAN Finite Element Airframe Model

A NASTRAN Finite Element (FE) model of the Apache helicopter airframe has been obtained from the Boeing Company, in Mesa, Arizona. A plot of the NASTRAN model is shown in *Figure 5.1*. The model is composed with 2198 node points, 7300 finite elements, and 8000 degrees-of-freedom. NASTRAN element types utilized in the model formulation are rod, beam, rigid, and shear panel elements. The airframe model obtained from Boeing is in the form of a NASTRAN input data file, which consists of 13,183 lines of column delimited text commands. As received, the NASTRAN input file is configured to construct the airframe model and perform an eigenvalue analysis. The computed eigenvalues are listed in tabular form in *Appendix C*. New lines of command code are added to the NASTRAN input file in order to compute and plot airframe mode shapes. A representative sampling of airframe mode shape plots are displayed in *Appendix C*. The large FE model of the Apache airframe is utilized to verify and compare the optimization results obtained from the reduced order airframe model analysis, study actuation concepts, and examine structural stresses.

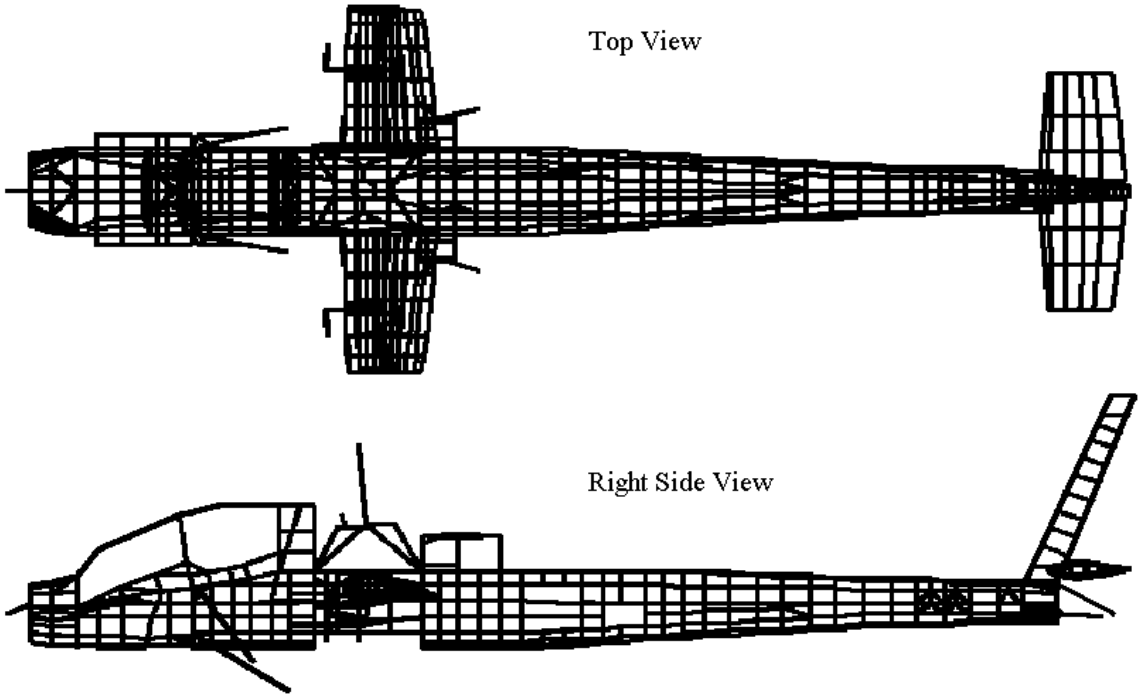

Figure 5.1: Apache helicopter NASTRAN Finite Element model

5.3 Airframe Models Response Comparison

Two airframe models are used within the ODARM methodology, and the recommended reduction procedure creates a reduced order model from a high fidelity finite element model. Therefore, a high degree of correlation between the reduced order and finite element airframe models is expected. Both airframe models were obtained from Boeing, and engineers at Boeing were responsible for applying the reduction procedure to create the reduced order model. Unfortunately, the reduction procedure was applied to a NASTRAN finite element model that differs from the NASTRAN model used in this study. The large NASTRAN model, obtained from Boeing, was created in the

mid 1980's. The Apache reduced order airframe model was created from an early 1990's version of the Apache NASTRAN model, which underwent a number of refinements over the years. Boeing was unable to release the early 1990's version of the NASTRAN model for proprietary and confidentiality reasons. The degree of refinement to the NASTRAN model is uncertain, and the effect of the refinements on model correlations is unknown. Fortunately, as will be shown, vibration predictions of the Reduced Order Model (ROM) and the obtained NASTRAN Finite Element (FE) model still agree fairly well in this research study.

The vibration responses of the ROM and the NASTRAN FE model are compared to substantiate a reasonable correlation between the two models. Each model node of the ROM is geometrically equivalent to a node of the NASTRAN FE model. Therefore, model nodes that are common to both airframe models are examined to compare vibration responses. The uncontrolled vibration response of the ROM is displayed in *Figure 5.2*. Displayed in *Figure 5.3*, is the uncontrolled vibration response of the NASTRAN FE model at model nodes corresponding to the ROM nodes. To generate the following results, both airframe models are excited by the same set of external loads, which are described in Chapter 3.

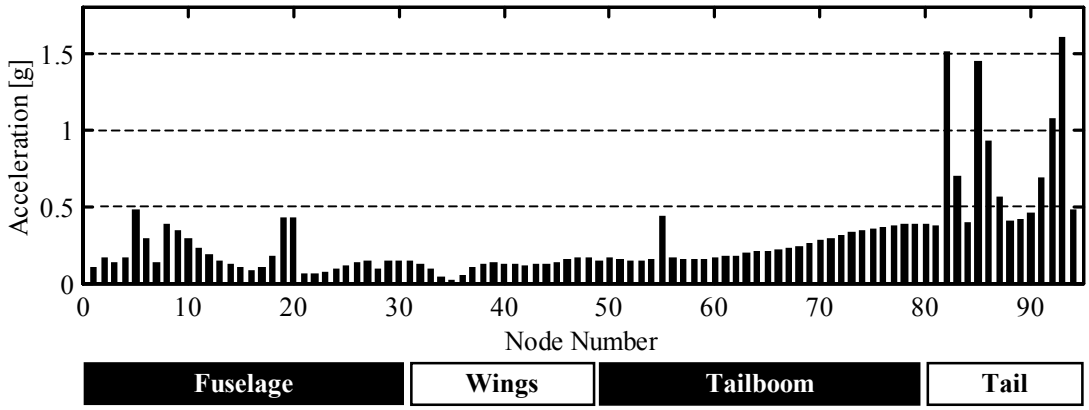

Figure 5.2: Reduced Order Model, uncontrolled vibration response to hub and tail excitation

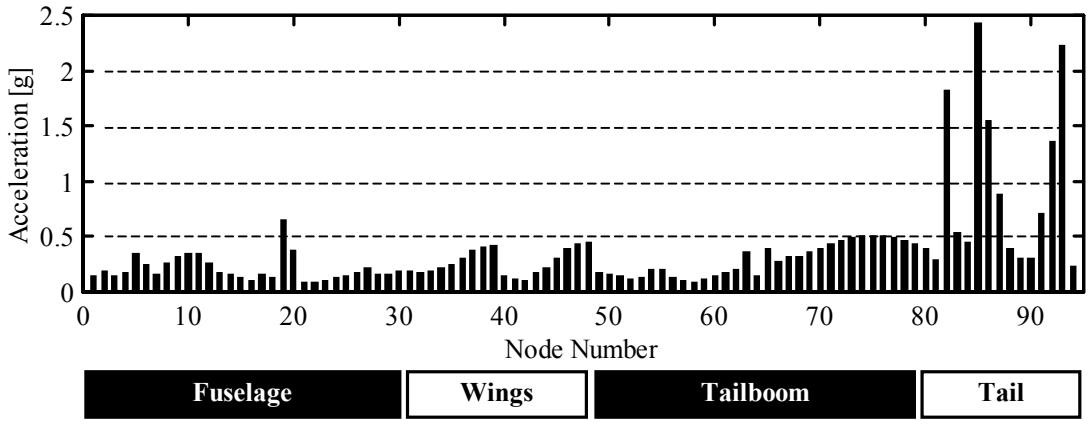

Figure 5.3: NASTRAN model, uncontrolled vibration response to hub and tail excitation

The uncontrolled vibration response of the NASTRAN FE model and Reduced Order Model of the Apache airframe exhibit similar characteristics. Although they differ to some degree in the absolute magnitude of the vibration, certain vibration trends are common to both airframe models. The largest 4/rev vibration levels occur in the horizontal and vertical tail section. Vibration levels in the tailboom section between

nodes 59 and 75 exhibit an increasing trend for nodes closest to the tail end. Vibration levels in the forward fuselage between nodes 10 and 16 exhibit a decreasing trend. Vibration levels in the middle fuselage region between nodes 21 and 30 exhibit an increasing trend. Nodes 1 through 7 correspond to the main rotor mast and support struts in both airframe models, and the vibration response trend of both models is quite similar. Although response of the wings does appear to have the most discrepancy between the two models, the Reduced Order airframe Model (ROM) replicates the global dynamic trends of the much larger NASTRAN Finite Element (FE) model quit well. In addition, a high level of confidence can be inferred upon the optimal actuator placement results, which utilized the ROM. Within the optimization process, certain airframe model nodes are targeted for vibration suppression. In this study, the airframe nodes selected for vibration suppression are model nodes corresponding to the copilot station, pilot station, and avionics bays. The ROM uncontrolled vibration response at the target nodes is displayed in *Figure 5.4*, and the respective NASTRAN FE model response in *Figure 5.5*. Vibration at the target nodes is between 0.1 and 0.4 g for both airframe models.

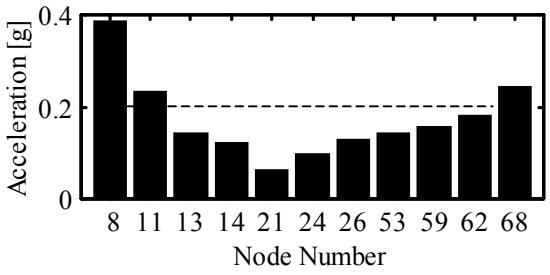

Figure 5.4: Reduced Order Model: Uncontrolled vibration at target nodes

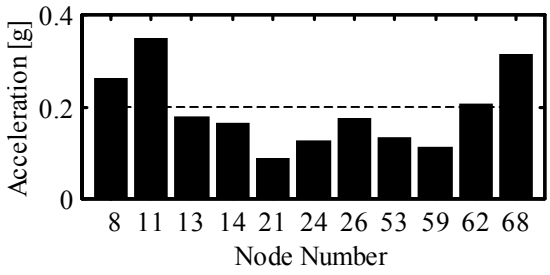

Figure 5.5: NASTRAN model: Uncontrolled vibration at target nodes

5.4 Distributed Actuation Analytical Realization

The optimally distributed actuation locations and control action results from prior research, which utilized the reduced order airframe model, will be used to guide the comparison study. The optimization process will not be applied utilizing the larger FE airframe model, but the optimized actuation locations predicted with the ROM will be used to specify actuation regions for the large NASTRAN FE airframe model. The airframe of the Apache is of semi-monocoque construction consisting of frames, bulkheads, longerons, and stringers covered with stressed skin. A helpful geometric equivalence relationship exists between the reduced order airframe model nodes and the large finite element model nodes, which are located, near the center of each frame member. Prior research did not incorporate any particular actuator, only actuation forces and moments that were applied at specific locations on the reduced order model. Actuation concepts that mimic the actuation forces and moments applied to the ROM are studied. One actuation concept is to apply forces at the intersection of the longeron/stringer and the frame member, as illustrated in *Figure 5.6*. The actuation concept could be realized by replacing the longerons with active structural elements, or could be realized by placing actuators in parallel with the longerons between frame members. This actuation concept can be configured to realize the dual point force or dual point bending moment types that are applied to the reduced order model. Actuation force directions and magnitudes are computed to produce a net force or moment at the airframe cross-section corresponding to a frame member. A pair of dual point actuation forces is applied at each stringer around the entire perimeter of the airframe cross section. The

magnitudes of the actuation forces are varied linearly from zero at the cross section geometric center to a maximum value at perimeter locations furthest from the center.

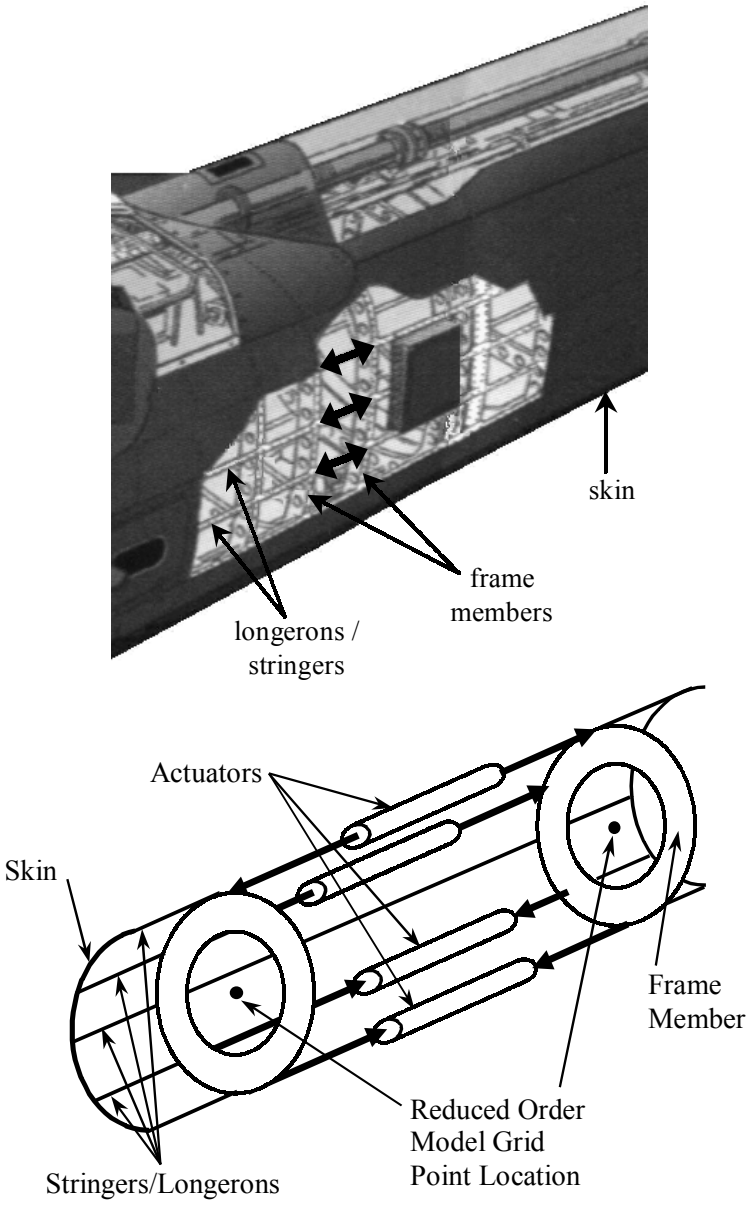

Figure 5.6: Dual-point actuation concept applied to semi-monocoque structure

The NASTRAN model input data file is edited to incorporate command codes that implement the dual-point actuation concept [45, 46]. A sample listing of the added command lines can be found in *Appendix C*. The input file is edited to implement the centralized actuation configuration and the dual-point actuation concept at 11 airframe locations. From the ROM optimization results, eleven Actuation Units (8, 33, 38, 41, 45, 56, 59, 107, 113, 129, and 142) are selected for implementation in the NASTRAN FE model. Location and definition of dual-point actuation on the airframe applied to the NASTRAN FE model is listed in *Appendix C*. In the following analyses, distributed dual-point actuation concepts are assessed analytically and compared with a centralized actuator configuration. Localized stresses are examined to insure that levels remain within the elastic limits of the structure.

A number of observations can be made when centralized control is applied to the reduced order model. The centralized control of ROM vibration at the target nodes is displayed in *Figure 5.7*. Significant vibration suppression, relative to uncontrolled vibration *Figure 5.4*, is achieved at all target nodes. Vibration is reduced below 0.08 g at the copilot (node 14) and pilot (node 24) stations. Centralized actuator control applied to the NASTRAN FE model produces similar results. Centralized control of the NASTRAN model vibration at the target nodes is displayed in *Figure 5.8*. Relative to *Figure 5.5*, vibration is suppressed at all target nodes. Vibration suppression is slightly better for centralized control applied to the NASTRAN model.

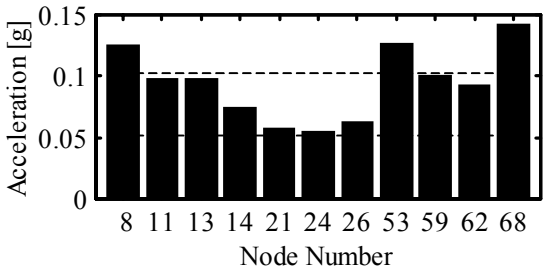

Figure 5.7: Reduced Order Model: Centralized actuation, Controlled vibration at target nodes

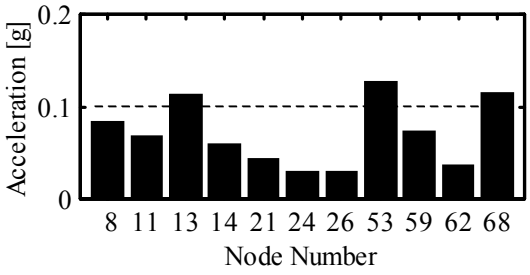

Figure 5.8: NASTRAN model: Centralized actuation, Controlled vibration at target nodes

The distributed actuation control of reduced order model vibration at the target nodes is displayed in *Figure 5.9*. Significant vibration suppression, below 0.04 g, is achieved at all target nodes, and vibration is reduced below 0.02 g at the copilot (node 14) and pilot (node 24) stations. Distributed control applied to the NASTRAN FE model produces similar results (*Figure 5.10*). Vibration is significantly reduced at target nodes, and vibration at the pilot stations, nodes 14 and 24, are reduced below 0.05 g.

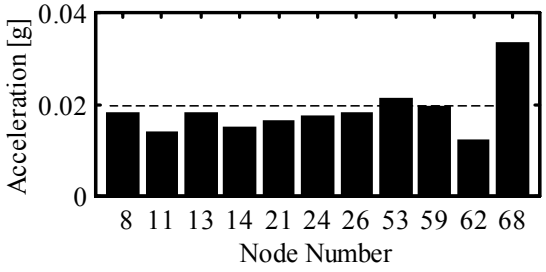

Figure 5.9: Reduced Order Model: Distributed actuation, Controlled vibration at target nodes

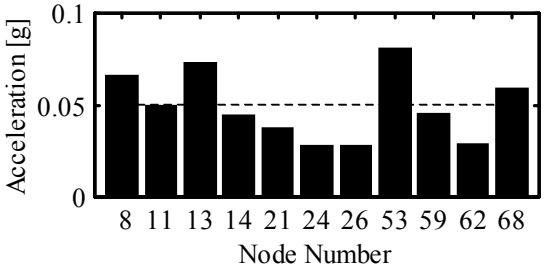

Figure 5.10: NASTRAN model: Distributed actuation, Controlled vibration at target nodes

To further evaluate the distributed actuation concept and compare with centralized actuation, three performance indices are defined. A vibration index is defined as the root-mean-square value of vibration at the target nodes. A control index is defined as the root-mean-square value of the actuation control effort. The third index is the maximum control effort of the active control system. These performance metrics are used to compare the centralized and distributed actuation configurations. A summary of the performance indices is depicted graphically in *Figure 5.11*, for the reduced order model, and *Figure 5.12* for the NASTRAN FE model analysis. Centralized control, applied to the ROM, reduced the vibration index by 49% from 0.111 g to 0.057 g with a control index of 2521 lb. and a maximum control effort of 4000 lb. Centralized control, applied to the NASTRAN FE model, reduced the vibration index by 61% from 0.170 g to 0.066 g with a control index of 2473 lb. and a maximum control effort of 4000 lb. Distributed control, applied to the ROM, reduced the vibration index by 90% from 0.111 g to 0.011 g with a control index of 1261 lb. and a

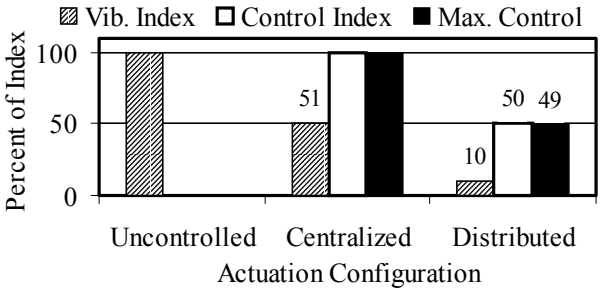

Figure 5.11: Reduced Order Model: Comparison of performance indices

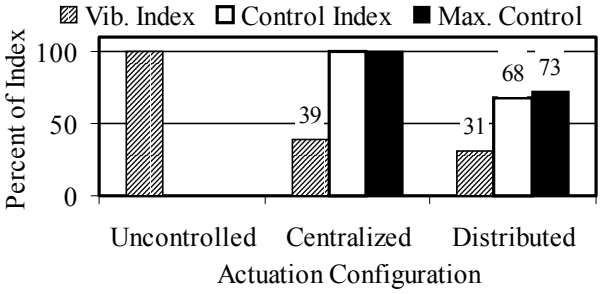

Figure 5.12: NASTRAN Model: Comparison of performance indices

maximum control effort of 1960 lb. Distributed control, applied to the NASTRAN FE model, reduced the vibration index by 69% from 0.170 g to 0.053 g with a control index of 1684 lb. and a maximum control effort of 2903 lb.

The reduced order model analysis indicates that the centralized control configuration is able to suppress vibration by 49% with a control index of 2521 lb. In contrast, the distributed control configuration reduced vibration by 90% and required 50% less control effort. Thus, distributed actuation is capable of greater vibration suppression and requires less control effort than a centralized actuator configuration. The NASTRAN FE model analysis indicates that the centralized control configuration is able to suppress vibration by 61 percent with a control index of 2473 lb. The distributed control configuration, applied to the NASTRAN model, reduced vibration by 69% and required 32% less control effort. The NASTRAN model analysis also indicates that distributed control is superior to centralized control. Greater vibration suppression is achieved with less control effort. However, the disparity between centralized and distributed actuation is not as pronounced with the NASTRAN model analysis. That is, centralized actuation is more effective on the NASTRAN model, and distributed actuation is less effective on the NASTRAN model.

A potential reason for the loss in disparity, between centralized and distributed control, may be that the actuation locations are not optimal for the NASTRAN FE model, due to differences between the two models. To test this hypothesis, the optimization

procedure is applied utilizing the NASTRAN FE model and a restricted set of potential actuation locations. The actuation locations are restricted to a set of nineteen candidate locations. Eight locations corresponding to the eight main rotor mast supporting struts, and eleven actuation locations that appeared most frequently in the ROM analysis results. Applying the optimization procedure with a restricted set of candidate actuation locations produces the following results, displayed in *Figure 5.13*, for a distribution of eight actuation locations. The vibration index is reduced from 0.170 g to 0.046 g with a control index of 1234 lb. and maximum control effort of 2089 lb. Some performance improvement is realized when compared with the actuation locations determined by the ROM analysis, *Figure 5.12*. The vibration index is reduced an additional 4%, the control index is reduced an additional 18%, and the maximum control effort is reduced an additional 20 percent. The re-optimized actuator distribution, using a limited set of potential locations, shows minimal improvement with respect to the vibration index, but substantial reductions of the required control effort are realized.

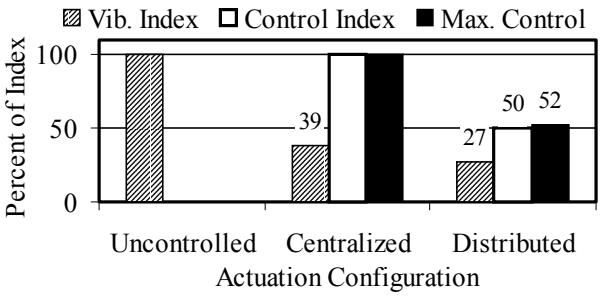

Figure 5.13: NASTRAN Model: Comparison of performance indices, re-optimized locations

All results presented thus far have been for a simultaneous hub and tail excitation condition. The hub only excitation condition was also examined, and the results are

contained in *Appendix C*. To avoid repetition, the hub only excitation results are not presented here, because similar vibration and control effort reduction trends are exhibited.

5.5 Airframe Dynamic Stress

An important engineering concern, associated with any active vibration control configuration, is the airframe dynamic stress levels introduced by the control system. The NASTRAN FE model is utilized to examine the dynamic stresses introduced by the centralized and distributed control configurations. Dynamic stress levels for the uncontrolled vibration condition are used as a baseline for comparison. The uncontrolled vibration condition is a reasonable baseline, because the helicopter airframe strength is designed to withstand numerous hours of normal operating flight. The dynamic stress levels for the 5497 elastic elements of the NASTRAN model are examined for the uncontrolled vibration condition, and the results are displayed in *Figure 5.14*.

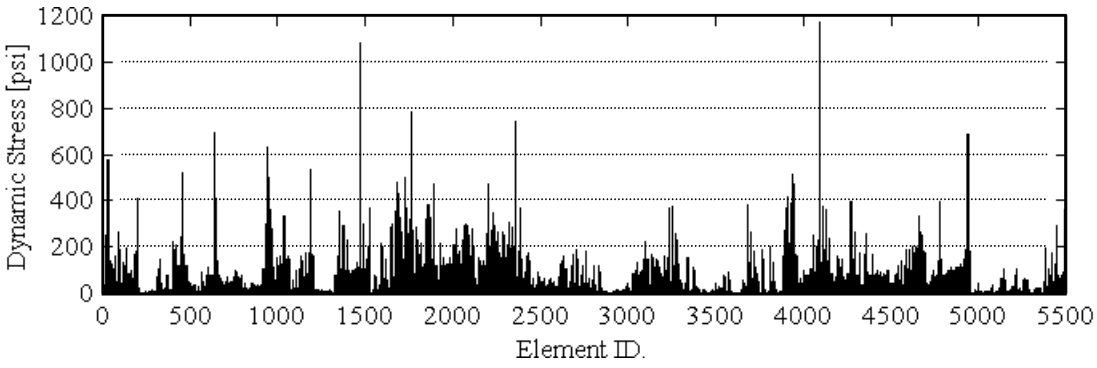

Figure 5.14: Finite Element dynamic stress from hub and tail excitation (uncontrolled)

The maximum observed stress level is 1170 psi, and only two elements have stresses in the 800 psi to 1200 psi range. Most of the element stresses, 99.2%, are less than 400 psi. A more precise breakdown is 84% in the 0.0 to 100 psi range, 11% in the 100 to 200 psi range, 3.3% in the 200 to 300 psi range, 0.9% in the 300 to 400 psi range, and 0.8% in the 400 to 1200 psi range.

Dynamic element stress levels are examined for the centralized control configuration, and the maximum observed stress is 700 psi. The dynamic stress values are displayed in *Figure 5.15*. Most of the element stresses (99.8%) are less than 400 psi. A number of observations can be made by comparing the dynamic stress levels for the centralized control configuration to the baseline uncontrolled condition.

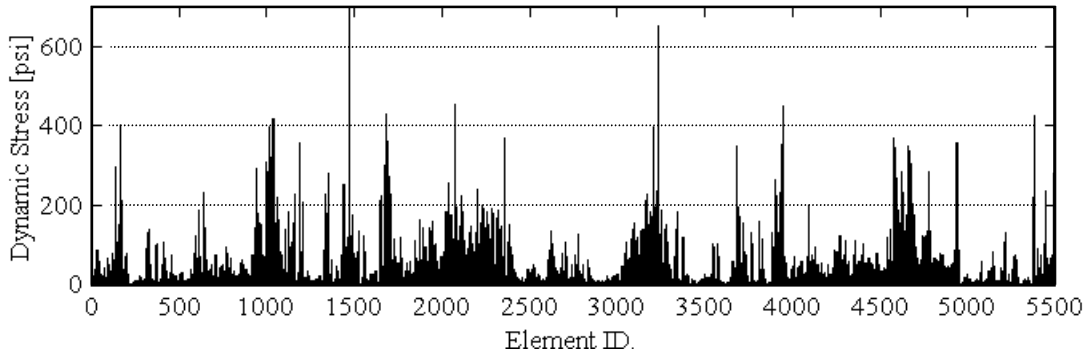

Figure 5.15: Finite Element dynamic stress, Centralized control of hub and tail excitation

The change in stress, as compared to the baseline uncontrolled stress, is illustrated in *Figure 5.16*. Dynamic stress levels are reduced in 68% of the finite elements, which is a logical expectation since the overall vibration levels of the airframe are reduced by the centralized control. A vibration increase is observed for 32% of the elements with a

maximum stress increase of 550 psi. However, a stress increase below 100 psi occurs for 30.8% of the elements. All elements with stress levels exceeding 600 psi for the uncontrolled vibration condition were reduced when centralized control is applied.

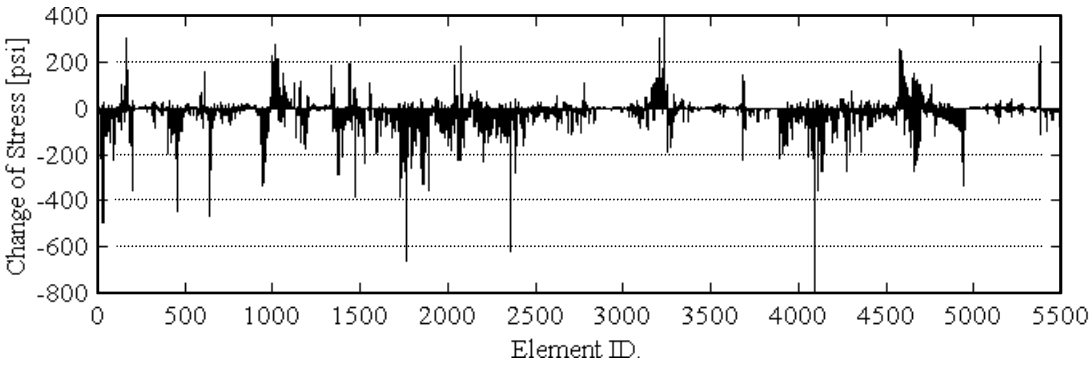

Figure 5.16: Change of element stress from uncontrolled to centralized control

The dynamic element stress levels are examined for the distributed actuation control configuration, and the maximum observed stress is 667 psi. The dynamic stress values are displayed in *Figure 5.17*. Most of the element stresses (99.9%) are less than 400 psi.

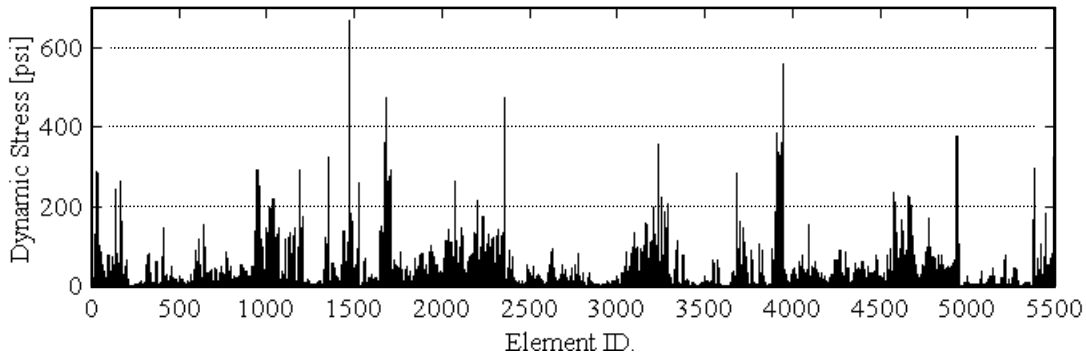

Figure 5.17: Finite Element dynamic stress, Distributed control of hub and tail excitation

A number of observations can be made by comparing the dynamic stress levels for the distributed control configuration to the baseline uncontrolled condition. The change in stress, as compared to the baseline uncontrolled stress, is illustrated in *Figure 5.18*. Dynamic stress levels are reduced in 83% of the finite elements. A vibration increase is observed for 17% of the elements with a maximum stress increase of 250 psi. However, a stress increase below 100 psi occurs for 16.5% of the elements. All elements with stress levels exceeding 600 psi for the uncontrolled vibration condition were reduced when distributed control is applied. Comparison of the change in element stress level for centralized control with the distributed control reveals two observations. Dynamic stress levels in more of the finite elements are reduced by the distributed control, 82% versus 68% for centralized control. The maximum stress increase of 250 psi for the distributed control is less than half of the increase with centralized control (550 psi). These two observations are reasonable, because the distributed control is producing greater vibration suppression and applying smaller control inputs.

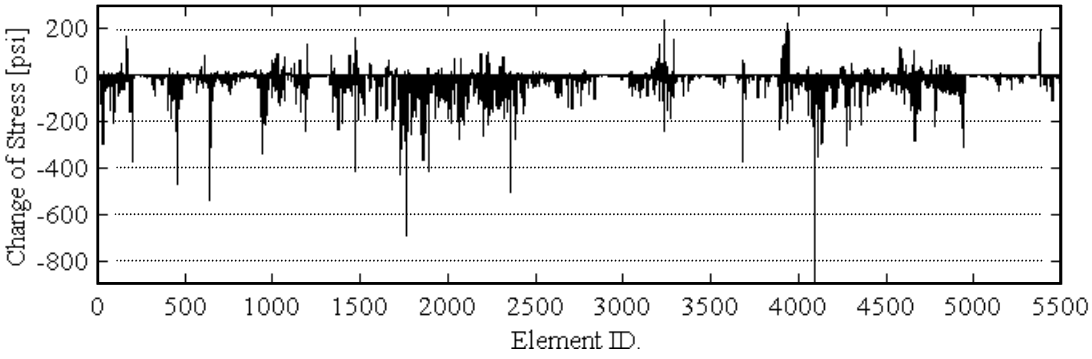

Figure 5.18: Change of element stress from uncontrolled to distributed control

Another interesting observation from the dynamic stress analysis data is that the largest dynamic stresses are not always near the location of external loads or actuation loads. To illustrate this observation, a contour plot of dynamic stresses for a distributed control configuration is shown in *Figure 5.19*. Low stress levels are indicated by dark colored regions and the highest stress areas are indicated by the lightest shading.

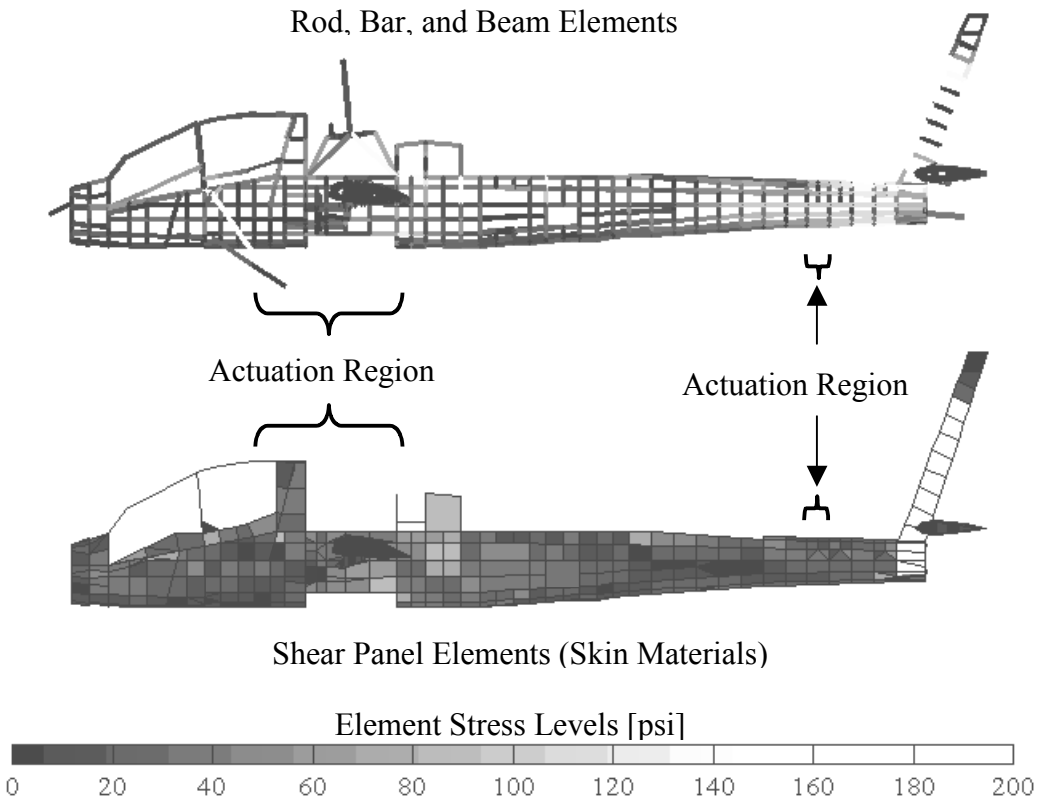

Figure 5.19: Dynamic stress levels for distributed control of hub and tail excitation

Actuation locations are identified by horizontal brackets in the figure. The largest stresses appear in the tailboom end and vertical stabilizer, not in the areas of actuation. Determination of the highest stress regions in a complex structure is not necessarily

intuitive, and is highly dependent upon which airframe structural modes are being excited. Therefore, an active control system designer needs to be cautious and examine stress levels in all regions of the aircraft, as well as, regions in the vicinity of control actuation.

5.6 Summary and Conclusion

Results of the feasibility study indicate that distributed actuation, applied to the reduced order airframe model, is capable of greater vibration suppression and requires less control effort than a centralized configuration. Vibration and distributed actuation analysis is also conducted with a large NASTRAN finite element model of the helicopter airframe. The uncontrolled vibration predictions of the reduced order model and the NASTRAN model are found to be similar. Distributed actuation control and centralized actuation control are applied to the NASTRAN airframe model. The distributed actuation control predicts a 73% vibration reduction and requires 50% less control effort than centralized actuation. When compared to the reduced order model analysis, the disparity between centralized control and distributed control is not as pronounced with the NASTRAN model analysis. However, distributed actuation control is still superior to centralized control, producing greater vibration suppression with less control effort. Dynamic stresses of the NASTRAN airframe model are examined for both the uncontrolled and controlled vibration conditions. For a controlled vibration condition, the majority of the element stresses are reduced. Dynamic stress levels in more of the finite elements are reduced by the distributed control, 82% versus 68% for the centralized

control. It was observed that the largest dynamic stresses are not always near the location of external or actuation applied loads. Thus, stress levels need to be examined in all regions of the airframe.

Chapter 6

SCALED TAILBOOM MODEL STRUCTURE AND EXPERIMENTAL STUDY

6.1 Introduction

A semi-monocoque test-bed structure is designed and fabricated for active vibration control studies. The structure is a scaled model of a helicopter tailboom that is fabricated with traditional semi-monocoque type aircraft construction. The structure is constructed and tested with several objectives in mind:

(a) To investigate the actuation design and realization issues associated with integrating dual-point actuation into a semi-monocoque structure;

(b) To examine a dual-point actuator configuration that produces a bending moment within the structure to suppress vibration;

(c) To demonstrate the correlation between the physical structure and the analytical model is reliable enough to make engineering decisions about the actuation design;

(d) To formulate an analysis procedure and establish guidelines for realizing dual-point actuation in a semi-monocoque structure;

(e) To evaluate the potential of piezoelectric stack actuators as a dual-point actuation device.

The previous analytical studies produced design guidelines and some candidate active structure designs to realize distributed actuation for helicopter active vibration control. One particular finding of significant interest is that dual-point bending moment actuation in the airframe tailboom is in general quite effective for vibration control. In addition, actuation in the tailboom was found to be especially beneficial when the airframe is excited by harmonic tail loads in conjunction with hub loads. Most rotorcraft experience considerable harmonic tail loading in some portion of their flight envelope; consequently, the above observations may be applicable to many helicopters. These observations are motivational factors in the formulation and design of the experimental study. A straightforward experimental and analytical case study is conducted to investigate and demonstrate a dual-point actuation concept applied to a semi-monocoque structure. Design and construction of the tailboom model is described. A detailed Finite Element model and a reduced order beam equivalent Finite Element model of the scaled tailboom structure are created. The tailboom FE models are utilized to analytically study a dual-point bending moment actuation concept. Actuators are installed in the scaled tailboom structure to realize the dual-point actuation concept. Vibration testing is conducted to experimentally demonstrate the predictions of the analytical models. Dynamics of the tailboom structure are examined and compared before and after the actuation installation. The influence of the actuation installation on the tailboom structure's dynamic stress levels is examined. Active vibration control by the actuator installation is demonstrated.

6.2 Tailboom Construction and Design

The experimental test-bed structure is a 0.3 scale model of a helicopter tailboom section, based on the Apache AH64-A helicopter. A diagram and photograph of the scaled tailboom model is shown in *Figure 6.1*. Overall dimensions of the tailboom model are 81 inches long, 40 inches wide, and 38 inches high. The tailboom structure is fabricated with aluminum materials and a semi-monocoque construction technique. The boom section is a rectangular shaped and tapered box beam with seven frame members, eight perimeter stringers, and covered by 0.032-inch aluminum skin material. Four stringer members, one on each corner, are 0.75-inch aluminum angles. Four stringer members, one at the middle of each side, are 1.0-inch by 0.125-inch aluminum flat stock. The root end of the boom section is a 14-inch by 11-inch cross-section and tapers to 7.25-inch by 7.25-inch cross-section. The horizontal and vertical tail surfaces of the tailboom structure are fabricated with 2-inch square aluminum tubing. All structural members

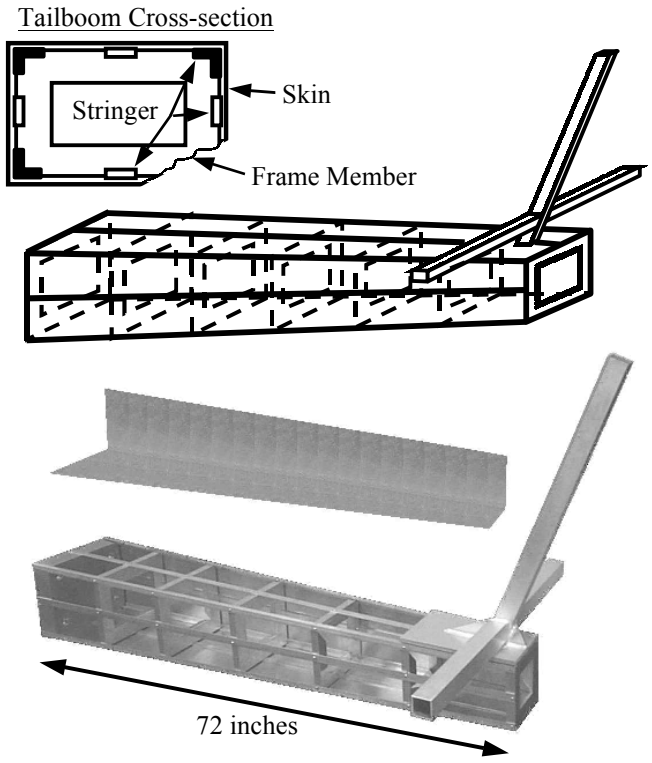

Figure 6.1: Tailboom model, 0.3 scale semi-monocoque structure

are fastened with screws to permit efficient disassembly and modifications. The total weight of the tailboom model is 60 pounds, which includes 22.5 pounds of inertial mass at the free ends of the tail surfaces.

Design of the test-bed structure is based on the Apache helicopter. The first decision in designing the tailboom model was choosing a scale factor and how much of the Apache helicopter tail section to consider. The rearmost 237 inches of the Apache tail section is selected, beginning at a bulkhead aft of the engines and an avionics bay. A test-bed structure length of 72 inches is selected due to space constraints in the laboratory and size limitations of instrumentation. Thus, the geometric scale factor based on tailboom length is 72 over 237, which equals 0.304. The model scale factor is then applied to the overall height and width of the Apache tailboom. At the selected bulkhead location of the Apache, the approximate height and width are 36 inches and 46 inches respectively. Applying the scale factor, these dimensions translate to 11-inch height and 14-inch width for the model structure. The Apache helicopter tailboom is tapered from a nearly rectangular cross-section to a 24-inch diameter circular cross-section at the tail end, which scales to 7.25 inches. In order to simplify fabrication and assembly the scaled tailboom model cross-section is rectangular throughout. However, the boom section is tapered to a 7.25-inch square cross-section at the end. Modeling of the horizontal and vertical tail surfaces is simplified by using hollow tubing, rather than semi-monocoque construction. The added complexity is deemed unnecessary for the objectives of this study. Geometric scaling of the horizontal tail width and vertical tail height is applied.

The resulting scaled width and height are 38.9 inches and 30.8 inches respectively. Engineering drawings of the scaled tailboom model components are listed in *Appendix D*.

Another design goal for the scaled model is to mimic the fundamental dynamics of the Apache helicopter tail section. The Reduced Order Model (ROM) of the Apache airframe is utilized for dynamic computations. The ROM is modified to simulate a cantilevered tail configuration. The root end of the cantilevered tailboom corresponds to ROM node number 62, which is the location of the bulkhead selected for geometric scaling. Natural frequencies and mode shapes of the cantilevered ROM tail are computed as target dynamic parameters for the scaled model design. A custom MATLAB computer code, which can be found in *Appendix D*, is written to formulate a beam equivalent elastic line model of the scaled tailboom structure. The analytical model is comprised of 13 beam elements and 14 nodes. A diagram of the computer model is displayed in *Figure 6.2*. Each node point has six degrees-of-freedom, three translational and three rotational.

The Beam Equivalent Model (BEM) is used to assess the design of the scaled tailboom structure to finalize detailed design parameters. Parameters to be determined with the BEM analysis are skin material thickness, frame member dimensions, stringer dimensions,

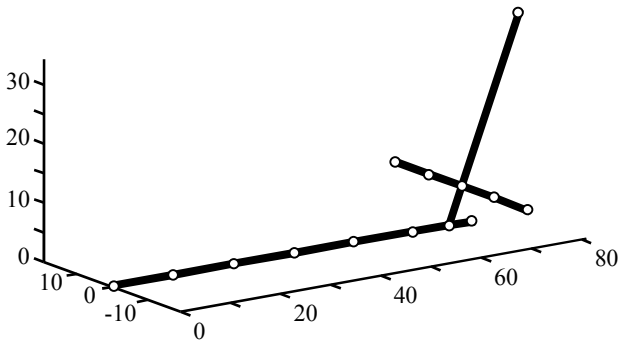

Figure 6.2: Scaled tailboom Beam Equivalent Model (BEM)

and inertial mass quantities. An iterative analytical procedure is conducted to search for model parameters that yield a scaled structure with natural frequencies matching the cantilevered ROM. Numerous design configurations are analyzed; unfortunately, a frequency matched design could not be achieved with practical and standard component sizes. Direct geometric scaling of component dimensions yields small component sizes that are not readily available. All of the trial designs were stiffer than the cantilevered ROM resulting in higher natural frequencies. Thus, an altered design approach is followed. Standard component dimensions are used and mode shape matching is attempted with less emphasis on natural frequency values. For the finalized scale model design, mode shape matching is achieved with much greater success. A comparison of the first two mode shapes of the final BEM design and the cantilevered ROM is displayed in *Figure 6.3*.

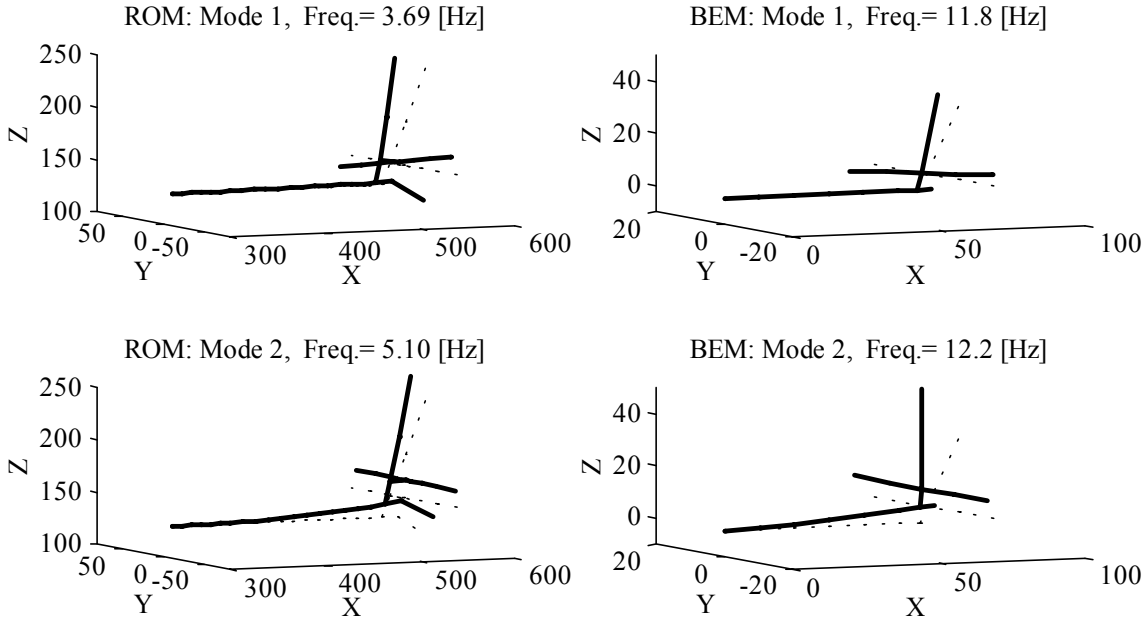

Figure 6.3: Cantilevered ROM and BEM mode shape comparison

Additional mode shape comparisons, up to mode eight, are listed in *Appendix D*. Cantilevered ROM natural frequencies and the resulting BEM natural frequencies are listed in *Table 6.1*.

Table 6.1: Cantilevered ROM and scaled BEM natural frequencies

Mode Number	ROM Natural Frequency [Hz]	BEM Natural Frequency [Hz]
1	3.69	11.85
2	5.10	12.22
3	9.49	23.87
4	10.65	26.60
5	19.16	38.31
6	24.05	48.78
7	28.52	54.49
8	31.65	72.08

The finalized tailboom structure design is used to purchase and fabricate the necessary components. In conjunction with the tailboom fabrication and assembly, a detailed finite element model is created for further analysis and design of the actuator installation. The detailed tailboom Finite Element Model (FEM) is comprised of beam elements, membrane elements, rod elements, and discrete spring elements. The model, shown in *Figure 6.4,* contains 120 nodes and 267 elements with a total global degree-of-freedom of 536. A custom MATLAB computer code was written to create the FEM, and a listing of the source code is contained in *Appendix D*. Static deflections and natural frequency predictions of the custom MATLAB code were verified with a commercial finite element package. Natural frequency and mode shape predictions of the FEM are

presented in later sections. The detailed FEM is utilized to design and evaluate actuator configurations that produce the desired control action within the tailboom structure.

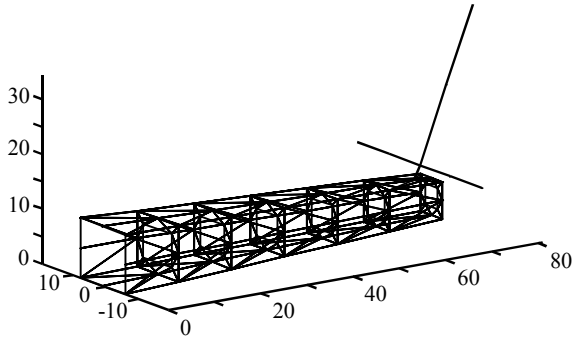

Figure 6.4: Scaled tailboom Finite Element Model (FEM)

6.3 Experimental Setup

The assembled tailboom structure is coupled with other testing hardware to create an experimental testing apparatus for vibration control studies and comparison with analytical model predictions. A diagram and photograph of the tailboom model and experimental setup are shown in *Figure 6.5*. The tailboom model is cantilevered at the root end from a rigid base structure. An electromechanical shaker is attached

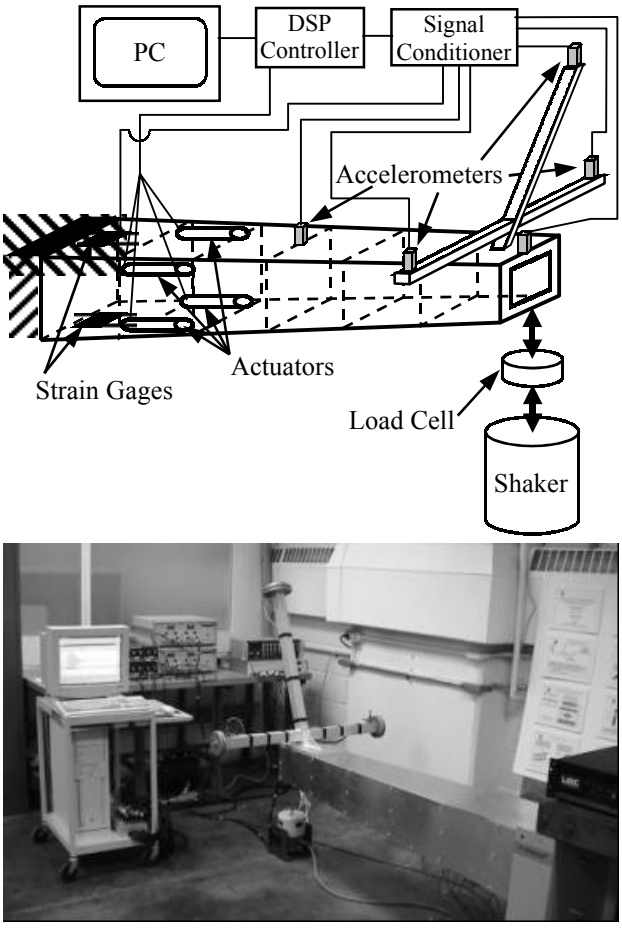

Figure 6.5: Tailboom model and experimental setup

to the tail end to excite the tailboom, and the shaker inputs are monitored with a piezoelectric load cell. Twelve accelerometers are installed on the tailboom to measure vibration levels. Four piezoelectric stack actuators are installed at the corner stringers between the second and third frames of the tailboom. A load cell is installed in series with the stack actuator to monitor the loads generated by the actuators. Twenty strain gages are installed on the corner stringers near the actuator installation to monitor the dynamic strains of the structure. All sensor signals are channeled to a signal-conditioning unit, then to a digital signal processor, and forwarded to a desktop PC for data collection. An equipment list for the experimental setup is detailed in *Appendix D*.

6.4 Actuation Design and Installation

6.4.1 Actuation Concept

A case study is formulated to investigate the actuation design and realization issues associated with integrating dual-point actuation into a semi-monocoque structure. A straightforward vibration control scenario is devised. The vibration control objective is to design a dual-point actuator configuration that will counteract the vibrations caused by a vertical load applied to the end of the tailboom structure. The actuation concept is to introduce a bending moment within the tailboom structure near the cantilevered end. This study is also formulated to evaluate piezoelectric stack actuators for realizing the actuation concept; thus, four stack actuators are installed near the root end of the tailboom model. The bending moment is realized by placing two actuators in the upper

left and right of the tailboom structure and placing two actuators in the lower left and right of the tailboom cross-section. A bending moment is created by commanding the top actuators out-of-phase with the bottom actuators.

6.4.2 Predicted Actuation Parameters

The dual point actuation concept, described above, is examined with the tailboom FE analysis model in order to select a commercial stack actuator. Actuator selection is based upon the static tail deflection produced by actuation. To establish a target tail deflection, bending moment actuation is applied to the cantilevered ROM. The resulting tail deflection is scaled for tailboom FE model analysis. Actuation is applied to the tailboom FE model to determine the appropriate actuator forces, which replicate the scaled tail deflection.

Examination of the optimization results, presented in Chapter 4, reveals that some distributed actuation configurations contained moment actuation in the tail section. One particular configuration, emphasizing both vibration and control effort reduction, contained Actuation Unit number 107. This AU produces bending moment actuation and is located near ROM node 62, which is the node selected for tailboom model scaling. Optimal control law computations for this distributed configuration indicates that a 23,200 in-lb moment is required by AU 107. The 23,200 in-lb moment is applied at nodes 69 and 70 of the cantilevered ROM to compute the static deflection at the end of the tail section. The computed tail deflection is 3.95×10^{-3} inches, which scales to 1.2×10^{-3} inches

by applying the 0.304 geometric scale factor. Next, actuation loads are applied at the corner stringers between frames 2 and 3 of the scaled tailboom FE model. The actuation loads are configured to mimic dual-point actuation with each actuator replacing the four corner stringer sections between frames 2 and 3. Loads are applied to simulate actuator expansion at the top and actuator contraction at the bottom of the tailboom section. Thus, the net result is a bending moment producing downward deflection of the tail end. Analysis results indicate that a 57-pound actuation force is required to produce the $1.2x10^{-3}$ inch scaled tail deflection. In conjunction with the computed actuator force, a $1.1x10^{-3}$ inch actuator stroke is predicted to produce the tail deflection.

6.4.3 Actuator Selection

A commercially available piezoelectric stack actuator is selected based upon the computed actuator force, actuator stroke, and the local structural stiffness that each actuator is working against. A photograph of the selected piezoelectric stack actuator is displayed in *Figure 6.6*, and the specifications are listed in *Table 6.2*.

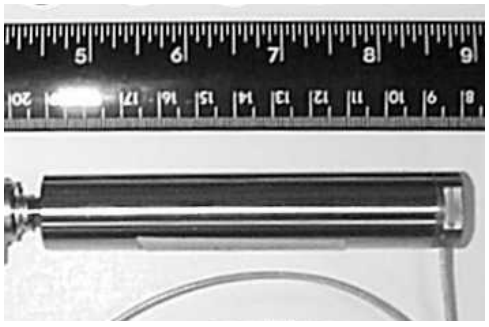

Figure 6.6: APC Pst 150/14/100 piezoelectric stack actuator

Table 6.2: Stack actuator specifications

Manufacturer	American Piezo Ceramics
Model	Pst 150/14/100
Blocked Force	1102 lb.
Free Stroke	$3.94x10^{-3}$ in.
Stiffness	$2.28x10^{5}$ lb/in
Input Voltage	0 volt to +150 volt
Weight	0.386 lb_f

Piezoelectric stack actuators directly transform input electrical energy into output mechanical energy through the principle of piezoelectricity. The Lead Zirconate Titanate (PZT) stack consists of many thin layers of electroactive material alternatively connected to positive and negative terminals of a voltage source (*Figure 6.7*). When an electrical voltage is applied, each PZT material layer expands and produces a net output displacement. The one-dimensional constitutive equations of linear piezoelectricity for a freestanding PZT stack describe the relation between mechanical and electrical variables [51].

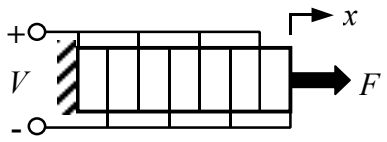

Figure 6.7: Piezoelectric stack element

$$S_3 = s_{33}^E T_3 + d_{33} E_3 \qquad (6.1)$$

$$D_3 = d_{33} T_3 + \varepsilon_3^T E_3 \qquad (6.2)$$

Where S_3 is the mechanical strain, T_3 is the mechanical stress, s_{33}^E is the mechanical compliance of the PZT material, E_3 is the applied electric field, D_3 is the electrical displacement, ε_3^T is the dielectric permittivity, and d_{33} is the piezoelectric coupling coefficient between mechanical and electrical variables. For a PZT stack, equation (6.1) can be rewritten as:

$$\frac{x}{nt} = s_{33}^E \frac{F}{A} + d_{33} \frac{V}{t} \qquad (6.3)$$

where x is the stack displacement, n is the number of material layers, t is the layer thickness, F is the applied external force, A is the stack cross-sectional area, and V is the

input voltage. Stack actuators typically have an internal mechanical preload spring (K_{sp}) in parallel with the stack element. The linear relationship between actuator displacement, actuator force, input voltage, and internal spring stiffness can be arranged into a convenient form:

$$F = K_a\, x - F_{ind} \qquad (6.4)$$

$$K_a = \frac{A}{n\, t\, s_{33}^E} + K_{sp} \qquad (6.5)$$

$$F_{ind} = \frac{A\, d_{33}}{t\, s_{33}^E} V \qquad (6.6)$$

where K_a is the actuator stiffness and F_{ind} is the piezoelectric induced force of the stack. When an electric voltage is applied to the stack, in the absence of an external force, the resulting actuator displacement is termed the characteristic free stroke (x_o). The characteristic blocked force (F_b), the force generated by the actuator when the net displacement is zero, is equivalent to the external force required to return the free stroke displacement back to the original actuator length.

$$x_o = F_{ind} / K_a \qquad \text{(Free stroke)} \qquad (6.7)$$

$$F_b = -F_{ind} \qquad \text{(Blocked force)} \qquad (6.8)$$

The internal mechanical energy of a piezoelectric stack actuator is equivalent to the work done by the piezoelectric induced force to overcome the internal stiffness and produce the free stroke displacement [51].

$$W_a = \frac{1}{2} K_a x_o^2 = \frac{1}{2} F_b x_o \qquad (6.9)$$

In practice, a stack actuator operates against an external load (F_e) with an external stiffness (K_e). When operating against an external load, the output displacement of the stack actuator is a fraction of the actuator's free stroke displacement (x_o) and is dependent upon the external stiffness.

$$x = \frac{K_a}{K_a + K_e} x_o = \frac{F_e}{K_e} \qquad (6.10)$$

The output energy of the actuator is equivalent to the work done on the external load, which is a fraction of the internal mechanical energy, and can be expressed as [51]:

$$W_e = \frac{1}{2} F_e x = \frac{1}{2} K_e x^2 = \left[\frac{K_e K_a}{(K_e + K_a)^2} \right] \left[\frac{1}{2} K_a x_o^2 \right] \qquad (6.11)$$

The stack actuator output energy is dependent upon the external stiffness and can be maximized when K_e equals K_a. This is known as the stiffness (impedance) matching principle [51]. The maximum output energy of a stack actuator is defined as one quarter of the internal mechanical energy (W_a) or can be expressed as one eighth of the blocked force times the free stroke.

$$W_e^{\max} = \frac{1}{4} W_a = \frac{1}{8} K_a x_o^2 = \frac{1}{8} F_b x_o = \frac{1}{8} \frac{F_{ind}^2}{K_a} \qquad (6.12)$$

Selecting an appropriate piezoelectric stack actuator is done by using the above actuator relations, the actuator specifications, and a graphical technique. Four lines are

plotted on two axes of actuator force versus actuator displacement. Two lines are constructed that represent the characteristic linear force and displacement relationship of the actuator. One line is plotted using the actuator free stroke and blocked force corresponding to the maximum voltage input. A second line, parallel to the first, is plotted for a voltage input equal to one-half the maximum. The third line is constructed to represent the stiffness of the stack actuator, and the fourth line represents the stiffness of the external structure upon which the actuator is operating. Such a graphical representation is displayed in *Figure 6.8* for the scaled tailboom structure and the stack actuator selected for this study.

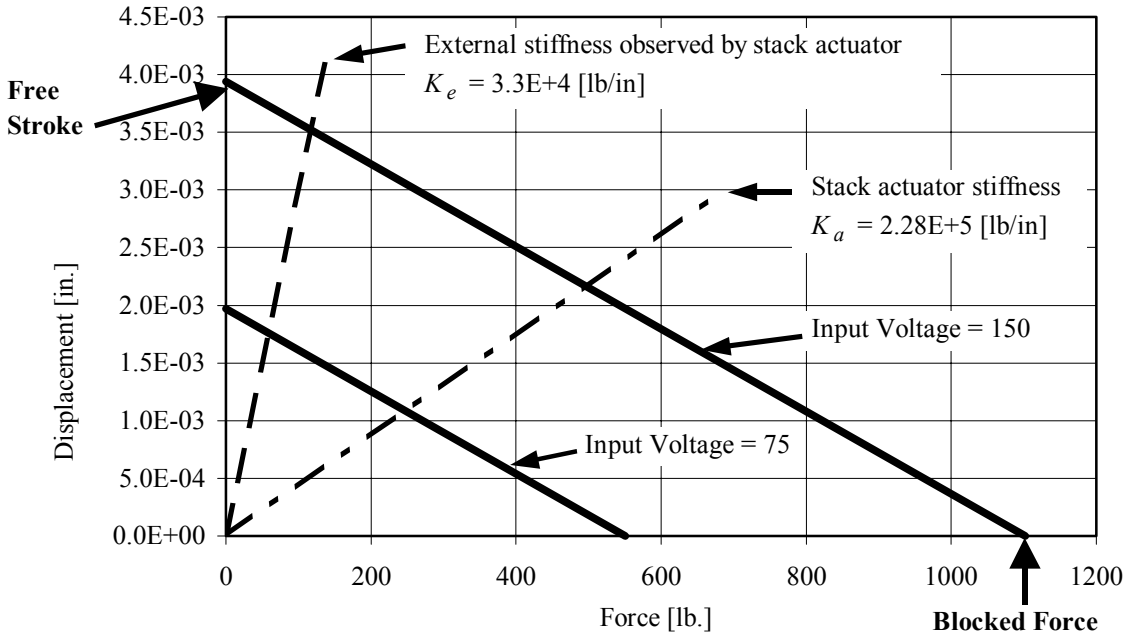

Figure 6.8: Stack actuator force and displacement relation

The actuator operating conditions can be extracted from *Figure 6.8* and are governed by the external structure stiffness and the characteristic stack actuator force and displacement relation. To illustrate the graphical analysis technique, a portion of *Figure 6.8* is reconstructed and displayed in *Figure 6.9.* The operational actuator force amplitude and corresponding stroke amplitude are identified from the intersection (points **A** and **B**) of the external stiffness line and the two characteristic actuator force and displacement lines. For the tailboom application, the actuator input voltage is varied about a positive DC bias of 75 volt; therefore, the maximum input variation is ±75 volt. Thus, the maximum achievable actuator force variation is the change in force between points **A** and **B** on the chart. The corresponding actuator stroke variation is identified by the change in displacement between points **A** and **B** or equivalently between points **A** and **C**.

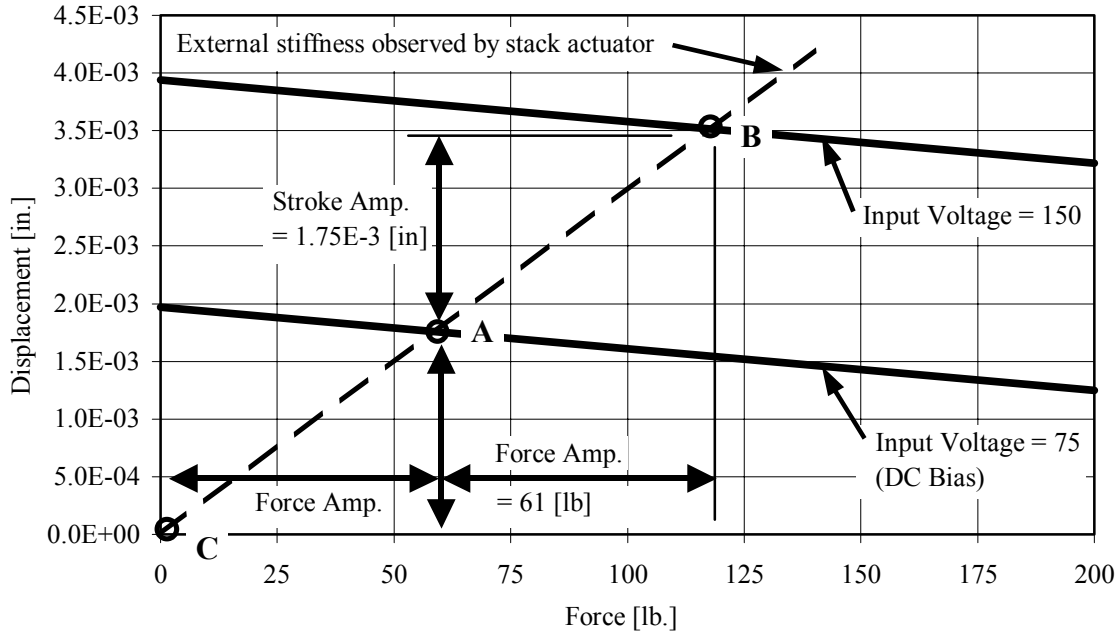

Figure 6.9: Stack actuator operating conditions

For the selected piezoelectric stack actuator, the predicted force amplitude is 61 pounds and the predicted stroke amplitude is 1.75×10^{-3} inches. Both values exceed the 57-pound force and 1.1×10^{-3} inch actuator stroke required to produce the target static tailboom deflection. Thus, the selected actuator has adequate output characteristics for the prescribed tailboom application. It is worth noting that a more efficient stack actuator would be stiffness matched with the external structure ($K_a = K_e$). A stiffness-matched actuator maximizes the actuator output energy and would transfer maximum energy to the tailboom structure. Stack actuator stiffness can be tailored by changing the stack length or changing the cross-sectional area. However, a stiffness-matched actuator that meets all performance specifications would most likely have to be custom manufactured.

6.4.4 Stack Actuator Installation

A photograph of the actuator installation is shown in *Figure 6.10*. The corner stringers between the second and third frame sections are removed and replaced with an actuator assembly. The top and bottom actuators, on each side, are attached to aluminum C-channels at each end of the actuator. One end of each actuator is bolted to the C-channel with a set of spherical washers to accommodate misalignment. The opposite end of each actuator is fastened to the C-channel through a spherical ball joint to prevent the transmission of moments between the actuator and the tailboom structure. This type of actuator connection is required for piezoelectric stack type actuators to protect the brittle piezoelectric material within the actuator. Force transducers are installed in series with

two of the actuators on opposite corners to monitor actuator loads. The stack actuator assembly and the attachment hardware are illustrated in more detail with photos displayed in *Figure 6.11*.

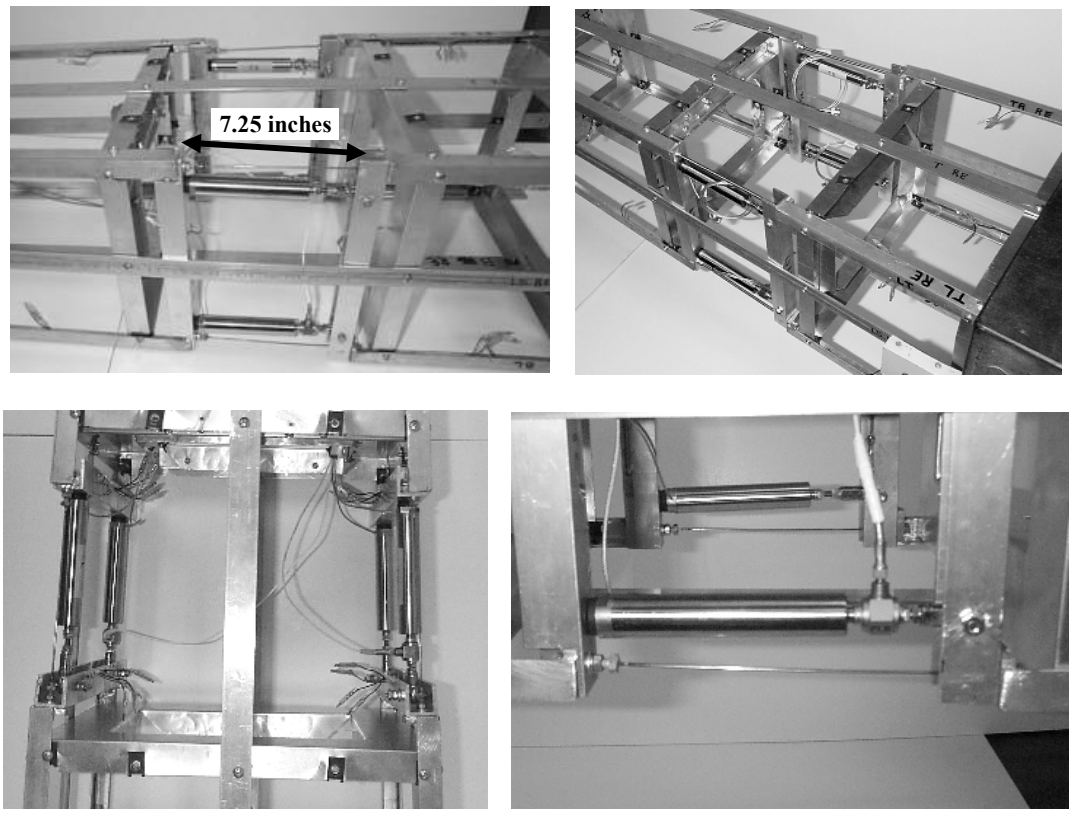

Figure 6.10: Piezoelectric stack actuator installation

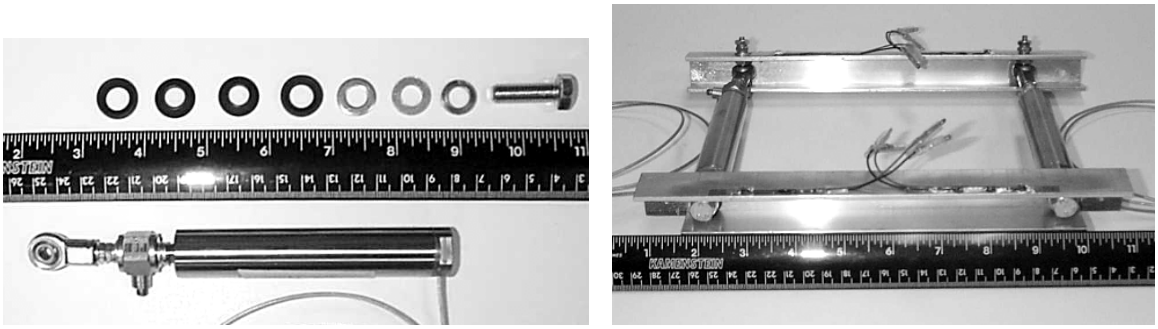

Figure 6.11: Stack actuator attachment and installation hardware

A thin steel rod is placed in parallel with and close to each actuator. The parallel steel rod serves two purposes: a device to preload the stack actuator assembly, and a mechanism to tailor the stiffness of the actuator assembly. One engineering challenge associated with using stack actuators is their one-directional force generating nature. Stack actuators are primarily pushing devices. Their ability to push against external loads is typically 7 times greater than the pulling force that can be generated. To minimize the effects of this limitation, actuators in the tailboom installation are pre-compressed by the surrounding tailboom structure. The stack actuators are installed through an access panel after the tailboom is completely assembled. A spreading tool is used to expand the opening between actuator attachment C-channels, then the actuator is installed and the spreading tool released. In addition, the actuators are operated with a DC bias input voltage that causes the stack to expand to a median length and introduce additional pre-stress. The actuators are pre-stressed by the tailboom structure, and vice versa, the tailboom structure is pre-stressed by the actuators. When the stack input voltage is decreased, the actuator length contracts and the tailboom structure elastically springs back. Therefore, the stack actuator's poor pulling ability is assisted by the structural pre-load.

6.5 Static Deflection Analysis

Both tailboom analytical models are utilized to examine static deflections and compare with experimentally measured data from the physical tailboom structure. One test case is determining the static deflection of the tailboom to a load applied at the free

end of the tailboom. Loads are applied with the electromagnetic shaker and displacements are measured with a linear potentiometer. Initial predictions of the analytical models did not correlate well with the experimental data and required adjustment of the model boundary condition. Initially, the cantilevered boundary condition was modeled as a fully constrained support and deflections were under-predicted. The boundary condition was altered to incorporate elasticity of the tailboom mounting and the pedestal base structure. A discrete spring element was added to the analytical models to account for flexibility at the mounting location. The added spring element stiffness had a negligible effect on the analytical model's natural frequency predictions, but the modeling adjustment greatly improved the static deflection predictions. A summary of the results is displayed in *Table 6.3*. Excellent agreement between the analytical models and the physical tailboom structure is achieved. In addition, the experimental data indicates the static deflection of the tailboom structure is linear.

Table 6.3: Static deflection at free end of tailboom

Applied Load [lb.]	BEM Model [in.]	FEM Model [in.]	Physical Model [in.]
10.7	0.0055	0.0056	0.0052
14.8	0.0076	0.0077	0.0075
18.9	0.0098	0.0098	0.0096

Another test case is formulated to examine the static deflection induced by the actuator installation. The top actuators are commanded to expand and the bottom

actuators are commanded to contract; thus, a bending moment is created and the free end of the tailboom deflects downward. Displacement at the free end and actuator stroke is measured with a linear displacement potentiometer. A summary of the results is displayed in *Table 6.4*. Fair agreement of the tailboom end deflection trend is observed; however, the measured actuator stroke is nearly twice the FEM predicted value. The results indicate the FEM is not accurately modeling the compliance of the actuator installation.

Table 6.4: Actuator induced static deflection of tailboom free end

Stack Actuator Force [lb.]	FEM Model End Disp. [in.]	FEM Model Actuator Stroke [in.]	Physical Model End Disp. [in.]	Physical Model Actuator Stroke [in.]
42.1	0.00099	0.0008	0.00078	0.0014
52.9	0.00124	0.0010	0.00140	0.0018
63.9	0.00150	0.0012	0.00166	0.0020

6.6 Dynamic Analysis and Vibration Control

The fundamental structural dynamics of the tailboom are determined through an experimental modal analysis to determine its natural frequencies and mode shapes. Natural frequencies and mode shapes are also computed for the analytical models. Listed in *Table 6.5* are the first eight natural frequencies of the analytical models and the physical tailboom structure. Natural frequencies computed from the analytical models are in good agreement with the experimentally measured values. The natural frequency

predictions of the analytical models are within 15% of the experimentally measured values. Five of the eight analytical predictions are within 5% of the measured values. Although not shown here, fair mode shape correlation is also observed between the analytical models and the tailboom structure. Mode shape plots are listed in *Appendix D*.

Table 6.5: Tailboom natural frequencies

Mode Number	BEM Model [Hz]	FEM Model [Hz]	Physical Model [Hz]
1	11.9	11.9	11.7
2	12.2	13.5	14.0
3	23.9	24.1	25.1
4	26.6	29.6	26.8
5	38.3	38.2	38.6
6	48.8	39.8	46.8
7	54.5	55.2	55.4
8	72.1	72.2	71.5

Helicopter airframes are designed to avoid resonance situations; specifically, the airframe is designed such that natural frequencies do not coincide with harmonics of the *N*/rev main rotor frequency. The installation of an active vibration control system must adhere to the same principle. In other words, the actuator installation should not shift the airframe natural frequencies to coincide with the *N*/rev harmonics. Design of the piezoelectric stack actuator installation in the tailboom structure is conducted following this principle. The detailed finite element model of the tailboom is utilized to design and

analyze an actuator installation that does not significantly alter the structure's natural frequencies. Successful design of the actuator installation is accomplished. The combined stiffness of the stack actuator and the pre-stress rod is designed to be nearly equivalent to the stiffness of the removed corner stringer segment. The added mass of the actuator installation had a negligible effect; even though, the added mass (0.814 lb_m) is 6.6 times larger than the removed corner stringer mass (0.123 lb_m). Listed in *Table 6.6* are the experimentally measured natural frequencies of the baseline tailboom, before the actuator installation, and the natural frequencies measured after installation of the actuators. The actuator installation had a negligible effect on the structure's natural frequencies. The largest shift of natural frequency is 6% for mode four.

Vibration control authority of the piezoelectric stack actuator installation is investigated. The design intent of the actuator installation is to produce a bending moment within the tailboom structure that counters vertical inputs at the free end. Actuator induced vibration of the tailboom is examined both analytically with the FEM model and experimentally with the tailboom structure. The tailboom FEM model is used to compute the frequency response transfer

Table 6.6: Tailboom natural frequencies before and after actuator installation

Mode Number	Before Actuator Installation [Hz]	After Actuator Installation [Hz]
1	11.5	11.7
2	14.0	14.0
3	25.5	25.1
4	28.5	26.8
5	39.0	38.6
6	47.0	46.8
7	55.5	55.4
8	72.5	71.5

function between the stack actuator inputs and the resulting vibration response. Displayed in *Figure 6.12* is the transfer function for the vertical vibration response at the top of the vertical tail, which is produced by a unit actuator force. The largest vibration levels, produced by the actuator installation, occur at three frequencies (13.5, 24.1, 72.2 Hz), which are commensurate with the natural frequencies of the second, third, and eighth vibration modes of the tailboom structure. In other words, vibrations at or very near these frequencies can be most effectively controlled by the actuator installation.

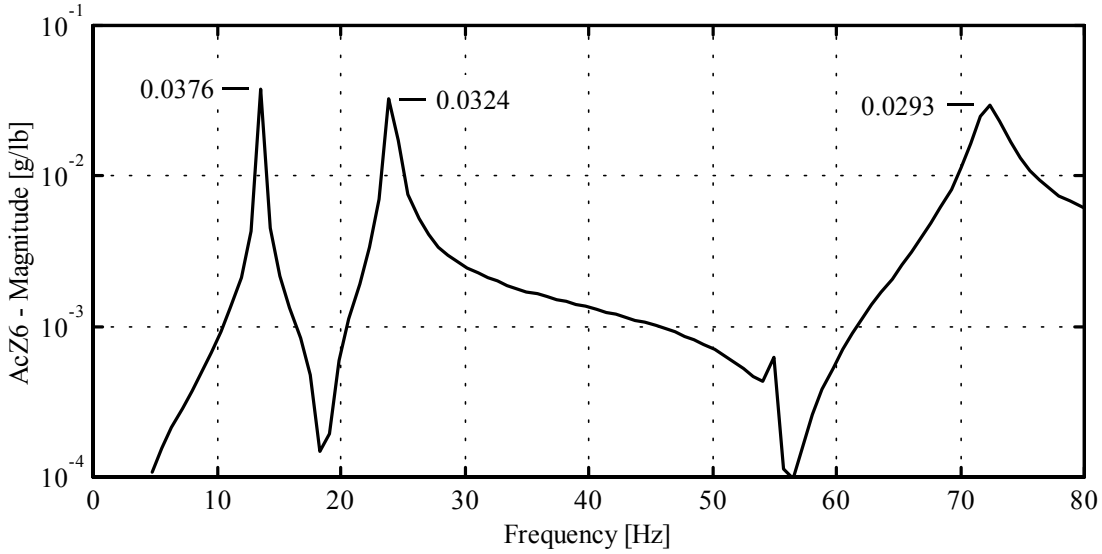

Figure 6.12: FEM analytical transfer function between actuator inputs and vertical response at tip of vertical tail

Transfer functions between the actuators and the twelve accelerometer sensors are computed from experimental data. A sine sweep method is used to collect the necessary vibration response data over the 10 Hz to 80 Hz frequency range. The actuators are commanded at a specific sinusoidal frequency to produce a bending moment and excite the tailboom structure. After the vibrations reach a steady state level, the accelerometer

signals are captured for a short time period. The data capture process is repeated multiple times at numerous frequencies in the 10 to 80 Hz range. The experimental data is post-processed to compute the transfer function, which is defined as the ratio of measured acceleration amplitude to the measured actuator force amplitude. An experimentally determined transfer function for the vertical tail vibration is displayed in *Figure 6.13.* The largest vibration levels, produced by the actuator installation, occur at three frequencies (14, 25.1, 71.5 Hz), which correspond to experimentally determined natural frequencies. The overall shape of the transfer function and the peak values are comparable to FEM analysis transfer function (*Figure 6.12*).

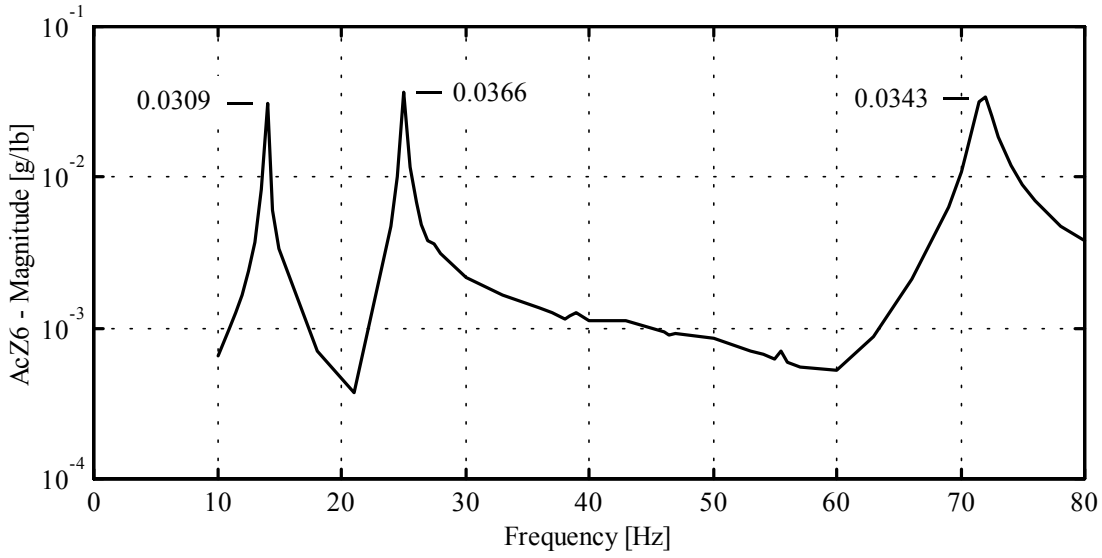

Figure 6.13: Experimental transfer function between actuator inputs and vertical response at tip of vertical tail

Vibrations at or very near the peak value frequencies can be most effectively controlled by the actuator installation. To illustrate a specific example consider actuator inputs at a 14 Hz frequency, the maximum force output of the actuator is 64 pounds; therefore, the maximum actuator induced vibration would be 1.98 g (0.0309 * 64). Thus, electromagnetic shaker inputs at 14 Hz, which produce 1.98 g at the vertical tail, can be suppressed by the stack actuator installation. The transfer function can be used similarly to assess the control authority of the actuator installation at other excitation frequencies.

To demonstrate the vibration control ability of the actuator installation, a test case is formulated. First, the tailboom model is excited at 14 Hz by the electromagnetic shaker to produce 0.6 g of vibration at the vertical tail. The shaker-induced vibration is then cancelled by the actuator induced bending moment. For demonstration safety purposes, the shaker input is chosen to be conservative; however, the actuator installation is able to suppress 1.98 g vibration levels.

A time history plot of the vibration control test is shown in *Figure 6.14*. Initially the vibration amplitude is 0.6 g, and the vibration amplitude quickly decays below 0.1 g after the actuators are activated.

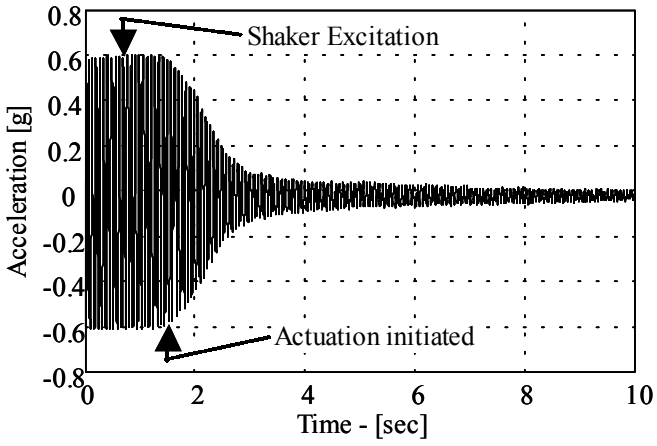

Figure 6.14: Tailboom active vibration control demonstration

Dynamic strain and stress in the vicinity of the actuator installation is examined to determine the effect of the actuator installation on the structure stresses. The tailboom is instrumented with strain gages on the four corner stringers and the actuator attachment frames. On the stringers, strain gages are installed near the root end and near both ends of the stack actuator. Strain gages are also installed on the actuator attachment frames near the point of actuator attachment. Dynamics strains are measured on the baseline tailboom structure, before the actuator installation, and after the actuators are installed. Three vibration scenarios are formulated and examined for comparison. On the baseline structure, dynamic strains are measured when the tailboom is excited by the electromagnetic shaker. The shaker input is commanded at 14 Hz, to excite the first vertical bending mode, and produce 1.0 g of vibration at the free end of the tailboom vertical stabilizer. It is worth noting that the tailboom response is linear, and the following results can be scaled with respect to initial vibration level. After the actuators are installed, the tailboom is again excited by the shaker, and strain data is collected. The third case studied is a vibration cancellation scenario, where the piezoelectric stack actuators are commanded to produce a bending moment that cancels the tailboom vibration caused by the electromagnetic shaker input. Dynamic stress values are computed from the experimentally measured strain data collected for each case study. A comparison of the dynamic stress results is illustrated in *Figure 6.15*. In the corner stringers, a measurable reduction of stress is observed after installation of the actuators. Substantial stress reductions in the corner stringers are evident when comparing case two and case three.

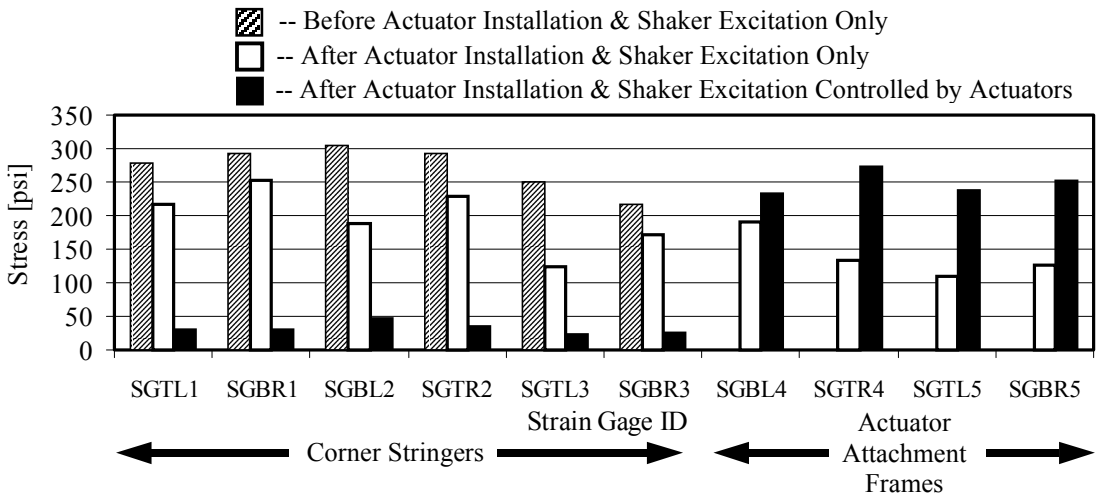

Figure 6.15: Comparison of tailboom dynamic stress levels, before and after actuator installation

These stress reductions are expected since the vibration and tailboom motion are being reduced by the actuator actions. However, stress levels in the actuator attachment frames are nearly doubled for the vibration cancellation scenario. The increase of stress in the attachment frames is however not detrimental, because the stress levels remain well below the endurance limit of 9000 psi for aluminum materials [47].

6.7 Summary and Conclusion

An analytical and experimental investigation is conducted on a scaled model of a helicopter tailboom. The scaled tailboom model is used to study the actuation design and realization issues associated with integrating dual-point actuation into a semi-monocoque airframe structure. Excellent correlation of static deflection and dynamic response is observed between the analytical tailboom model predictions and the experimental data. A

piezoelectric stack actuator configuration is designed and installed on the tailboom model. Successful design of the actuator installation is accomplished without altering the natural frequencies of the tailboom structure. Fair correlation of the frequency response transfer functions is observed between the analytical FEM model prediction and the experimentally determined transfer function. Experimental tests indicate the stack actuator configuration is able to produce a bending moment and suppress vibration induced by external shaker loads. The actuator installation does not significantly alter the uncontrolled dynamic stresses of the tailboom structure. In other words, vibration suppression is achieved without creating excessive stress in the structure near the actuator installation.

Chapter 7

CONCLUSION AND FUTURE RESEARCH

7.1 Thesis Summary and Conclusions

Reducing helicopter airframe vibrations has numerous payoffs with regard to passenger comfort, weapons sighting, structural fatigue, production costs, and maintenance costs. Airframe vibrations are caused by several important excitation sources; however, the dominant sources are the *N*/rev main rotor hub forces and moments. Historically, helicopter vibrations have been addressed with passive control methods, and considerable progress has been made in designing rotorcraft with lower vibration levels. However, vibration specifications continue to be ever more stringent, and there are continued efforts to strive for more effective vibration control measures. Therefore, active vibration control methods are receiving considerable attention and study. An extensive literature search on helicopter active vibration control methods was conducted. Helicopter active vibration control can be broadly categorized as either rotor-based or airframe-based. Rotor-based systems apply control actions in the main rotor system, and control actions of the airframe-based systems are applied within the helicopter airframe structure. Rotor-based active control methods reduce the oscillatory hub loads, but may not be capable or efficient at controlling excitations that do not enter the airframe through the main rotor hub. Until all problematic excitation sources are

eliminated, some type of airframe-based control system is required to meet more stringent vibration specifications.

One of the more promising airframe-based active control approaches is commonly referred to as Active Control of Structural Response (ACSR). In general terms, an ACSR system consists of airframe mounted sensors, a control computer, and a set of force actuators mounted on the airframe. Vibration control is achieved by the superposition of an actuator-induced airframe response with the response caused by external loads. Numerous analytical and experimental studies have been conducted on variations of the ACSR control approach. Study and flight-testing of airframe-based approaches have demonstrated significant vibration suppression and enough promise to begin appearing on production rotorcraft. Limitations of the current airframe-based active control approaches were identified from the literature search materials. Actuator placement, in the airframe-based systems, is based largely upon engineering experience and limitations imposed by retrofitting an existing airframe structure. Some researchers have concluded that actuator locations, different from their selected locations, may yield a more effective active vibration control system. They also concluded that a larger number of small actuators may be more effective than a fewer number of large actuator devices. Thus, smaller actuators could be placed at more locations in the airframe and avoid the unfortunate circumstance of placing all actuators near modal nodes. The helicopter airframe is a complex structure, and it has a complex dynamic response; therefore, determining the best actuator locations is not a simple task. Distributing actuators at optimal locations in

the airframe needs to be studied to investigate feasibility and examine the potential for improving vibration suppression.

A literature review has been conducted on actuator placement techniques. Numerous approaches have been formulated to determine actuator locations for the active control of flexible structures. The actuator placement problem is typically solved by an optimization technique to maximize or minimize a cost function. The optimization problem has been solved with gradient-based techniques and non-gradient techniques. Various performance metrics have been formulated for the optimization cost function, such as; metrics based on the entries of the actuator influence matrix, metrics formed from the controllability grammian, metrics to maximize the energy dissipation, and metrics to minimize the system energy. A formal optimization procedure for actuator placement has not been applied to the helicopter for active structural control purposes. Therefore, a need exists to formulate an optimization procedure for the unique features of actuator placement in rotorcraft active vibration control. The majority of present day helicopter airframes are of semi-monocoque construction; therefore, actuator placement within an airframe is most likely relegated to a finite number of distinct locations. Unlike simple continuous beam or plate structures, the actuator placement in helicopter airframes is discrete in nature, and non-gradient optimization algorithms are well suited for the discrete actuator placement problem. In addition, the non-gradient approaches are less likely to converge to a local minimum solution. Helicopter vibration excitation is known to occur at discrete frequencies, rather than excitation over a broad frequency range.

Active control of specific structural modes has been attempted by other researchers; however, such an approach requires a priori knowledge of which modes are significant or which modes are to be controlled. Researchers have demonstrated the influence of control laws and performance objectives on the actuator placement problem; therefore, an optimization procedure for actuator placement in the helicopter airframe should incorporate a control law. Drawing on the knowledge acquired from previous researchers, an optimization procedure is formulated for the unique characteristics of helicopter airframe vibration control.

To overcome the limitations of present active control systems and advance the state-of-the-art, a new actuator placement and active structure design methodology is proposed and explored. The proposed methodology is termed the Optimally Distributed Actuation Realization Methodology (ODARM), which is versatile enough to be applied to any rotorcraft. ODARM is a four-part methodology that relies heavily on numerical computation, modeling, and analysis. The first step of ODARM is to create a detailed numerical finite element model of the helicopter airframe. The second step is to create a reduced order model of the airframe and apply an optimization procedure to determine actuation placement and control action. The optimization procedure is applied to the reduced order airframe model, and the results indicate the actuation locations, types of actuation, and the necessary control effort. In the third step of the ODARM, the detailed airframe finite element model is utilized for analysis and design. The third step is to use the optimization results for guidance, and design a detailed actuator configuration that

produces the desired control actions. The fourth and final step of the ODARM is to utilize the analytical knowledge acquired in the previous steps to install the hardware and realize the active vibration control system in the actual helicopter structure.

Two dynamic models of the helicopter airframe and an optimization procedure are utilized within the ODARM methodology. One of the dynamic models is a reduced order representation of the helicopter airframe. Airframe model reduction is an essential part of the ODARM methodology in order to reduce the optimization problem to a manageable size. Numerous model reduction techniques exist, however, one particular reduction method is recommended for the proposed design methodology. The recommended reduction procedure creates the mass and stiffness matrices of a reduced order elastic line model representation from the mass and stiffness matrices of a much larger finite element model of the helicopter airframe. The reduced mass and stiffness matrices are produced by separate static condensation routines. Unlike some other reduction techniques, this method retains a geometric relationship between the large finite element model and the reduced order model. Each node of the reduced order elastic line model geometrically corresponds to one node of the detailed finite element model. Thus, an actuator location in the reduced order model is easily translated to a geometric region in the larger finite element model.

An optimization procedure is developed to simultaneously determine the actuation type, the optimal actuation locations, and the optimal control action. The

proposed optimization method is a hybrid approach that couples a control law and an optimization routine for actuator placement. The selected control law is based on optimal control theory and is commonly used for rotorcraft active vibration control applications. The optimization procedure is formulated as a constrained minimization problem with a quadratic objective function. The optimization algorithm to be coupled with the control law is called Simulated Annealing. The Simulated Annealing algorithm is a probabilistic search technique to find a global minimizer. This algorithm is selected for the optimization procedure, because it is compatible with certain features of the design problem. The actuation locations are confined to discrete positions at reduced order model nodes; therefore, the design variables are discontinuous. Unlike gradient-based techniques, the Simulated Annealing algorithm is compatible with discrete design variables. In addition, our analysis revealed that the objective function contains multiple local minima. The Simulated Annealing routine is capable of escaping local minima and more likely to find a global minimum.

A new approach has been formulated to examine the feasibility and effectiveness of optimal actuation placement for active control of helicopter vibrations. A numerical study was performed, on a reduced order airframe model, comparing distributed actuation configurations to a representative state-of-the-art centralized actuation configuration. The following observations were made with regard to the investigation results. The optimally distributed actuation configurations are significantly more effective than centralized actuation. One case study shows the centralized actuation reduced vibration by 49%, but

the distributed configuration achieved a 96% vibration reduction with similar control effort. The optimization procedure can be tailored to emphasize both vibration and control effort reductions. In another case study, the distributed actuation configuration achieves a 90% reduction of vibration and requires 50% less control effort than the centralized configuration. The optimization procedure and a multi-objective function can be utilized to search for an actuation configuration that performs effectively for multiple excitation conditions. A case study demonstrated that the multi-objective optimized actuation configuration outperforms the centralized configuration for each excitation condition. The optimization procedure can be applied to determine the minimum number of actuation locations for adequate vibration suppression. In the scenario studied, it is found that four optimally distributed actuation locations are more effective than centralized configuration. The four distributed configuration achieves 10% more vibration reduction and requires 41% less control effort relative to the centralized configuration.

Vibration and distributed actuation analysis was conducted with a large NASTRAN finite element model of the helicopter airframe. Distributed actuation control and centralized actuation control were applied to the NASTRAN airframe model. Distributed control predicted a 73% vibration reduction and required 50% less control effort than centralized actuation. When compared to the reduced order model analysis, the disparity between centralized control and distributed control was not as pronounced with the NASTRAN model analysis. However, distributed actuation control is still

superior to centralized control, producing greater vibration suppression with less control effort. Dynamic stresses of the NASTRAN airframe model were examined for both the uncontrolled and controlled vibration conditions. For a controlled vibration condition, the majority of the element stresses were reduced. Dynamic stress levels in more of the finite elements are reduced by the distributed control, 82% versus 68% for the centralized control. It was observed that the largest dynamic stresses were not always near the location of external or actuation applied loads. Thus, stress levels need to be examined in all regions of the airframe.

An analytical and experimental investigation was conducted on a scaled model of a helicopter tailboom. The scaled tailboom model was used to study the actuation design and realization issues associated with integrating dual-point actuation into a semi-monocoque airframe structure. Excellent correlation of static deflection and dynamic response was observed between the analytical tailboom model predictions and the experimental data. A piezoelectric stack actuator configuration was designed and installed on the tailboom model. Successful design of the actuator installation was accomplished without altering the natural frequencies of the tailboom structure. Experimental results indicate the stack actuator configuration is able to produce a bending moment to suppress vibration induced by external shaker loads at the tailboom end. The actuator installation did not significantly alter the uncontrolled dynamic stresses of the tailboom structure. In other words, vibration suppression is achieved without creating excessive localized stress in the structure.

7.2 Future Research Recommendations

A comprehensive research project has been conducted and many findings have been discovered with respect to distributed actuation to control helicopter vibrations. Although the project was executed with specific objectives and many inquiries were addressed, new research issues arose during the course of the project. Some of the new issues are beyond the scope of this research program or could not be investigated due to the time constraints associated with a finite project length. Continuing research programs can be formulated to address many related topics; however, the following topics are recommended in order to make significant contributions to rotorcraft active vibration control.

Distributed actuation applied to the NASTRAN FE model was restricted to one dual-point actuation concept (*Figure 5.6*). Control forces are applied at the intersection of stringers and adjacent frame members of the airframe structure. The dual-point actuation concept can be commanded to produce a net force or bending moment within the localized structure. Another research topic worthy of investigation is to formulate and examine other dual-point actuation concepts that mimic the control actions applied to the reduced order airframe model. For example, a new actuation concept illustrated in *Figure 7.1* could be the formulation of an active frame member to replace an existing passive frame member of the airframe. The active frame member would generate a force and displacement distribution around its perimeter. Forces would then be transferred to the stringers and skin, which are connected to both sides of the active frame member.

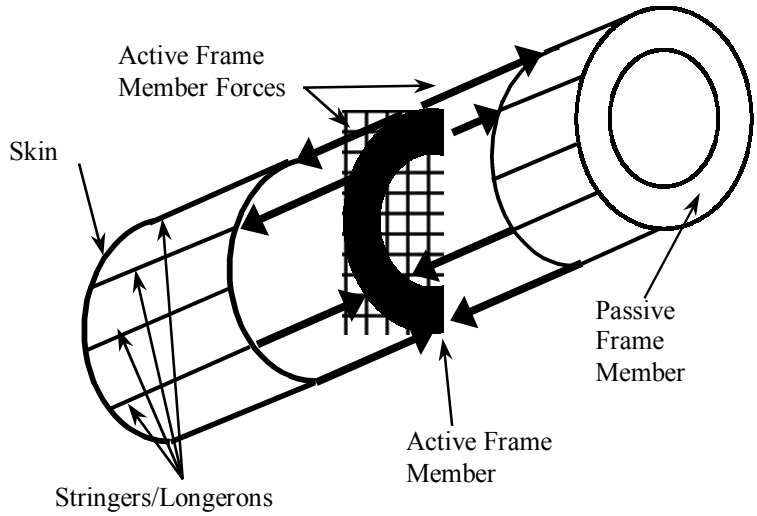

Figure 7.1: Active frame member actuation concept (future research)

Specific actuator devices were not selected or modeled in the present study to realize distributed actuation systems. The intent was to keep the analysis general and robust by not committing to a particular actuator device. In addition, actuator selection can be delayed until the later stages of the Optimally Distributed Actuation Realization Methodology. Thus, a future research topic could be an actuator selection and comparison study or an actuator design study for this specific application. Actuator types worth considering are hydraulic actuators, electro-mechanical, piezoelectric, or some hybrid combination.

A scaled tailboom structure, which incorporates conventional piezoelectric stack actuators, was fabricated for vibration control studies. Control authority of the actuator installation was limited by the one-directional (push only) nature of the commercial stack actuators. The actuator installation required structural preload, which added complexity

to the installation. A recommendation for future research is to install push-pull actuation devices in the tailboom structure and assess their control authority relative to the currently installed conventional stack actuators. Bi-directional push and pull actuators may eliminate the need for structural preload, which simplifies the actuator installation and may improve the actuation authority. One possible actuator recommended for consideration is a new piezoelectric stack actuator design developed by Heverly et al. [52] in a study independent of the research contained in this thesis. Their stack actuator design is a push-pull device, does not require preload, and produces greater output than a conventional piezoelectric stack actuator design. A detailed report on the new stack actuator design can be found in reference 52.

In the early stages of the research investigation, an engineering decision was made that restricted actuation to dual-point concepts for analysis and study. In light of the fact that dual-point actuation may require up to 6 actuator devices to realize an airframe bending moment, the weight penalty of single-point actuation may not be as dramatic as initially anticipated. Therefore, future research should revisit the distributed actuation optimization and incorporate single-point actuation concepts. It may be found that the optimal distribution may include both single-point and dual-point actuation. In addition, a penalty function, based on actuation device weight, could be formulated and added to the optimization objective function to distinguish between single-point and dual-point actuation.

BIBLIOGRAPHY

1. Loewy, R. G., "Helicopter Vibrations: A Technological Perspective," *Journal of the American Helicopter Society*, Vol. 29, No. 4, Oct. 1984, pp. 4-30.

2. Johnson, W., "Helicopter Theory," New York, Dover Publications, Inc., 1994, pp. 694-707.

3. Bielawa, R. L., "Rotary Wing Structural Dynamics and Aeroelasticity," Washington DC, American Institute of Aeronautics and Astronautics, AIAA Education Series, 1992, pp. 163-208.

4. Friedmann, P. P., and Millott, T. A., "Vibration Reduction in Rotorcraft Using Active Control: A Comparison of Various Approaches," *Proceedings of the 1994 American Helicopter Society Aeromechanics Specialists Conference*, San Francisco, CA, 1994, pp. 7.6-1 to 7.6-19.

5. Teal, R. S., McCorvey, D. L., and Malloy, D., "Active Vibration Suppression for the CH-47D," *Proceedings of the 53rd Annual Forum of the American Helicopter Society*, Virginia Beach, VA, 1997, pp. 211-219.

6. King, S. P., and Staple, A. E., "Minimization of Helicopter Vibration through Active Control of Structural Response," *Proceedings of AGARD Conference, Rotorcraft Design for Operations*, AGARD, 1986, (N88-1164903-05).

7. Staple, A. E., "Evaluation of Active Control of Structural Response as a Means of Reducing Helicopter Vibration," *Proceedings of the 46th Annual Forum of the American Helicopter Society*, Washington, DC, 1990, pp. 3-17.

8. Goodman, R. K., and Millott, T. A., "Design, Development, and Flight Testing of the Active Vibration Control System for the Sikorsky S-92," *Proceedings of the 56th Annual Forum of the American Helicopter Society*, Virginia Beach, VA, 2000, pp. 764-771.

9. Welsh, W. A., Von Hardenberg, P. C., Von Hardenberg, P. W., and Staple, A. E., "Test and Evaluation of Fuselage Vibration Utilizing Active Control of Structural Response (ACSR) Optimized to ADS-27," *Proceedings of the 46th Annual Forum of the American Helicopter Society*, Washington, DC, 1990, pp. 21-37.

10. Kvaternik, R., G., "The NASA/Industry Design Analysis Methods for Vibrations (DAMVIBS) Program – A Government Overview," *Proceedings of the*

AIAA/ASME/ASCE/AHS/ASC, 33rd Structures, Structural Dynamics, and Materials Conference, AIAA, Washington, DC, 1992, pp. 1103-1112 (AIAA 92-2200-CP).

11. Cronkhite, J., "The NASA/Industry Design Analysis Methods for Vibrations (DAMVIBS) Program – Bell Helicopter Textron Accomplishments," *Proceedings of the AIAA/ASME/ASCE/AHS/ASC, 33rd Structures, Structural Dynamics, and Materials Conference*, AIAA, Washington, DC, 1992, pp. 1113-1125 (AIAA 92-2201-CP).

12. Gabel, R., Lang, P., and Reed, D., "The NASA/Industry Design Analysis Methods for Vibrations (DAMVIBS) Program – Boeing Helicopters Airframe Finite Element Modeling," *Proceedings of the AIAA/ASME/ASCE/AHS/ASC, 33rd Structures, Structural Dynamics, and Materials Conference*, AIAA, Washington, DC, 1992, pp. 1126-1137 (AIAA 92-2202-CP).

13. Toossi, M., Weisenburger, R., and Hashemi-Kia, M., "The NASA/Industry Design Analysis Methods for Vibrations (DAMVIBS) Program – McDonnell Douglas Helicopter Company Achievements," *Proceedings of the AIAA/ASME/ASCE/AHS/ASC, 33rd Structures, Structural Dynamics, and Materials Conference*, AIAA, Washington, DC, 1992, pp. 1138-1148 (AIAA 92-2203-CP).

14. Twomey, W., "The NASA/Industry Design Analysis Methods for Vibrations (DAMVIBS) Program – Sikorsky Aircraft – Advances Toward Interacting With The Airframe Design Process," *Proceedings of the AIAA/ASME/ASCE/AHS/ASC, 33rd Structures, Structural Dynamics, and Materials Conference*, AIAA, Washington, DC, 1992, pp. 1149-1158 (AIAA 92-2204-CP).

15. Hashemi-kia, M. and Toossi, M., "Finite Element Model Reduction Application to Parametric Studies and Optimization of Rotorcraft Structures," *Proceedings of the 46th Annual Forum of the American Helicopter Society*, Washington, DC, 1990, pp. 139-154.

16. Chiu, T., and Friedmann, P. P., "A Coupled Helicopter Rotor/Fuselage Aeroelastic Response Model For ACSR," *Proceedings of the AIAA/ASME/ASCE/AHS/ASC, 36th Structures, Structural Dynamics, and Materials Conference*, AIAA, New Orleans, LA, 1995, pp. 574-600 (AIAA Paper 95-1226-CP).

17. Chiu, T., and Friedmann, P. P., "Vibration Suppression in Helicopter Rotor/Flexible Fuselage System Using the ACSR Approach With Disturbance

Rejection," *Proceedings of the 52nd Annual Forum of the American Helicopter Society*, Washington, DC, 1996, pp. 736-757.

18. Cribbs, R. C., and Friedmann, P. P., "Vibration Suppression in Helicopters Using The ACSR Approach With Improved Aerodynamic Modeling," *Proceedings of the AIAA/ASME/ASCE/AHS/ASC, 40th Structures, Structural Dynamics, and Materials Conference*, AIAA, St. Louis, MO, 1999, pp. 110-125 (AIAA Paper 99-1218).

19. Hanagud, S., and Babu, G. L., "Smart Structures in the Control of Airframe Vibrations," *Journal of the American Helicopter Society*, Vol. 39, No. 2, 1994, pp. 69-72.

20. Schrage, D. P., and Peskar, R. E., "Helicopter Vibration Requirements," *Proceedings of the 33rd Annual Forum of the American Helicopter Society*, Washington, DC, 1977, pp. 77.33-33-1 to 77.33-33-9.

21. Crews, S. T., "Rotorcraft Vibration Criteria, A New Perspective," *Proceedings of the 43rd Annual Forum of the American Helicopter Society*, St Louis, MO, 1987, pp. 991-998.

22. Welsh, W., Fredrickson, C., and Rauch, C., "Flight Test of an Active Vibration Control System on the UH-60 Black Hawk Helicopter," *Proceedings of the 51st Annual Forum of the American Helicopter Society*, Fort Worth, TX, 1995, pp. 393-402.

23. Kawaguchi, H., Bandoh, S., and Niwa, Y., "The Test Results of AVR (Active Vibration Reduction) System," *Proceedings of the 52nd Annual Forum of the American Helicopter Society*, Washington, DC, 1996, pp. 123-136.

24. Aso, M., and Bandoh, S., "The Development of the Total Vibration Reduction (TVR) System," *Proceedings of the 55th Annual Forum of the American Helicopter Society*, Montreal, Quebec, Canada, 1999, pp. 202-208.

25. Settle, T. B., and Nixon, M. W., "MAVSS Control of an Active Flaperon for Tiltrotor Vibration Reduction," *Proceedings of the 53rd Annual Forum of the American Helicopter Society*, Virginia Beach, VA, 1997, pp. 1177-1193.

26. Lim, K. B., "Method for Optimal Actuator and Sensor Placement for Large Flexible Structures," *Journal of Guidance, Control, and Dynamics*, Vol. 15, No. 1, 1992, pp. 49-57.

27. Xu, K., Warnitchai, P., and Igusa, T., "Optimal Placement and Gains of Sensors and Actuators for Feedback Control," *Journal of Guidance, Control, and Dynamics*, Vol. 17, No. 5, 1994, pp. 929-934.

28. Schulz, G., and Heimbold, G., "Dislocated Actuator/Sensor Positioning and Feedback Design for Flexible Structures," *Journal of Guidance, Control, and Dynamics*, Vol. 6, No. 5, 1983, pp. 361-367.

29. DeLorenzo, M. L., "Sensor and Actuator Selection for Large Space Structural Control," *Journal of Guidance, Control, and Dynamics*, Vol. 13, No. 2, 1990, pp. 249-257.

30. Choe, K., and Baruh, H., "Actuator Placement in Structural Control," *Journal of Guidance, Control, and Dynamics*, Vol. 15, No. 1, 1992, pp. 40-48.

31. Singiresu, R., and Tzong-Shii, P., "Optimal Placement of Actuators in Actively Controlled Structures Using Genetic Algorithms," *AIAA Journal*, Vol. 29, No. 6, 1991, pp. 942-944.

32. Kirby, G., Matic, P., and Lindner, D., "Optimal Actuator Size and Location Using Genetic Algorithms for Multivariable Control," *Proceedings of the ASME International Congress and Exposition,* ASME, Chicago, IL, Vol. 45, 1994, pp. 325-335.

33. Sepulveda, A., Jin, I., and Schmit, L., "Optimal Placement of Active Elements in Control Augmented Structural Synthesis," *Proceedings of the AIAA/ASME/ASCE/AHS/ASC, 33rd Structures, Structural Dynamics, and Materials Conference*, AIAA, Washington, DC, 1992, pp. 2768-2787 (AIAA 92-2557-CP).

34. Maghami, P., and Joshi, S., "Sensor-Actuator Placement for Flexible Structures with Actuator Dynamics," *Journal of Guidance, Control, and Dynamics*, Vol. 16, No. 2, 1993, pp. 301-307.

35. Lindberg, R., and Longman, R., "On the Number and Placement of Actuators for Independent Modal Space Control," *Journal of Guidance, Control, and Dynamics*, Vol. 7, No. 2, 1984, pp. 215-221.

36. Venkatesan, C., and Udayasankar, A., "Selection of Sensor Locations for Active Vibration Control of Helicopter Fuselages," *Journal of Aircraft*, Vol. 36, No. 2, 1999, pp. 434-442.

37. Devore, J. L., "Probability and Statistics for Engineering and the Sciences," Monterey, CA, Wadsworth, Inc., 1987, pp. 46-52.

38. Gangwani, S. T., "Calculation of Rotor Wake Induced Empennage Airloads," *Journal of the American Helicopter Society*, Vol. 28, No. 2, 1983, pp. 37-46.

39. Yeo, H. and Chopra, I., "Coupled Rotor/Fuselage Vibration Analysis Using Detailed 3-D Airframe Models," *Proceedings of the AIAA/ASME/ASCE/ AHS/ASC, 40th Structures, Structural Dynamics, and Materials Conference*, AIAA, St. Louis, MO, 1999, pp. 126-145 (AIAA Paper 99-1219).

40. Johnson, W., "Self-Tuning Regulators for Multicyclic Control of Helicopter Vibration," *NASA Technical Paper*, NAS 1.60:1996, A-8719, 1982, (ISSN: 0148-8341).

41. Haftka, R. T., and Gurdal, Z., "Elements of Structural Optimization," Kluwer Academic Publishers, Third Edition, 1992, pp. 145-149.

42. Corana, A., Marchesi, M., Martini, C., and Ridella, S., "Minimizing Multimodal Functions of Continuous Variables with the "Simulated Annealing" Algorithm," *Association for Computing Machinery Transactions on Mathematical Software*, ACM, Vol. 13, No. 3, 1987, pp. 262-280.

43. Huang, M. W., and Arora J. S., "Optimal Design with Discrete Variables: Some Numerical Experiments," *International Journal for Numerical Methods in Engineering*, Vol. 40, 1997, pp. 165-188.

44. The Math Works Inc., "MATLAB, Technical Computing Software, Version 5," The Math Works Inc., Natick, MA, 1996.

45. The Math Works Inc., "Using MATLAB," The Math Works Inc., Natick, MA, Version 5, 1996.

46. MacNeal-Schwendler Corp., "MSC/Nastran User's Manual," MacNeal-Schwendler Corporation, Los Angeles, CA, Version 66, Vol. 1, 1988.

47. MacNeal-Schwendler Corp., "MSC/Nastran User's Manual," MacNeal-Schwendler Corporation, Los Angeles, CA, Version 66, Vol. 2, 1988.

48. Spotts, M. F., "Design of Machine Elements," 6th edition, Englewood Cliffs, Prentice-Hall, 1985.

49. Ross, C. T. F., "Finite Element Methods in Structural Mechanics," Chichester, Ellis Horwood, 1985.

50. NASA, "NASTRAN Theoretical Manual," National Aeronautics and Space Administration, Washington D.C., 1981, NASA SP-221(06).

51. Giurgiutiu, V., and Rogers, C. A., "Power and Energy Characteristics of Solid-State Induced-Strain Actuators for Static and Dynamic Applications," *Journal of Intelligent Material Systems and Structures*, Vol. 8, 1997, pp. 738-750.

52. Heverly, D. E., Wang, K. W., and Smith, E. C., "A New Dual Stack Piezoelectric Actuation Device with Improved Performance," *Proceedings of SPIE Conference on Smart Structures and Materials*, Vol. 4701, 2002, San Diego, CA.

Appendix A

HELICOPTER AIRFRAME MODEL AND COMPUTER SOURCE CODES

Reduced Order Model (ROM) description, node numbering, and coordinate locations

ROM Node Number	Nastran FEM Node Number	X Global Coordinate [in.]	Y Global Coordinate [in.]	Z Global Coordinate [in.]	Location Description
1	5	202.571	14.0	170.612	Mast base right side
2	18	188.624	0.0	169.392	Mast base front
3	29	217.514	0.0	171.919	Mast base rear
4	41	202.571	-14.0	170.612	Mast base left side
5	54	198.6	0.0	215.8	Main rotor shaft C-line
6	62	199.6	0.0	204.1	Main rotor mast top
7	500	202.571	0.0	170.612	Mast base-bottom/center
8	3499	35.5	0.0	129.2	Forward fuselage 1st Frame
9	4600	46.1	0.0	129.2	Forward fuselage 2nd Frame
10	5700	57.5	0.0	129.2	Forward fuselage 3rd Frame
11	6900	69.8	0.0	129.2	Forward fuselage 4th Frame
12	8000	80.5	0.0	129.2	Forward fuselage 5th Frame
13	9056	206.2	0.0	129.2	Below main rotor shaft
14	9101	98.5	0.0	129.2	Forward fuselage 6th Frame
15	10514	105.0	0.0	129.2	Forward fuselage 7th Frame
16	11501	115.0	0.0	129.2	Forward fuselage 8th Frame
17	12002	120.0	30.0	135.2	Main landing gear – Right
18	12004	120.0	-30.0	135.2	Main landing gear – Left
19	12031	163.6	40.00000	79.9	Main landing gear – Right
20	12032	163.6	-40.00000	79.9	Main landing gear – Left
21	12501	125.0	0.0	129.2	Landing gear attachment
22	13501	135.0	0.0	129.2	Middle fuselage 10th Frame

ROM Node Number	Nastran FEM Node Number	X Global Coordinate [in.]	Y Global Coordinate [in.]	Z Global Coordinate [in.]	Location Description
23	14401	144.5	0.0	129.2	Middle fuselage 11th Frame
24	15400	154.3	0.0	129.2	Middle fuselage 12th Frame
25	16300	163.4	0.0	129.2	Middle fuselage 13th Frame
26	17600	176.0	0.0	129.2	Middle fuselage 14th Frame
27	17616	176.0	23.75	145.5	Right front airframe attachment point for mast base supporting strut
28	17619	176.0	-23.75	145.5	Left front airframe attachment point for mast base supporting strut
29	18800	188.4	0.0	129.2	Middle fuselage 15th Frame
30	19900	199.8	0.0	129.2	Middle fuselage 16th Frame
31	20050	206.2	24.13	129.2	Right wing root
32	20051	206.2	33.0	129.2	Right wing
33	20052	206.2	46.0	129.2	Right wing
34	20053	206.2	60.0	129.2	Right wing
35	20054	206.2	66.0	129.2	Right wing
36	20055	206.2	78.0	129.2	Right wing
37	20056	206.2	90.0	129.2	Right wing
38	20057	206.2	96.0	129.2	Right wing
39	20058	206.2	98.0	129.2	Right wing tip
40	20060	206.2	-24.13	129.2	Left wing root
41	20061	206.2	-33.0	129.2	Left wing
42	20062	206.2	-46.0	129.2	Left wing
43	20063	206.2	-60.0	129.2	Left wing
44	20064	206.2	-66.0	129.2	Left wing
45	20065	206.2	-78.0	129.2	Left wing
46	20066	206.2	-90.0	129.2	Left wing
47	20067	206.2	-96.0	129.2	Left wing
48	20068	206.2	-98.0	129.2	Left wing tip
49	21400	214.5	0.0	129.2	Rear fuselage 17th Frame
50	22999	230.0	0.0	129.2	Rear fuselage 18th Frame

ROM Node Number	Nastran FEM Node Number	X Global Coordinate [in.]	Y Global Coordinate [in.]	Z Global Coordinate [in.]	Location Description
51	23010	230.0	23.75	145.5	Right rear airframe attachment point for mast base supporting strut
52	23011	230.0	-23.75	145.5	Left rear airframe attachment point for mast base supporting strut
53	23800	238.9	0.0	129.2	Engine attachment
54	24000	239.6	38.3	165.3	Engine right
55	24001	239.5	-37.2	165.3	Engine left
56	24700	247.7	0.0	129.2	Tailboom frames
57	25800	258.5	0.0	129.2	Tailboom frames
58	26900	269.2	0.0	129.2	Tailboom frames
59	28000	280.0	0.0	129.2	Tailboom frames
60	29000	290.0	0.0	129.2	Tailboom frames
61	30000	300.0	0.0	129.2	Tailboom frames
62	31000	310.0	0.0	129.2	Tailboom frames
63	32000	320.0	0.0	129.2	Tailboom frames
64	33000	330.0	0.0	129.2	Tailboom frames
65	34000	340.0	0.0	129.2	Tailboom frames
66	35000	350.0	0.0	129.2	Tailboom frames
67	36000	360.0	0.0	129.2	Tailboom frames
68	37000	370.0	0.0	129.2	Tailboom frames
69	38300	383.0	0.0	129.2	Tailboom frames
70	39600	396.6	0.0	129.2	Tailboom frames
71	40900	409.9	0.0	129.2	Tailboom frames
72	42300	423.2	0.0	129.2	Tailboom frames
73	43600	436.5	0.0	129.2	Tailboom frames
74	45000	450.0	0.0	129.2	Tailboom frames
75	46300	463.3	0.0	129.2	Tailboom frames
76	47600	476.6	0.0	129.2	Tailboom frames
77	48900	489.9	0.0	129.2	Tailboom frames
78	50300	503.2	0.0	129.2	Tailboom frames

ROM Node Number	Nastran FEM Node Number	X Global Coordinate [in.]	Y Global Coordinate [in.]	Z Global Coordinate [in.]	Location Description
79	51600	516.5	0.0	129.2	Tailboom frames
80	53000	530.1	0.0	129.2	Frame at Vertical Stabilizer
81	54700	547.2	0.0	129.2	Tailboom frame (Tail end)
82	55401	576.7	0.0	242.2	Vertical Stabilizer Top
83	55403	554.8	0.0	189.2	Vertical Stabilizer
84	55404	538.5	0.0	149.6	Vertical Stabilizer
85	56501	553.8	-64.0	147.2	Horizontal Stabilizer Left
86	56502	553.8	-40.0	147.2	Horizontal Stabilizer
87	56503	553.8	-21.0	147.2	Horizontal Stabilizer
88	56504	553.8	-5.7	147.2	Horizontal Stabilizer
89	56505	553.8	0.0	147.2	Horizontal Stabilizer Center
90	56506	553.8	5.7	147.2	Horizontal Stabilizer
91	56507	553.8	21.0	147.2	Horizontal Stabilizer
92	56508	553.8	40.0	147.2	Horizontal Stabilizer
93	56509	553.8	64.0	147.2	Horizontal Stabilizer Right
94	57004	578.0	0.0	109.8	Tail landing gear

Reduced Order Model (ROM) element topology and node connectivity

ROM Element Number	Start Node Number	End Node Number	ROM Element Number	Start Node Number	End Node Number
1	5	6	51	42	43
2	6	7	52	43	44
3	2	7	53	44	45
4	1	7	54	45	46
5	3	7	55	46	47
6	4	7	56	47	48
7	27	2	57	13	49
8	28	2	58	49	50

ROM Element Number	Start Node Number	End Node Number	ROM Element Number	Start Node Number	End Node Number
9	27	1	59	50	53
10	51	1	60	53	54
11	51	3	61	53	55
12	52	3	62	53	56
13	52	4	63	56	57
14	28	4	64	57	58
15	26	27	65	58	59
16	26	28	66	59	60
17	50	51	67	60	61
18	50	52	68	61	62
19	8	9	69	62	63
20	9	10	70	63	64
21	10	11	71	64	65
22	11	12	72	65	66
23	12	14	73	66	67
24	14	15	74	67	68
25	15	16	75	68	69
26	16	21	76	69	70
27	21	17	77	70	71
28	17	19	78	71	72
29	21	18	79	72	73
30	18	20	80	73	74
31	21	22	81	74	75
32	22	23	82	75	76
33	23	24	83	76	77
34	24	25	84	77	78
35	25	26	85	78	79
36	26	29	86	79	80
37	29	30	87	80	81
38	30	13	88	81	94
39	13	31	89	80	84
40	31	32	90	84	83

ROM Element Number	Start Node Number	End Node Number	ROM Element Number	Start Node Number	End Node Number
41	32	33	91	83	82
42	33	34	92	84	89
43	34	35	93	85	86
44	35	36	94	86	87
45	36	37	95	87	88
46	37	38	96	88	89
47	38	39	97	89	90
48	13	40	98	90	91
49	40	41	99	91	92
50	41	42	100	92	93

Reduced Order Model (ROM) eigenvalues and natural frequencies

ROM Mode Number	ROM Eigenvalue [rad2/sec2]	ROM Natural Frequency [rad/sec]	ROM Natural Frequency [Hz]
1	810.0110	28.4607	4.5297
2	1454.5899	38.1391	6.0700
3	2797.6076	52.8924	8.4181
4	2844.6105	53.3349	8.4885
5	3437.5566	58.6307	9.3314
6	3793.7209	61.5932	9.8029
7	4407.6180	66.3899	10.5663
8	5681.0616	75.3728	11.9960
9	5792.8408	76.1107	12.1134
10	6845.1728	82.7356	13.1678
11	7912.9089	88.9545	14.1576
12	8263.5344	90.9040	14.4678
13	9667.1921	98.3219	15.6484
14	10432.5112	102.1397	16.2560
15	11195.6122	105.8093	16.8401

ROM Mode Number	ROM Eigenvalue [rad2/sec2]	ROM Natural Frequency [rad/sec]	ROM Natural Frequency [Hz]
16	13055.0758	114.2588	18.1849
17	13456.7049	116.0030	18.4625
18	19127.3352	138.3016	22.0114
19	19768.7459	140.6014	22.3774
20	20435.1590	142.9516	22.7515
21	21087.2903	145.2146	23.1116
22	22221.1291	149.0675	23.7248
23	24027.8629	155.0092	24.6705
24	27334.2541	165.3307	26.3132
25	29676.7177	172.2693	27.4175
26	31407.1545	177.2206	28.2055
27	33231.0449	182.2938	29.0130
28	39731.0999	199.3266	31.7238
29	42476.6994	206.0988	32.8016
30	44601.5953	211.1909	33.6121
31	45086.5751	212.3360	33.7943
32	46092.2201	214.6910	34.1691
33	47672.9382	218.3413	34.7501
34	52420.9350	228.9562	36.4395
35	55489.3864	235.5619	37.4908
36	57416.7301	239.6179	38.1364
37	59120.5900	243.1473	38.6981
38	65891.3587	256.6931	40.8540
39	69329.5299	263.3050	41.9063
40	72250.9632	268.7954	42.7801

The first twenty modes shapes of the Reduced Order Model are displayed in the following figures.

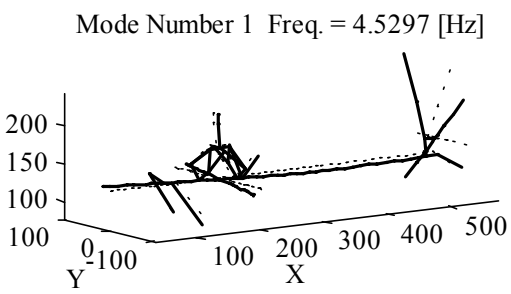
Mode Number 1 Freq. = 4.5297 [Hz]
200
150
100
100
0
-100
Y
100 200 300 400 500
X

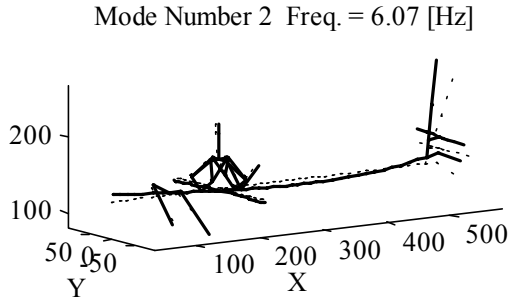
Mode Number 2 Freq. = 6.07 [Hz]
200
100
50 0 -50
Y
100 200 300 400 500
X

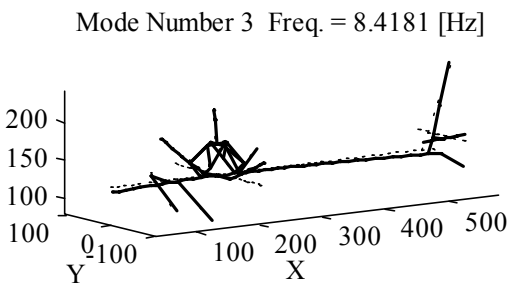
Mode Number 3 Freq. = 8.4181 [Hz]
200
150
100
100
0
-100
Y
100 200 300 400 500
X

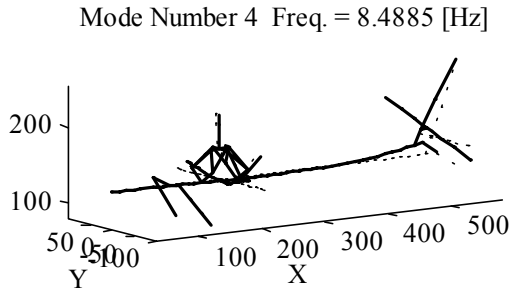
Mode Number 4 Freq. = 8.4885 [Hz]
200
100
50 0 -50
Y
100 200 300 400 500
X

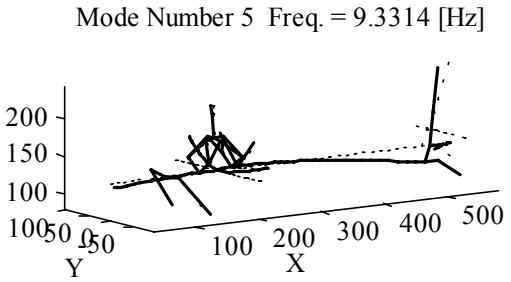
Mode Number 5 Freq. = 9.3314 [Hz]
200
150
100
100
50 0 -50
Y
100 200 300 400 500
X

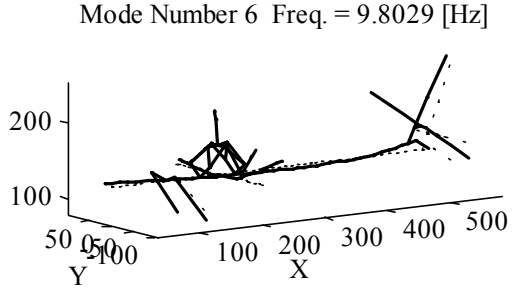
Mode Number 6 Freq. = 9.8029 [Hz]
200
100
50 0 -50
Y
100 200 300 400 500
X

Mode Number 7 Freq. = 10.5663 [Hz]

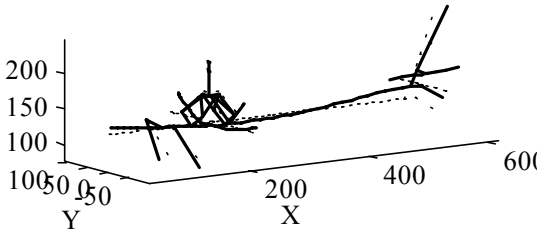

Mode Number 8 Freq. = 11.996 [Hz]

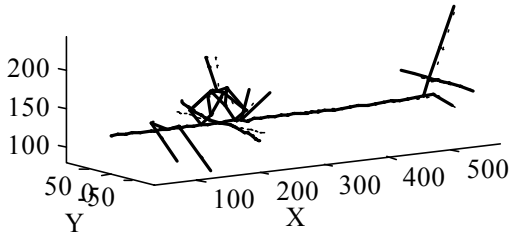

Mode Number 9 Freq. = 12.1134 [Hz]

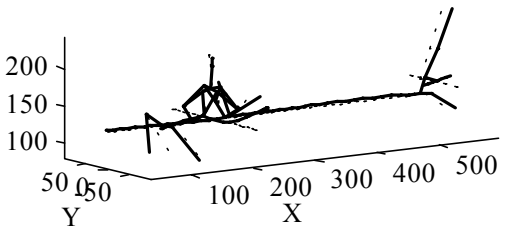

Mode Number 10 Freq. = 13.1678 [Hz]

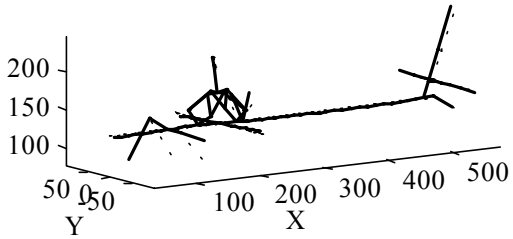

Mode Number 11 Freq. = 14.1576 [Hz]

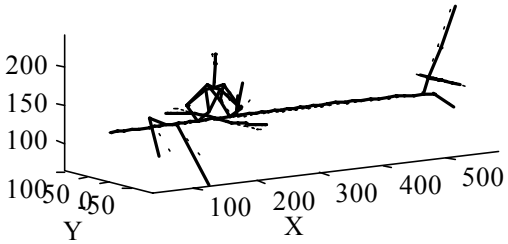

Mode Number 12 Freq. = 14.4678 [Hz]

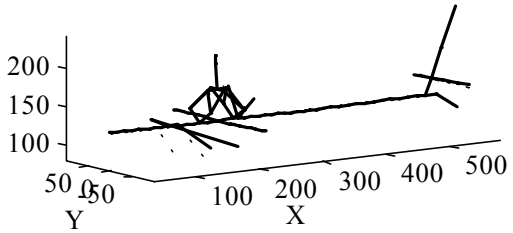

Mode Number 13 Freq. = 15.6484 [Hz]

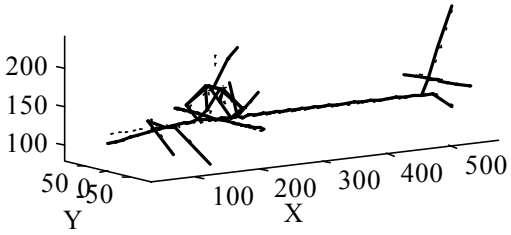

Mode Number 14 Freq. = 16.256 [Hz]

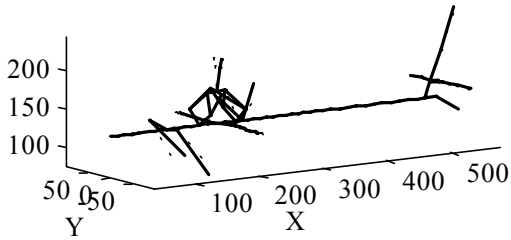

Mode Number 15 Freq. = 16.8401 [Hz]

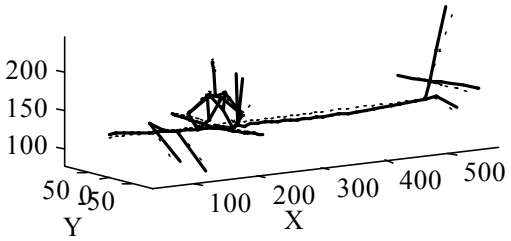

Mode Number 16 Freq. = 18.1849 [Hz]

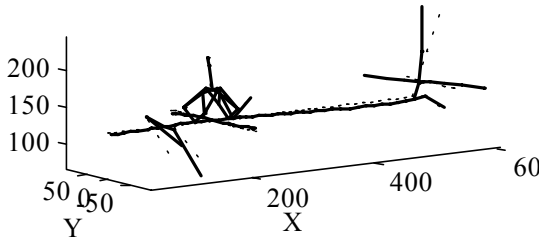

Mode Number 17 Freq. = 18.4625 [Hz]

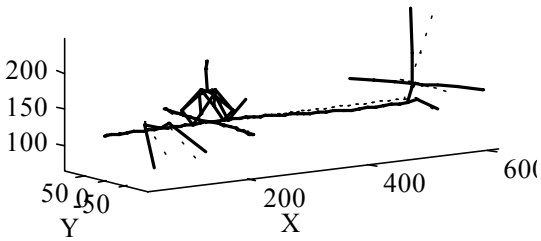

Mode Number 18 Freq. = 22.0114 [Hz]

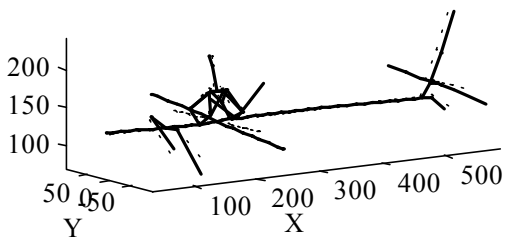

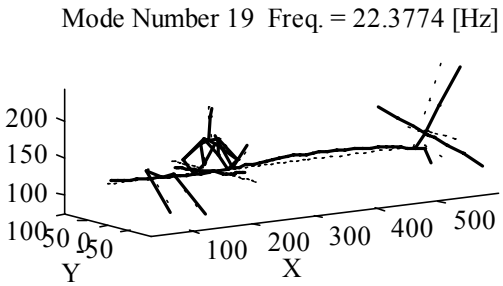

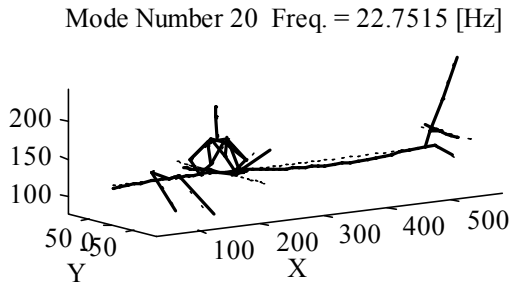

Actuation Unit definitions and relation to ROM

Actuation Unit Identification Number	Actuation Unit Type	First ROM Node Number	First ROM Global D.O.F.	Second ROM Node Number	Second ROM Global D.O.F.	Elastic Axis Offset [in.]
1	FAU	8	43	9	49	1
2	MAU	8	47	9	53	17
3	MAU	8	48	9	54	18
4	FAU	9	49	10	55	1
5	MAU	9	53	10	59	17
6	MAU	9	54	10	60	18
7	FAU	10	55	11	61	1
8	MAU	10	59	11	65	17
9	MAU	10	60	11	66	20
10	FAU	11	61	12	67	1
11	MAU	11	65	12	71	9
12	MAU	11	66	12	72	23
13	FAU	12	67	14	79	1
14	MAU	12	71	14	83	9
15	MAU	12	72	14	84	24
16	FAU	14	79	15	85	1

Actuation Unit Identification Number	Actuation Unit Type	First ROM Node Number	First ROM Global D.O.F.	Second ROM Node Number	Second ROM Global D.O.F.	Elastic Axis Offset [in.]
17	MAU	14	83	15	89	9
18	MAU	14	84	15	90	24
19	FAU	15	85	16	91	1
20	MAU	15	89	16	95	9
21	MAU	15	90	16	96	24
22	FAU	16	91	21	121	1
23	MAU	16	95	21	125	9
24	MAU	16	96	21	126	24
25	FAU	21	121	22	127	1
26	MAU	21	125	22	131	9
27	MAU	21	126	22	132	24
28	FAU	22	127	23	133	1
29	MAU	22	131	23	137	9
30	MAU	22	132	23	138	24
31	FAU	23	133	24	139	1
32	MAU	23	137	24	143	9
33	MAU	23	138	24	144	24
34	FAU	24	139	25	145	1
35	MAU	24	143	25	149	9
36	MAU	24	144	25	150	24
37	FAU	25	145	26	151	1
38	MAU	25	149	26	155	9
39	MAU	25	150	26	156	24
40	FAU	26	151	29	169	1
41	MAU	26	155	29	173	20
42	MAU	26	156	29	174	24
43	FAU	29	169	30	175	1
44	MAU	29	173	30	179	20
45	MAU	29	174	30	180	24
46	FAU	30	175	13	73	1
47	MAU	30	179	13	77	20
48	MAU	30	180	13	78	24

Actuation Unit Identification Number	Actuation Unit Type	First ROM Node Number	First ROM Global D.O.F.	Second ROM Node Number	Second ROM Global D.O.F.	Elastic Axis Offset [in.]
49	FAU	31	182	32	188	1
50	MAU	31	184	32	190	5
51	MAU	31	186	32	192	6
52	FAU	40	236	41	242	1
53	MAU	40	238	41	244	5
54	MAU	40	240	41	246	6
55	FAU	13	73	49	289	1
56	MAU	13	77	49	293	20
57	MAU	13	78	49	294	24
58	FAU	49	289	50	295	1
59	MAU	49	293	50	299	20
60	MAU	49	294	50	300	24
61	FAU	50	295	53	313	1
62	MAU	50	299	53	317	20
63	MAU	50	300	53	318	24
64	FAU	53	313	56	331	1
65	MAU	53	317	56	335	20
66	MAU	53	318	56	336	24
67	FAU	56	331	57	337	1
68	MAU	56	335	57	341	20
69	MAU	56	336	57	342	24
70	FAU	57	337	58	343	1
71	MAU	57	341	58	347	20
72	MAU	57	342	58	348	24
73	FAU	58	343	59	349	1
74	MAU	58	347	59	353	20
75	MAU	58	348	59	354	24
76	FAU	59	349	60	355	1
77	MAU	59	353	60	359	19
78	MAU	59	354	60	360	23
79	FAU	60	355	61	361	1
80	MAU	60	359	61	365	19

Actuation Unit Identification Number	Actuation Unit Type	First ROM Node Number	First ROM Global D.O.F.	Second ROM Node Number	Second ROM Global D.O.F.	Elastic Axis Offset [in.]
81	MAU	60	360	61	366	23
82	FAU	61	361	62	367	1
83	MAU	61	365	62	371	19
84	MAU	61	366	62	372	23
85	FAU	62	367	63	373	1
86	MAU	62	371	63	377	19
87	MAU	62	372	63	378	22
88	FAU	63	373	64	379	1
89	MAU	63	377	64	383	19
90	MAU	63	378	64	384	22
91	FAU	64	379	65	385	1
92	MAU	64	383	65	389	18
93	MAU	64	384	65	390	21
94	FAU	65	385	66	391	1
95	MAU	65	389	66	395	18
96	MAU	65	390	66	396	21
97	FAU	66	391	67	397	1
98	MAU	66	395	67	401	17
99	MAU	66	396	67	402	20
100	FAU	67	397	68	403	1
101	MAU	67	401	68	407	17
102	MAU	67	402	68	408	20
103	FAU	68	403	69	409	1
104	MAU	68	407	69	413	16
105	MAU	68	408	69	414	19
106	FAU	69	409	70	415	1
107	MAU	69	413	70	419	15
108	MAU	69	414	70	420	18
109	FAU	70	415	71	421	1
110	MAU	70	419	71	425	15
111	MAU	70	420	71	426	17
112	FAU	71	421	72	427	1

Actuation Unit Identification Number	Actuation Unit Type	First ROM Node Number	First ROM Global D.O.F.	Second ROM Node Number	Second ROM Global D.O.F.	Elastic Axis Offset [in.]
113	MAU	71	425	72	431	14
114	MAU	71	426	72	432	16
115	FAU	72	427	73	433	1
116	MAU	72	431	73	437	14
117	MAU	72	432	73	438	15
118	FAU	73	433	74	439	1
119	MAU	73	437	74	443	13
120	MAU	73	438	74	444	14
121	FAU	74	439	75	445	1
122	MAU	74	443	75	449	13
123	MAU	74	444	75	450	14
124	FAU	75	445	76	451	1
125	MAU	75	449	76	455	12
126	MAU	75	450	76	456	13
127	FAU	76	451	77	457	1
128	MAU	76	455	77	461	12
129	MAU	76	456	77	462	13
130	FAU	77	457	78	463	1
131	MAU	77	461	78	467	12
132	MAU	77	462	78	468	13
133	FAU	78	463	79	469	1
134	MAU	78	467	79	473	12
135	MAU	78	468	79	474	12
136	FAU	87	518	88	524	1
137	MAU	87	520	88	526	4
138	MAU	87	522	88	528	7
139	FAU	90	536	91	542	1
140	MAU	90	538	91	544	4
141	MAU	90	540	91	546	7
142	MAU	80	479	84	503	6
143	MAU	83	497	84	503	6

Actuation Unit Identification Number	Actuation Unit Type	First ROM Node Number	First ROM Global D.O.F.	Second ROM Node Number	Second ROM Global D.O.F.	Elastic Axis Offset [in.]
144	FAU	83 83	493 495	84 84	499 501	1 1
145	FAU	80 80	475 477	84 84	499 501	1 1
146	MAU	83 83	496 498	84 84	502 504	5 5
147	MAU	80 80	478 480	84 84	502 504	5 5
148	CA	3 3 3	13 14 15	51 51 51	301 302 303	1 1 1
149	CA	1 1 1	1 2 3	51 51 51	301 302 303	1 1 1
150	CA	1 1 1	1 2 3	27 27 27	157 158 159	1 1 1
151	CA	2 2 2	7 8 9	27 27 27	157 158 159	1 1 1
152	CA	2 2 2	7 8 9	28 28 28	163 164 165	1 1 1
153	CA	4 4 4	19 20 21	28 28 28	163 164 165	1 1 1
154	CA	4 4 4	19 20 21	52 52 52	307 308 309	1 1 1
155	CA	3 3 3	13 14 15	52 52 52	307 308 309	1 1 1

Hydraulic Actuator, Model RD-41 specification data sheet, page 1 of 2

RD-Series, Precision Production Cylinders

ENERPAC
Hydraulic Technology Worldwide

▼ Shown from left to right: **RD-2510, RD-96, RD-256, RD-41, RD-166**

High Precision and High Cycle Performance

Golden Ring Design

Enerpac RD-Cylinders are provided with the Golden Ring Design, for long, trouble-free performance.

This paper mill uses RD cylinders for precision when trimming. ▶

- **Designed for long life, the best choice for production applications**
- **Unique mounting configurations simplify fixturing**
- **Baked enamel finish for increased corrosion resistance**
- **Double-acting operation develops force in both directions, providing maximum versatility**
- **Plunger wiper reduces contamination, extending cylinder life**

Nominal Cylinder Capacity (tons)	Stroke (in)	Model Number	Max. Cylinder Capacity (tons)		Cylinder Effective Area (in²)		Oil Capacity (in³)		Col. Height A (in)	Ext. Height B (in)	Body Length C (in)	Cyl. Dia. D (in)	Cyl. Bore Dia. E (in)	Plgr. Dia. F (in)
			Advance	Retract	Advance	Retract	Advance	Retract						
4	1.13	**RD-41**	4	2	.79	.34	.88	.38	7.31	8.44	6.38	2.00	1.00	.75
	3.13	**RD-43**	4	2	.79	.34	2.45	1.07	9.31	12.44	8.38	2.00	1.00	.75
	6.13	**RD-46**	4	2	.79	.34	4.81	2.10	12.31	18.44	11.38	2.00	1.00	.75
9	1.13	**RD-91**	9	5	1.77	.90	1.99	1.10	8.75	9.88	7.80	2.50	1.50	1.00
	3.13	**RD-93**	9	5	1.77	.90	5.52	3.07	10.75	13.91	9.80	2.50	1.50	1.00
	6.13	**RD-96**	9	5	1.77	.98	10.82	6.01	13.75	19.91	12.80	2.50	1.50	1.00
	10.13	**RD-910**	9	5	1.77	.90	17.89	9.94	17.75	27.91	16.81	2.50	1.50	1.00
16	6.25	**RD-166**	16	8	3.14	1.66	19.63	10.25	15.31	21.56	14.13	3.00	2.00	1.38
	10.25	**RD-1610**	16	8	3.14	1.66	32.20	16.89	19.31	29.56	18.11	3.00	2.00	1.38
25	6.25	**RD-256**	25	11	4.91	2.15	30.68	13.42	16.69	22.94	15.69	3.63	2.50	1.88
	10.25	**RD-2510**	25	11	4.91	2.15	50.31	22.01	20.69	30.94	19.61	3.63	2.50	1.88

Hydraulic Actuator, Model RD-41 specification data sheet, page 2 of 2

Double-Acting, Precision Production Cylinders

▼ RD CYLINDER ATTACHMENTS

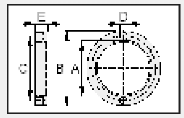

Retainer Nut
For locking foot or flange mountings. Tightens onto cylinder collar threads (included with foot and flange mounting kits)

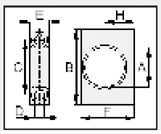

Foot Mounting
Mounts onto cylinder collar

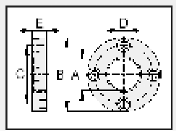

Flange Mounting
Mounts onto cylinder collar

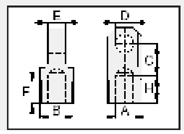

Clevis Eye
Threads onto plunger or into cylinder base

Model Number	RD-Cyl. (tons)	Dimensions (in)						
		A	B	C	D	E	F	H
Foot Mounting with Retainer Nut								
AD-141	**4**	1.38	3.[illegible]	2.[illegible]	.4[illegible]	.76	2.2[illegible]	1.2[illegible]
AD-171	**9**	2.00	4.[illegible]	2.55	.55	1.00	3.2[illegible]	1.7[illegible]
AD-181	**16**	2.63	5.[illegible]	[illegible].75	.78	1.38	4.00	2.06
AD-191	**25**	3.25	6.25	4.62	1.03	1.76	4.88	2.50
Flange Mounting with Retainer Nut								
AD-142	**4**	1.38	3.22	3.[illegible]	.4[illegible]	.75		
AD-172	**9**	2.00	4.75	[illegible].88	.4[illegible]	1.00	–	–
AD-182	**16**	2.63	5.63	4.56	.53	1.38	–	–
AD-192	**25**	3.25	6.[illegible]	[illegible].31	.60	1.75		
Retainer Nut								
AD-143	**4**	1⁵⁄₁₆"-12 UNF	2.25	1.8[illegible]	.25	.38	–	–
AD-173	**9**	2"-12	3.[illegible]	2.50	.27	.50	–	–
AD-183	**16**	2⅝"-16	3.62	3.12	.27	.75		
AD-193	**25**	3¼"-16	4.2[illegible]	3.75	.27	1.00		
Clevis Eye*								
AD-150	**4**	½"-20	1 [illegible]-20	52.4	.63	.63	.75	23,8
AD-151	**9**	¾"-16	1 [illegible]-12	67,[illegible]	.75	1.00	1.00	25.8
AD-152	**16**	1⅛"-12	2⁵⁄₁₆"-16	77,5	1.00	1.25	1.00	30.2
AD-153	**25**	1⅛"-12	2[illegible]-16	77.8	1.25	1.50	1.00	27,0

RD Series

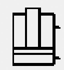

Capacity:
4-25 tons

Stroke:
1.13-10.25 inch

Maximum Operating Pressure:
10,000 psi

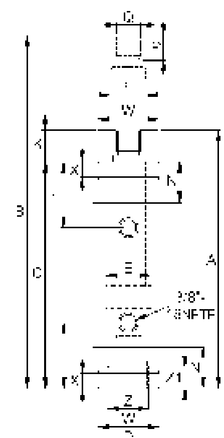

Top to Ret. Port H (in)	Bottom to Adv. Port I (in)	Plunger Protrusion K (in)	Neck Length N (in)	Plunger Thread Length P (in)	Plunger External Thread G (in)	Cylinder Mounting Dimensions (in)					Weight (lbs)	Model Number
						Collar Thread W	Collar Thread Length X	Int. Base Thread Z	Int. Base Thread Length Z1	Pin to Pin with Clevis Eyes Fitted*		
1.84	1.84	.94	1.13	.75	½"-20	1⁵⁄₁₆"-12	.44	1⅛"-20	.35	10.15	4.5	**RD-41**
1.84	1.84	.94	1.13	.75	½"-20	1⁵⁄₁₆"-12	.44	1⅛"-20	.35	12.15	6.4	**RD-43**
1.84	1.84	.94	1.13	.75	½"-20	1⁵⁄₁₆"-12	.44	1⅛"-20	.35	15.15	9.0	**RD-46**
2.25	2.25	.98	1.50	.75	¾"-16	2"-12	.56	1¹¹⁄₁₆"-16	.55	11.78	9.0	**RD-91**
2.25	2.25	.98	1.50	.75	¾"-16	2"-12	.56	1¹¹⁄₁₆"-16	.55	13.79	11.0	**RD-93**
2.25	2.25	.98	1.50	.75	¾"-16	2"-12	.56	1¹¹⁄₁₆"-16	.55	16.78	14.0	**RD-96**
2.25	2.25	.98	1.50	.75	¾"-16	2"-12	.56	1¹¹⁄₁₆"-16	.55	20.78	18.0	**RD-910**
2.88	2.88	1.19	2.13	1.00	1⅛"-12	2⅝"-16	.56	2⁵⁄₁₆"-16	.94	20.31	22.0	**RD-166**
2.88	2.88	1.19	2.13	1.00	1⅛"-12	2⅝"-16	.56	2⁵⁄₁₆"-16	.94	2[illegible].31	28.0	**RD-1610**
3.50	3.50	1.06	2.75	1.00	1⅛"-12	3¼"-16	1.13	2¾"-16	1.02	20.79	36.0	**RD-256**
3.50	3.50	1.06	2.75	1.00	1⅛"-12	3¼"-16	1.13	2¾"-16	1.02	24.79	46.0	**RD-2510**

Program to read airframe model information and save in matrix format

```
% This MATLAB program is part of a computer software package for
% helicopter vibration analysis, active vibration control, and
optimized
% actuator placement studies.
%
% Written by: David E. Heverly II                          2/22/99
%             Mechanical Engineering Ph.D. Candidate
%             The Pennsylvania State University
%*********************************************************
% Filename = readin.m
%*********************************************************
% Routine to read the data file "mat.dat" and stores the result
% in the specified matrix & file.
% "mat.dat" contains the Apache helicopter Reduced Order Model
% mass and stiffness matrix information.
% The (564 X 564) "mass" & "stif" matrix data is stored in row format.
% Each line of "mat.dat" has three entries, therefore the first 188
% lines of "mat.dat" compose the first row of the mass matrix.
%
%************ Variable names/definitions ******************
% Input: mat.dat - ASCII text file of airframe model information
%
% Output:   mass - 564 X 564 mass matrix
%           stif - 564 x 564 stiffness matrix
%           stk-m-k.mat - binary output file containing mass, stif
%
%*********************************************************

clear     % Clear variables from computer memory
fid=fopen('mat.dat');    % Open data file

disp('Reading Mass Matrix')
str1=fscanf(fid,'%4s',1);
m=fscanf(fid,'%3d',2);

disp(['Number of read elements should be = ',num2str(m(1)*m(2))])
[mass, count]=fscanf(fid, '%g %g %g',[m(1),m(2)]);
mass=mass';

disp(['Number of elements read = ',num2str(count)])
disp(' ')

disp('Reading Stiffness Matrix')
str1=fscanf(fid,'%4s',1);
m=fscanf(fid,'%3d',2);

disp(['Number of read elements should be = ',num2str(m(1)*m(2))])
[stif, count]=fscanf(fid, '%g %g %g',[m(1),m(2)]);
stif=stif';

disp(['Number of elements read = ',num2str(count)])
```

Program to read airframe model information and save in matrix format

```
disp(' ')
fclose(fid);    % Close data file

%  Save variables in binary output file "stk-m-k.mat"
%************************************************
disp('Saving "mass" & "stif" matrices to binary file: "stk-m-k.mat"')
save stk-m-k mass stif
%***************** End of File *************************
```

Program to compute eigenvalues and eigenvectors

```
% This MATLAB program is part of a computer software package for
% helicopter vibration analysis, active vibration control, and
optimized
% actuator placement studies.
%
% Written by: David E. Heverly II                          2/22/99
%             Mechanical Engineering Ph.D. Candidate
%             The Pennsylvania State University
%*******************************************************
% Filename = eignanal.m
%*******************************************************
% The program loads the structure's mass and stiffness
% matricies that have been stored in a binary data file.
% An eigenanalysis is performed to compute the eigenvalues
% (natural frequencies) and eigenvectors (mode shapes). The
% eigenvectors are normalized with-respect-to the mass matrix
% such that the norm (magnidude) of each eigenvector = one.
%
%  NOTE: The eigenvectors are mormalized w.r.t the mass matrix
%         such that  [evecs]'*[mass]*[evecs] = [I]
%
% The first 100 eigenvalues and corresponding eigenvectors are
% stored in a binary output file.
%
%************ Variable names/definitions **************
% Input: mass - Ng x Ng mass matrix
%        stif - Ng x Ng stiffness matrix
%        Ng - No. global physical d.o.f. (Ng=564)
%
% Output:   eval - 100 X 1 vector of natural frequencies
%           evec - Ng x 100 matrix of eigenvectors
%           eigen.mat - binary output file containing evals,evecs
%
%*******************************************************
```

Program to compute eigenvalues and eigenvectors

```
% Load mass & stiffness matrices
%*******************************************************
clear variables      % Clears all variables from computer memory
load stk-m-k.mat     % Loads binary mass, stif file
mass=0.5*(mass'+mass);
stif=0.5*(stif'+stif);
[Ng,N]=size(mass);
N=100;               % Number of eigenvalues to save and print
%**************************

% Compute eigenvalues and eigenvectors
%**************************
disp('Computing eigenvalues and eigenvectors')
[V,lamda]=eig(stif,mass);
for i=1:Ng
   lam(i,1)=sqrt((abs(lamda(i,i))));
end

[dum,II]=sort(lam);
for i=1:N                                  % Eliminate first 6 rigid
body modes
   eval(i,1)=dum(i+6);
   freqs(i,1)=(dum(i+6))^2;                % Natural frequency in
rad^2/sec^2
   freqs(i,2)=dum(i+6);                    % Natural frequency in
rad/sec
   freqs(i,3)=(dum(i+6))/(2*pi);           % Natural frequency in Hz
   vec(:,i)=real(V(:,II(i+6)));            % eigenvector
end

disp('Normalizing eigenvectors wrt mass matrix')
%  Normalize eigenvectors (mode shapes) w.r.t. mass matrix
%  ******************************************************
for i=1:N
  norm=abs(((vec(:,i))')*mass*(vec(:,i)));
  evec(:,i)=(vec(:,i))/sqrt(norm);
end

% Save matricies in binary output file
%*************************************
disp('Saving natural frequencies and normalized eigenvectors to file:
"eigen.mat"')
save eigen eval evec Ng

disp(' ')
disp('Natural Frequencies')
disp('w^2 [rad^2/sec^2]    w [rad/sec]    f=w/2pi [Hz]')
disp('*************************************')
for i=1:N
   disp([num2str(freqs(i,1)),',      ',num2str(freqs(i,2)),',
```

Program to compute eigenvalues and eigenvectors

```
',num2str(freqs(i,3))])
end
%***************** End of File *************************
```

Program to formulate a State Space model

```
% This MATLAB program is part of a computer software package for
% helicopter vibration analysis, active vibration control, and
optimized
% actuator placement studies.
%
% Written by: David E. Heverly II                          3/2/99
%             Mechanical Engineering Ph.D. Candidate
%             The Pennsylvania State University
%*********************************************************
% Filename = ssmodel.m
%*********************************************************
% The program loads the structure's mass, stiffness, and
% eigenvector matricies that have been stored in binary data files.
% Using the selected number of modes (up to 100), the equations of
% motion are transformed to modal coordinates in second order form.
% The equation of motion is then transformed to state space form
% (first order) with the option of adding modal damping.  Finally,
% the state space matricies are saved in binary format.
%
%  NOTE: The eigenvectors (mode shapes) have been mormalized w.r.t
%        the mass matrix in subroutine "eignanal.m" such that
%        [phi]'*[mass]*[phi] = [Mm] = [I]
%
%************ Variable names/definitions **************
% Input: mass - 564x564 mass matrix
%        stif - 564x564 stiffness matrix
%        evec - 564x100  eigenvector matrix (normalized wrt [mass])
%
%        Km - modal mass matrix
%        Cm - modal damping matrix
%        zeta - modal damping ratio
%        e - vector of Actuation Unit moment arms
%
% Output:   A - 2N x 2N  State matrix
%           B - 2N x Ng  Actuation Input matrix
%           N - No. modes used in modal reduction
%           Ng=564 - No. global physical d.o.f.
%           phi - Ng x N Matrix of normalized mode shapes
%
```

Program to formulate a State Space model

```
%***************** Revisions/comments *****************
% Revision 1/5/00 - increase modes to 100
% Revision 1/5/00 - Added moment arm matrix for inputs so
%                   that input loads have consistent units [lbs.]
%*********************************************************

% Load mass & stiffness matricies & eigenvectors
%*****************************************************************
clear                % Clears all variables from computer memory
load stk-m-k.mat     % Loads binary mass, stif file
load eigen.mat       % Loads binary eigenvector file
%**************************

Ng=564;     % Global degrees-of-freedom of full model
N=25;       % No. of modes used in modal reduction
% Define modal transformation matrix
%**************************
for i=1:N
 phi(1:Ng,i)=evec(1:Ng,i);
end

% Transform to modal space
%**************************
disp('Transforming to modal coordinates')
% Note: Mm=(phi')*mass*phi=[I];
Km=diag(diag((phi')*stif*phi));

% Add 0.2% modal damping matrix
%******************************
disp('Adding modal damping')
zeta=0.002;    % Modal damping ratio
Cm=eye(N);
for i=1:N
 Cm(i,i)=2*zeta*(sqrt(Km(i,i)));
end

% Transform to State Space form
%******************************
% NOTE: [Mm]=[I] ==> inv(Mm)=[I]
disp('Transforming to state space')
A(1:N,1:N)=zeros(N,N);
A(1:N,N+1:N*2)=eye(N);
A(N+1:N*2,1:N)=-Km;
A(N+1:N*2,N+1:N*2)=-Cm;

% Specify moment arm matrix
% for actuation influence matrix
%**************************
e=ones(1,Ng);
e(47)=17;   e(48)=18;   % Node #8
e(53)=17;   e(54)=18;   % Node #9
```

Program to formulate a State Space model

```
e(59)=17;   e(60)=20;   % Node #10
e(65)=9;    e(66)=23;   % Node #11
e(71)=9;    e(72)=24;   % Node #12
e(77)=20;   e(78)=24;   % Node #13
e(83)=9;    e(84)=24;   % Node #14
e(89)=9;    e(90)=24;   % Node #15
e(95)=9;    e(96)=24;   % Node #16
e(125)=9;   e(126)=24;  % Node #21
e(131)=9;   e(132)=24;  % Node #22
e(137)=9;   e(138)=24;  % Node #23
e(143)=9;   e(144)=24;  % Node #24
e(149)=9;   e(150)=24;  % Node #25
e(155)=20;  e(156)=24;  % Node #26
e(173)=20;  e(174)=24;  % Node #29
e(179)=20;  e(180)=24;  % Node #30
e(184)=5;   e(186)=6;   % Node #31
e(190)=5;   e(192)=6;   % Node #32
e(238)=5;   e(240)=6;   % Node #40
e(244)=5;   e(246)=6;   % Node #41
e(293)=20;  e(294)=24;  % Node #49
e(299)=20;  e(300)=24;  % Node #50
e(317)=20;  e(318)=24;  % Node #53
e(335)=20;  e(336)=24;  % Node #56
e(341)=20;  e(342)=24;  % Node #57
e(347)=20;  e(348)=24;  % Node #58
e(353)=19;  e(354)=23;  % Node #59
e(359)=19;  e(360)=23;  % Node #60
e(365)=19;  e(366)=23;  % Node #61
e(371)=19;  e(372)=22;  % Node #62
e(377)=19;  e(378)=22;  % Node #63
e(383)=18;  e(384)=21;  % Node #64
e(389)=18;  e(390)=21;  % Node #65
e(395)=17;  e(396)=20;  % Node #66
e(401)=17;  e(402)=20;  % Node #67
e(407)=16;  e(408)=19;  % Node #68
e(413)=15;  e(414)=18;  % Node #69
e(419)=15;  e(420)=17;  % Node #70
e(425)=14;  e(426)=16;  % Node #71
e(431)=14;  e(432)=15;  % Node #72
e(437)=13;  e(438)=14;  % Node #73
e(443)=13;  e(444)=14;  % Node #74
e(449)=12;  e(450)=13;  % Node #75
e(455)=12;  e(456)=13;  % Node #76
e(461)=12;  e(462)=13;  % Node #77
e(467)=12;  e(468)=12;  % Node #78
e(473)=12;  e(474)=12;  % Node #79
e(478)=5;   e(479)=6;   e(480)=5;   % Node #80
e(496)=5;   e(497)=6;   e(498)=5;   % Node #83
e(502)=5;   e(503)=6;   e(504)=5;   % Node #84
e(520)=4;   e(521)=4;   e(522)=7;   % Node #87
e(526)=4;   e(527)=4;   e(528)=7;   % Node #88
```

Program to formulate a State Space model

```
e(538)=4;   e(539)=4;   e(540)=7;   % Node #90
e(544)=4;   e(545)=4;   e(546)=7;   % Node #91
E=diag(e);  % form matrix with "e" on diagonal

B(1:N,1:Ng)=zeros(N,Ng);   % Input matrix for Force & Moment actuation
Units
B(N+1:2*N,1:Ng)=phi'*E;    % which are dual point actuation
%*******************************

% Save matricies in binary output file
%************************************
disp('Saving state space model to file: statemod.mat')
save statemod A B phi Ng N
%***************** End of File *************************
```

Program to formulate a Transfer Function model

```
% This MATLAB program is part of a computer software package for
% helicopter vibration analysis, active vibration control, and
optimized
% actuator placement studies.
%
% Written by: David E. Heverly II                              3/7/99
%             Mechanical Engineering Ph.D. Candidate
%             The Pennsylvania State University
%*******************************************************
% Filename = tfmodel.m
%*******************************************************
% The program computes the Complex Transfer Function Matrices
(input/output
% relationship in the frequency domain) of the helicopter airframe
% model at the specified frequency.  The actuation model assumes
% the actuators are placed between nodes to generate loads equal
% in magnitude but opposite in direction.  The defined actuation
% types are: 1) Force Actuation Unit (FAU) 2) Moment Actuation Unit
(MAU)
% 3) Centralized Actuation (CA).  There are a total of 147 airframe
% Actuation Units (FAU or MAU) and 8 CA at the main rotor/airframe
interface.
% The computation method assumes a linear global model of the
airframe.
%
%************ Variable names/definitions **************
%  Z = Zo + [T]*u
%  Z = 3 tranlational vibrations (acceleration) at airframe nodes
```

Program to formulate a Transfer Function model

```
%      (complex output vector)
%  Zo = uncontrolled vibration level due to vibratory hub loads
%  u = actuation input vector (complex - magnitude & phase)
%  T = Transfer Function Matrix (complex)
%
%  [TFF1] = Complex Transfer Function matrix between actuation input &
output.
%           Output being the complex disp. response for each airframe
d.o.f.
%           (3 tranlational & 3 Rotational).
%
%  [TFF2] = Complex Transfer Function matrix between actuation input &
output.
%           Output being a complex vector of the translational (x,y,z)
%           accelerations at each airframe node.
%
%***************** Revisions/comments *****************
% Revision 1/7/00 - Added moment arm matrix for inputs so
%                    that input loads have consistent units [lbs.]
% Revision 1/11/00 - Removal of specific actuators (reduced from 218
to 155)
%*********************************************************

clear             % Clears all variables from computer memory
omega=30.264;     % rotor speed [rad/s]
w=4*omega;        % excitation frequency
eta=1.17966;      % Vertical Stabilizer angle [radians]=67.589 degrees
gees=(w^2)/386.4; % conversion factor to accel. in G's
% Note: acceleration = w^2 * displacement

% Load state space equations and mode shapes
% for the helicopter airframe model.
%************************************
load statemod.mat

% Define system output matrix "y=C1*z+D1*u"
% for system translational & rotational
% displacement response.
%****************************************
C1(1:Ng,1:N)=phi;
C1(1:Ng,N+1:2*N)=zeros(Ng,N);
D1=zeros(Ng,Ng);

% Define transformation matrix to extract
% the x,y,z translational response
% where C2=psi*C1.
%****************************************
psi=zeros(Ng/2,Ng);
for i=1:(Ng/6)
  j=6*(i-1)+1;
  ii=3*(i-1)+1;
```

Program to formulate a Transfer Function model

```
  psi(ii,j)=1;
  psi(ii+1,j+1)=1;
  psi(ii+2,j+2)=1;
end
%**********************************

disp('Wait, the program is working.')
disp('Computing the frequency responses')

% Compute frequency response for all 6
% inputs at each airframe node.
%**********************************
[mag1,phase1]=bode(A,B,C1,D1,[1:1:Ng],w);
for i=1:Ng
   mag(i,:)=mag1(((i-1)*Ng+1):(i*Ng));
   phase(i,:)=phase1(((i-1)*Ng+1):(i*Ng));
end
%**********************************

% Define the Actuation Unit topology
%*****************************
% Atop(i,1 or 2)= j;   i=Actuation Unit number, j=global d.o.f.
Atop(1,1)=43;   Atop(1,2)=49;   Atop(2,1)=47;   Atop(2,2)=53;
   Atop(3,1)=48;   Atop(3,2)=54;
Atop(4,1)=49;   Atop(4,2)=55;   Atop(5,1)=53;   Atop(5,2)=59;
Atop(6,1)=54;   Atop(6,2)=60;
Atop(7,1)=55;   Atop(7,2)=61;   Atop(8,1)=59;   Atop(8,2)=65;
   Atop(9,1)=60;   Atop(9,2)=66;
Atop(10,1)=61;  Atop(10,2)=67;  Atop(11,1)=65;  Atop(11,2)=71;
Atop(12,1)=66;  Atop(12,2)=72;
Atop(13,1)=67;  Atop(13,2)=79;  Atop(14,1)=71;  Atop(14,2)=83;
Atop(15,1)=72;  Atop(15,2)=84;
Atop(16,1)=79;  Atop(16,2)=85;  Atop(17,1)=83;  Atop(17,2)=89;
Atop(18,1)=84;  Atop(18,2)=90;
Atop(19,1)=85;  Atop(19,2)=91;  Atop(20,1)=89;  Atop(20,2)=95;
Atop(21,1)=90;  Atop(21,2)=96;
Atop(22,1)=91;  Atop(22,2)=121;  Atop(23,1)=95;  Atop(23,2)=125;
Atop(24,1)=96;  Atop(24,2)=126;
Atop(25,1)=121;  Atop(25,2)=127;  Atop(26,1)=125;  Atop(26,2)=131;
Atop(27,1)=126;  Atop(27,2)=132;
Atop(28,1)=127;  Atop(28,2)=133;  Atop(29,1)=131;  Atop(29,2)=137;
Atop(30,1)=132;  Atop(30,2)=138;
Atop(31,1)=133;  Atop(31,2)=139;  Atop(32,1)=137;  Atop(32,2)=143;
Atop(33,1)=138;  Atop(33,2)=144;
Atop(34,1)=139;  Atop(34,2)=145;  Atop(35,1)=143;  Atop(35,2)=149;
Atop(36,1)=144;  Atop(36,2)=150;
Atop(37,1)=145;  Atop(37,2)=151;  Atop(38,1)=149;  Atop(38,2)=155;
Atop(39,1)=150;  Atop(39,2)=156;
Atop(40,1)=151;  Atop(40,2)=169;  Atop(41,1)=155;  Atop(41,2)=173;
Atop(42,1)=156;  Atop(42,2)=174;
Atop(43,1)=169;  Atop(43,2)=175;  Atop(44,1)=173;  Atop(44,2)=179;
```

Program to formulate a Transfer Function model

```
Atop(45,1)=174;  Atop(45,2)=180;
Atop(46,1)=175;  Atop(46,2)=73;   Atop(47,1)=179;  Atop(47,2)=77;
Atop(48,1)=180;  Atop(48,2)=78;
Atop(49,1)=182;  Atop(49,2)=188;  Atop(50,1)=184;  Atop(50,2)=190;
Atop(51,1)=186;  Atop(51,2)=192;
Atop(52,1)=236;  Atop(52,2)=242;  Atop(53,1)=238;  Atop(53,2)=244;
Atop(54,1)=240;  Atop(54,2)=246;
Atop(55,1)=73;   Atop(55,2)=289;  Atop(56,1)=77;   Atop(56,2)=293;
Atop(57,1)=78;   Atop(57,2)=294;
Atop(58,1)=289;  Atop(58,2)=295;  Atop(59,1)=293;  Atop(59,2)=299;
Atop(60,1)=294;  Atop(60,2)=300;
Atop(61,1)=295;  Atop(61,2)=313;  Atop(62,1)=299;  Atop(62,2)=317;
Atop(63,1)=300;  Atop(63,2)=318;
Atop(64,1)=313;  Atop(64,2)=331;  Atop(65,1)=317;  Atop(65,2)=335;
Atop(66,1)=318;  Atop(66,2)=336;
Atop(67,1)=331;  Atop(67,2)=337;  Atop(68,1)=335;  Atop(68,2)=341;
Atop(69,1)=336;  Atop(69,2)=342;
Atop(70,1)=337;  Atop(70,2)=343;  Atop(71,1)=341;  Atop(71,2)=347;
Atop(72,1)=342;  Atop(72,2)=348;
Atop(73,1)=343;  Atop(73,2)=349;  Atop(74,1)=347;  Atop(74,2)=353;
Atop(75,1)=348;  Atop(75,2)=354;
Atop(76,1)=349;  Atop(76,2)=355;  Atop(77,1)=353;  Atop(77,2)=359;
Atop(78,1)=354;  Atop(78,2)=360;
Atop(79,1)=355;  Atop(79,2)=361;  Atop(80,1)=359;  Atop(80,2)=365;
Atop(81,1)=360;  Atop(81,2)=366;
Atop(82,1)=361;  Atop(82,2)=367;  Atop(83,1)=365;  Atop(83,2)=371;
Atop(84,1)=366;  Atop(84,2)=372;
Atop(85,1)=367;  Atop(85,2)=373;  Atop(86,1)=371;  Atop(86,2)=377;
Atop(87,1)=372;  Atop(87,2)=378;
Atop(88,1)=373;  Atop(88,2)=379;  Atop(89,1)=377;  Atop(89,2)=383;
Atop(90,1)=378;  Atop(90,2)=384;
Atop(91,1)=379;  Atop(91,2)=385;  Atop(92,1)=383;  Atop(92,2)=389;
Atop(93,1)=384;  Atop(93,2)=390;
Atop(94,1)=385;  Atop(94,2)=391;  Atop(95,1)=389;  Atop(95,2)=395;
Atop(96,1)=390;  Atop(96,2)=396;
Atop(97,1)=391;  Atop(97,2)=397;  Atop(98,1)=395;  Atop(98,2)=401;
Atop(99,1)=396;  Atop(99,2)=402;
Atop(100,1)=397;  Atop(100,2)=403;  Atop(101,1)=401;  Atop(101,2)=407;
Atop(102,1)=402;  Atop(102,2)=408;
Atop(103,1)=403;  Atop(103,2)=409;  Atop(104,1)=407;  Atop(104,2)=413;
Atop(105,1)=408;  Atop(105,2)=414;
Atop(106,1)=409;  Atop(106,2)=415;  Atop(107,1)=413;  Atop(107,2)=419;
Atop(108,1)=414;  Atop(108,2)=420;
Atop(109,1)=415;  Atop(109,2)=421;  Atop(110,1)=419;  Atop(110,2)=425;
Atop(111,1)=420;  Atop(111,2)=426;
Atop(112,1)=421;  Atop(112,2)=427;  Atop(113,1)=425;  Atop(113,2)=431;
Atop(114,1)=426;  Atop(114,2)=432;
Atop(115,1)=427;  Atop(115,2)=433;  Atop(116,1)=431;  Atop(116,2)=437;
Atop(117,1)=432;  Atop(117,2)=438;
Atop(118,1)=433;  Atop(118,2)=439;  Atop(119,1)=437;  Atop(119,2)=443;
Atop(120,1)=438;  Atop(120,2)=444;
```

Program to formulate a Transfer Function model

```
Atop(121,1)=439;  Atop(121,2)=445;  Atop(122,1)=443;  Atop(122,2)=449;
Atop(123,1)=444;  Atop(123,2)=450;
Atop(124,1)=445;  Atop(124,2)=451;  Atop(125,1)=449;  Atop(125,2)=455;
Atop(126,1)=450;  Atop(126,2)=456;
Atop(127,1)=451;  Atop(127,2)=457;  Atop(128,1)=455;  Atop(128,2)=461;
Atop(129,1)=456;  Atop(129,2)=462;
Atop(130,1)=457;  Atop(130,2)=463;  Atop(131,1)=461;  Atop(131,2)=467;
Atop(132,1)=462;  Atop(132,2)=468;
Atop(133,1)=463;  Atop(133,2)=469;  Atop(134,1)=467;  Atop(134,2)=473;
Atop(135,1)=468;  Atop(135,2)=474;
Atop(136,1)=518;  Atop(136,2)=524;  Atop(137,1)=520;  Atop(137,2)=526;
Atop(138,1)=522;  Atop(138,2)=528;
Atop(139,1)=536;  Atop(139,2)=542;  Atop(140,1)=538;  Atop(140,2)=544;
Atop(141,1)=540;  Atop(141,2)=546;

% Actuators in vertical stabilizer
Atop(142,1)=479;  Atop(142,2)=503;  Atop(143,1)=503;  Atop(143,2)=497;
Avfin(1,1)=493; Avfin(1,2)=499; Avfin(1,3)=495; Avfin(1,4)=501;
Avfin(2,1)=499; Avfin(2,2)=475; Avfin(2,3)=501; Avfin(2,4)=477;
Avfin(3,1)=498; Avfin(3,2)=504; Avfin(3,3)=496; Avfin(3,4)=502;
Avfin(4,1)=504; Avfin(4,2)=480; Avfin(4,3)=502; Avfin(4,4)=478;

% Centralized actuators
Ac(1,1)=301; Ac(1,2)=13; Ac(1,3)=302; Ac(1,4)=14; Ac(1,5)=303;
Ac(1,6)=15;
Ac(2,1)=301; Ac(2,2)=1;  Ac(2,3)=302; Ac(2,4)=2;  Ac(2,5)=303;
Ac(2,6)=3;
Ac(3,1)=157; Ac(3,2)=1;  Ac(3,3)=158; Ac(3,4)=2;  Ac(3,5)=159;
Ac(3,6)=3;
Ac(4,1)=157; Ac(4,2)=7;  Ac(4,3)=158; Ac(4,4)=8;  Ac(4,5)=159;
Ac(4,6)=9;
Ac(5,1)=163; Ac(5,2)=7;  Ac(5,3)=164; Ac(5,4)=8;  Ac(5,5)=165;
Ac(5,6)=9;
Ac(6,1)=163; Ac(6,2)=19; Ac(6,3)=164; Ac(6,4)=20; Ac(6,5)=165;
Ac(6,6)=21;
Ac(7,1)=307; Ac(7,2)=19; Ac(7,3)=308; Ac(7,4)=20; Ac(7,5)=309;
Ac(7,6)=21;
Ac(8,1)=307; Ac(8,2)=13; Ac(8,3)=308; Ac(8,4)=14; Ac(8,5)=309;
Ac(8,6)=15;
Dcos(1,1)=0.3316;  Dcos(1,2)=0.6307;  Dcos(1,3)=-0.7016;
Dcos(2,1)=0.7135;  Dcos(2,2)=0.2536;  Dcos(2,3)=-0.6532;
Dcos(3,1)=-0.7022; Dcos(3,2)=0.2577;  Dcos(3,3)=-0.6637;
Dcos(4,1)=-0.3509; Dcos(4,2)=0.6602;  Dcos(4,3)=-0.6641;
Dcos(5,1)=-0.3509; Dcos(5,2)=-0.6602; Dcos(5,3)=-0.6641;
Dcos(6,1)=-0.7022; Dcos(6,2)=-0.2577; Dcos(6,3)=-0.6637;
Dcos(7,1)=0.7135;  Dcos(7,2)=-0.2536; Dcos(7,3)=-0.6532;
Dcos(8,1)=0.3316;  Dcos(8,2)=-0.6307; Dcos(8,3)=-0.7016;
%********************

disp('Computing transfer function matrices')
% Compute transfer function for each Actuation Unit
```

Program to formulate a Transfer Function model

```
% ********************************************
TFF1=zeros(Ng,155);
TFF2=zeros(Ng/2,155);
i=sqrt(-1);
for jjj=1:143
  Z=zeros(1,Ng);
  for jj=1:2
   ang=(pi/180)*phase(Atop(jjj,jj),:); % convert to radians
   ang=ang-((jj-1)*pi*ones(1,Ng));
   Z=Z+((mag(Atop(jjj,jj),:)).*(exp(i*ang)));   % make complex vector
& sum
  end
  TFF1(:,jjj)=Z.';      % magnitude of summed frequency response
end
% ************************************

% Compute transfer function for each Actuation Unit in vertical
stabilizer
%
**************************************************************************
*
% Axial force actuators
i=sqrt(-1);
ang=zeros(1,Ng);
ang2=zeros(1,Ng);
ang3=zeros(1,Ng);
for iii=1:2
  Z1=zeros(1,Ng);
  Z2=zeros(1,Ng);
  for ii=1:2
   ang=(pi/180)*phase(Avfin(iii,ii),:);   % convert to radians
   ang=ang-((ii-1)*pi*ones(1,Ng));
   Z1=Z1+((mag(Avfin(iii,ii),:)).*(exp(i*ang)));   % make complex
vector & sum

   ang2=(pi/180)*phase(Avfin(iii,ii+2),:);   % convert to radians
   ang2=ang2-((ii-1)*pi*ones(1,Ng));
   Z2=Z2+((mag(Avfin(iii,ii+2),:)).*(exp(i*ang2)));   % make complex
vector & sum
  end
  Z=(cos(eta).*(Z1))+(sin(eta).*(Z2));
  TFF1(:,(143+iii))=Z.';         % magnitude of summed frequency
response
end
% Lateral bending moment actuators
i=sqrt(-1);
for iii=3:4
  Z1=zeros(1,Ng);
  Z2=zeros(1,Ng);
  for ii=1:2
   ang=(pi/180)*phase(Avfin(iii,ii),:);   % convert to radians
```

Program to formulate a Transfer Function model

```
   ang=ang-((ii-1)*pi*ones(1,Ng));
   Z1=Z1+((mag(Avfin(iii,ii),:)).*(exp(i*ang)));   % make complex
vector & sum

   ang2=(pi/180)*phase(Avfin(iii,ii+2),:);   % convert to radians
   ang2=ang2-((ii-1)*pi*ones(1,Ng));
   Z2=Z2+((mag(Avfin(iii,ii+2),:)).*(exp(i*ang2)));   % make complex
vector & sum
  end
  Z=((sin(eta).*(Z2)-cos(eta).*(Z1)));
  TFF1(:,(143+iii))=Z.';          % magnitude of summed frequency
response
end
% ************************************************************

% Compute transfer function for each actuation pair in centralized
configuration
%
**********************************************************************
*******
i=sqrt(-1);
for iii=1:8
  Z1=zeros(1,Ng);
  Z2=zeros(1,Ng);
  Z3=zeros(1,Ng);
  for ii=1:2
   ang=(pi/180)*phase(Ac(iii,ii),:);   % convert to radians
   ang=ang-((ii-1)*pi*ones(1,Ng));
   Z1=Z1+((mag(Ac(iii,ii),:)).*(exp(i*ang)));   % make complex vector
& sum

   ang2=(pi/180)*phase(Ac(iii,ii+2),:);   % convert to radians
   ang2=ang2-((ii-1)*pi*ones(1,Ng));
   Z2=Z2+((mag(Ac(iii,ii+2),:)).*(exp(i*ang2)));   % make complex
vector & sum

   ang3=(pi/180)*phase(Ac(iii,ii+4),:);   % convert to radians
   ang3=ang3-((ii-1)*pi*ones(1,Ng));
   Z3=Z3+((mag(Ac(iii,ii+4),:)).*(exp(i*ang3)));   % make complex
vector & sum
  end
  Z=((Dcos(iii,1)).*(Z1))+((Dcos(iii,2)).*(Z2))+((Dcos(iii,3)).*(Z3));
  TFF1(:,(147+iii))=Z.';          % magnitude of summed frequency
response
end
% ************************************************************
TFF2=gees*(psi*TFF1); % Transfer function for output of x,y,z
translational components

% Save transfer function matrices
% to binary output file "tfmodel.mat".
```

Program to formulate a Transfer Function model

```
%*******************************************
disp('Saving transfer function model matrices to file "tfmodel.mat"')
save tfmodel TFF1 TFF2
%***************** End of File ************************
```

Coupled optimal control and optimization program

```
% This MATLAB program is part of a computer software package for
% helicopter vibration analysis, active vibration control, and
optimized
% actuator placement studies.
%
% Written by: David E. Heverly II                          8/31/99
%             Mechanical Engineering Ph.D. Candidate
%             The Pennsylvania State University
%*********************************************************
% Filename = saoptim.m
%*********************************************************
%
% Hybrid optimization routine: Simulated Annealing + Active Control
%
% The program is a coupled optimal control (actuation effort) and
% passive (actuation placement) optimization routine. A standard
% Simulated Annealing optimization algorithm is modified to
% incorporate the active control computation. The main program
% is a general-purpose format code, and makes calls to user
% supplied subroutines for objective function evaluation, new
% trial designs, and an uncontrolled vibration response vector.
%
%***************** Variable names/definitions ******************
%
%  n =     number of design variables
%  x =     vector (length n) of design variables (Actuation Unit No.)
%  xp =    vector (length n) of trial design variables
%  xopt = optimal vector of design variables
%  f =     objective function value (scalar) to be minimized
%  fp =   objective function value of trial design
%  fopt = optimal objective function
%  T =     temperature parameter to control acceptance probability
%  step = vector (length n) new design step size
%  smax = vector (length n) of maximum step size
%  smin = vector (length n) of minimum step size
%  eps =  termination criteriion on objective function (% change)
%  Neps = number of temperature reductions to test for termination
%  Ns =   number of iterations to test for step size adjustment
```

Coupled optimal control and optimization program

```
%  c =    scalar step size variation criterion
%  Nt =   number of cycles for temperature reduction
%  rt =   temperature reduction coefficient
%  h =    index denoting coordinate direction h=1,2, ... ,n
%  i =    index of successive trial designs
%  j =    index of successive cycles along every coordinate direction
*
%  k =    index of successive temperature reductions
%  m =    index of successive step size adjustments
%  nu =   vector (length n) of accepted trial designs for each
variable *
%  fstr = vector (length Neps) of past function values for termination
*
%  maxtry = maximum number of trial designs before termination
%
%
%  ucvibs = user supplied subroutine that computes the uncontrolled
*
%           vibration response, which is sent to "funcn"
*
%
%  trial = user supplied subroutine that randomly generates a feasible
*
%          set of design variables: Syntax is: "xp=trial(x,h,step(h))"
%
%  funcn = user supplied subroutine that computes and returns the
*
%          objective function for given set of design variables:
%          Syntax is:  "fp=funcn(xp)"
%*****************************************************************
***

% Initialize parameters
clear
n=8;
eps=1e-3;
Neps=3;
Ns=10;
Nt=5;
c=2;
rt=0.85;
i=1; j=0; k=1; m=0; h=1;
maxtry=100000;
wuu=1e-10;     % Control effort weighting

% Compute uncontrolled vibration
zo=ucvibs(0);     % Hub Loading Only
%zo=ucvibs(1);    % Hub & Tail Loading

% Initial guess of Actuation Unit Numbers
x=[148; 149; 150; 151; 152; 153; 154; 155];  % Centralized Actuation
```

Coupled optimal control and optimization program

```
% Initialize parameters
xopt=x;
f=funcn(x,zo,wuu);
fopt=f;
T=1*fopt;
for ii=1:n
 nu(ii)=0;
 step(ii)=1000;
 smax(ii)=2000;
 smin(ii)=1;
end
for ii=1:Neps
 fstr(ii)=ii;
end

% Write current results to screen
disp('Opt. Func.       Func.       No. Iter.       Temp.')
disp('************************************************************')
disp([fopt,f,i,T])
disp('Current actuators')
disp('**********************')
disp([xopt(:)'])

while i<maxtry    % Beginning of while loop #1
  while m<Nt      % Beginning of while loop #2
    while j<Ns    % Beginning of while loop #3

%   Randomly perturb each design variable individually
      while h<=n     % Beginning of while loop #4
        xp=trial(x,h,step(h));   % Call "trial" to find new trial
design
        fp=funcn(xp,zo,wuu);  % Call "funcn" to compute objective
function
        dF=fp-f;

%       Accept new design if objective function decreases
        if dF<=0.0
          x=xp;
          f=fp;
          i=i+1;
          nu(h)=nu(h)+1;
          if fp<fopt
            xopt=xp;
            fopt=fp;
          end

%       Accept/Reject an increase based on probability
        else
          z=rand;
          p=exp(-dF/T);
```

Coupled optimal control and optimization program

```
          if z<p
            x=xp;
            f=fp;
            i=i+1;
            nu(h)=nu(h)+1;
          end
        end

        h=h+1;
      end   % End of while loop #4

      h=1;
      j=j+1;
    end     % End of while loop #3

%   Adjust step size for each design variable
    for jj=1:n
      if nu(jj)>(0.6*Ns)
        step(jj)=step(jj)*(1+c*(((nu(jj)/Ns)-0.6)/0.4));
      end
      if nu(jj)<(0.4*Ns)
        step(jj)=step(jj)/(1+c*((0.4-(nu(jj)/Ns))/0.4));
      end
      if step(jj)>smax(jj)
        step(jj)=smax(jj);
      end
      if step(jj)<smin(jj)
        step(jj)=smin(jj);
      end
    end
    j=0;
    m=m+1;
    for ii=1:n
      nu(ii)=0;
    end

  end % End of while loop #2

% Write current results to screen
disp('Opt. Func.       Func.       No. Iter.       Temp.')
disp('************************************************************')
disp([fopt,f,i,T])
disp('Current actuators')
disp('**********************')
disp([x(:)'])
disp('Optimal actuators')
disp('**********************')
disp([xopt(:)'])

% Reduce temperature for next cycle
  T=rt*T;
```

Coupled optimal control and optimization program

```
  k=k+1;
  fstr(1)=f;
  m=0;

% Check termination criteria
  gout=0;          % Flag to break out of loop
  for jj=1:Neps-1
    if (abs((fstr(jj)-fstr(jj+1))/fstr(jj))) <= eps
      gout=gout+1;
    end
  end
  if ((fstr(1)-fopt)/fopt) <= eps
    gout=gout+1;
  end
  if gout>=Neps
    disp('Converged: Objective function NOT changing')
    break
  end
  gout=0;
  for jj=Neps:-1:2
    fstr(jj)=fstr(jj-1);
  end

  i=i+1;
  x=xopt;
  f=fopt;
  if i>=maxtry
   disp('Program Stopped: Maximum number of trials reached')
   break
  end

end   % End of while loop #1

% Write final results to screen
disp('Opt. Func.     Control weighting       No. Iter.       Temp.')
disp('************************************************************')
disp([fopt,wuu,i,T])
disp('Optimal actuators')
disp('**********************')
disp([xopt(:)'])
%***************** End of File *************************
```

Subroutine for uncontrolled vibration response computation

```
function zo=ucvibs(flag)
%UCVIBS
%
% This MATLAB program is part of a computer software package for
% helicopter vibration analysis, active vibration control, and
optimized
% actuator placement studies.
%
% Written by: David E. Heverly II                              3/5/99
%             Mechanical Engineering Ph.D. Candidate
%             The Pennsylvania State University
%*********************************************************
% Filename = ucvibs.m
%*********************************************************
% The function m-file (subroutine) computes the uncontrolled vibratory
% response of the airframe model at the specified harmonic (4/rev).
%
%***************** Variable names/definitions ******************
%
%  Output:  zo = uncontrolled vibration response vector (complex)
%           both magnitude and phase for x,y,z directions
%
%        omega = fundamental frequency
%        flag = 0 ==> Hub only excitation
%        flag = 1 ==> Hub & Tail excitation
%
%*************************************************************

omega=30.264;  % rotor speed [rad/s]
w=4*omega;     % excitation and response frequency (4/rev)

%  Load state space equations and mode shapes
%  for the helicopter airframe model.
%***************************************
load statemod.mat

% Define the external excitation loads
%*************************************
if flag==1
  vdof=[25 26 27 28 29 531 532 533];   % Global dof of input
excitations
  Ne=length(vdof);      % No. of external excitations
  B2=zeros(2*N,Ne);     % State Space input matrix
  for i=1:Ne
    B2(:,i)=B(:,vdof(i));
  end

  % Excitation loads, magnitude and phase
  v(1)=185;       % Fx 4/rev hub load [lbs], Global dof #25
  theta(1)=0;     % phase angle [deg] of Fx
  v(2)=185;       % Fy 4/rev hub load [lbs] Global dof #26
```

Subroutine for uncontrolled vibration response computation

```
  theta(2)=90;    % phase angle [deg] of Fy
  v(3)=920;       % Fz 4/rev hub load [lbs] Global dof #27
  theta(3)=90;    % phase angle [deg] of Fz
  v(4)=920;       % Mx 4/rev hub load [in-lbs] Global dof #28
  theta(4)=90;    % phase angle [deg] of Mx
  v(5)=920;       % My 4/rev hub load [in-lbs] Global dof #29
  theta(5)=180;   % phase angle [deg] of My
  v(6)=250;       % Ftz 4/rev Tail load [lbs] Global dof #531
  theta(6)=-90;   % phase angle [deg] of Ftz
  v(7)=5400;      % Mtx 4/rev Tail load Global dof #532
  theta(7)=195;   % phase angle [deg] of Mtx
  v(8)=1300;      % Mty 4/rev Tail load Global dof #533
  theta(8)=130;   % phase angle [deg] of Mty
elseif flag==0
  vdof=[25 26 27 28 29];   % Global dof of input excitations
  Ne=length(vdof);         % No. of external excitations
  B2=zeros(2*N,Ne);        % State Space input matrix
  for i=1:Ne
    B2(:,i)=B(:,vdof(i));
  end

  % Excitation loads, magnitude and phase
  v(1)=185;       % Fx 4/rev hub load [lbs], Global dof #25
  theta(1)=0;     % phase angle [deg] of Fx
  v(2)=185;       % Fy 4/rev hub load [lbs] Global dof #26
  theta(2)=90;    % phase angle [deg] of Fy
  v(3)=920;       % Fz 4/rev hub load [lbs] Global dof #27
  theta(3)=90;    % phase angle [deg] of Fz
  v(4)=920;       % Mx 4/rev hub load [in-lbs] Global dof #28
  theta(4)=90;    % phase angle [deg] of Mx
  v(5)=920;       % My 4/rev hub load [in-lbs] Global dof #29
  theta(5)=180;   % phase angle [deg] of My
else
   disp('ERROR: Excitation condition NOT specified properly')
   disp('flag=0 ==> Hub loading')
   disp('flag=1 ==> Hub &Tail loading')
   pause
end
%*******************************

% Define system output matrix "y=C*z"
% for system translational displacement response
%*********************************
for i=1:(Ng/6)
  j=6*(i-1)+1;
  ii=3*(i-1)+1;
  psi(ii,1:N)=phi(j,1:N);
  psi(ii+1,1:N)=phi(j+1,1:N);
  psi(ii+2,1:N)=phi(j+2,1:N);
end
C(1:(Ng/2),1:N)=psi;
```

Subroutine for uncontrolled vibration response computation

```
C(1:(Ng/2),N+1:2*N)=zeros((Ng/2),N);
D1=zeros((Ng/2),Ne);
%**********************************

% Compute freq. response to each individual
% hub load and sum for total response.
%**************************************
[mag1,phase1]=bode(A,B2,C,D1,[1:1:Ne],w);
for ii=1:Ne
   mag(ii,:)=mag1(((ii-1)*(Ng/2)+1):(ii*(Ng/2)));
   phase(ii,:)=phase1(((ii-1)*(Ng/2)+1):(ii*(Ng/2)));
end
%**********************************
Z=zeros(1,(Ng/2));
i=sqrt(-1);
phase=(pi/180)*phase;      % convert to radians
for ii=1:Ne
 theta(ii)=theta(ii)*(pi/180);   % convert to radians
 Z=Z+(v(ii)*(mag(ii,:).*exp(i*(phase(ii,:)+theta(ii)))));   % make
complex vector & sum
end
gees=(w^2)/386.4;    % conversion factor to accel. in G's
zo=gees*(Z);         % magnitude & phase of total acceleration
frequency response
zo=zo.';             % Non-conjugate transpose
%***************** End of File ***************************
```

Subroutine to generate new trial design variable sets

```
function xp=trial(x,h,step)
%TRIAL
%
% This MATLAB program is part of a computer software package for
% helicopter vibration analysis, active vibration control, and
optimized
% actuator placement studies.
%
% Written by: David E. Heverly II                              8/31/99
%             Mechanical Engineering Ph.D. Candidate
%             The Pennsylvania State University
%*******************************************************
% Filename = trial.m
%*******************************************************
%
% Function m-file (subroutine) to randomly generate a new feasible
```

Subroutine to generate new trial design variable sets

```
% (within constraints) set of passive design variables (Actuation
% Unit locations).  Only one component of vector "x" is randomly
% varied for each call to "trial" all other components are fixed.
%
%************ Variable names/definitions **************
%  INPUTS:
%  x = vector of design variables
%  h = component index of vector "x" to be varied
%  step = step size variable
%  Constraint: 1 <= xp(h) <= 155
%
%  OUTPUT:
%  xp = new feasible design vector
%
%*********************************************************

out=1;
n=length(x);
iter=0;
while out>0.0
  out=0;
  xp=x;
% Generate random number between -1.0 and 1.0
  inc=(2*rand)-1;
  dX=step*inc;    % step size increment
  xp(h)=x(h)+round(dX); % New trial design variable

% Check constraints
  if xp(h)>155
    out=1;
  end
  if xp(h)<1
    out=1;
  end
  for i=1:n
    if i ~= h
      if xp(h)==xp(i)
        out=1;
      end
    end
  end

  iter=iter+1;
  if iter>20
    xp=x;
    break
  end
end
%***************** End of File *************************
```

Subroutine to compute the objective function for the optimization program

```
function fp=funcn(xp,zo,wuu)
%FUNCN
%
% This MATLAB program is part of a computer software package for
% helicopter vibration analysis, active vibration control, and
optimized
% actuator placement studies.
%
% Written by: David E. Heverly II                              8/31/99
%             Mechanical Engineering Ph.D. Candidate
%             The Pennsylvania State University
%*******************************************************
% Filename = funcn.m
%*******************************************************
%
% Function m-file (subroutine) to compute the objective function
% to be minimized by the Simulated Annealling optimization program.
%
%************ Variable names/definitions **************
%
% Global Model:   {z} = {zo} + [T]{u}
%
% Objective Function:   J = {z}'[Wz]{z} + {u}'[Wu]{u}+{p}'[Wp]{p}
%
% z = controlled vibration response
% zo = uncontrolled vibration response
% T = Transfer function between actuation inputs and response outputs
% u = vector of optimal actuation inputs
%
% z2 = controlled vibration response at target nodes
% zo2 = uncontrolled vibration response at target nodes
% T2 = Transfer function between for response at target nodes
%
% Wz = [I] = vibration response weighting matrix
% Wu = wuu*[I] = control effort weighting matrix
% Wp = [I] = penalty function weighting matrix
% p = penalty function vector (constraint violation)
%
%*******************************************************

%  Load the transfer function matrix
%  for the helicopter airframe model.
%**************************************
load tfmodel.mat
%**************************************
[m,n]=size(TFF2);
n=length(xp);

% Define transfer function matrix for
% actuator locations given in "xp"
%**************************************
```

Subroutine to compute the objective function for the optimization program

```
T=zeros(m,n);  % Initialize transfer function matrix
for i=1:n
  T(:,i)=TFF2(:,xp(i));
end

% Define transfer function matrix for
% actuator locations given in "xp"
% and output at target nodes for vibration suppression
%**************************************
rp=[8 11 13 14 21 24 26 53 59 62 68];  % Target nodes
m2=length(rp);
% Uncontrolled vibration response at target nodes
for i=1:m2
   for j=1:3
      zo2((3*(i-1)+j),1)=zo((3*(rp(i)-1)+j));
   end
end
% Transfer function for target nodes
T2=zeros(3*m2,n); % Initialize transfer function matrix
for i=1:n
   for j=1:m2
      for ii=1:3
         T2((3*(j-1)+ii),i)=T((3*(rp(j)-1)+ii),i);
      end
   end
end

% Define weighting matricies
Wu=wuu*eye(n);
Wz=eye(3*m2);

% Compute control inputs
u=((T2'*Wz*T2)+Wu)\(-(T2'*Wz*zo2));

% Compute response from transfer functions
z=zo+T*u;      % Controlled response at all airframe nodes
z2=zo2+T2*u;   % Controlled response at target nodes

% Compute penalty function
%**************************************
% Compute a vector sum of translational vibration components (x, y, z)
for i=1:(m/3)
 zz(i)=sqrt((abs(z(3*(i-1)+1)))^2+(abs(z(3*(i-1)+2)))^2+(abs(z(3*(i-
1)+3)))^2);
end

j=1;
for i=31:48    % check vibration magnitudes at nodes 31 thru 48
   p(j,1)=zz(i)/0.4; % Vibration level not to be exceeded = 0.4
   if p(j)<=1.0
      p(j)=0;
```

Subroutine to compute the objective function for the optimization program

```
   end
   j=j+1;
end
for i=82:93    % check vibration magnitudes at nodes 82 thru 93
   p(j,1)=zz(i)/1.7; % Vibration level not to be exceeded = 1.7
   if p(j)<=1.0
      p(j)=0;
   end
   j=j+1;
end
Wp=eye(length(p));   % Weighting matrix for penalty function

% Compute objective function
fp=abs(z2'*Wz*z2)+abs(u'*Wu*u)+(p'*Wp*p);
%***************** End of File *************************
```

Program to display and plot the optimization results

```
% This MATLAB program is part of a computer software package for
% helicopter vibration analysis, active vibration control, and
optimized
% actuator placement studies.
%
% Written by: David E. Heverly II                          8/31/99
%             Mechanical Engineering Ph.D. Candidate
%             The Pennsylvania State University
%*********************************************************
% Filename = plott1.m
%*********************************************************
%
% The program plots the frequency response of the Global linear
% helicopter airframe model. User inputs are the excitation
% condition, actuation locations/types, and the weighting
% on control effort.
%
%************ Variable names/definitions **************
%
% Global Model:   {z} = {zo} + [T]{u}
%
% Objective Function:   J = {z}'[Wz]{z} + {u}'[Wu]{u}+{p}'[Wp]{p}
%
% z = controlled vibration response
% zo = uncontrolled vibration response
% T = Transfer function between actuation inputs and response outputs
% u = vector of optimal actuation inputs
```

Program to display and plot the optimization results

```
%
% Wz = [I] = vibration response weighting matrix
% Wu = wuu*[I] = control effort weighting matrix
% Wp = [I] = penalty function weighting matrix
% p = penalty function vector (constraint violation)
%
% Input: xp - vector of Actuation Unit numbers
%        rp - vector of node numbers at target response locations
%        wuu - scale factor for control weighting matrix
%        flag = 0 ==> Hub only excitation
%        flag = 1 ==> Hub & Tail excitation
%
% Subroutines: ucvibs.m, funcn.m
%
%************************************************************

clear  % Clear variables from computer memory


%*********************************************
% User supplied information.
% Uncomment the appropriate variables
% to execute the desired analysis.
%*********************************************
%*********************************************

% Specify excitation condition
flag=0;     % Hub loads only
%flag=1;    % Hub & Tail loads

% Actuation Unit definitions for active control
%*********************************************
% Centralized Actuation (CA)
xp=[148 149 150 151 152 153 154 155];
wuu=4.32e-10;        % Control weighting for Hub excitation
%wuu=7.013e-10;      % Control weighting for Hub & Tail excitation

% Optimally distributed actuation Hub excitation condition
%xp=[8 41 45 47 149 150 151 152];   % Hub, Maximum control effort case
%wuu=1e-20;
%xp=[8 38 41 59 148 152 154 155];   % Hub, Vibration reduction similar
to CA
%wuu=1e-8;
%xp=[8 33 38 56 148 151 154 155];      % Hub, Intermediate case
%wuu=1e-10;

% Optimally distributed actuation Hub excitation condition
%xp=[8 38 45 47 129 152 154 155];   % Hub & Tail, Maximum control
effort case
%wuu=1e-20;
%xp=[8 38 41 142 151 152 154 155];  % Hub & Tail, Vibration reduction
```

Program to display and plot the optimization results

```
similar to CA
%wuu=2.5e-8;
%xp=[8 38 107 113 142 148 150 155]; % Hub & Tail Intermediate case
%wuu=2e-10;
%*********************************************
%*********************************************

% Display results to screen
if flag==0
   disp('Hub Excitation Condition')
   disp(' ')
end
if flag==1
   disp('Hub + Tail Excitation Condition')
   disp(' ')
end

%  Load the transfer function matrix
%  for the helicopter airframe model.
%***************************************
load tfmodel.mat
%***************************************
zo=ucvibs(flag); % Call subroutine to compute uncontrolled vibration
response
disp('Actuation Unit Numbers')   % Display results to screen
disp(xp)
[m,n]=size(TFF2);
n=length(xp);
Tp=zeros(m,n);
rp=[8 11 13 14 21 24 26 53 59 62 68];
% Display results to screen
disp('Response to be minimized at airframe target nodes')
disp(rp)
m2=length(rp);
Tp2=zeros(3*m2,n);
% Uncontrolled response at target nodes
for i=1:m2
   for j=1:3
      zoo((3*(i-1)+j),1)=zo((3*(rp(i)-1)+j));
   end
end

% Define transfer function matrices for
% actuator locations given in "xp"
for i=1:n
  Tp(:,i)=TFF2(:,xp(i));
  for j=1:m2
     for ii=1:3
        Tp2((3*(j-1)+ii),i)=TFF2((3*(rp(j)-1)+ii),xp(i));
     end
 end
```

Program to display and plot the optimization results

```
end

% Define weighting matricies
Wz=eye(3*m2);
Wu=wuu*eye(n);
% Display results to screen
disp(['Control weighting = ',num2str(wuu)])
disp(' ')

u=((Tp2'*Wz*Tp2)+Wu)\(-(Tp2'*Wz*zoo));

% Display results to screen
disp('Actuation Effort: Magnitude and Phase')
disp(u)

% Compute control effort for FAU's & MAU's
for i=1:n
  if xp(i)<=147
    % For FAU's & MAU's
    uuu(i)=(u(i))/2;
  else
    % For Centralized Actuation
    uuu(i)=u(i);
  end
end
maxx=max(abs(uuu));
% Display results to screen
disp('Actuation Effort Magnitude')
disp(abs(uuu))
disp(' ')
disp('Actuation Effort Phase')
disp((angle(u)*(180/pi))')
disp(' ')

% Compute controlled response from transfer functions
z=zo+Tp*u;     % response of all airframe nodes
z2=zoo+Tp2*u;  % response for nodes targeted for vibration suppression

% Compute vector sum of translational vibration components (x, y, z)
for i=1:(m/3)
 zzo(i)=sqrt((abs(zo(3*(i-1)+1)))^2+(abs(zo(3*(i-
1)+2)))^2+(abs(zo(3*(i-1)+3)))^2);
 zz(i)=sqrt((abs(z(3*(i-1)+1)))^2+(abs(z(3*(i-1)+2)))^2+(abs(z(3*(i-
1)+3)))^2);
end
for i=1:m2
 zz2(i,1)=sqrt((abs(z2(3*(i-1)+1)))^2+(abs(z2(3*(i-
1)+2)))^2+(abs(z2(3*(i-1)+3)))^2);
 zoo2(i,1)=sqrt((abs(zoo(3*(i-1)+1)))^2+(abs(zoo(3*(i-
1)+2)))^2+(abs(zoo(3*(i-1)+3)))^2);
end
```

Program to display and plot the optimization results

```
% Compute objective function
fopt=funcn(xp,zo,wuu);

% Display results to screen
disp(['Uncontrolled Vibration Index for target nodes =
',num2str(sqrt(abs((zoo2'*zoo2)/(3*m2))))])
disp(' ')
disp(['Controlled Vibration Index for target nodes =
',num2str(sqrt(abs((zz2'*zz2)/(3*m2))))])
disp(' ')
disp(['Control Index = ',num2str(sqrt(abs((uuu*uuu')/n)))])
disp(' ')
disp(['Max. Control Effort = ',num2str(maxx)])
disp(' ')
disp(['Objective function value = ',num2str(abs(fopt))])

% Plot response of uncontrolled system
%**********************************
figure
subplot(2,1,1)
stem(zzo,'ro','r-')
grid on
xlabel('Node Number')
ylabel('Acceleration [g]')
if flag==0
   axx=axis;
   axis([0 95 0 axx(4)])
   title(['Uncontrolled Response to 4/rev Hub Loads'])
end
if flag==1
   axx=axis;
   axis([0 95 0 axx(4)])
   title(['Uncontrolled Response to 4/rev Hub & Tail Loads'])
end
%**************************************

% Plot response of controlled system
%********************************************
subplot(2,1,2)
stem(zz,'ro','r-')
grid on
xlabel('Node Number')
ylabel('Acceleration [g]')
if flag==0
   axis([0 95 0 axx(4)])
   title(['Controlled Response to 4/rev Hub Loads'])
end
if flag==1
   axis([0 95 0 axx(4)])
   title(['Controlled Response to 4/rev Hub & Tail Loads'])
```

Program to display and plot the optimization results

```
end
%**************************************
%***************** End of File ************************
```

Appendix B

ADDITIONAL ACTUATION PLACEMENT RESULTS

Optimized Actuation Unit locations for hub and tail excitation, emphasizing control effort reduction.		
Actuation Unit Number	Location: Airframe Nodes	Applied Load
8	10-11	Pitch Moment
38	25-26	Pitch Moment
41	26-29	Pitch Moment
142	80-84	Pitch Moment
151	2-27	Axial Force
152	2-28	Axial Force
154	4-52	Axial Force
155	3-52	Axial Force

Optimized Actuation Unit locations for hub and tail excitation, emphasizing both vibration and control effort reduction.		
Actuation Unit Number	Location: Airframe Nodes	Applied Load
8	10-11	Pitch Moment
38	25-26	Pitch Moment
107	69-70	Pitch Moment
113	71-72	Pitch Moment
142	80-84	Pitch Moment
148	3-51	Axial Force
150	1-27	Axial Force
155	3-52	Axial Force

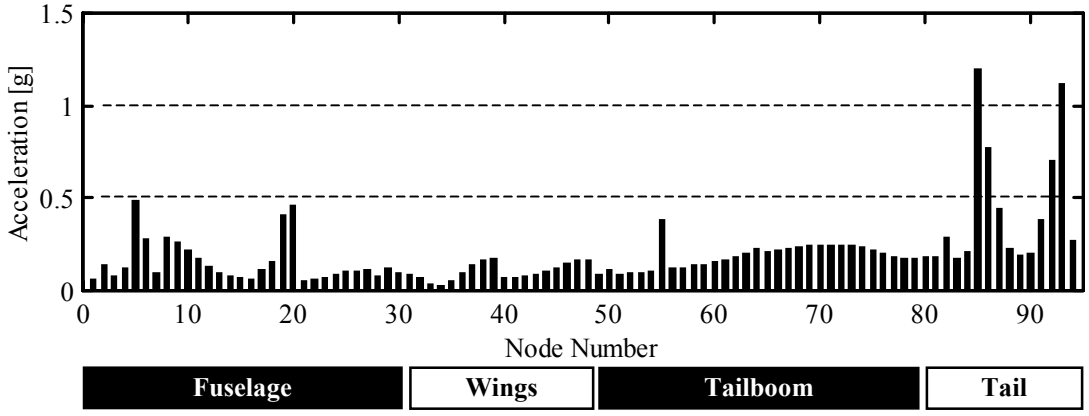

ROM: Uncontrolled airframe response to hub excitation

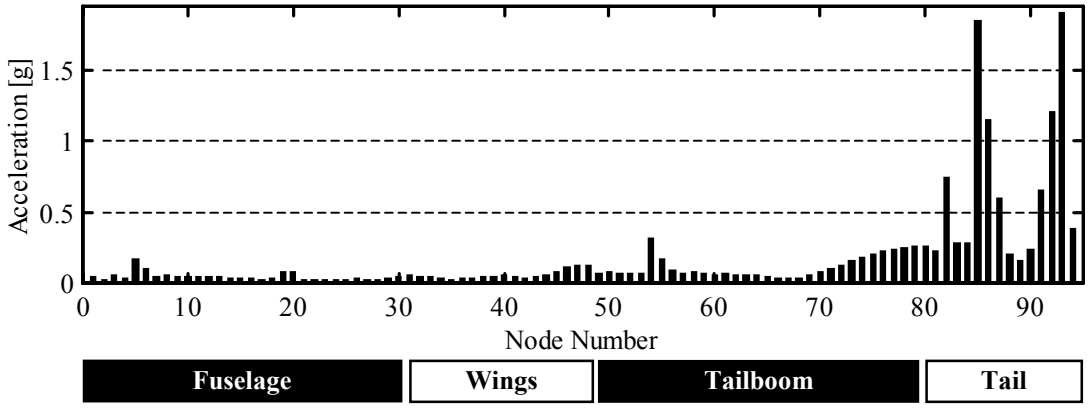

ROM: CAC controlled airframe response to hub excitation.

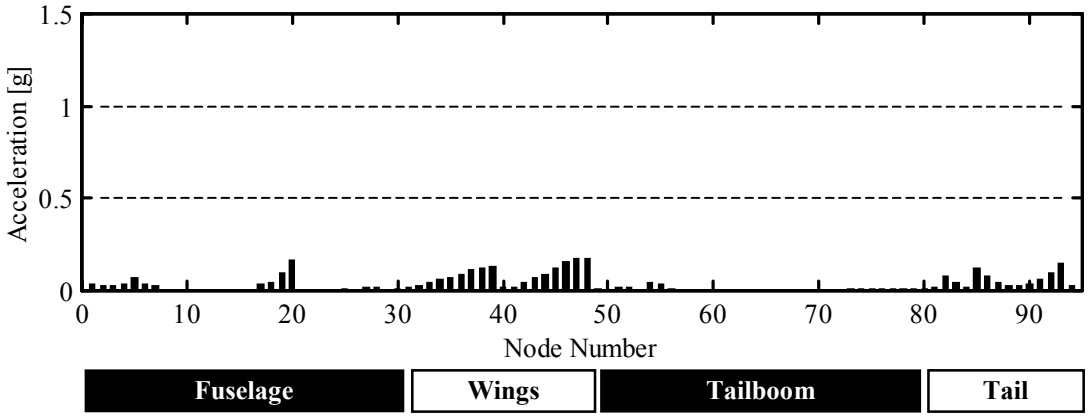

ROM: DAUC controlled airframe response to hub excitation.

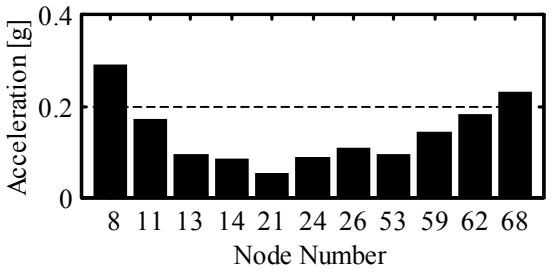

ROM: Uncontrolled vibration response at target nodes (hub excitation).

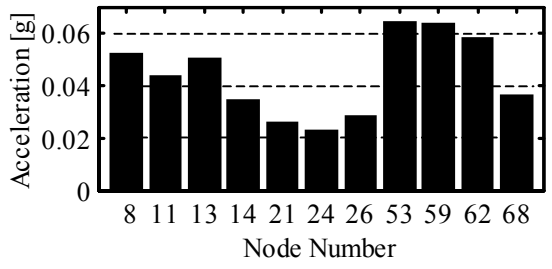

ROM: CAC controlled vibration response at target nodes (hub excitation).

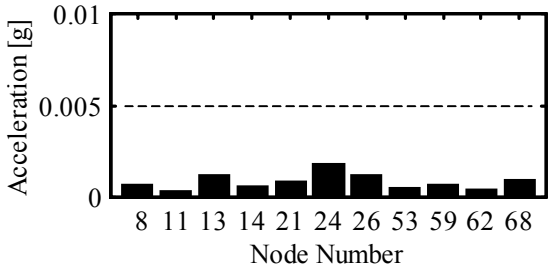

ROM: DAUC controlled vibration response at target nodes (hub excitation).

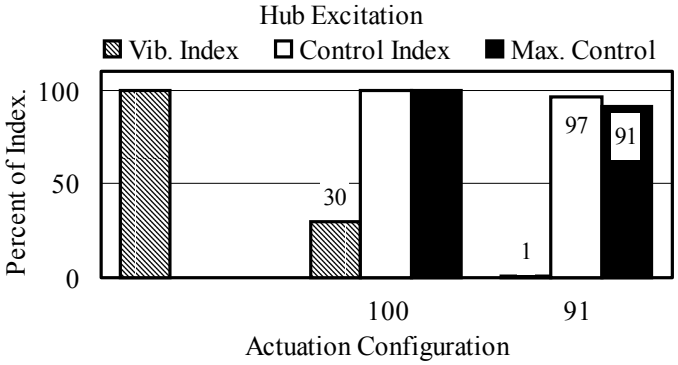

ROM: Optimized DAUC emphasizing vibration reduction.

Optimized Actuation Unit locations for hub excitation, emphasizing vibration reduction.		
Actuation Unit Number	Location: Airframe Nodes	Applied Load
8	10-11	Pitch Moment
41	26-29	Pitch Moment
45	29-30	Yaw Moment
47	31-13	Pitch Moment
149	1-51	Axial Force
150	1-27	Axial Force
151	2-27	Axial Force
152	2-28	Axial Force

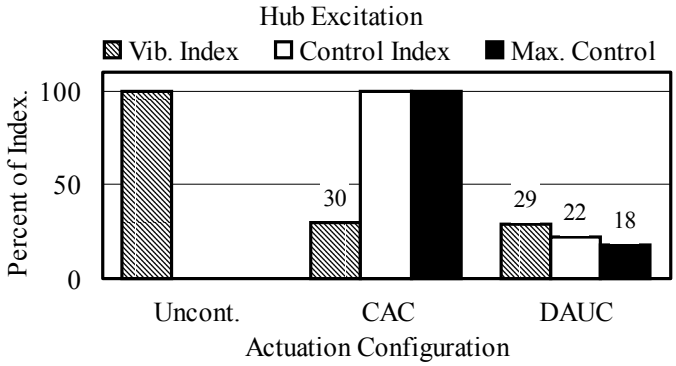

ROM: Optimized DAUC emphasizing control effort reduction.

Optimized Actuation Unit locations for hub excitation, emphasizing control effort reduction.		
Actuation Unit Number	Location: Airframe Nodes	Applied Load
8	10-11	Pitch Moment
38	25-26	Pitch Moment
41	26-29	Pitch Moment
59	49-50	Pitch Moment
148	3-51	Axial Force
152	2-28	Axial Force
154	4-52	Axial Force
155	3-52	Axial Force

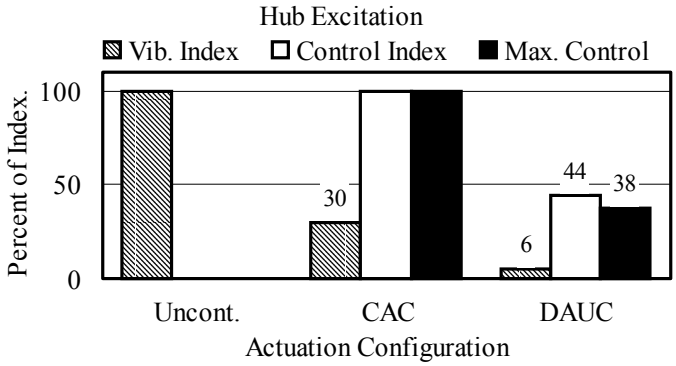

ROM: Optimized DAUC emphasizing both control effort and vibration reduction.

Optimized Actuation Unit locations for hub excitation, emphasizing both control effort and vibration reduction.		
Actuation Unit Number	Location: Airframe Nodes	Applied Load
8	10-11	Pitch Moment
33	23-24	Yaw Moment
38	25-26	Pitch Moment
56	13-49	Pitch Moment
148	3-51	Axial Force
151	2-27	Axial Force
154	4-52	Axial Force
155	3-52	Axial Force

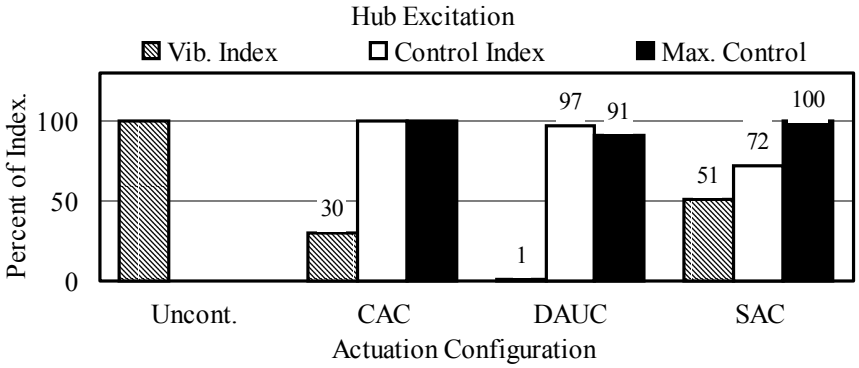

ROM: Evaluation indices for various actuation configurations.

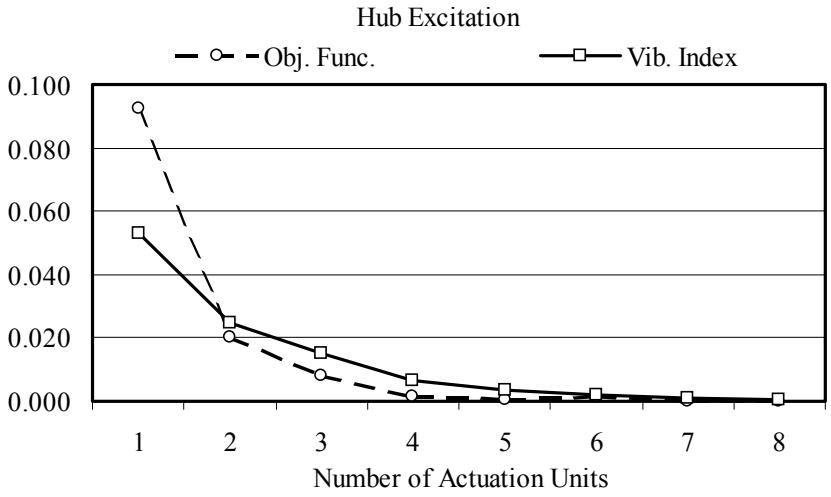

Optimization objective function and vibration index versus number of Actuation Units

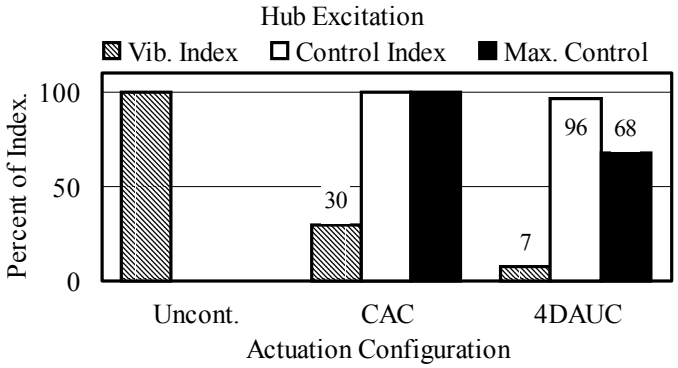

Evaluation indices of CAC and 4 optimally distributed Actuation Unit configuration

Actuation Unit Numbers = [8, 47, 152, 154]

Appendix C

DISTRIBUTED ACTUATION REALIZATION ANALYSIS RESULTS

Apache helicopter Nastran airframe model eigenvalue analysis results. The first 6 modes are rigid body modes, and modes 6 through 12 are very localized structure modes. The first global dynamic structural mode is number 13 at 4.145 [Hz].

Mode No.	Eigenvalue [rad^2/sec^2]	Radians [rad/sec]	Cycles [Hz]	Generalized Mass	Generalized Stiffness
1	2.9060E-09	5.3907E-05	8.5796E-06	1.0000E+00	2.9060E-09
2	3.9388E-09	6.2760E-05	9.9885E-06	1.0000E+00	3.9388E-09
3	8.8416E-09	9.4030E-05	1.4965E-05	1.0000E+00	8.8416E-09
4	5.7618E-07	7.5906E-04	1.2081E-04	1.0000E+00	5.7618E-07
5	2.2912E-06	1.5137E-03	2.4091E-04	1.0000E+00	2.2912E-06
6	1.0098E-05	3.1778E-03	5.0576E-04	1.0000E+00	1.0098E-05
7	1.3796E+02	1.1746E+01	1.8694E+00	1.0000E+00	1.3796E+02
8	1.5879E+02	1.2601E+01	2.0056E+00	1.0000E+00	1.5879E+02
9	1.8545E+02	1.3618E+01	2.1674E+00	1.0000E+00	1.8545E+02
10	1.8563E+02	1.3624E+01	2.1684E+00	1.0000E+00	1.8563E+02
11	1.9083E+02	1.3814E+01	2.1986E+00	1.0000E+00	1.9083E+02
12	1.9689E+02	1.4032E+01	2.2332E+00	1.0000E+00	1.9689E+02
13	678.416	26.046	4.145	1.000	678.416
14	735.769	27.125	4.317	1.000	735.769
15	761.384	27.593	4.392	1.000	761.384
16	963.244	31.036	4.940	1.000	963.244
17	982.474	31.344	4.989	1.000	982.474
18	1133.478	33.667	5.358	1.000	1133.478
19	1346.107	36.689	5.839	1.000	1346.107
20	1989.824	44.607	7.099	1.000	1989.824
21	2375.411	48.738	7.757	1.000	2375.411

Mode No.	Eigenvalue [rad^2/sec^2]	Radians [rad/sec]	Cycles [Hz]	Generalized Mass	Generalized Stiffness
22	2980.899	54.598	8.689	1.000	2980.899
23	3210.526	56.662	9.018	1.000	3210.526
24	3811.226	61.735	9.825	1.000	3811.226
25	5016.515	70.827	11.273	1.000	5016.515
26	5390.046	73.417	11.685	1.000	5390.046
27	6066.628	77.889	12.396	1.000	6066.628
28	6679.901	81.731	13.008	1.000	6679.901
29	6827.713	82.630	13.151	1.000	6827.713
30	7418.970	86.133	13.709	1.000	7418.970
31	7570.051	87.006	13.847	1.000	7570.051
32	8629.388	92.895	14.785	1.000	8629.388
33	9028.369	95.018	15.123	1.000	9028.369
34	9377.566	96.838	15.412	1.000	9377.566
35	9720.283	98.592	15.691	1.000	9720.283
36	9925.175	99.625	15.856	1.000	9925.175
37	10516.800	102.551	16.322	1.000	10516.800
38	11064.720	105.189	16.741	1.000	11064.720
39	11646.670	107.920	17.176	1.000	11646.670
40	12584.060	112.179	17.854	1.000	12584.060
41	14619.600	120.912	19.244	1.000	14619.600
42	15518.930	124.575	19.827	1.000	15518.930
43	15823.240	125.791	20.020	1.000	15823.240
44	17812.760	133.464	21.242	1.000	17812.760
45	18494.220	135.994	21.644	1.000	18494.220
46	19014.840	137.894	21.947	1.000	19014.840
47	20482.650	143.118	22.778	1.000	20482.650
48	21667.680	147.200	23.428	1.000	21667.680
49	22619.130	150.397	23.936	1.000	22619.130
50	22732.030	150.771	23.996	1.000	22732.030
51	22736.240	150.785	23.998	1.000	22736.240
52	23447.160	153.125	24.371	1.000	23447.160

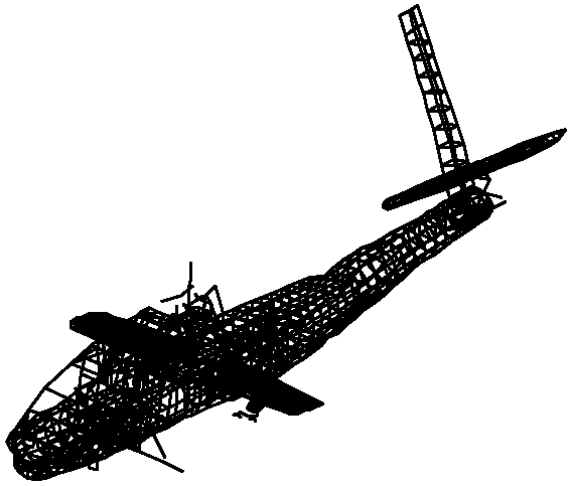

Nastran Model: Mode shape, Frequency = 4.15 [Hz], Tailboom torsion

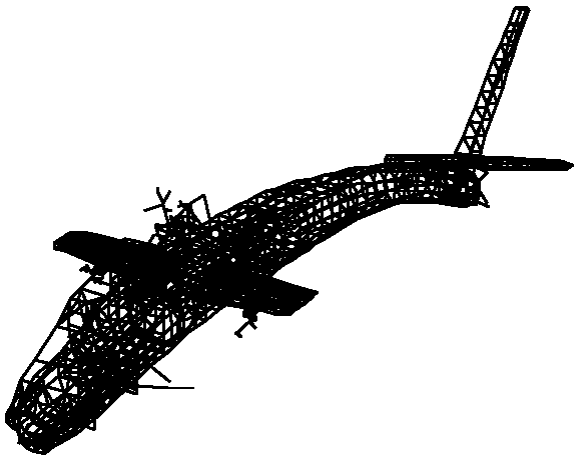

Nastran Model: Mode shape, Frequency = 5.36 [Hz], Vertical bending

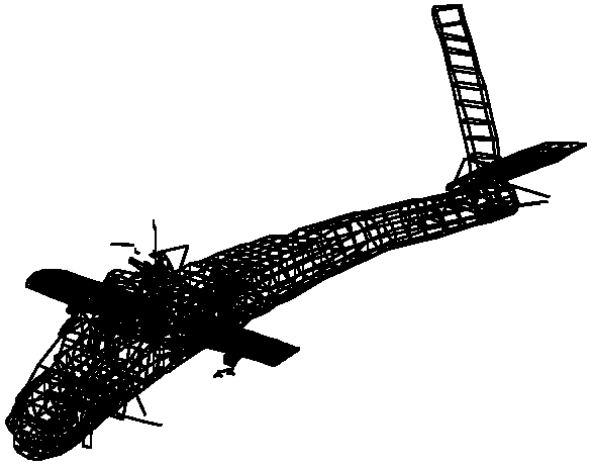

Nastran Model: Mode shape, Frequency = 8.69 [Hz], Lateral bending & torsion

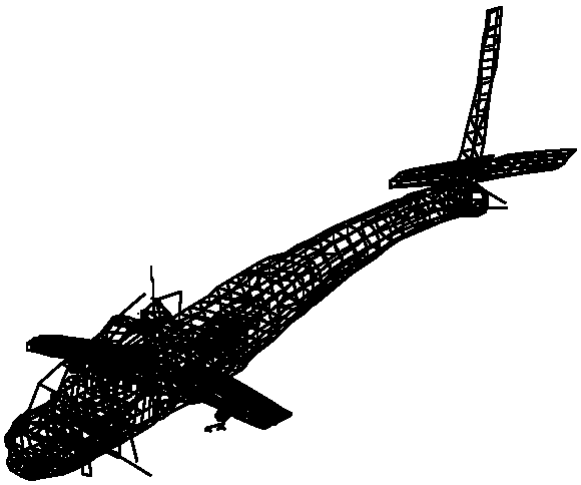

Nastran Model: Mode shape, Frequency = 9.83 [Hz], Second vertical bending

Definition of dual-point actuation applied to both airframe models					
Nastran FE Model			Reduced Order Model		
Actuation ID Label	Node No. Or Frame No.	Net Actuation Load	Actuation Unit Number	Model Node Numbers	Actuation Type
1	29, 23010	Force, *x,y,z*	148	3, 51	CA
2	5, 23010	Force, *x,y,z*	149	1, 51	CA
3	5, 17616	Force, *x,y,z*	150	1, 27	CA
4	18, 17616	Force, *x,y,z*	151	2, 27	CA
5	18, 17619	Force, *x,y,z*	152	2, 28	CA
6	41, 17619	Force, *x,y,z*	153	4, 28	CA
7	41, 23011	Force, *x,y,z*	154	4, 52	CA
8	29, 23011	Force, *x,y,z*	155	3, 52	CA
9	57, 69	Moment, *Y*	8	10, 11	MAU, *Y*
10	144, 154	Moment, *Z*	33	23, 24	MAU, *Z*
11	163, 176	Moment, *Y*	38	25, 26	MAU, *Y*
12	182, 188	Moment, *Y*	41	26, 29	MAU, *Y*
13	188, 199	Moment, *Z*	45	29, 30	MAU, *Z*
14	199, 214	Moment, *Y*	56	13, 49	MAU, *Y*
15	214, 230	Moment, *Y*	59	49, 50	MAU, *Y*
16	383, 396	Moment, *Y*	107	69, 70	MAU, *Y*
17	409, 423	Moment, *Y*	113	71, 72	MAU, *Y*
18	476, 489	Moment, *Z*	129	76, 77	MAU, *Z*
19	530, 547	Moment, *Y*	142	80, 84	MAU, *Y*

NASTRAN source code, sample of added command lines

```
$OOOOOOOOOOOOOOOOOOOOOOOOOOOOOOOOOOOOOOOOOOOOOOOOOOOOOOOOOOOOOOOOOOOOOOOOOOOOOOOOOOOOOOOOOOOOOOOOO
$OOOOOOOOOOOOOOOOOOOOOOOOOOOOOOOOOOOOOOOOOOOOOOOOOOOOOOOOOOOOOOOOOOOOOOOOOOOOOOOOOOOOOOOOOOOOOOOOO
$ THE FOLLOWING SECTIONS WERE ADDED BY DAVID HEVERLY ON 11/7/01
$
$ EXECUTIVE CONTROL DECK
$EEEEEEEEEEEEEEEEEEEEEEEEEEEEEEEEEEEEEEEEEEEEEEEEEEEEEEEEEEEEEEEEEEEEEEEEEEEEEEEEEEEEEEEEEEEEEEEEE
$000000100000002000000030000000400000005000000060000000700000008000000090000001O
ID DEH,AH64A
TIME 15
$ Dynamic analysis solution for dynamic excitation
$***********************************************
SOL 11
CEND
$EEEEEEEEEEEEEEEEEEEEEEEEEEEEEEEEEEEEEEEEEEEEEEEEEEEEEEEEEEEEEEEEEEEEEEEEEEEEEEEEEEEEEEEEEEEEEEEEE
$
$
$ CASE CONTROL DECK
$CCCCCCCCCCCCCCCCCCCCCCCCCCCCCCCCCCCCCCCCCCCCCCCCCCCCCCCCCCCCCCCCCCCCCCCCCCCCCCCCCCCCCCCCCCCCCCCCCC
TITLE=AH64A, Dynamic Analysis, Hub & Tail Loads
SUBTITLE=Distributed Control (Inter. Case), Element Stress
FREQUENCY=66631
MPC=10
METHOD=100
ECHO=NONE
SDAMPING=66611
DLOAD=66603
$
$ NASTRAN model grid points = Reduced Order Model (ROM) nodes
SET 66621=5,18,29,41,54,62,500,3499,4600,5700,6900,8000,9056,9101,10514,
          11501,12002,12004,12031,12032,12501,13501,14401,15400,16300,
         17600,17616,17619,18800,19900,20050,20051,20052,20053,20054,
         20055,20056,20057,20058,20060,20061,20062,20063,20064,20065,
         20066,20067,20068,21400,22999,23010,23011,23800,24000,24001,
         24700,25800,26900,28000,29000,30000,31000,32000,33000,34000,
         35000,36000,37000,38300,39600,40900,42300,43600,45000,46300,
         47600,48900,50300,51600,53000,54700,55401,55403,55404,56501,
         56502,56503,56504,56505,56506,56507,56508,56509,57004
$
$ NASTRAN model grid points = Reduced Order Model (ROM) target nodes
SET 66622=3499,6900,9056,9101,12501,15400,17600,23800,28000,
          31000,37000
$
$ Case 1 = Distributed control, response at all ROM nodes
SUBCASE 1
SUBTITLE=Distributed control, response at all ROM nodes
ACCELERATION=66621
$
$ Case 2 = Distributed control, response at target nodes
SUBCASE 2
SUBTITLE=Distributed control, response at target nodes
ACCELERATION=66622
```

NASTRAN source code, sample of added command lines

```
$
$ Case 3 = Dynamic stress for all elements
SUBCASE 3
SUBTITLE=Dynamic stress for all elements
ELSTRESS(PRINT,PHASE)=ALL
$
BEGIN BULK
$CCCCCCCCCCCCCCCCCCCCCCCCCCCCCCCCCCCCCCCCCCCCCCCCCCCCCCCCCCCCCCCCCCCCCCCCCCCCC
$
$ THE FOLLOWING SECTIONS WERE ADDED BY DAVID HEVERLY ON 11/7/01
$
$ BULK DATA DECK ADDITIONS
$BBBBBBBBBBBBBBBBBBBBBBBBBBBBBBBBBBBBBBBBBBBBBBBBBBBBBBBBBBBBBBBBBBBBBBBBBBBBB
$00000001000000020000000300000004000000050000000600000007000000080000000900000010
$
SUPORT        54  123456
EIGRL        100      4.      40.
INCLUDE AH64BULK.DATA
FREQ       66631   19.2
TABDMP1    66611    CRIT
             0.0   0.02   10.0+9   0.02     ENDT
$
$
$ This section is for the Hub & Tail loading condition
DLOAD      66601     1.0   185.0   77701   185.0   77702   920.0   77703 +DLHpT
+DLHpT     920.0   77704   920.0   77705    62.5   77706    62.5   77707 +DLHpT2
+DLHpT2   368.25   77708  368.25   77709   88.65   77710   88.65   77711
RLOAD1     77701   77751           77771   77901
RLOAD1     77702   77752           77772   77901
RLOAD1     77703   77753           77773   77901
RLOAD1     77704   77754           77774   77901
RLOAD1     77705   77755           77775   77901
RLOAD1     77706   77756           77776   77901
RLOAD1     77707   77757           77777   77901
RLOAD1     77708   77758           77778   77901
RLOAD1     77709   77759           77779   77901
RLOAD1     77710   77760           77780   77901
RLOAD1     77711   77761           77781   77901
DAREA      77751      54       1     1.0
DAREA      77752      54       2     1.0
DAREA      77753      54       3     1.0
DAREA      77754      54       4     1.0
DAREA      77755      54       5     1.0
DAREA      77756   56050       3     1.0   56051       3     1.0
DAREA      77757   56054       3     1.0   56055       3     1.0
DAREA      77758   56050       2    -1.0   56051       2     1.0
DAREA      77759   56054       2    -1.0   56055       2     1.0
DAREA      77760   56050       1     1.0   56051       1    -1.0
DAREA      77761   56054       1     1.0   56055       1    -1.0
DPHASE     77771      54       1     0.0
DPHASE     77772      54       2    90.0
```

NASTRAN source code, sample of added command lines

```
DPHASE    77773      54        3     0.0
DPHASE    77774      54        4    90.0
DPHASE    77775      54        5   180.0
DPHASE    77776   56050        3   270.0   56051       3   270.0
DPHASE    77777   56054        3   270.0   56055       3   270.0
DPHASE    77778   56050        2   195.0   56051       2   195.0
DPHASE    77779   56054        2   195.0   56055       2   195.0
DPHASE    77780   56050        1   130.0   56051       1   130.0
DPHASE    77781   56054        1   130.0   56055       1   130.0
TABLED1   77901                                                      +TB1
+TB1        0.0     1.0  10.0+9     1.0    ENDT
$
$
$ This section is for Centralized actuator control
$000000100000002000000030000000400000005000000060000000700000008000000090000001 0
$ Centralized Actuator 148
RLOAD1    78051   78101           78251   77901
RLOAD1    78052   78102           78252   77901
RLOAD1    78053   78103           78253   77901
RLOAD1    78054   78104           78254   77901
RLOAD1    78055   78105           78255   77901
RLOAD1    78056   78106           78256   77901
$ Centralized Actuator 149
RLOAD1    78057   78107           78257   77901
RLOAD1    78058   78108           78258   77901
RLOAD1    78059   78109           78259   77901
RLOAD1    78060   78110           78260   77901
RLOAD1    78061   78111           78261   77901
RLOAD1    78062   78112           78262   77901
$ Centralized Actuator 150
RLOAD1    78063   78113           78263   77901
RLOAD1    78064   78114           78264   77901
RLOAD1    78065   78115           78265   77901
RLOAD1    78066   78116           78266   77901
RLOAD1    78067   78117           78267   77901
RLOAD1    78068   78118           78268   77901
$ Centralized Actuator 151
RLOAD1    78069   78119           78269   77901
RLOAD1    78070   78120           78270   77901
RLOAD1    78071   78121           78271   77901
RLOAD1    78072   78122           78272   77901
RLOAD1    78073   78123           78273   77901
RLOAD1    78074   78124           78274   77901
$ Centralized Actuator 152
RLOAD1    78075   78125           78275   77901
RLOAD1    78076   78126           78276   77901
RLOAD1    78077   78127           78277   77901
RLOAD1    78078   78128           78278   77901
RLOAD1    78079   78129           78279   77901
RLOAD1    78080   78130           78280   77901
$ Centralized Actuator 153
```

NASTRAN source code, sample of added command lines

```
RLOAD1    78081   78131           78281   77901
RLOAD1    78082   78132           78282   77901
RLOAD1    78083   78133           78283   77901
RLOAD1    78084   78134           78284   77901
RLOAD1    78085   78135           78285   77901
RLOAD1    78086   78136           78286   77901
$ Centralized Actuator 154
RLOAD1    78087   78137           78287   77901
RLOAD1    78088   78138           78288   77901
RLOAD1    78089   78139           78289   77901
RLOAD1    78090   78140           78290   77901
RLOAD1    78091   78141           78291   77901
RLOAD1    78092   78142           78292   77901
$ Centralized Actuator 155
RLOAD1    78093   78143           78293   77901
RLOAD1    78094   78144           78294   77901
RLOAD1    78095   78145           78295   77901
RLOAD1    78096   78146           78296   77901
RLOAD1    78097   78147           78297   77901
RLOAD1    78098   78148           78298   77901
$
$ Centralized Actuator 148
DAREA     78101      29       1  -.3316
DAREA     78102      29       2  -.6307
DAREA     78103      29       3  0.7016
DAREA     78104   23010       1  0.3316
DAREA     78105   23010       2  0.6307
DAREA     78106   23010       3  -.7016
$ Centralized Actuator 149
DAREA     78107       5       1  -.7135
DAREA     78108       5       2  -.2536
DAREA     78109       5       3  0.6532
DAREA     78110   23010       1  0.7135
DAREA     78111   23010       2  0.2536
DAREA     78112   23010       3  -.6532
$ Centralized Actuator 150
DAREA     78113       5       1  0.7022
DAREA     78114       5       2  -.2577
DAREA     78115       5       3  0.6637
DAREA     78116   17616       1  -.7022
DAREA     78117   17616       2  0.2577
DAREA     78118   17616       3  -.6637
$ Centralized Actuator 151
DAREA     78119      18       1  0.3509
DAREA     78120      18       2  -.6602
DAREA     78121      18       3  0.6641
DAREA     78122   17616       1  -.3509
DAREA     78123   17616       2  0.6602
DAREA     78124   17616       3  -.6641
$ Centralized Actuator 152
DAREA     78125      18       1  0.3509
```

NASTRAN source code, sample of added command lines

```
DAREA     78126      18       2  0.6602
DAREA     78127      18       3  0.6641
DAREA     78128   17619       1  -.3509
DAREA     78129   17619       2  -.6602
DAREA     78130   17619       3  -.6641
$ Centralized Actuator 153
DAREA     78131      41       1  0.7022
DAREA     78132      41       2  0.2577
DAREA     78133      41       3  0.6637
DAREA     78134   17619       1  -.7022
DAREA     78135   17619       2  -.2577
DAREA     78136   17619       3  -.6637
$ Centralized Actuator 154
DAREA     78137      41       1  -.7135
DAREA     78138      41       2  0.2536
DAREA     78139      41       3  0.6532
DAREA     78140   23011       1  0.7135
DAREA     78141   23011       2  -.2536
DAREA     78142   23011       3  -.6532
$ Centralized Actuator 155
DAREA     78143      29       1  -.3316
DAREA     78144      29       2  0.6307
DAREA     78145      29       3  0.7016
DAREA     78146   23011       1  0.3316
DAREA     78147   23011       2  -.6307
DAREA     78148   23011       3  -.7016
$
$00000010000000200000003000000040000000500000006000000070000000800000009000000010
$ Centralized Actuator 148
DPHASE    78251      29       1     0.0
DPHASE    78252      29       2     0.0
DPHASE    78253      29       3     0.0
DPHASE    78254   23010       1     0.0
DPHASE    78255   23010       2     0.0
DPHASE    78256   23010       3     0.0
$ Centralized Actuator 149
DPHASE    78257       5       1   203.7
DPHASE    78258       5       2   203.7
DPHASE    78259       5       3   203.7
DPHASE    78260   23010       1   203.7
DPHASE    78261   23010       2   203.7
DPHASE    78262   23010       3   203.7
$ Centralized Actuator 150
DPHASE    78263       5       1     0.0
DPHASE    78264       5       2     0.0
DPHASE    78265       5       3     0.0
DPHASE    78266   17616       1     0.0
DPHASE    78267   17616       2     0.0
DPHASE    78268   17616       3     0.0
$ Centralized Actuator 151
DPHASE    78269      18       1   205.0
```

NASTRAN source code, sample of added command lines

```
DPHASE    78270      18       2   205.0
DPHASE    78271      18       3   205.0
DPHASE    78272   17616       1   205.0
DPHASE    78273   17616       2   205.0
DPHASE    78274   17616       3   205.0
$ Centralized Actuator 152
DPHASE    78275      18       1     0.0
DPHASE    78276      18       2     0.0
DPHASE    78277      18       3     0.0
DPHASE    78278   17619       1     0.0
DPHASE    78279   17619       2     0.0
DPHASE    78280   17619       3     0.0
$ Centralized Actuator 153
DPHASE    78281      41       1     0.0
DPHASE    78282      41       2     0.0
DPHASE    78283      41       3     0.0
DPHASE    78284   17619       1     0.0
DPHASE    78285   17619       2     0.0
DPHASE    78286   17619       3     0.0
$ Centralized Actuator 154
DPHASE    78287      41       1     0.0
DPHASE    78288      41       2     0.0
DPHASE    78289      41       3     0.0
DPHASE    78290   23011       1     0.0
DPHASE    78291   23011       2     0.0
DPHASE    78292   23011       3     0.0
$ Centralized Actuator 155
DPHASE    78293      29       1    43.4
DPHASE    78294      29       2    43.4
DPHASE    78295      29       3    43.4
DPHASE    78296   23011       1    43.4
DPHASE    78297   23011       2    43.4
DPHASE    78298   23011       3    43.4
$
$
$ This section is for distributed control - intermediate case
$00000010000000200000003000000040000005000000060000007000000080000009000000010
DLOAD     66603     1.0   185.0   77701   185.0   77702   920.0   77703 +DLIC1
+DLIC1    920.0   77704   920.0   77705    62.5   77706    62.5   77707 +DLIC2
+DLIC2   368.25   77708  368.25   77709   88.65   77710   88.65   77711 +DLIC3
+DLIC3   1575.0   78057  1575.0   78058  1575.0   78059  1575.0   78060 +DLIC4
+DLIC4   1575.0   78061  1575.0   78062   692.4   78069   692.4   78070 +DLIC5
+DLIC5    692.4   78071   692.4   78072   692.4   78073   692.4   78074 +DLIC6
+DLIC6   1127.0   78093  1127.0   78094  1127.0   78095  1127.0   78096 +DLIC7
+DLIC7   1127.0   78097  1127.0   78098   183.2   79017   183.2   79018 +DLIC8
+DLIC8    183.2   79019   183.2   79020   183.2   79021   183.2   79022 +DLIC9
+DLIC9    183.2   79023   183.2   79024   183.2   79025   183.2   79026 +DLIC10
+DLIC10   183.2   79027   183.2   79028   183.2   79029   183.2   79030 +DLIC11
+DLIC11   183.2   79031   183.2   79032  1294.5   79033  1294.5   79034 +DLIC12
+DLIC12  1294.5   79035  1294.5   79036  1294.5   79037  1294.5   79038 +DLIC13
+DLIC13  1294.5   79039  1294.5   79040  1294.5   79041  1294.5   79042 +DLIC14
```

NASTRAN source code, sample of added command lines

```
+DLIC14  1294.5   79043  1294.5   79044  1294.5   79045  1294.5   79046 +DLIC15
+DLIC15  1294.5   79047  1294.5   79048   425.9   79061   425.9   79062 +DLIC16
+DLIC16   425.9   79063   425.9   79064   425.9   79065   425.9   79066 +DLIC17
+DLIC17   425.9   79067   425.9   79068   425.9   79069   425.9   79070 +DLIC18
+DLIC18   425.9   79071   425.9   79072   425.9   79073   425.9   79074 +DLIC19
+DLIC19   425.9   79075   425.9   79076   425.9   79077   425.9   79078 +DLIC20
+DLIC20   425.9   79079   425.9   79080  2089.1   79081  2089.1   79082 +DLIC21
+DLIC21  2089.1   79083  2089.1   79084  2089.1   79085  2089.1   79086 +DLIC22
+DLIC22  2089.1   79087  2089.1   79088  2089.1   79089  2089.1   79090 +DLIC23
+DLIC23  2089.1   79091  2089.1   79092  2089.1   79093  2089.1   79094 +DLIC24
+DLIC24  2089.1   79095  2089.1   79096  1303.0   79153  1303.0   79154 +DLIC25
+DLIC25  1303.0   79155  1303.0   79156  1303.0   79157  1303.0   79158 +DLIC26
+DLIC26  1303.0   79159  1303.0   79160  1303.0   79161  1303.0   79162 +DLIC27
+DLIC27  1303.0   79163  1303.0   79164  1303.0   79165  1303.0   79166 +DLIC28
+DLIC28  1303.0   79167  1303.0   79168  1303.0   79169  1303.0   79170 +DLIC29
+DLIC29  1303.0   79171  1303.0   79172
$
$
$ This section is for distributed actuation loads
$00000010000000200000003000000040000000500000006000000070000000800000009000000010
$ Distributed Actuator 8
RLOAD1    79001   79301           79601   77901
RLOAD1    79002   79302           79602   77901
RLOAD1    79003   79303           79603   77901
RLOAD1    79004   79304           79604   77901
RLOAD1    79005   79305           79605   77901
RLOAD1    79006   79306           79606   77901
RLOAD1    79007   79307           79607   77901
RLOAD1    79008   79308           79608   77901
RLOAD1    79009   79309           79609   77901
RLOAD1    79010   79310           79610   77901
RLOAD1    79011   79311           79611   77901
RLOAD1    79012   79312           79612   77901
RLOAD1    79013   79313           79613   77901
RLOAD1    79014   79314           79614   77901
RLOAD1    79015   79315           79615   77901
RLOAD1    79016   79316           79616   77901
$ Distributed Actuator 33
RLOAD1    79017   79317           79617   77901
RLOAD1    79018   79318           79618   77901
RLOAD1    79019   79319           79619   77901
RLOAD1    79020   79320           79620   77901
RLOAD1    79021   79321           79621   77901
RLOAD1    79022   79322           79622   77901
RLOAD1    79023   79323           79623   77901
RLOAD1    79024   79324           79624   77901
RLOAD1    79025   79325           79625   77901
RLOAD1    79026   79326           79626   77901
RLOAD1    79027   79327           79627   77901
RLOAD1    79028   79328           79628   77901
RLOAD1    79029   79329           79629   77901
```

NASTRAN source code, sample of added command lines

```
RLOAD1    79030   79330           79630   77901
RLOAD1    79031   79331           79631   77901
RLOAD1    79032   79332           79632   77901
$ Distributed Actuator 38
RLOAD1    79033   79333           79633   77901
RLOAD1    79034   79334           79634   77901
RLOAD1    79035   79335           79635   77901
RLOAD1    79036   79336           79636   77901
RLOAD1    79037   79337           79637   77901
RLOAD1    79038   79338           79638   77901
RLOAD1    79039   79339           79639   77901
RLOAD1    79040   79340           79640   77901
RLOAD1    79041   79341           79641   77901
RLOAD1    79042   79342           79642   77901
RLOAD1    79043   79343           79643   77901
RLOAD1    79044   79344           79644   77901
RLOAD1    79045   79345           79645   77901
RLOAD1    79046   79346           79646   77901
RLOAD1    79047   79347           79647   77901
RLOAD1    79048   79348           79648   77901
$ Distributed Actuator 41
RLOAD1    79049   79349           79649   77901
RLOAD1    79050   79350           79650   77901
RLOAD1    79051   79351           79651   77901
RLOAD1    79052   79352           79652   77901
RLOAD1    79053   79353           79653   77901
RLOAD1    79054   79354           79654   77901
RLOAD1    79055   79355           79655   77901
RLOAD1    79056   79356           79656   77901
RLOAD1    79057   79357           79657   77901
RLOAD1    79058   79358           79658   77901
RLOAD1    79059   79359           79659   77901
RLOAD1    79060   79360           79660   77901
$ Distributed Actuator 45
RLOAD1    79061   79361           79661   77901
RLOAD1    79062   79362           79662   77901
RLOAD1    79063   79363           79663   77901
RLOAD1    79064   79364           79664   77901
RLOAD1    79065   79365           79665   77901
RLOAD1    79066   79366           79666   77901
RLOAD1    79067   79367           79667   77901
RLOAD1    79068   79368           79668   77901
RLOAD1    79069   79369           79669   77901
RLOAD1    79070   79370           79670   77901
RLOAD1    79071   79371           79671   77901
RLOAD1    79072   79372           79672   77901
RLOAD1    79073   79373           79673   77901
RLOAD1    79074   79374           79674   77901
RLOAD1    79075   79375           79675   77901
RLOAD1    79076   79376           79676   77901
RLOAD1    79077   79377           79677   77901
```

NASTRAN source code, sample of added command lines

```
RLOAD1    79078   79378           79678   77901
RLOAD1    79079   79379           79679   77901
RLOAD1    79080   79380           79680   77901
$ Distributed Actuator 56
RLOAD1    79081   79381           79681   77901
RLOAD1    79082   79382           79682   77901
RLOAD1    79083   79383           79683   77901
RLOAD1    79084   79384           79684   77901
RLOAD1    79085   79385           79685   77901
RLOAD1    79086   79386           79686   77901
RLOAD1    79087   79387           79687   77901
RLOAD1    79088   79388           79688   77901
RLOAD1    79089   79389           79689   77901
RLOAD1    79090   79390           79690   77901
RLOAD1    79091   79391           79691   77901
RLOAD1    79092   79392           79692   77901
RLOAD1    79093   79393           79693   77901
RLOAD1    79094   79394           79694   77901
RLOAD1    79095   79395           79695   77901
RLOAD1    79096   79396           79696   77901
$ Distributed Actuator 59
RLOAD1    79097   79397           79697   77901
RLOAD1    79098   79398           79698   77901
RLOAD1    79099   79399           79699   77901
RLOAD1    79100   79400           79700   77901
RLOAD1    79101   79401           79701   77901
RLOAD1    79102   79402           79702   77901
RLOAD1    79103   79403           79703   77901
RLOAD1    79104   79404           79704   77901
RLOAD1    79105   79405           79705   77901
RLOAD1    79106   79406           79706   77901
RLOAD1    79107   79407           79707   77901
RLOAD1    79108   79408           79708   77901
RLOAD1    79109   79409           79709   77901
RLOAD1    79110   79410           79710   77901
RLOAD1    79111   79411           79711   77901
RLOAD1    79112   79412           79712   77901
$ Distributed Actuator 107
RLOAD1    79113   79413           79713   77901
RLOAD1    79114   79414           79714   77901
RLOAD1    79115   79415           79715   77901
RLOAD1    79116   79416           79716   77901
RLOAD1    79117   79417           79717   77901
RLOAD1    79118   79418           79718   77901
RLOAD1    79119   79419           79719   77901
RLOAD1    79120   79420           79720   77901
RLOAD1    79121   79421           79721   77901
RLOAD1    79122   79422           79722   77901
RLOAD1    79123   79423           79723   77901
RLOAD1    79124   79424           79724   77901
RLOAD1    79125   79425           79725   77901
```

NASTRAN source code, sample of added command lines

```
RLOAD1    79126   79426           79726   77901
RLOAD1    79127   79427           79727   77901
RLOAD1    79128   79428           79728   77901
RLOAD1    79129   79429           79729   77901
RLOAD1    79130   79430           79730   77901
RLOAD1    79131   79431           79731   77901
RLOAD1    79132   79432           79732   77901
$ Distributed Actuator 113
RLOAD1    79133   79433           79733   77901
RLOAD1    79134   79434           79734   77901
RLOAD1    79135   79435           79735   77901
RLOAD1    79136   79436           79736   77901
RLOAD1    79137   79437           79737   77901
RLOAD1    79138   79438           79738   77901
RLOAD1    79139   79439           79739   77901
RLOAD1    79140   79440           79740   77901
RLOAD1    79141   79441           79741   77901
RLOAD1    79142   79442           79742   77901
RLOAD1    79143   79443           79743   77901
RLOAD1    79144   79444           79744   77901
RLOAD1    79145   79445           79745   77901
RLOAD1    79146   79446           79746   77901
RLOAD1    79147   79447           79747   77901
RLOAD1    79148   79448           79748   77901
RLOAD1    79149   79449           79749   77901
RLOAD1    79150   79450           79750   77901
RLOAD1    79151   79451           79751   77901
RLOAD1    79152   79452           79752   77901
$ Distributed Actuator 129
RLOAD1    79153   79453           79753   77901
RLOAD1    79154   79454           79754   77901
RLOAD1    79155   79455           79755   77901
RLOAD1    79156   79456           79756   77901
RLOAD1    79157   79457           79757   77901
RLOAD1    79158   79458           79758   77901
RLOAD1    79159   79459           79759   77901
RLOAD1    79160   79460           79760   77901
RLOAD1    79161   79461           79761   77901
RLOAD1    79162   79462           79762   77901
RLOAD1    79163   79463           79763   77901
RLOAD1    79164   79464           79764   77901
RLOAD1    79165   79465           79765   77901
RLOAD1    79166   79466           79766   77901
RLOAD1    79167   79467           79767   77901
RLOAD1    79168   79468           79768   77901
RLOAD1    79169   79469           79769   77901
RLOAD1    79170   79470           79770   77901
RLOAD1    79171   79471           79771   77901
RLOAD1    79172   79472           79772   77901
$ Distributed Actuator 142
RLOAD1    79173   79473           79773   77901
```

NASTRAN source code, sample of added command lines

```
RLOAD1    79174   79474           79774   77901
RLOAD1    79175   79475           79775   77901
RLOAD1    79176   79476           79776   77901
RLOAD1    79177   79477           79777   77901
RLOAD1    79178   79478           79778   77901
RLOAD1    79179   79479           79779   77901
RLOAD1    79180   79480           79780   77901
$
$000000010000000200000003000000040000005000000060000000700000008000000090000001O
$ Distributed Actuator 8
DAREA     79301    5708       1    0.17
DAREA     79302    5709       1    0.17
DAREA     79303    5710       1    0.36
DAREA     79304    5711       1    0.36
DAREA     79305    5714       1    0.50
DAREA     79306    5715       1    0.50
DAREA     79307    5719       1     1.0
DAREA     79308    5720       1     1.0
DAREA     79309    6904       1   -0.17
DAREA     79310    6903       1   -0.17
DAREA     79311    6906       1   -0.36
DAREA     79312    6905       1   -0.36
DAREA     79313    6908       1    -0.5
DAREA     79314    6907       1    -0.5
DAREA     79315    6919       1    -1.0
DAREA     79316    6920       1    -1.0
$ Distributed Actuator 33
DAREA     79317   14408       1   -0.25
DAREA     79318   14410       1   -0.25
DAREA     79319   14412       1   -0.25
DAREA     79320   14414       1   -0.25
DAREA     79321   14409       1    0.25
DAREA     79322   14411       1    0.25
DAREA     79323   14413       1    0.25
DAREA     79324   14415       1    0.25
DAREA     79325   15468       1    0.25
DAREA     79326   15406       1    0.25
DAREA     79327   15408       1    0.25
DAREA     79328   15410       1    0.25
DAREA     79329   15467       1   -0.25
DAREA     79330   15407       1   -0.25
DAREA     79331   15409       1   -0.25
DAREA     79332   15411       1   -0.25
$ Distributed Actuator 38
DAREA     79333   16303       1   -1.00
DAREA     79334   16306       1   -1.00
DAREA     79335   16309       1    0.30
DAREA     79336   16314       1    0.30
DAREA     79337   16313       1    0.30
DAREA     79338   16318       1    0.30
DAREA     79339   16317       1    0.40
```

NASTRAN source code, sample of added command lines

```
DAREA     79340   16322       1    0.40
DAREA     79341   17619       1    1.00
DAREA     79342   17616       1    1.00
DAREA     79343   17677       1   -0.30
DAREA     79344   17680       1   -0.30
DAREA     79345   17691       1   -0.30
DAREA     79346   17688       1   -0.30
DAREA     79347   17703       1   -0.40
DAREA     79348   17700       1   -0.40
$ Distributed Actuator 41
DAREA     79349   18202       1   -1.00
DAREA     79350   18203       1   -1.00
DAREA     79351   18208       1    0.50
DAREA     79352   18209       1    0.50
DAREA     79353   18212       1    0.50
DAREA     79354   18213       1    0.50
DAREA     79355   18808       1    1.00
DAREA     79356   18807       1    1.00
DAREA     79357   18814       1   -0.50
DAREA     79358   18813       1   -0.50
DAREA     79359   18818       1   -0.50
DAREA     79360   18817       1   -0.50
$ Distributed Actuator 45
DAREA     79361   18804       1   -0.20
DAREA     79362   18806       1   -0.20
DAREA     79363   18810       1   -0.20
DAREA     79364   18814       1   -0.20
DAREA     79365   18818       1   -0.20
DAREA     79366   18805       1    0.20
DAREA     79367   18807       1    0.20
DAREA     79368   18809       1    0.20
DAREA     79369   18813       1    0.20
DAREA     79370   18817       1    0.20
DAREA     79371   19908       1    0.20
DAREA     79372   19920       1    0.20
DAREA     79373   19930       1    0.20
DAREA     79374   19940       1    0.20
DAREA     79375   19948       1    0.20
DAREA     79376   19909       1   -0.20
DAREA     79377   19921       1   -0.20
DAREA     79378   19933       1   -0.20
DAREA     79379   19943       1   -0.20
DAREA     79380   19951       1   -0.20
$ Distributed Actuator 56
DAREA     79381   19908       1   -0.60
DAREA     79382   19909       1   -0.60
DAREA     79383   19920       1   -0.40
DAREA     79384   19921       1   -0.40
DAREA     79385   19940       1    0.40
DAREA     79386   19943       1    0.40
DAREA     79387   19948       1    0.60
```

NASTRAN source code, sample of added command lines

```
DAREA     79388   19951       1    0.60
DAREA     79389   21408       1    0.60
DAREA     79390   21409       1    0.60
DAREA     79391   21414       1    0.40
DAREA     79392   21415       1    0.40
DAREA     79393   21432       1   -0.40
DAREA     79394   21435       1   -0.40
DAREA     79395   21438       1   -0.60
DAREA     79396   21441       1   -0.60
$ Distributed Actuator 59
DAREA     79397   21408       1   -0.60
DAREA     79398   21409       1   -0.60
DAREA     79399   21414       1   -0.40
DAREA     79400   21415       1   -0.40
DAREA     79401   21432       1    0.40
DAREA     79402   21435       1    0.40
DAREA     79403   21438       1    0.60
DAREA     79404   21441       1    0.60
DAREA     79405   23010       1    0.60
DAREA     79406   23011       1    0.60
DAREA     79407   23020       1    0.40
DAREA     79408   23023       1    0.40
DAREA     79409   23038       1   -0.40
DAREA     79410   23041       1   -0.40
DAREA     79411   23042       1   -0.60
DAREA     79412   23045       1   -0.60
$ Distributed Actuator 107
DAREA     79413   38301       1   -0.20
DAREA     79414   38302       1   -0.20
DAREA     79415   38303       1   -0.20
DAREA     79416   38304       1   -0.20
DAREA     79417   38305       1   -0.20
DAREA     79418   38310       1    0.20
DAREA     79419   38311       1    0.20
DAREA     79420   38312       1    0.20
DAREA     79421   38313       1    0.20
DAREA     79422   38317       1    0.20
DAREA     79423   39601       1    0.20
DAREA     79424   39602       1    0.20
DAREA     79425   39603       1    0.20
DAREA     79426   39604       1    0.20
DAREA     79427   39605       1    0.20
DAREA     79428   39610       1   -0.20
DAREA     79429   39611       1   -0.20
DAREA     79430   39612       1   -0.20
DAREA     79431   39613       1   -0.20
DAREA     79432   39617       1   -0.20
$ Distributed Actuator 113
DAREA     79433   40901       1   -0.20
DAREA     79434   40902       1   -0.20
DAREA     79435   40903       1   -0.20
```

NASTRAN source code, sample of added command lines

```
DAREA     79436   40904       1   -0.20
DAREA     79437   40905       1   -0.20
DAREA     79438   40910       1    0.20
DAREA     79439   40911       1    0.20
DAREA     79440   40912       1    0.20
DAREA     79441   40913       1    0.20
DAREA     79442   40917       1    0.20
DAREA     79443   42301       1    0.20
DAREA     79444   42302       1    0.20
DAREA     79445   42303       1    0.20
DAREA     79446   42304       1    0.20
DAREA     79447   42305       1    0.20
DAREA     79448   42308       1   -0.20
DAREA     79449   42309       1   -0.20
DAREA     79450   42310       1   -0.20
DAREA     79451   42311       1   -0.20
DAREA     79452   42313       1   -0.20
$ Distributed Actuator 129
DAREA     79453   47602       1   -0.20
DAREA     79454   47604       1   -0.20
DAREA     79455   47606       1   -0.20
DAREA     79456   47608       1   -0.20
DAREA     79457   47610       1   -0.20
DAREA     79458   47603       1    0.20
DAREA     79459   47605       1    0.20
DAREA     79460   47607       1    0.20
DAREA     79461   47609       1    0.20
DAREA     79462   47611       1    0.20
DAREA     79463   48902       1    0.20
DAREA     79464   48904       1    0.20
DAREA     79465   48906       1    0.20
DAREA     79466   48908       1    0.20
DAREA     79467   48910       1    0.20
DAREA     79468   48903       1   -0.20
DAREA     79469   48905       1   -0.20
DAREA     79470   48907       1   -0.20
DAREA     79471   48909       1   -0.20
DAREA     79472   48911       1   -0.20
$ Distributed Actuator 142
DAREA     79473   53022       3   -0.50
DAREA     79474   53035       3   -0.50
DAREA     79475   54755       3    0.50
DAREA     79476   54756       3    0.50
DAREA     79477   55062       3    0.50
DAREA     79478   55061       3    0.50
DAREA     79479   55063       3   -0.50
DAREA     79480   55064       3   -0.50
$
$000000100000002000000030000000400000005000000060000000700000008000000090000001 0
$ Distributed Actuator 8
DPHASE    79601    5708       1     0.0
```

NASTRAN source code, sample of added command lines

```
DPHASE    79602    5709       1     0.0
DPHASE    79603    5710       1     0.0
DPHASE    79604    5711       1     0.0
DPHASE    79605    5714       1     0.0
DPHASE    79606    5715       1     0.0
DPHASE    79607    5719       1     0.0
DPHASE    79608    5720       1     0.0
DPHASE    79609    6904       1     0.0
DPHASE    79610    6903       1     0.0
DPHASE    79611    6906       1     0.0
DPHASE    79612    6905       1     0.0
DPHASE    79613    6908       1     0.0
DPHASE    79614    6907       1     0.0
DPHASE    79615    6919       1     0.0
DPHASE    79616    6920       1     0.0
$ Distributed Actuator 33
DPHASE    79617   14408       1   255.2
DPHASE    79618   14410       1   255.2
DPHASE    79619   14412       1   255.2
DPHASE    79620   14414       1   255.2
DPHASE    79621   14409       1   255.2
DPHASE    79622   14411       1   255.2
DPHASE    79623   14413       1   255.2
DPHASE    79624   14415       1   255.2
DPHASE    79625   15468       1   255.2
DPHASE    79626   15406       1   255.2
DPHASE    79627   15408       1   255.2
DPHASE    79628   15410       1   255.2
DPHASE    79629   15467       1   255.2
DPHASE    79630   15407       1   255.2
DPHASE    79631   15409       1   255.2
DPHASE    79632   15411       1   255.2
$ Distributed Actuator 38
DPHASE    79633   16303       1   185.3
DPHASE    79634   16306       1   185.3
DPHASE    79635   16309       1   185.3
DPHASE    79636   16314       1   185.3
DPHASE    79637   16313       1   185.3
DPHASE    79638   16318       1   185.3
DPHASE    79639   16317       1   185.3
DPHASE    79640   16322       1   185.3
DPHASE    79641   17619       1   185.3
DPHASE    79642   17616       1   185.3
DPHASE    79643   17677       1   185.3
DPHASE    79644   17680       1   185.3
DPHASE    79645   17691       1   185.3
DPHASE    79646   17688       1   185.3
DPHASE    79647   17703       1   185.3
DPHASE    79648   17700       1   185.3
$ Distributed Actuator 41
DPHASE    79649   18202       1     0.0
```

NASTRAN source code, sample of added command lines

```
DPHASE    79650   18203       1     0.0
DPHASE    79651   18208       1     0.0
DPHASE    79652   18209       1     0.0
DPHASE    79653   18212       1     0.0
DPHASE    79654   18213       1     0.0
DPHASE    79655   18808       1     0.0
DPHASE    79656   18807       1     0.0
DPHASE    79657   18814       1     0.0
DPHASE    79658   18813       1     0.0
DPHASE    79659   18818       1     0.0
DPHASE    79660   18817       1     0.0
$ Distributed Actuator 45
DPHASE    79661   18804       1   249.3
DPHASE    79662   18806       1   249.3
DPHASE    79663   18810       1   249.3
DPHASE    79664   18814       1   249.3
DPHASE    79665   18818       1   249.3
DPHASE    79666   18805       1   249.3
DPHASE    79667   18807       1   249.3
DPHASE    79668   18809       1   249.3
DPHASE    79669   18813       1   249.3
DPHASE    79670   18817       1   249.3
DPHASE    79671   19908       1   249.3
DPHASE    79672   19920       1   249.3
DPHASE    79673   19930       1   249.3
DPHASE    79674   19940       1   249.3
DPHASE    79675   19948       1   249.3
DPHASE    79676   19909       1   249.3
DPHASE    79677   19921       1   249.3
DPHASE    79678   19933       1   249.3
DPHASE    79679   19943       1   249.3
DPHASE    79680   19951       1   249.3
$ Distributed Actuator 56
DPHASE    79681   19908       1   174.3
DPHASE    79682   19909       1   174.3
DPHASE    79683   19920       1   174.3
DPHASE    79684   19921       1   174.3
DPHASE    79685   19940       1   174.3
DPHASE    79686   19943       1   174.3
DPHASE    79687   19948       1   174.3
DPHASE    79688   19951       1   174.3
DPHASE    79689   21408       1   174.3
DPHASE    79690   21409       1   174.3
DPHASE    79691   21414       1   174.3
DPHASE    79692   21415       1   174.3
DPHASE    79693   21432       1   174.3
DPHASE    79694   21435       1   174.3
DPHASE    79695   21438       1   174.3
DPHASE    79696   21441       1   174.3
$ Distributed Actuator 59
DPHASE    79697   21408       1     0.0
```

NASTRAN source code, sample of added command lines

```
DPHASE    79698   21409       1     0.0
DPHASE    79699   21414       1     0.0
DPHASE    79700   21415       1     0.0
DPHASE    79701   21432       1     0.0
DPHASE    79702   21435       1     0.0
DPHASE    79703   21438       1     0.0
DPHASE    79704   21441       1     0.0
DPHASE    79705   23010       1     0.0
DPHASE    79706   23011       1     0.0
DPHASE    79707   23020       1     0.0
DPHASE    79708   23023       1     0.0
DPHASE    79709   23038       1     0.0
DPHASE    79710   23041       1     0.0
DPHASE    79711   23042       1     0.0
DPHASE    79712   23045       1     0.0
$ Distributed Actuator 107
DPHASE    79713   38301       1     0.0
DPHASE    79714   38302       1     0.0
DPHASE    79715   38303       1     0.0
DPHASE    79716   38304       1     0.0
DPHASE    79717   38305       1     0.0
DPHASE    79718   38310       1     0.0
DPHASE    79719   38311       1     0.0
DPHASE    79720   38312       1     0.0
DPHASE    79721   38313       1     0.0
DPHASE    79722   38317       1     0.0
DPHASE    79723   39601       1     0.0
DPHASE    79724   39602       1     0.0
DPHASE    79725   39603       1     0.0
DPHASE    79726   39604       1     0.0
DPHASE    79727   39605       1     0.0
DPHASE    79728   39610       1     0.0
DPHASE    79729   39611       1     0.0
DPHASE    79730   39612       1     0.0
DPHASE    79731   39613       1     0.0
DPHASE    79732   39617       1     0.0
$ Distributed Actuator 113
DPHASE    79733   40901       1     0.0
DPHASE    79734   40902       1     0.0
DPHASE    79735   40903       1     0.0
DPHASE    79736   40904       1     0.0
DPHASE    79737   40905       1     0.0
DPHASE    79738   40910       1     0.0
DPHASE    79739   40911       1     0.0
DPHASE    79740   40912       1     0.0
DPHASE    79741   40913       1     0.0
DPHASE    79742   40917       1     0.0
DPHASE    79743   42301       1     0.0
DPHASE    79744   42302       1     0.0
DPHASE    79745   42303       1     0.0
DPHASE    79746   42304       1     0.0
```

NASTRAN source code, sample of added command lines

```
DPHASE    79747   42305       1     0.0
DPHASE    79748   42308       1     0.0
DPHASE    79749   42309       1     0.0
DPHASE    79750   42310       1     0.0
DPHASE    79751   42311       1     0.0
DPHASE    79752   42313       1     0.0
$ Distributed Actuator 129
DPHASE    79753   47602       1    57.2
DPHASE    79754   47604       1    57.2
DPHASE    79755   47606       1    57.2
DPHASE    79756   47608       1    57.2
DPHASE    79757   47610       1    57.2
DPHASE    79758   47603       1    57.2
DPHASE    79759   47605       1    57.2
DPHASE    79760   47607       1    57.2
DPHASE    79761   47609       1    57.2
DPHASE    79762   47611       1    57.2
DPHASE    79763   48902       1    57.2
DPHASE    79764   48904       1    57.2
DPHASE    79765   48906       1    57.2
DPHASE    79766   48908       1    57.2
DPHASE    79767   48910       1    57.2
DPHASE    79768   48903       1    57.2
DPHASE    79769   48905       1    57.2
DPHASE    79770   48907       1    57.2
DPHASE    79771   48909       1    57.2
DPHASE    79772   48911       1    57.2
$ Distributed Actuator 142
DPHASE    79773   53022       3     0.0
DPHASE    79774   53035       3     0.0
DPHASE    79775   54755       3     0.0
DPHASE    79776   54756       3     0.0
DPHASE    79777   55062       3     0.0
DPHASE    79778   55061       3     0.0
DPHASE    79779   55063       3     0.0
DPHASE    79780   55064       3     0.0
$
$
$ ADD GRID POINTS
$00000010000000200000003000000040000005000000060000007000000080000009000000010
GRID       3499            35.5     0.0   129.2                       100
GRID       9056           206.2     0.0   129.2                       100
GRID      20050           206.2   23.75   129.2                       100
GRID      20051           206.2    33.0   129.2                       100
GRID      20052           206.2    46.0   129.2                       100
GRID      20053           206.2    60.0   129.2                       100
GRID      20054           206.2    66.0   129.2                       100
GRID      20055           206.2    78.0   129.2                       100
GRID      20056           206.2    90.0   129.2                       100
GRID      20057           206.2    96.0   129.2                       100
GRID      20058           206.2    98.0   129.2                       100
```

NASTRAN source code, sample of added command lines

```
GRID      20060           206.2  -23.75   129.2                    100
GRID      20061           206.2   -33.0   129.2                    100
GRID      20062           206.2   -46.0   129.2                    100
GRID      20063           206.2   -60.0   129.2                    100
GRID      20064           206.2   -66.0   129.2                    100
GRID      20065           206.2   -78.0   129.2                    100
GRID      20066           206.2   -90.0   129.2                    100
GRID      20067           206.2   -96.0   129.2                    100
GRID      20068           206.2   -98.0   129.2                    100
GRID      22999           230.0     0.0   129.2                    100
GRID      55401           576.7     0.0   242.2                    100
GRID      55403           554.8     0.0   189.2                    100
GRID      55404           538.5     0.0   149.6                    100
GRID      56501           553.8   -64.0   147.2                    100
GRID      56502           553.8   -40.0   147.2                    100
GRID      56503           553.8   -21.0   147.2                    100
GRID      56504           553.8    -5.7   147.2                    100
GRID      56505           553.8     0.0   147.2                    100
GRID      56506           553.8     5.7   147.2                    100
GRID      56507           553.8    21.0   147.2                    100
GRID      56508           553.8    40.0   147.2                    100
GRID      56509           553.8    64.0   147.2                    100
$ ADD PLOTTING ELEMENTS
$000000100000002000000300000040000005000000600000070000008000000900000010
PLOTEL    99001      54      62
PLOTEL    99002      62     500
PLOTEL    99003      18     500
PLOTEL    99004       5     500
PLOTEL    99005      29     500
PLOTEL    99006      41     500
PLOTEL    99007   17616      18
PLOTEL    99008   17619      18
PLOTEL    99009   17616       5
PLOTEL    99010   23010       5
PLOTEL    99011   23010      29
PLOTEL    99012   23011      29
PLOTEL    99013   23011      41
PLOTEL    99014   17619      41
PLOTEL    99015   17600   17616
PLOTEL    99016   17600   17619
PLOTEL    99017   22999   23010
PLOTEL    99018   22999   23011
PLOTEL    99019    3499    4600
PLOTEL    99020    4600    5700
PLOTEL    99021    5700    6900
PLOTEL    99022    6900    8000
PLOTEL    99023    8000    9101
PLOTEL    99024    9101   10514
PLOTEL    99025   10514   11501
PLOTEL    99026   11501   12501
PLOTEL    99027   12501   12002
```

NASTRAN source code, sample of added command lines

```
PLOTEL    99028   12002   12031
PLOTEL    99029   12501   12004
PLOTEL    99030   12004   12032
PLOTEL    99031   12501   13501
PLOTEL    99032   13501   14401
PLOTEL    99033   14401   15400
PLOTEL    99034   15400   16300
PLOTEL    99035   16300   17600
PLOTEL    99036   17600   18800
PLOTEL    99037   18800   19900
PLOTEL    99038   19900    9056
PLOTEL    99039    9056   20050
PLOTEL    99040   20050   20051
PLOTEL    99041   20051   20052
PLOTEL    99042   20052   20053
PLOTEL    99043   20053   20054
PLOTEL    99044   20054   20055
PLOTEL    99045   20055   20056
PLOTEL    99046   20056   20057
PLOTEL    99047   20057   20058
PLOTEL    99048    9056   20060
PLOTEL    99049   20060   20061
PLOTEL    99050   20061   20062
$00000010000000200000003000000040000000500000006000000070000000800000009000000010
PLOTEL    99051   20062   20063
PLOTEL    99052   20063   20064
PLOTEL    99053   20064   20065
PLOTEL    99054   20065   20066
PLOTEL    99055   20066   20067
PLOTEL    99056   20067   20068
PLOTEL    99057    9056   21400
PLOTEL    99058   21400   22999
PLOTEL    99059   22999   23800
PLOTEL    99060   23800   24000
PLOTEL    99061   23800   24001
PLOTEL    99062   23800   24700
PLOTEL    99063   24700   25800
PLOTEL    99064   25800   26900
PLOTEL    99065   26900   28000
PLOTEL    99066   28000   29000
PLOTEL    99067   29000   30000
PLOTEL    99068   30000   31000
PLOTEL    99069   31000   32000
PLOTEL    99070   32000   33000
PLOTEL    99071   33000   34000
PLOTEL    99072   34000   35000
PLOTEL    99073   35000   36000
PLOTEL    99074   36000   37000
PLOTEL    99075   37000   38300
PLOTEL    99076   38300   39600
PLOTEL    99077   39600   40900
```

NASTRAN source code, sample of added command lines

```
PLOTEL    99078   40900   42300
PLOTEL    99079   42300   43600
PLOTEL    99080   43600   45000
PLOTEL    99081   45000   46300
PLOTEL    99082   46300   47600
PLOTEL    99083   47600   48900
PLOTEL    99084   48900   50300
PLOTEL    99085   50300   51600
PLOTEL    99086   51600   53000
PLOTEL    99087   53000   54700
PLOTEL    99088   54700   57004
PLOTEL    99089   53000   55404
PLOTEL    99090   55404   55403
PLOTEL    99091   55403   55401
PLOTEL    99092   55404   56505
PLOTEL    99093   56501   56502
PLOTEL    99094   56502   56503
PLOTEL    99095   56503   56504
PLOTEL    99096   56504   56505
PLOTEL    99097   56505   56506
PLOTEL    99098   56506   56507
PLOTEL    99099   56507   56508
PLOTEL    99100   56508   56509
$ ADD RBE3 ELEMENTS TO RESEMBLE STICK MODEL OUTPUT
$00000010000000200000003000000040000000500000006000000070000000800000009000000010
$ Note the following RBE3 entry is duplicated later by RBE3 503500
RBE3      99908            3499  123456     1.0     123    3519    3520 +RB08
+RB08      3541    3542    3553    3554
RBE3      99909            4600  123456     1.0     123    4608    4609 +RB09
+RB09      4616    4617    4628    4629
RBE3      99910            5700  123456     1.0     123    5706    5707 +RB10
+RB10      5714    5715    5719    5720
RBE3      99911            6900  123456     1.0     123    6901    6902 +RB11
+RB11      6907    6908    6919    6920
RBE3      99912            8000  123456     1.0     123    8001    8002 +RB12
+RB12      8007    8008    8019    8020
RBE3      99913            9056  123456     1.0     123   19901   19908 +RB13
+RB13     19909   19948   19951   21401   21408   21409   21438   21441
RBE3      99914            9101  123456     1.0     123    9106    9107 +RB14
+RB14      9116    9117    9121    9122    9124
RBE3      99915           10514  123456     1.0     123   10501   10502 +RB15
+RB15     10507   10508   10511   10512
RBE3      99916           11501  123456     1.0     123   11506   11507 +RB16
+RB16     11536   11537   11544   11545
RBE3      99921           12501  123456     1.0     123   12506   12507 +RB21
+RB21     12520   12521   12528   12529
RBE3      99922           13501  123456     1.0     123   13506   13507 +RB22
+RB22     13514   13515   13518   13519
RBE3      99923           14401  123456     1.0     123   14406   14407 +RB23
+RB23     14414   14415   14418   14419
RBE3      99924           15400  123456     1.0     123   15401   15406 +RB24
```

NASTRAN source code, sample of added command lines

```
+RB24     15407   15412   15413   15414   15457   15458   15415
RBE3      99925           16300  123456     1.0     123   16302   16303 +RB25
+RB25     16306   16313   16318   16324
RBE3      99926           17600  123456     1.0     123   17634   17639 +RB26
+RB26     17688   17691   17708
RBE3      99929           18800  123456     1.0     123   18801   18804 +RB29
+RB29     18805   18817   18818
RBE3      99930           19900  123456     1.0     123   19901   19908 +RB30
+RB30     19909   19948   19951
$00000010000000200000003000000040000000500000006000000070000000800000009000000010
RBE3      99931           20050  123456     1.0     123   20106   20108 +RB31
+RB31     20118   20120
RBE3      99932           20051  123456     1.0     123   20134   20136 +RB32
+RB32     20146   20148
RBE3      99933           20052  123456     1.0     123   20162   20164 +RB33
+RB33     20174   20176
RBE3      99934           20053  123456     1.0     123   20190   20192 +RB34
+RB34     20198   20200
RBE3      99935           20054  123456     1.0     123   20214   20216 +RB35
+RB35     20226   20228
RBE3      99936           20055  123456     1.0     123   20242   20244 +RB36
+RB36     20254   20256
RBE3      99937           20056  123456     1.0     123   20270   20272 +RB37
+RB37     20282   20284
RBE3      99938           20057  123456     1.0     123   20294   20296 +RB38
+RB38     20306   20308
RBE3      99939           20058  123456     1.0     123   20314   20316 +RB39
+RB39     20326   20328
$
$00000010000000200000003000000040000000500000006000000070000000800000009000000010
RBE3      99940           20060  123456     1.0     123   20406   20408 +RB40
+RB40     20418   20420
RBE3      99941           20061  123456     1.0     123   20434   20436 +RB41
+RB41     20446   20448
RBE3      99942           20062  123456     1.0     123   20462   20464 +RB42
+RB42     20474   20476
RBE3      99943           20063  123456     1.0     123   20490   20492 +RB43
+RB43     20498   20500
RBE3      99944           20064  123456     1.0     123   20514   20516 +RB44
+RB44     20526   20528
RBE3      99945           20065  123456     1.0     123   20542   20544 +RB45
+RB45     20554   20556
RBE3      99946           20066  123456     1.0     123   20570   20572 +RB46
+RB46     20582   20584
RBE3      99947           20067  123456     1.0     123   20594   20596 +RB47
+RB47     20606   20608
RBE3      99948           20068  123456     1.0     123   20614   20616 +RB48
+RB48     20626   20628
$00000010000000200000003000000040000000500000006000000070000000800000009000000010
RBE3      99949           21400  123456     1.0     123   21401   21408 +RB49
+RB49     21409   21438   21441
```

NASTRAN source code, sample of added command lines

```
RBE3     99950          22999  123456     1.0     123   23001   23010 +RB50
+RB50    23011  23042   23045   23057
RBE3     99953          23800  123456     1.0     123   23801   23804 +RB53
+RB53    23805  23812   23813   23819
RBE3     99956          24700  123456     1.0     123   24701   24706 +RB56
+RB56    24707  24714   24715   24721
RBE3     99957          25800  123456     1.0     123   25801   25804 +RB57
+RB57    25805  25812   25813   25819
RBE3     99958          26900  123456     1.0     123   26901   26904 +RB58
+RB58    26905  26912   26913   26919
RBE3     99959          28000  123456     1.0     123   28001   28004 +RB59
+RB59    28005  28012   28013   28019
RBE3     99960          29000  123456     1.0     123   29008   29009 +RB60
+RB60    29016  29017
RBE3     99961          30000  123456     1.0     123   30012   30013 +RB61
+RB61    30016  30017
RBE3     99962          31000  123456     1.0     123   31001   31004 +RB62
+RB62    31005  31012   31013   31019
RBE3     99963          32000  123456     1.0     123   32001   32004 +RB63
+RB63    32005  32012   32013   32019
RBE3     99964          33000  123456     1.0     123   33001   33004 +RB64
+RB64    33005  33012   33013   33019
RBE3     99965          34000  123456     1.0     123   34001   34004 +RB65
+RB65    34005  34012   34013   34019
RBE3     99966          35000  123456     1.0     123   35001   35006 +RB66
+RB66    35007  35010   35011   35019
RBE3     99967          36000  123456     1.0     123   36001   36006 +RB67
+RB67    36007  36010   36011   36019
RBE3     99968          37000  123456     1.0     123   37001   37004 +RB68
+RB68    37005  37008   37009   37017
RBE3     99969          38300  123456     1.0     123   38301   38306 +RB69
+RB69    38307  38317
$00000010000000200000003000000040000000500000006000000070000000800000009000000010
RBE3     99970          39600  123456     1.0     123   39601   39606 +RB70
+RB70    39607  39617
RBE3     99971          40900  123456     1.0     123   40901   40906 +RB71
+RB71    40907  40917
RBE3     99972          42300  123456     1.0     123   42301   42306 +RB72
+RB72    42307  42313
RBE3     99973          43600  123456     1.0     123   43601   43606 +RB73
+RB73    43607  43613
RBE3     99974          45000  123456     1.0     123   45001   45006 +RB74
+RB74    45007  45013
RBE3     99975          46300  123456     1.0     123   46301   46306 +RB75
+RB75    46307  46313
RBE3     99976          47600  123456     1.0     123   47601   47606 +RB76
+RB76    47607  47613
RBE3     99977          48900  123456     1.0     123   48901   48906 +RB77
+RB77    48907  48913
RBE3     99978          50300  123456     1.0     123   50301   50306 +RB78
+RB78    50307  50313
```

NASTRAN source code, sample of added command lines

```
RBE3      99979           51600  123456     1.0     123   51601   51606 +RB79
+RB79     51607   51613
RBE3      99980           53000  123456     1.0     123   53003   53012 +RB80
+RB80     53015   53033
RBE3      99981           54700  123456     1.0     123   54701   54710 +RB81
+RB81     54711   54733
RBE3      99982           55401  123456     1.0     123   55041   55042 +RB82
+RB82     55043   55044
RBE3      99983           55403  123456     1.0     123   55021   55022 +RB83
+RB83     55023   55024
RBE3      99984           55404  123456     1.0     123   55005   55006 +RB84
+RB84     55007   55008
RBE3      99985           56501  123456     1.0     123   56044   56045 +RB85
+RB85     56096   56097
RBE3      99986           56502  123456     1.0     123   56046   56047 +RB86
+RB86     56098   56099
RBE3      99987           56503  123456     1.0     123   56048   56049 +RB87
+RB87     56100   56101
RBE3      99988           56504  123456     1.0     123   56050   56051 +RB88
+RB88     56102   56103
RBE3      99989           56505  123456     1.0     123   56050   56051 +RB89
+RB89     56054   56055   56102   56103   56106   56107
RBE3      99990           56506  123456     1.0     123   56054   56055 +RB90
+RB90     56106   56107
RBE3      99991           56507  123456     1.0     123   56056   56057 +RB91
+RB91     56108   56109
RBE3      99992           56508  123456     1.0     123   56058   56059 +RB92
+RB92     56110   56111
RBE3      99993           56509  123456     1.0     123   56060   56061 +RB93
+RB93     56112   56113
$
ENDDATA
$
$BBBBBBBBBBBBBBBBBBBBBBBBBBBBBBBBBBBBBBBBBBBBBBBBBBBBBBBBBBBBBBBBBBBBBBBBBBBBBBB
$ END OF ADDED SECTION BY DAVID HEVERLY
$OOOOOOOOOOOOOOOOOOOOOOOOOOOOOOOOOOOOOOOOOOOOOOOOOOOOOOOOOOOOOOOOOOOOOOOOOOOOO
$OOOOOOOOOOOOOOOOOOOOOOOOOOOOOOOOOOOOOOOOOOOOOOOOOOOOOOOOOOOOOOOOOOOOOOOOOOOOO
```

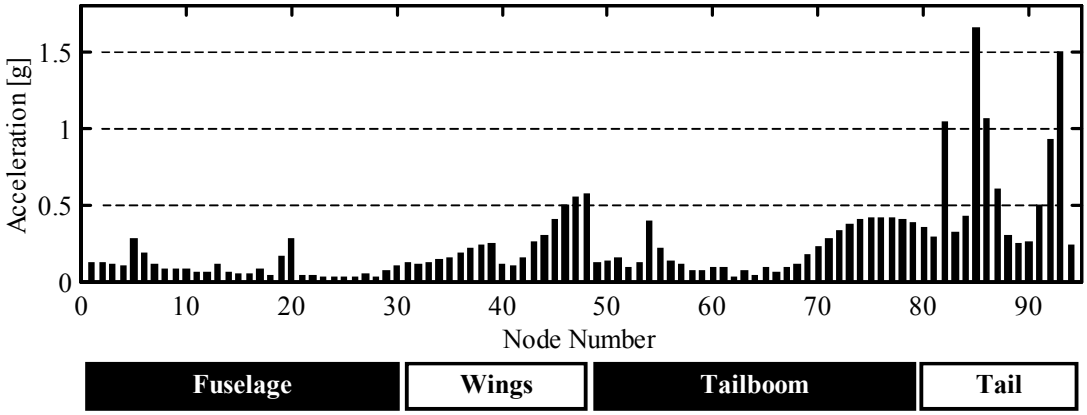

Nastran Model: Centralized Actuation, Controlled vibration response to hub and tail excitation

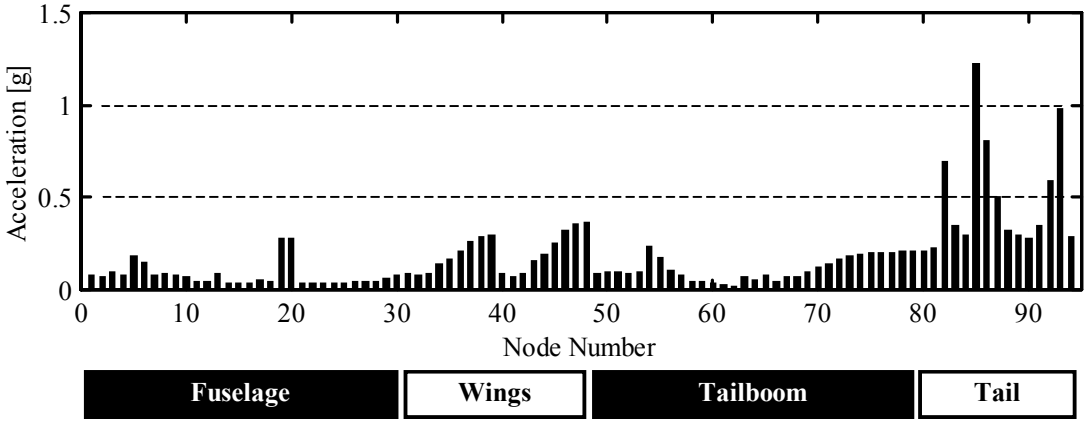

Nastran Model: Distributed Actuation, Controlled vibration response to hub and tail excitation

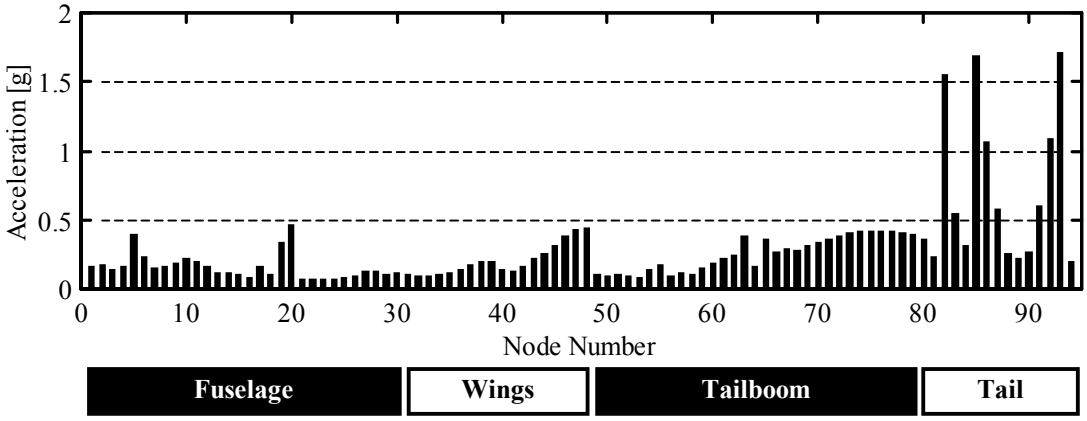

Nastran Model: Uncontrolled vibration response to hub excitation

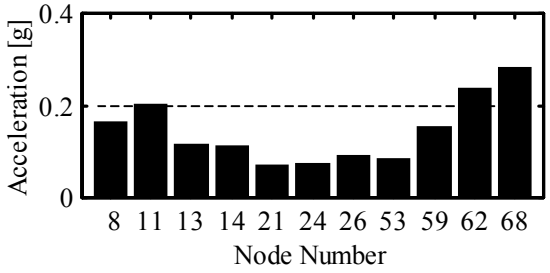

Nastran Model: Uncontrolled vibration at target nodes (hub excitation)

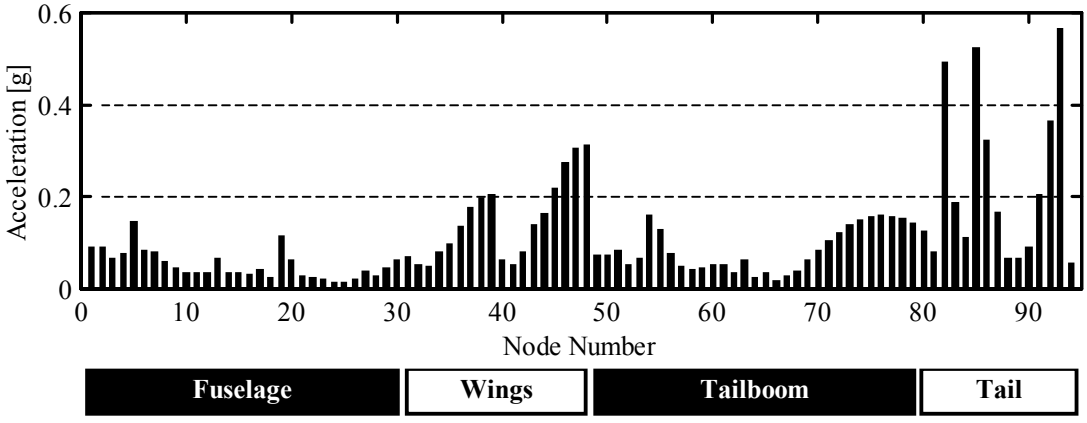

Nastran Model: Centralized Actuation, Controlled vibration response to hub excitation

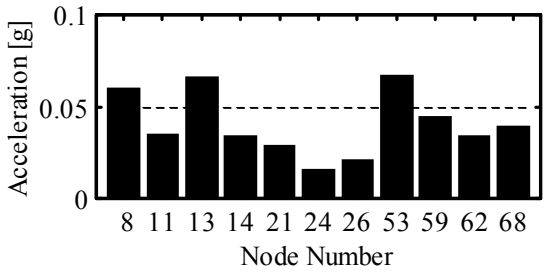

Nastran Model: Centralized Actuation, Controlled vibration at target nodes (hub excitation)

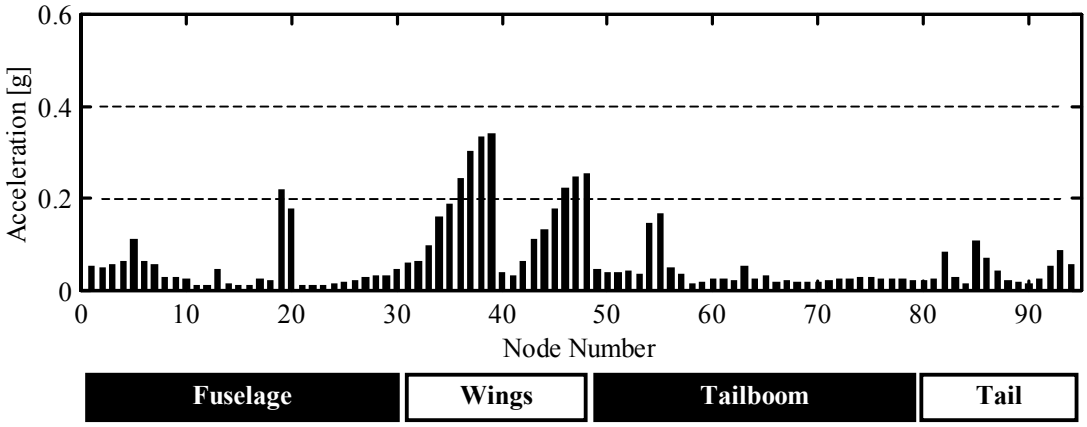

Nastran Model: Distributed Actuation, Controlled vibration response to hub excitation

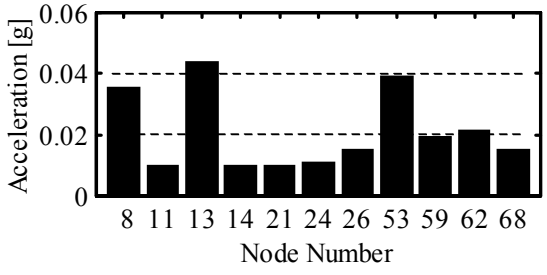

Nastran Model: Distributed Actuation, Controlled vibration at target nodes (hub excitation)

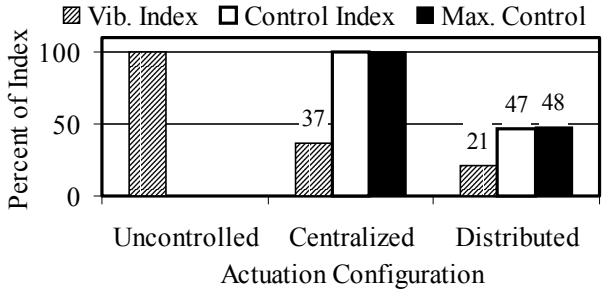

Nastran Model: Comparison of performance indices (hub excitation)

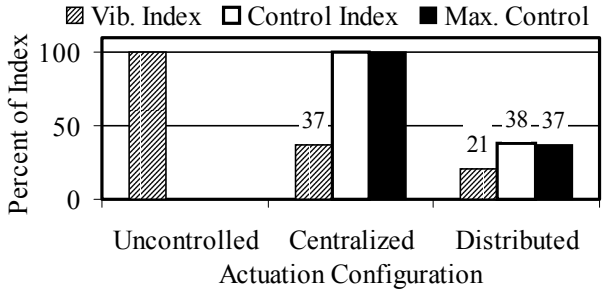

Nastran Model: Comparison of performance indices,
Re-optimized locations (hub excitation)

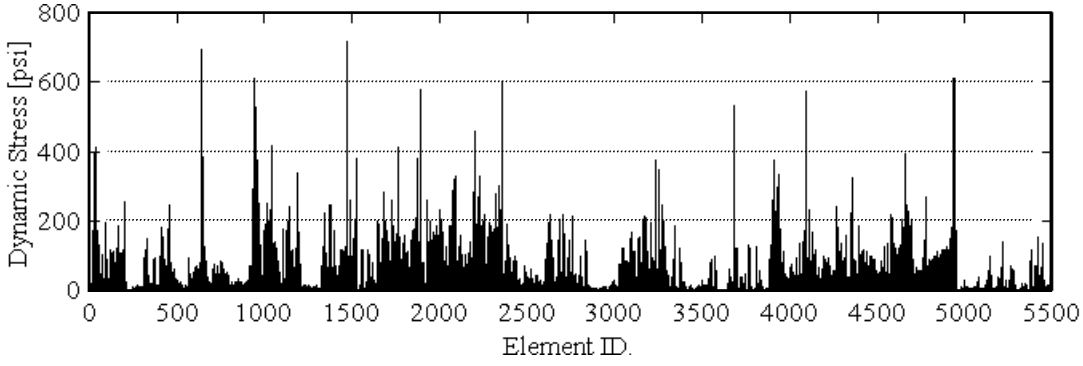

Nastran Finite Element dynamic stress from hub excitation (uncontrolled)

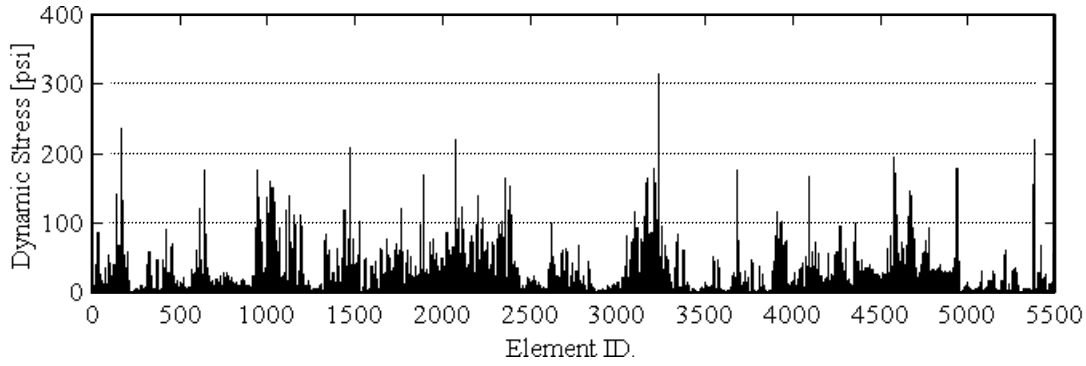

Nastran Finite Element dynamic stress, Centralized control of hub excitation

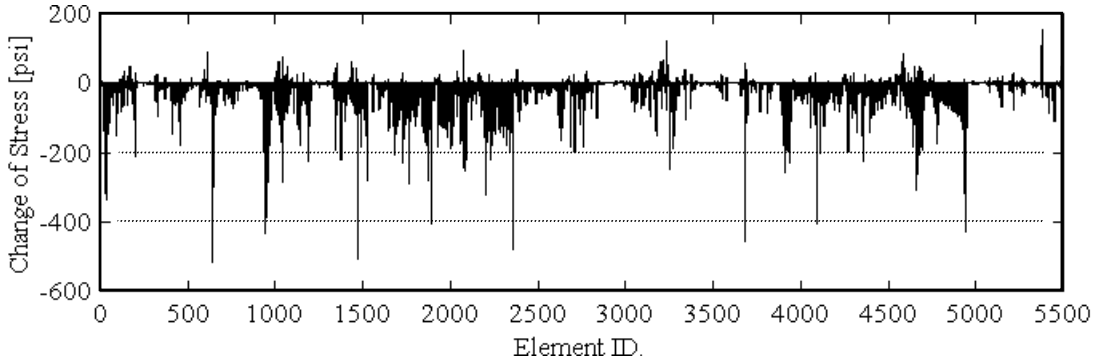

Change of element stress from uncontrolled to centralized control (hub excitation)

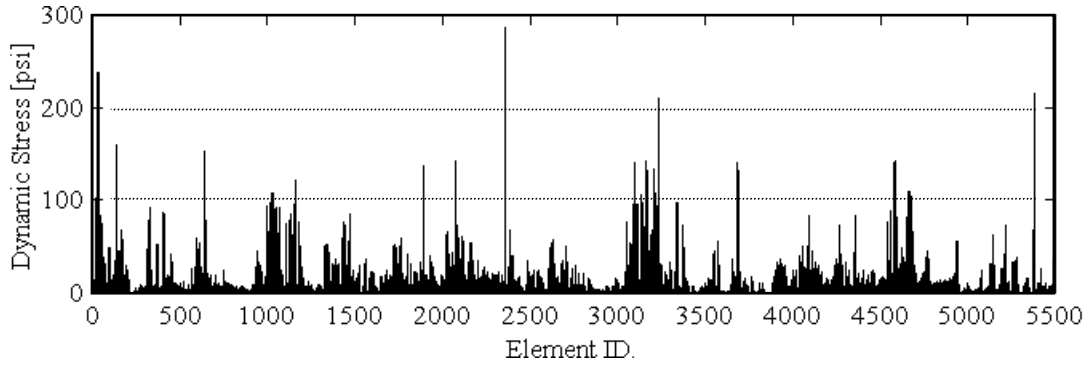

Nastran Finite Element dynamic stress, Distributed control of hub excitation

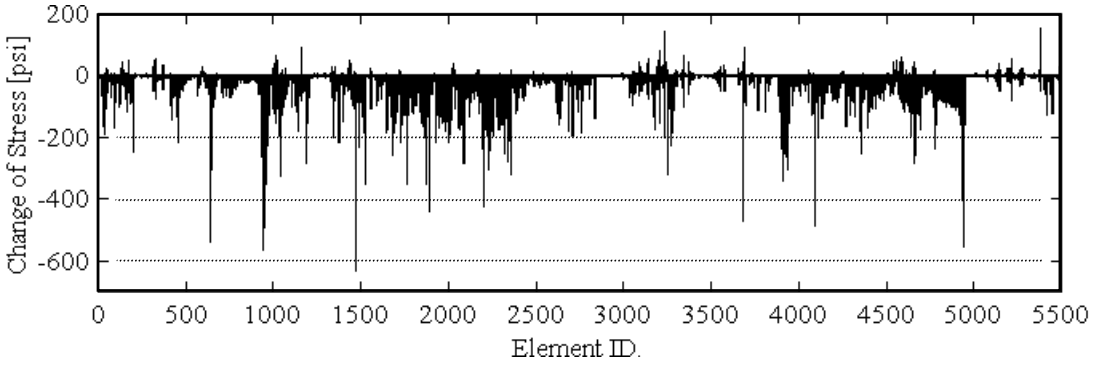

Change of element stress from uncontrolled to distributed control (hub excitation)

Appendix D

SCALED TAILBOOM MODEL SPECIFICATIONS AND ANALYSIS RESULTS

TITLE FRAME MEMBERS
QUANTITY = 6
MATERIAL .032 INCH ALUMINUM SHEET
DIMENSIONS: INCHES
PAGE 1 OF 1
ORGANIZATION PENN STATE
UNIVERSITY ROTORCRAFT CENTER

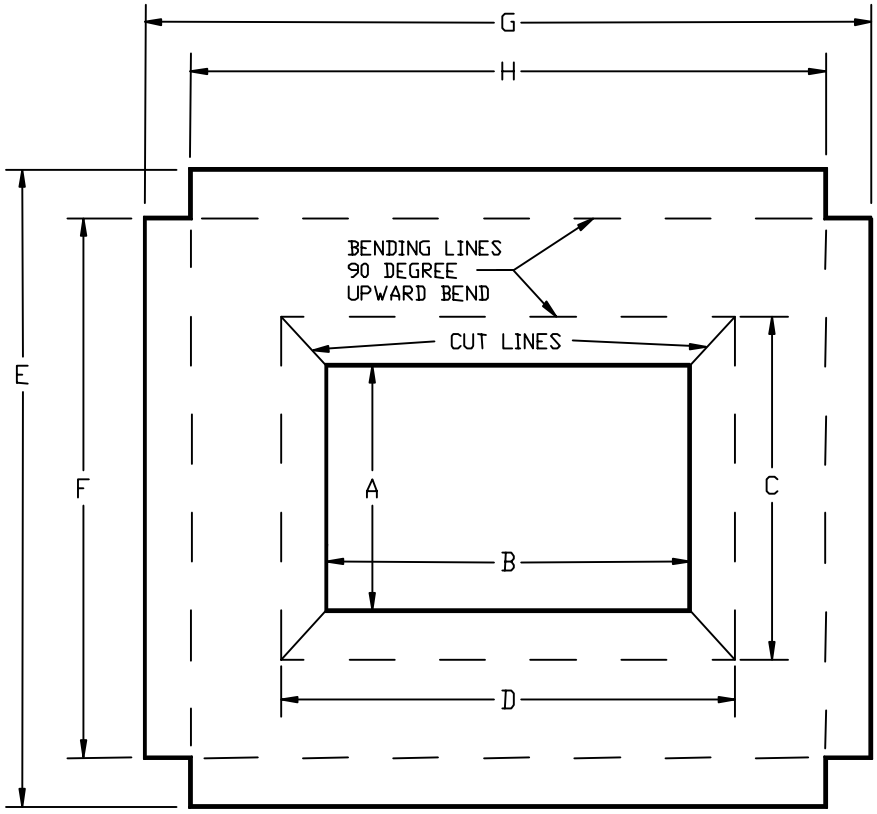

Scaled tailboom structure, Frame member layout, see accompanying table for dimensions

Scaled tailboom structure, Frame member dimensions								
	Dimension [inches]							
Frame No.	A	B	C	D	E	F	G	H
1	5.0	8.0	7.0	10.0	12.89	10.89	15.81	13.81
2	4.31	6.81	6.31	8.81	12.31	10.31	14.81	12.81
3	3.69	5.69	5.69	7.69	11.69	9.69	13.69	11.69
4	3.0	4.5	5.0	6.5	11.0	9.0	12.5	10.5
5	3.31	4.31	5.31	6.31	10.31	8.31	11.31	9.31
6	2.69	3.19	4.69	5.19	9.69	7.69	10.19	8.19

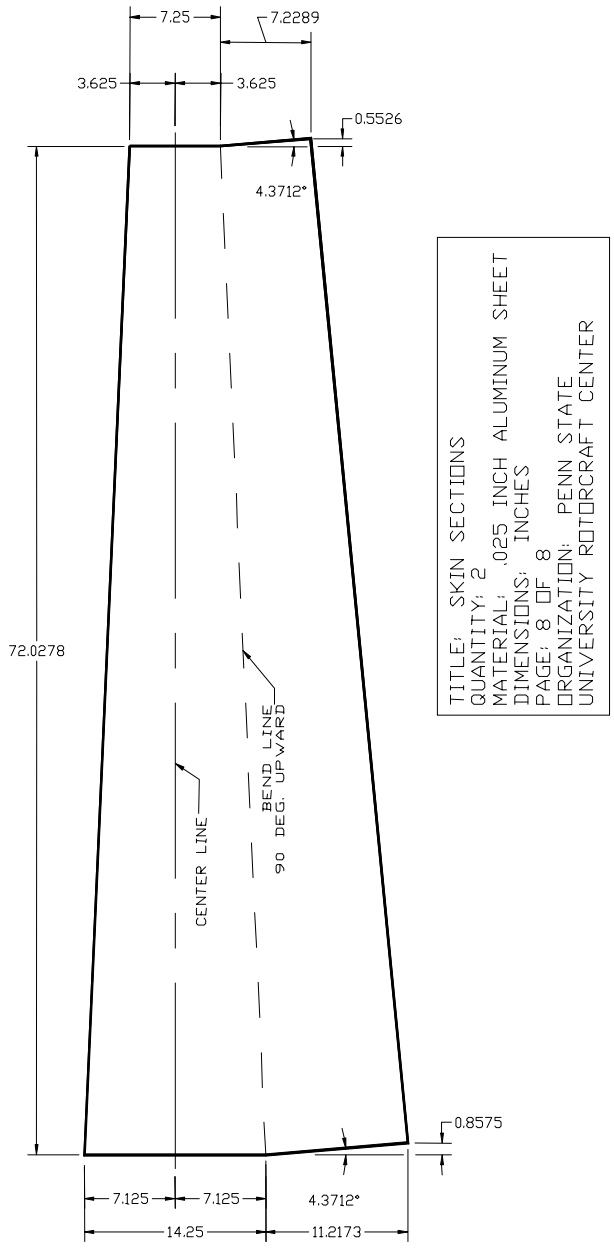

Scaled tailboom structure, Skin material layout and dimensions

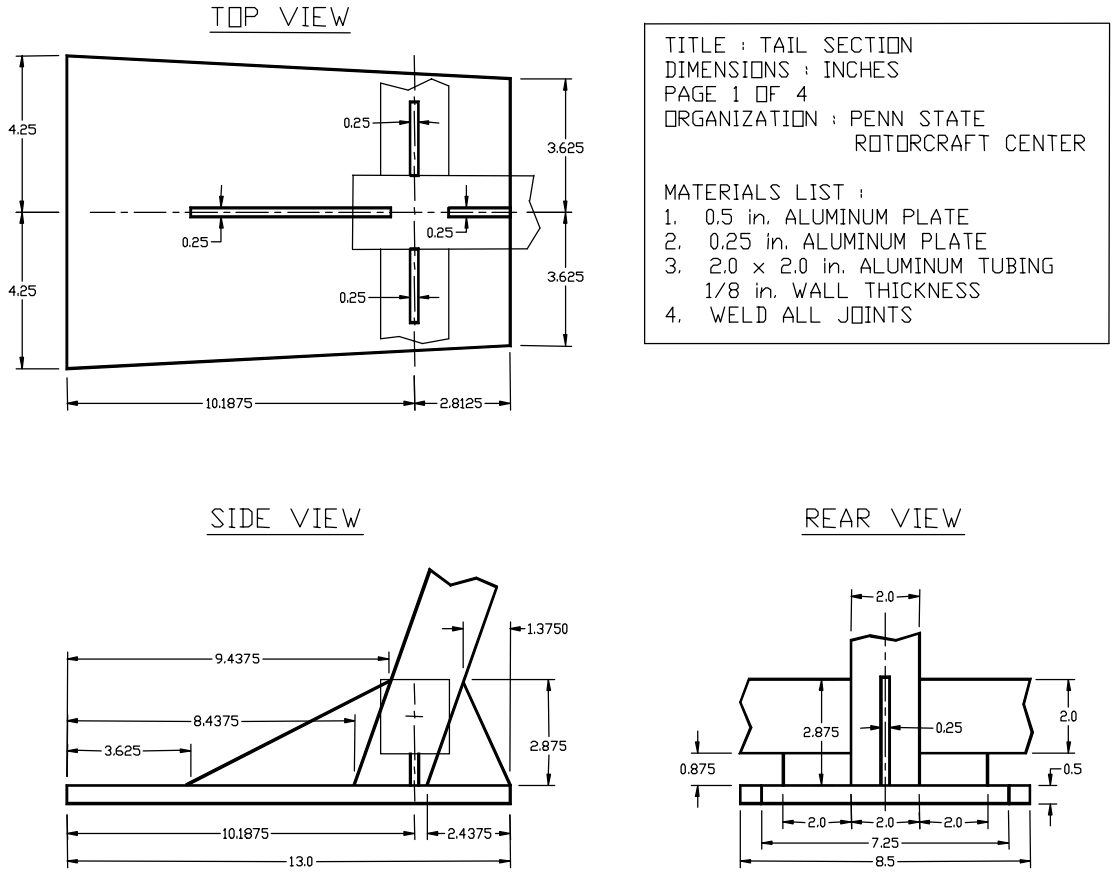

Scaled tailboom structure, Tail section layout and dimensions

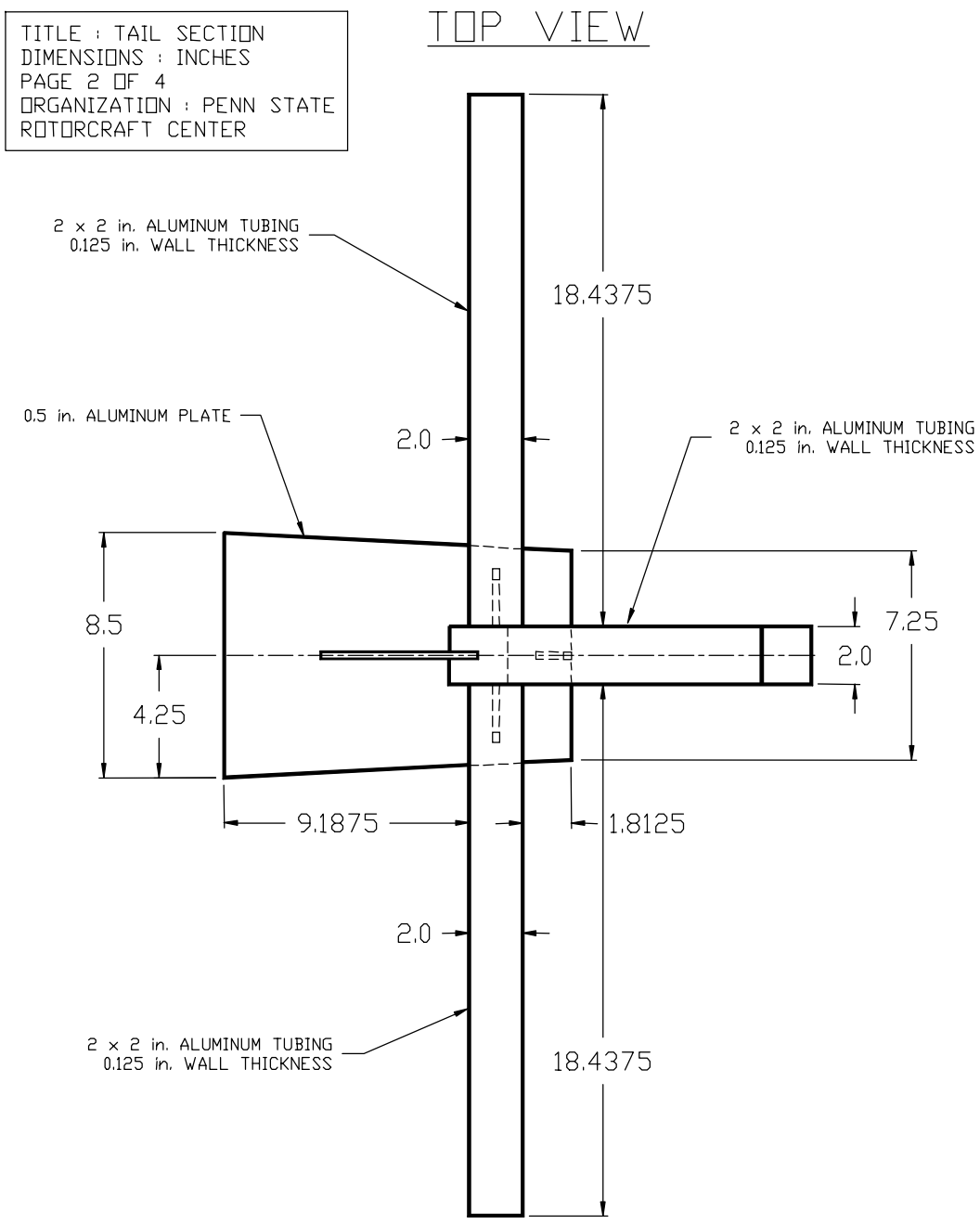

Scaled tailboom structure, Tail section layout and dimensions

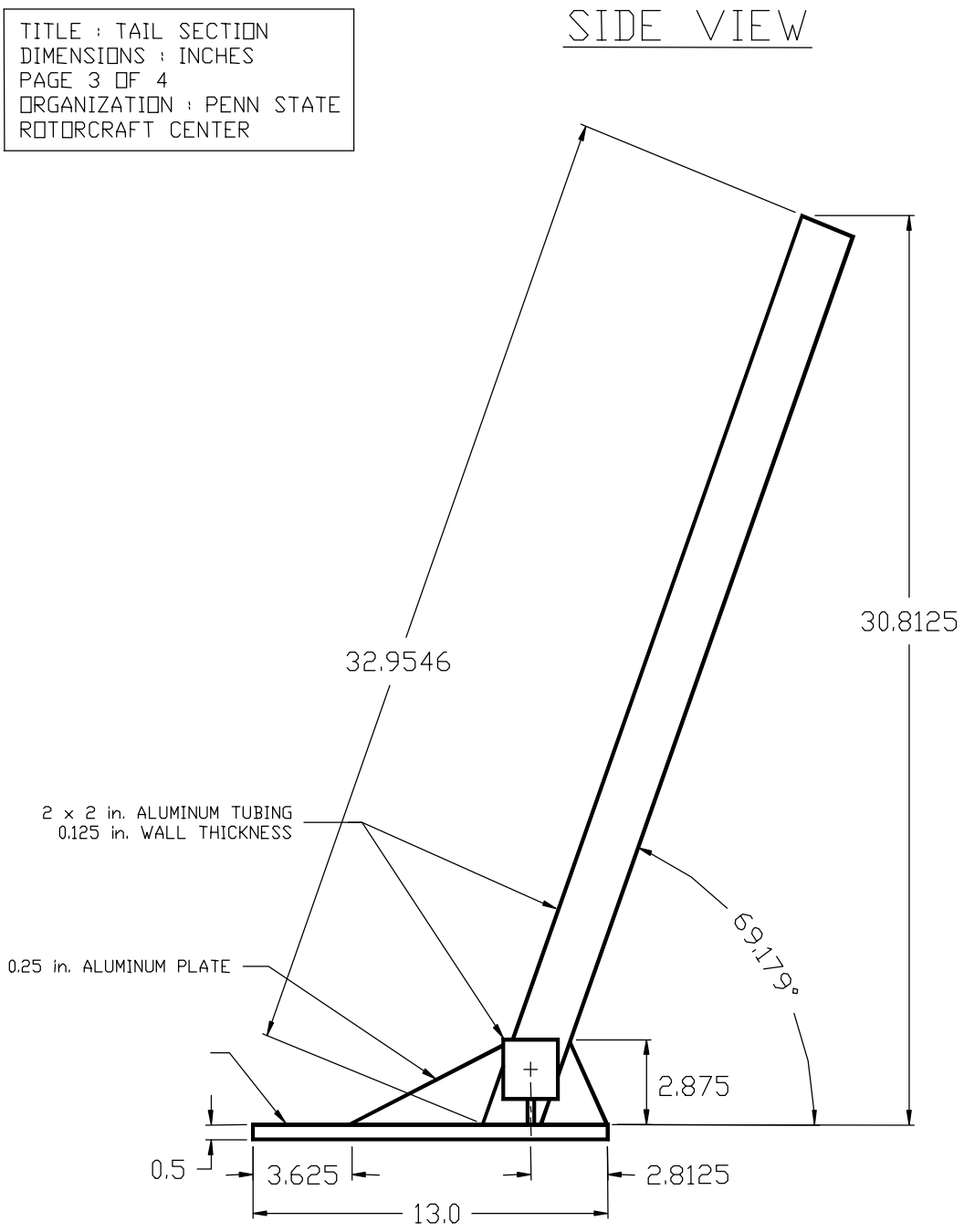

Scaled tailboom structure, Tail section layout and dimensions

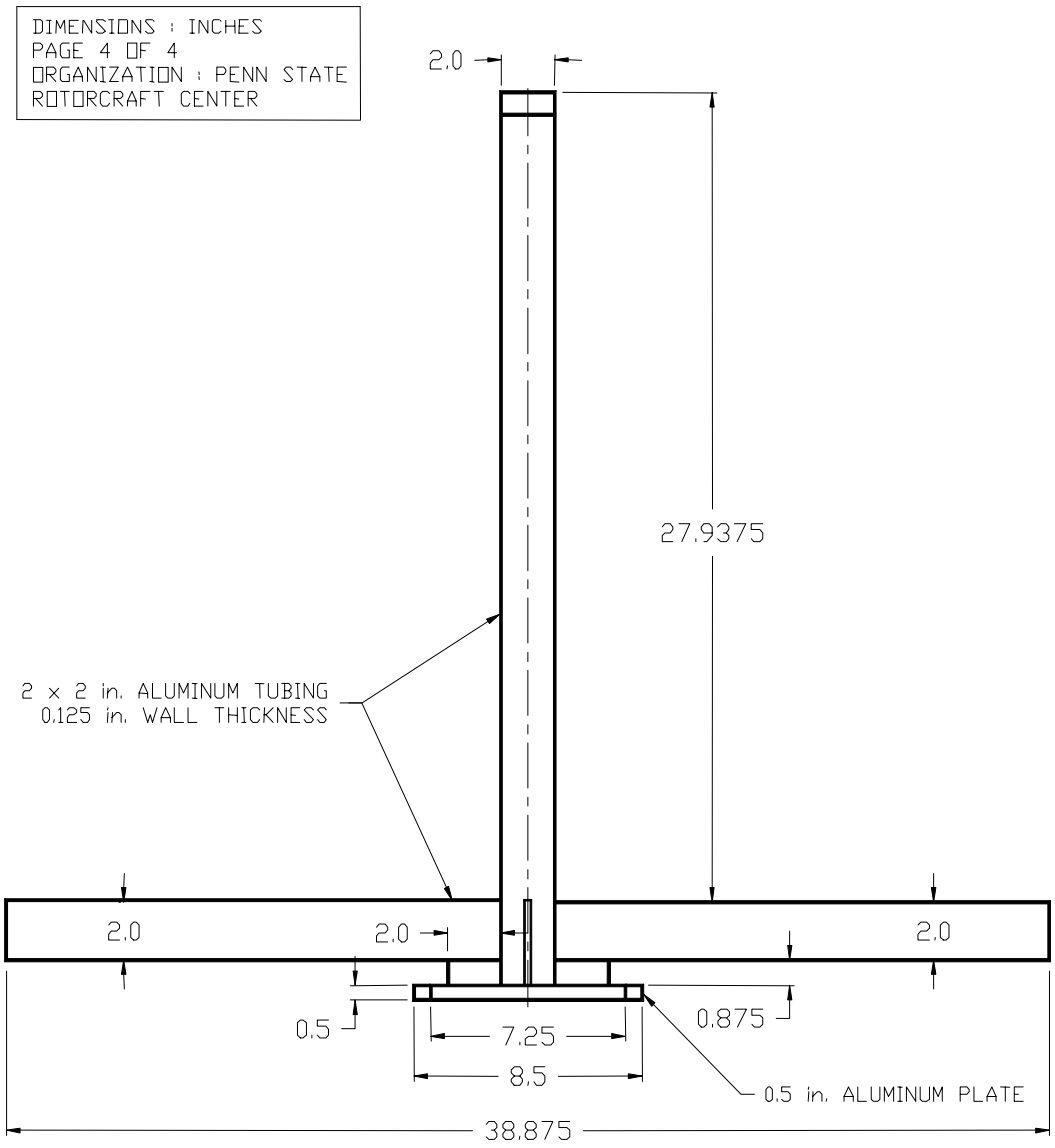

Scaled tailboom structure, Tail section layout and dimensions

TITLE : END PLATE
DIMENSIONS : INCHES
PAGE 1 OF 1
ORGANIZATION : PENN STATE ROTORCRAFT CENTER

MATERIALS LIST :
1. 0.5 in. ALUMINUM PLATE

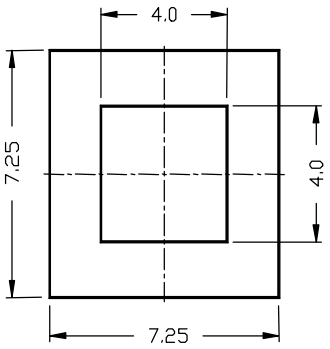

Scaled tailboom structure, End plate (last frame member) layout and dimensions

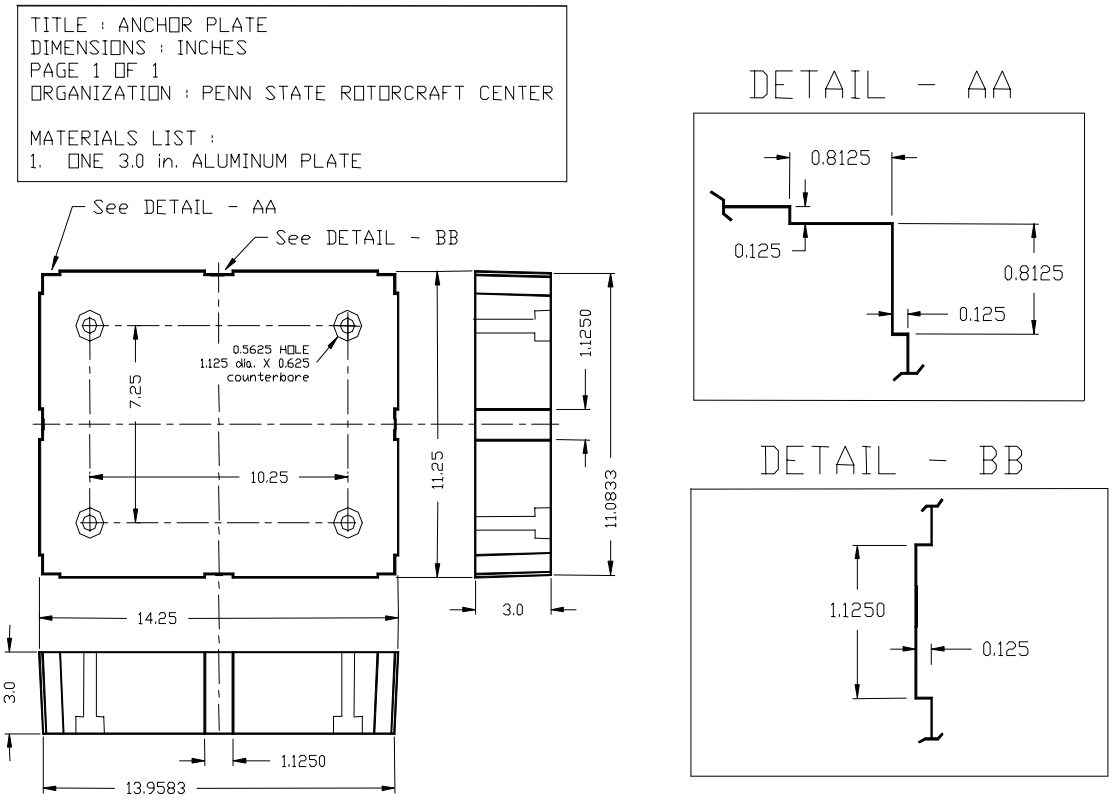

Scaled tailboom structure, Anchor plate (to base support) layout and dimensions

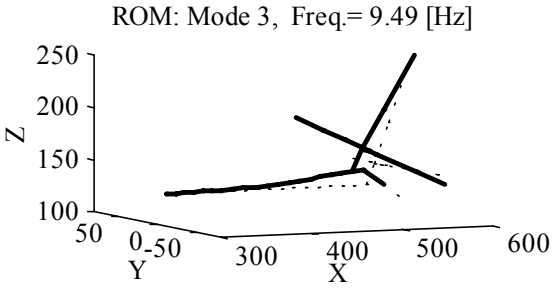

Apache Reduced Order Model (ROM) cantilevered tail section mode shape

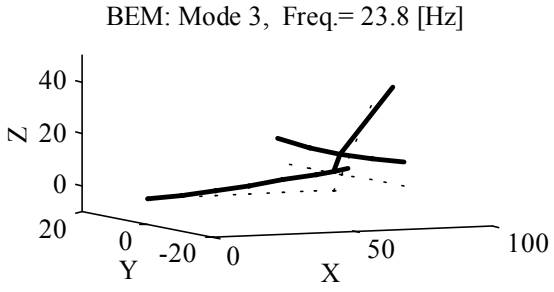

Scaled tailboom Beam Equivalent Model (BEM) mode shape

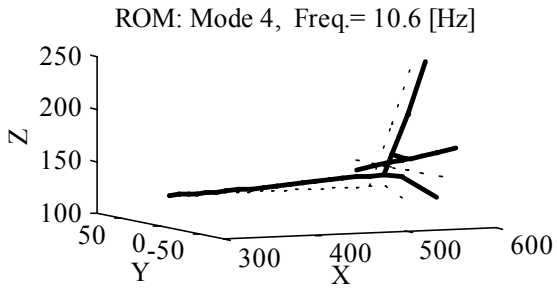

Apache Reduced Order Model (ROM) cantilevered tail section mode shape

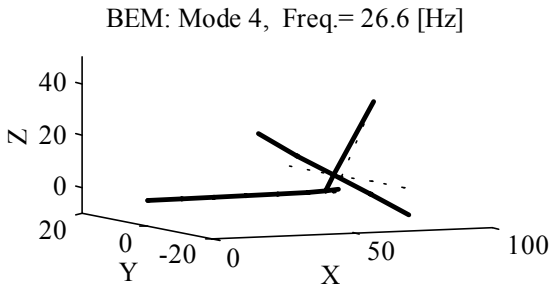

Scaled tailboom Beam Equivalent Model (BEM) mode shape

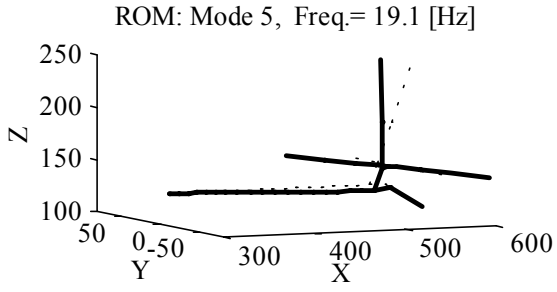

Apache Reduced Order Model (ROM) cantilevered tail section mode shape

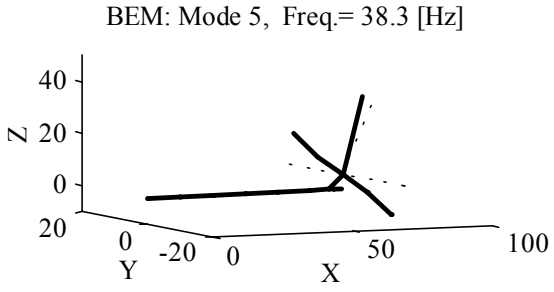

Scaled tailboom Beam Equivalent Model (BEM) mode shape

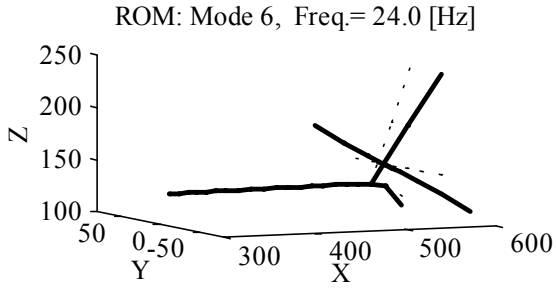

Apache Reduced Order Model (ROM) cantilevered tail section mode shape

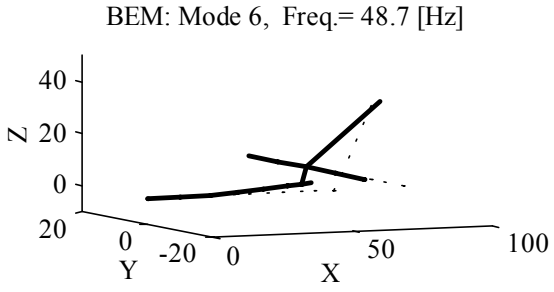

Scaled tailboom Beam Equivalent Model (BEM) mode shape

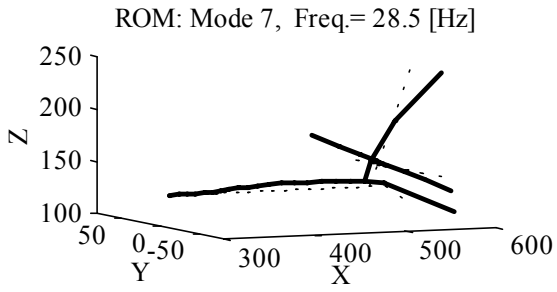

Apache Reduced Order Model (ROM) cantilevered tail section mode shape

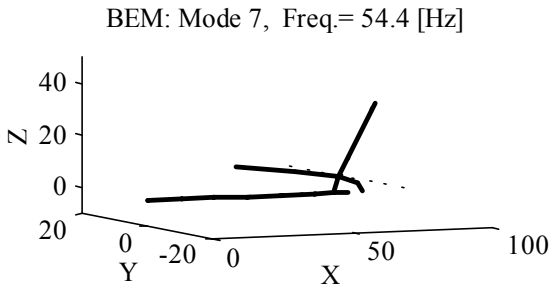

Scaled tailboom Beam Equivalent Model (BEM) mode shape

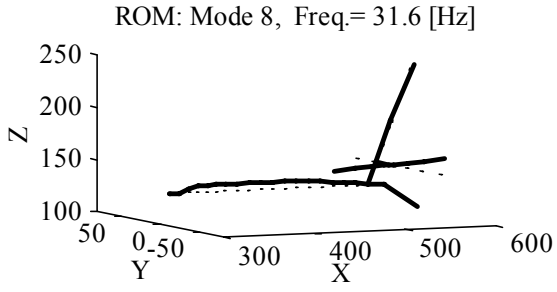

Apache Reduced Order Model (ROM) cantilevered tail section mode shape

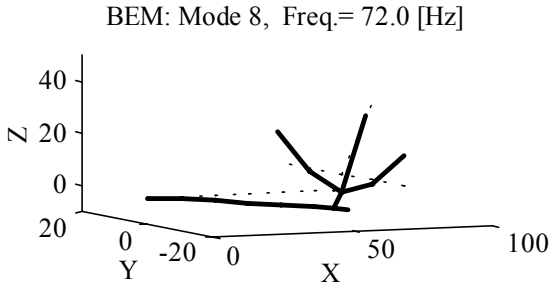

Scaled tailboom Beam Equivalent Model (BEM) mode shape

Program to formulate the tailboom BEM model parameters

```
% This MATLAB program is part of a computer software package for
% the design and analysis of a scaled tailboom structure model.
%
%
% Written by: David E. Heverly II                                  9/1/00
%             Mechanical Engineering Ph.D. Candidate
%             The Pennsylvania State University
%*********************************************************
% Filename = inframe.m
%*********************************************************
% This program creates an input data file for "frame.m" a Finite
% Element based analysis program of Rigid-jointed Space Frames.
```

Program to formulate the tailboom BEM model parameters

```
% "Frame.m" creates a beam equivalent model of the tailboom structure.
% This MATLAB m-file must be executed prior to executing "frame.m"
%
%************ Variable names/definitions **************
% Input:
%  nj - number of nodes
%  mems - number of elements
%  nmatl - number of element/material types/properties
%  nsup - number od supported/restrained nodes
%  Eref - reference elastic modulus
%  x,y,z - global coordinates of model node locations
%  Etop - element topology, node connectivity
%  *frm - frame member dimensions/properties
%  *st - stringer dimensions/properties
%  *sk - skin dimensions/properties
%  *vs - vertical stabilizer dimesions/properties
%  *hs - horizontal stabilizer dimesions/properties
%  E - elastic modulus
%  G - rigidity/shear modulus
%  dens - material density
%
%
% Output: (Beam Equivalent properties)
%  elast(i) - Elastic modulus
%  rigd(i) - Rigidity modulus
%  area(i) - Cross-sectional area
%  xin(i) - Torsional constant of cross section
%  yin(i) - 2nd moment of area of the cross section about x-y plane
%  zin(i) - 2nd moment of area of the cross section about x-z plane
%  xjp(i) - Polar 2nd moment of area of cross section
%  dens(i) - Material density
%
%*********************************************************

clear    % Clears all variables from computer memory

%General descriptive parameters
nj=14;          % Number of joints/nodes
mems=13;        % Number of elements or members
nmatl=9;        % Number of element/material types
nsup=1;         % Number of supported/restrained joints
nconc=10;       % Number of concentrated masses (at joints/nodes)
Eref = 9.99e6; % Reference elastic modulus [psi]


% Global coordinates of each structural joint, followed by the
% global coordinates of the imaginary nodes. Imaginary nodes are
% needed to define the principle "x-y" bending plane of each
% element, which may be an existing joint of the structure.
x(1)=0.0;       y(1)=0.0;       z(1)=0.0;
x(2)=12.0;      y(2)=0.0;       z(2)=0.0;
```

Program to formulate the tailboom BEM model parameters

```
x(3)=24.0;      y(3)=0.0;       z(3)=0.0;
x(4)=36.0;      y(4)=0.0;       z(4)=0.0;
x(5)=48.0;      y(5)=0.0;       z(5)=0.0;
x(6)=60.0;      y(6)=0.0;       z(6)=0.0;
x(7)=66.8125;   y(7)=0.0;       z(7)=0.0;
x(8)=72.0;      y(8)=0.0;       z(8)=0.0;
x(9)=69.37;     y(9)=0.0;       z(9)=6.202;
x(10)=80.978;   y(10)=0.0;      z(10)=34.35;
x(11)=69.37;    y(11)=-19.456;  z(11)=6.202;
x(12)=69.37;    y(12)=-9.5;     z(12)=6.202;
x(13)=69.37;    y(13)=9.5;      z(13)=6.202;
x(14)=69.37;    y(14)=19.456;   z(14)=6.202;
x(15)=0.0;      y(15)=70.0;     z(15)=6.202;% Imaginary node
x(16)=0.0;      y(16)=70.0;     z(16)=0.0;  % Imaginary node
x(17)=0.0;      y(17)=0.0;      z(17)=27.55;% Imaginary node

% NOTE: The principle "x-y" bending plane (in local element
coordinates)
%       of an element is defined by the triangular plane formed by the
%       "i,j,k" nodes. Node "k" may be an existing node of the
structure
%       or an imaginary node.
%  Element Topology
%   Start  End   Imaginary
%   Node   Node  Node
%     i     j     k     (Mat. Type) (Element type)
Etop=[1     2     16        1       1  % Element 1
      2     3     16        2       1  % Element 2
      3     4     16        3       1  % Element 3
      4     5     16        4       1  % Element 4
      5     6     16        5       1  % Element 5
      6     7     16        6       1  % Element 6
      7     8     16        7       1  % Element 7
      7     9     17        8       1  % Element 8
      9     10    17        8       1  % Element 9
      11    12    15        9       1  % Element 10
      12    9     15        9       1  % Element 11
      9     13    15        9       1  % Element 12
      13    14    15        9       1];% Element 13

% Frame members Dimensions (Aluminum sheet metal)
%*******************************************************
% Frame member width at element center between nodes
afrm(1)=13.42; afrm(2)=12.25; afrm(3)=11.08; afrm(4)=9.92;
afrm(5)=8.75; afrm(6)=7.84; afrm(7)=7.25;
% Frame member height at element center between nodes
bfrm(1)=10.67; bfrm(2)=10.0; bfrm(3)=9.33; bfrm(4)=8.67;
bfrm(5)=8.0; bfrm(6)=7.478; bfrm(7)=7.144;  %height
tfrm = .032;   % frame member thickness
densfrm = (0.0979/386.4);     % material density of the frame members
```

Program to formulate the tailboom BEM model parameters

```
% Stringer Dimensions
%*******************************************************
% Outer Stringer Dimensions (Aluminum angles)
lego = 0.75;   % height & width of angles, outer stringers
tst = 1/8;     % thickness of angles
% ybar distance from outer leg surface to center-of-gravity
cgdist = (lego^2+tst*lego-tst^2)/(4*lego-2*tst);
Est = 9.99e6;  % Modulus of elasticity:
densst = (0.0979/386.4);   % Material density
% Area moment of inertia about the stringers centroid
Ist = ((1/12)*(lego-tst)*(tst^3)+(lego-tst)*tst*(cgdist-
tst/2)^2)+((1/12)*tst*(lego^3)+((lego/2-cgdist)^2)*lego*tst);
areasto = 2*lego*tst-tst^2;  % cross section area of stringer
Length=72;        % Overall length of tailboom structure
legi=1.0;      % Width of inner stringers, rectangular shape
% Inner Stringer Dimensions (Aluminum flat stock)
areasti=legi*tst;  % Area of inner strigers
Isti=(1/12)*legi*tst^3; % Area moment of inertia
% Weight of all stringers in LBSf
strwght=(4*areasto+4*areasti)*densst*Length*386.4;

% Skin Dimensions (Aluminum sheet metal)
%*******************************************************
tsk = .032;             % thickness of skin
Esk = 9.99e6;           % Modulus of elasticity
Gsk = 3.77e6;           % Shear modulus
denssk = (0.0979/386.4);   % Material density

%*******************************************************
% Compute beam equivalent properties from component properties
%*******************************************************
totmass=0;
for i=1:7
   lel(i)=x(i+1)-x(i); % element length
  % Stringers
  % distance from stringer c.g. to global Y-axis
  ast(i) = afrm(i)/2+tst-cgdist;
  % distance from stringer c.g. to global Z-axis
  bst(i) = bfrm(i)/2+tst-cgdist;
  % Skin
  ask(i) = afrm(i);     % width at center between nodes
  bsk(i) = bfrm(i);     % height at center between nodes
  skwght(i)=(2*ask(i)+2*bsk(i))*tsk*denssk*lel(i)*386.4;

  % Equivalent moments of area, cross-sectional area
  if i>=6


IY(i)=(2*(Est/Eref)*(Isti+areasti*bst(i)^2))+(4*(Est/Eref)*(Ist+areasto
*bst(i)^2))+(2*(Esk/Eref)*(((1/12)*ask(i)*tsk^3)+(ask(i)*tsk*(bsk(i)/2)
^2)+((1/12)*tsk*bsk(i)^3)))+(((1/12)*afrm(i)*0.5^3)+(afrm(i)*0.5*(bfrm(
```

Program to formulate the tailboom BEM model parameters

```
i)/2+0.25)^2));


IZ(i)=(2*(Est/Eref)*(Isti+areasti*ast(i)^2))+(4*(Est/Eref)*(Ist+areasto
*ast(i)^2))+(2*(Esk/Eref)*(((1/12)*bsk(i)*tsk^3)+(bsk(i)*tsk*(ask(i)/2)
^2)+((1/12)*tsk*ask(i)^3)))+((1/12)*0.5*(afrm(i))^3);

    J(i)=((1/12)*((ask(i)*bsk(i)*(ask(i)^2+bsk(i)^2))-((ask(i)-
2*tsk)*(bsk(i)-2*tsk)*((ask(i)-2*tsk)^2+(bsk(i)-
2*tsk)^2))))+(((1/12)*afrm(i)*0.5^3)+(afrm(i)*0.5*(bfrm(i)/2+0.25)^2))+
((1/12)*0.5*(afrm(i))^3);


massdistrib(i)=(4*areasto+4*areasti)*densst+2*tsk*denssk*(ask(i)+bsk(i)
)+0.46*afrm(i)*densfrm;


Acs(i)=((2*ask(i)+2*bsk(i))*tsk*(Esk/Eref))+((4*areasto+4*areasti)*(Est
/Eref))+0.5*afrm(i);

 else


IY(i)=(2*(Est/Eref)*(Isti+areasti*bst(i)^2))+(4*(Est/Eref)*(Ist+areasto
*bst(i)^2))+(2*(Esk/Eref)*(((1/12)*ask(i)*tsk^3)+(ask(i)*tsk*(bsk(i)/2)
^2)+((1/12)*tsk*bsk(i)^3)));


IZ(i)=(2*(Est/Eref)*(Isti+areasti*ast(i)^2))+(4*(Est/Eref)*(Ist+areasto
*ast(i)^2))+(2*(Esk/Eref)*(((1/12)*bsk(i)*tsk^3)+(bsk(i)*tsk*(ask(i)/2)
^2)+((1/12)*tsk*ask(i)^3)));

    J(i)=(1/12)*((ask(i)*bsk(i)*(ask(i)^2+bsk(i)^2))-((ask(i)-
2*tsk)*(bsk(i)-2*tsk)*((ask(i)-2*tsk)^2+(bsk(i)-2*tsk)^2)));


massdistrib(i)=(4*areasto+4*areasti)*densst+2*tsk*denssk*(ask(i)+bsk(i)
);


Acs(i)=((2*ask(i)+2*bsk(i))*tsk*(Esk/Eref))+((4*areasto+4*areasti)*area
sto*(Est/Eref));

 end

  % Frame members
  hith=11-(4/72)*x(i+1);
  widt=14-(7/72)*x(i+1);
  % volume of frame material
  if i<=3
    volfrm(i)= ((widt)*(hith)-(widt-4)*(hith-4))*tfrm;
```

Program to formulate the tailboom BEM model parameters

```
  elseif i<=5
    volfrm(i)= ((widt)*(hith)-(widt-3)*(hith-3))*tfrm;
  elseif i==6
    volfrm(i)=0.0;
  else
    volfrm(i)=(((widt*hith)-((widt-3)*(hith-3)))*0.532);
  end
  frmwght(i)=volfrm(i)*densfrm*386.4; % Weight of all frames in LBSf
  pointmass(i) = volfrm(i)*densfrm; % frame member mass added at nodes;

  % Equivalent Beam Element Properties
  elast(i)=Eref;              % Elastic modulus - E
  rigd(i)=Gsk;                % Rigidity modulus - G
  area(i)=Acs(i);             % Cross-sectional area - A
  xin(i)=J(i);                % Torsional constant of cross section - J
  yin(i)=IY(i);               % 2nd moment of area about x-y plane - Iy
  zin(i)=IZ(i);               % 2nd moment of area about x-z plane - Iz
  xjp(i)=yin(i)+zin(i);% Polar 2nd moment of area of cross section - Ip
  dens(i)=massdistrib(i)/Acs(i);% Material density - rhoa
  totmass=totmass+(lel(i)*massdistrib(i))+pointmass(i);
end
%*********************************************************
%*********************************************************

UGmass=0.7*totmass;  % Point mass for tail rotor upper gearbox
HSmass=0.3*totmass;  % Point mass for tail rotor lower gearbox
tailbwgt=totmass*386.4;
UGwgt=UGmass*386.4;
HSwgt=2*HSmass*386.4;
disp(' ')
disp(['Vertical tail Mass = ',num2str(UGmass*386.4),' [lbs]'])
disp(' ')
disp(['Horizontal tail Masses = ',num2str(HSmass*386.4),' [lbs]'])
disp(' ')

% Vertical Stabilizer dimensions & properties
%*******************************************************
avs=2;                  % width of vertical stabilizer elements
bvs=2;                  % height of vertical stabilizer elements
tvs=1/8;                % wall thickness of vertical stabilizer tubing
dens(8)=(0.0979/386.4); % Material density - rhoa (Aluminum)
elast(8)=Eref;          % Elastic modulus - E (Aluminum)
rigd(8)=Gsk;            % Rigidity modulus - G (Aluminum)
area(8)=2*(avs+bvs-tvs-tvs)*tvs;       % Cross-sectional area - A

xin(8)=((1/12)*avs*bvs*(avs^2+bvs^2))-((1/12)*(avs-2*tvs)*(bvs-
2*tvs)*((avs-2*tvs)^2+(bvs-2*tvs)^2)); % Torsional constant of cross
section - J

yin(8)=2*(((1/12)*avs*tvs^3)+(avs*tvs*(bvs/2-
tvs/2)^2)+((1/12)*tvs*bvs^3)); % 2nd moment of area of the cross
```

Program to formulate the tailboom BEM model parameters

```
section about x-y plane - Iy

zin(8)=2*(((1/12)*bvs*tvs^3)+(bvs*tvs*(avs/2-
tvs/2)^2)+((1/12)*tvs*avs^3)); % 2nd moment of area of the cross
section about x-z plane - Iz

xjp(8)=xin(8);       % Polar 2nd moment of area of cross section - Ip

% Horizontal Stabilizer dimensions & properties
%*******************************************************
ahs=2;               % width of horizontal stabilizer elements
bhs=2;               % height of horizontal stabilizer elements
ths=1/8;             % wall thickness of horizontal stabilizer tubing
dens(9)=(0.0979/386.4); % Material density - rhoa (Aluminum)
elast(9)=Eref;          % Elastic modulus - E (Aluminum)
rigd(9)=Gsk;            % Rigidity modulus - G (Aluminum)
area(9)=2*(ahs+bhs-ths-ths)*ths;       % Cross-sectional area - A

xin(9)=((1/12)*ahs*bhs*(ahs^2+bhs^2))-((1/12)*(ahs-2*ths)*(bhs-
2*ths)*((ahs-2*ths)^2+(bhs-2*ths)^2)); % Torsional constant of cross
section - J

yin(9)=2*(((1/12)*ahs*ths^3)+(ahs*ths*(bhs/2-
ths/2)^2)+((1/12)*ths*bhs^3)); % 2nd moment of area of the cross
section about x-y plane - Iy

zin(9)=2*(((1/12)*bhs*ths^3)+(bhs*ths*(ahs/2-
ths/2)^2)+((1/12)*ths*ahs^3)); % 2nd moment of area of the cross
section about x-z plane - Iz

xjp(9)=xin(9);       % Polar 2nd moment of area of cross section - Ip

vswgt=(area(8)*dens(8)*(((x(10)-x(7))^2+(y(10)-y(7))^2+(z(10)-
z(7))^2)^0.5))*386.4;
hswgt=(area(9)*dens(9)*(((x(14)-x(11))^2+(y(14)-y(11))^2+(z(14)-
z(11))^2)^0.5))*386.4;
totweight=(totmass+UGmass+2*HSmass)*386.4+vswgt+hswgt;
disp(['Total Tailboom Weight = ',num2str(totweight),' [lbs]'])
disp(' ')

% Constrained Joints/Nodes
%*******************************************************
% NOTE: 0=No Restraint & 1=Full Restraint of specified d.o.f.
%     Joint #   X-tran  Y-tran  Z-tran  X-rot  Y-rot  Z-rot
Jrest=[ 1         1       1       1       1      0      1];

% Concentrated Translational Masses
%*******************************************************
% Note concentrated masses MUST be located at joints
nposn(1)=7;       % Unconstrained Global dof of joint at mass location
xmass(1)=pointmass(1);  % Value of concentrated mass
```

Program to formulate the tailboom BEM model parameters

```
nposn(2)=13;      % Unconstrained Global dof of joint at mass location
xmass(2)=pointmass(2);  % Value of concentrated mass
nposn(3)=19;      % Unconstrained Global dof of joint at mass location
xmass(3)=pointmass(3);  % Value of concentrated mass
nposn(4)=25;      % Unconstrained Global dof of joint at mass location
xmass(4)=pointmass(4);  % Value of concentrated mass
nposn(5)=31;      % Unconstrained Global dof of joint at mass location
xmass(5)=pointmass(5);  % Value of concentrated mass
nposn(6)=37;      % Unconstrained Global dof of joint at mass location
xmass(6)=pointmass(6);  % Value of concentrated mass
nposn(7)=43;      % Unconstrained Global dof of joint at mass location
xmass(7)=pointmass(7);  % Value of concentrated mass
nposn(8)=55;      % Unconstrained Global dof of joint at mass location
xmass(8)=UGmass;  % Value of concentrated mass
nposn(9)=61;      % Unconstrained Global dof of joint at mass location
xmass(9)=HSmass;  % Value of concentrated mass
nposn(10)=79;     % Unconstrained Global dof of joint at mass location
xmass(10)=HSmass; % Value of concentrated mass

save inframe   % Saves variables in binary file "inframe.mat"
               % to be loaded by "frame.m"
%********************** End of File ****************************
```

Main program to create the tailboom BEM finite element model

```
% This MATLAB program is part of a computer software package for
% the design and analysis of a scaled tailboom structure model.
%
%
% Written by: David E. Heverly II                                  9/1/00
%             Mechanical Engineering Ph.D. Candidate
%             The Pennsylvania State University
%*********************************************************
% Filename = frame.m
%*********************************************************
% Finite Element based analysis program to create a beam
% equivalent model of the scaled tailboom structure.
% The input data is created by "inframe.m" and loaded
% by this program. The main program calls the following
% subroutines/function m-files:
%  1.) assembl.m
%  2.) FEstiff.m
%  3.) FEmass.m
%
%************ Variable names/definitions **************
% Input:
```

Main program to create the tailboom BEM finite element model

```
%  nj - number of nodes
%  mems - number of elements
%  nmatl - number of element/material types/properties
%  nsup - number od supported/restrained nodes
%  x,y,z - global coordinates of model node locations
%  Etop - element topology, node connectivity
% (Beam Equivalent properties)
%  elast(i) - Elastic modulus
%  rigd(i) - Rigidity modulus - G
%  area(i) - Cross-sectional area - A
%  xin(i) - Torsional constant of cross section - J
%  yin(i) - 2nd moment of area of the cross section about x-y plane
%  zin(i) - 2nd moment of area of the cross section about x-z plane
%  xjp(i) - Polar 2nd moment of area of cross section
%  dens(i) - Material density
%
% Output:
%  Mg - global mass matrix
%  Kg - global stiffness matrix
%  evec - mass normalized eigenvectors
%  eval - eigenvalues
%
%************************************************************

%*****************************************************
% Start Main Program
%*****************************************************
clear all         % Clears variables from computer memory
load inframe      % Loads the binary input data file

dof=6*nj;         % Unrestrained global degrees of freedom

% Initialize Mass & Stiffness Matrices
stiff=zeros(dof,dof);
mass=zeros(dof,dof);

% Loop thru each element: compute element matrices
% & assemble global matrices
%************************
for mem=1:mems
 i=Etop(mem,1);
 j=Etop(mem,2);
 k=Etop(mem,3);
 matl=Etop(mem,4);
 E=elast(matl); rho=dens(matl); G=rigd(matl); csa=area(matl);
 TC=xin(matl); smay=yin(matl); smaz=zin(matl); xpol=xjp(matl);
 xi=x(i);  yi=y(i);  zi=z(i);
 xj=x(j);  yj=y(j);  zj=z(j);
 xk=x(k);  yk=y(k);  zk=z(k);
 % Form elemental Stiffness matrix
```

Main program to create the tailboom BEM finite element model

```
sk=FEstiff(Etop(mem,5),xi,yi,zi,xj,yj,zj,xk,yk,zk,csa,TC,smay,smaz,E,G)
;
 % Form elemental Mass matrix

sm=FEmass(Etop(mem,5),xi,yi,zi,xj,yj,zj,xk,yk,zk,csa,smay,smaz,xpol,rho
);
 stiff=assembl(stiff,sk,i,j,k,Etop(mem,5));% Assemble global stiffness
matrix
 mass=assembl(mass,sm,i,j,k,Etop(mem,5)); % Assemble global mass matrix
end
%**********************************

% Addition of concentrated translational masses to global mass matrix
%****************************************************
if nconc>0
 for ii=1:nconc
  n9=nposn(ii);
  mass(n9,n9)=mass(n9,n9)+xmass(ii);
  mass(n9+1,n9+1)=mass(n9+1,n9+1)+xmass(ii);
  mass(n9+2,n9+2)=mass(n9+2,n9+2)+xmass(ii);
 end
end
%***********************************************

% Apply boundary conditions/constraints by deleting rows
% and columns from Unconstrained global matrices.
%*****************************************************
nn1=6*nj;
if nsup>0
 nn2=0;
 for i=1:nsup
  b2=(6*(Jrest(i,1)-1))-nn2;
  xr(1:6)=Jrest(i,2:7);
  nn3=0;
  for j=1:6
   if xr(j)==1
    mm1=b2+j-nn3;
    for ii=mm1:(nn1-1)
     b1=ii+1;
     for jj=1:nn1
      stiff(ii,jj)=stiff(b1,jj);
      mass(ii,jj)=mass(b1,jj);
     end
     for jj=1:nn1
      stiff(jj,ii)=stiff(jj,b1);
      mass(jj,ii)=mass(jj,b1);
     end
    end
    nn1=nn1-1;
    nn2=nn2+1;
    nn3=nn3+1;
```

Main program to create the tailboom BEM finite element model

```
   end
  end
 end
end
%**********************************

% Add Y-rotational stiffness at the root end
%**************************************
stiff(1,1)=stiff(1,1)+2.1e7;
%**************************************

% Make copies of constrained Mass & Stiffness matrices
%******************************************************
for ii=1:nn1
 for jj=1:nn1
  Kg(ii,jj)=stiff(ii,jj);
  Mg(ii,jj)=mass(ii,jj);
 end
end
%******************************************************

%  COMPUTE EIGENVALUES AND EIGENVECTORS
%************************************
disp('Computing eigenvalues and eigenvectors')
[V,lamda]=eig(Kg,Mg);
[lam,II]=sort(diag(lamda));
for i=1:nn1
   eval(i,1)=sqrt(lamda(II(i),II(i)));
   frq(i,1)=(sqrt(lamda(II(i),II(i))))/(2*pi);
   vec(:,i)=V(:,II(i));
end
%  Normalize wrt mass matrix
for i=1:nn1
  norm=((vec(:,i))')*Mg*(vec(:,i));
  evec(:,i)=(vec(:,i))/sqrt(norm);
end
%************************************

disp('Natural Frequencies [Hz]')
disp(frq(1:10))

% Save model data
disp('Saving model data in file bem-M-K.mat')
%************************************
save bem-M-K  Kg Mg eval evec
%***************** End of File ********************************
```

Subroutine to compute finite element stiffness matrix

```
function
sk=FEstiff(type,xio,yio,zio,xjo,yjo,zjo,xko,yko,zko,A,TC,smay,smaz,E,G)
% This MATLAB subroutine is part of a computer software package for
% the design and analysis of a scaled tailboom structure model.
%
%
% Written by: David E. Heverly II                                   9/1/00
%             Mechanical Engineering Ph.D. Candidate
%             The Pennsylvania State University
%*******************************************************
% Filename = FEstiff.m
%*******************************************************
% Form elemental stiffness matrix for the Finite Element Model
%
% Subroutine "Glb2Loc.m" is called to transform from local
% element coordinates to global coordinates
%
%  xio - global X-coordinate of first element node
%  yio - global Y-coordinate of first element node
%  zio - global Z-coordinate of first element node
%  xjo - global X-coordinate of second element node
%  yjo - global Y-coordinate of second element node
%  zjo - global Z-coordinate of second element node
%  xko - global X-coordinate of third element node
%  yko - global Y-coordinate of third element node
%  zko - global Z-coordinate of third element node
%  A - Cross-sectional area
%  TC - Torsional constant of cross section
%  smay - 2nd moment of area of the cross section about x-y plane
%  smaz - 2nd moment of area of the cross section about x-z plane
%  E - Elastic modulus
%  G - Rigidity/shear modulus
%
% Four Finite Element Types can be used to construct the model
%
% Type 1: One dimensional Beam Element (2 nodes)
%         degrees-of-freedom: {u,v,w,THETAx,THETAy,THETAz} at each node
%
% Type 2: Two dimensional Triangular Membrane Element (3 nodes)
%         (Plane Stress)degrees-of-freedom: {u,v} at each node
%
% Type 3: One dimensional Rod Element (2 nodes)
%         degrees-of-freedom: {u} at each node
%
% Type 4: One dimensional Discrete Scalar Spring Element (2 nodes)
%         degrees-of-freedom: {u AND/OR theta} at each node
%         Translational stiffness AND/OR Torsional stiffness between
nodes

% Elemental Stiffness Matrix for type 1 Beam elements
if type == 1
```

Subroutine to compute finite element stiffness matrix

```
% Compute element stiffness matrix
sk=zeros(12,12); % Initialize element matrix
xl=sqrt((xjo-xio)^2+(yjo-yio)^2+(zjo-zio)^2);
sk(1,1)=(A*E/xl);
sk(7,7)=sk(1,1);
sk(7,1)=-sk(1,1);
sk(1,7)=-sk(1,1);
sk(2,2)=12*E*smaz/(xl^3);
sk(8,8)=sk(2,2);
sk(8,2)=-sk(2,2);
sk(2,8)=-sk(2,2);
sk(6,2)=6*E*smaz/(xl^2);
sk(2,6)=sk(6,2);
sk(12,2)=sk(6,2);
sk(2,12)=sk(6,2);
sk(3,3)=12*E*smay/(xl^3);
sk(9,9)=sk(3,3);
sk(9,3)=-sk(3,3);
sk(3,9)=-sk(3,3);
sk(5,3)=-6*E*smay/(xl^2);
sk(3,5)=sk(5,3);
sk(11,3)=sk(5,3);
sk(3,11)=sk(11,3);
sk(4,4)=G*TC/xl;
sk(10,10)=sk(4,4);
sk(10,4)=-sk(4,4);
sk(4,10)=-sk(4,4);
sk(5,5)=4*E*smay/xl;
sk(11,11)=sk(5,5);
sk(11,5)=sk(5,5)/2.0;
sk(5,11)=sk(11,5);
sk(9,5)=6*E*smay/(xl^2);
sk(5,9)=sk(9,5);
sk(6,6)=4*E*smaz/xl;
sk(12,12)=sk(6,6);
sk(12,6)=sk(6,6)/2.0;
sk(6,12)=sk(12,6);
sk(8,6)=-6*E*smaz/(xl^2);
sk(6,8)=sk(8,6);
sk(12,8)=-6*E*smaz/(xl^2);
sk(8,12)=sk(12,8);
sk(11,9)=6*E*smay/(xl^2);
sk(9,11)=sk(11,9);
% Tranform element matrix to global coordinates
% Compute transformation matrix
zeta=Glb2Loc(xio,yio,zio,xjo,yjo,zjo,xko,yko,zko);
PSI=zeros(12,12);
PSI(1:3,1:3)=zeta;
PSI(4:6,4:6)=zeta;
PSI(7:9,7:9)=zeta;
PSI(10:12,10:12)=zeta;
```

Subroutine to compute finite element stiffness matrix

```
   sk=(PSI')*sk*PSI;
end

% Elemental Stiffness Matrix for type 2 Triangular membrane elements
if type == 2
   % Length of element sides
   L1=sqrt((xjo-xio)^2+(yjo-yio)^2+(zjo-zio)^2);
   L2=sqrt((xko-xjo)^2+(yko-yjo)^2+(zko-zjo)^2);
   L3=sqrt((xko-xio)^2+(yko-yio)^2+(zko-zio)^2);
   theta=acos((L2^2-L1^2-L3^2)/(-2*L1*L3));
   % Element in local (planar) coordinates
   xi=0; yi=0;
   xj=L1; yj=0;
   xk=L3*cos(theta);  yk=L3*sin(theta);
   % Element area
   Ae=0.5*((xj*yk+xi*yj+yi*xk)-(yi*xj+yj*xk+xi*yk));
   % Element stiffness matrix in local coordinates
   BB(1,1:6)=[-(yk-yj), 0, -(yi-yk), 0, -(yj-yi), 0];
   BB(2,1:6)=[0, (xk-xj), 0, (xi-xk), 0, (xj-xi)];
   BB(3,1:6)=[(xk-xj), -(yk-yj), (xi-xk), -(yi-yk), (xj-xi), -(yj-yi)];
   nu=(E/(2*G))-1;
   EE=((E*A)/(4*Ae*(1-nu^2)))*[1, nu, 0; nu, 1, 0; 0, 0, 0.5*(1-nu)];
   Kuv=BB'*EE*BB;
   % Add zero rows and columns for out of plane disp. "w"
   Add=zeros(9,6);
   Add(1,1)=1; Add(2,2)=1; Add(4,3)=1; Add(5,4)=1; Add(7,5)=1;
Add(8,6)=1;
   Kuvw=Add*Kuv*Add';
   % Tranform element matrix to global coordinates
   % Compute transformation matrix
   zeta=Glb2Loc(xio,yio,zio,xjo,yjo,zjo,xko,yko,zko);
   PSI=zeros(9,9);
   PSI(1:3,1:3)=zeta;
   PSI(4:6,4:6)=zeta;
   PSI(7:9,7:9)=zeta;
   sk=(PSI')*Kuvw*PSI;
end

% Elemental Stiffness Matrix for type 3 Rod elements
if type == 3
   % Length of element
   L=sqrt((xjo-xio)^2+(yjo-yio)^2+(zjo-zio)^2);
   % Element stiffness matrix in local coordinates
   Kuvw(1:3,1:6)=[1,0,0,-1,0,0;0,0,0,0,0,0;0,0,0,0,0,0];
   Kuvw(4:6,1:6)=[-1,0,0,1,0,0;0,0,0,0,0,0;0,0,0,0,0,0];
   Kuvw=(A*E/L)*Kuvw;
   % Tranform element matrix to global coordinates
   % Compute transformation matrix
   zeta=Glb2Loc(xio,yio,zio,xjo,yjo,zjo,xko,yko,zko);
   PSI=zeros(6,6);
   PSI(1:3,1:3)=zeta;
```

Subroutine to compute finite element stiffness matrix

```
   PSI(4:6,4:6)=zeta;
   sk=(PSI')*Kuvw*PSI;
end

% Elemental Stiffness Matrix for type 4 Scalar Spring elements
% Translational stiffness OR Torsional stiffness between nodes
if type == 4
   % Element stiffness matrix in local coordinates
   Kuvw(1,1:12)=[E,0,0,0,0,0,-E,0,0,0,0,0];
   Kuvw(2,1:12)=[0,0,0,0,0,0,0,0,0,0,0,0];
   Kuvw(3,1:12)=[0,0,0,0,0,0,0,0,0,0,0,0];
   Kuvw(4,1:12)=[0,0,0,G,0,0,0,0,0,-G,0,0];
   Kuvw(5,1:12)=[0,0,0,0,0,0,0,0,0,0,0,0];
   Kuvw(6,1:12)=[0,0,0,0,0,0,0,0,0,0,0,0];
   Kuvw(7,1:12)=[-E,0,0,0,0,0,E,0,0,0,0,0];
   Kuvw(8,1:12)=[0,0,0,0,0,0,0,0,0,0,0,0];
   Kuvw(9,1:12)=[0,0,0,0,0,0,0,0,0,0,0,0];
   Kuvw(10,1:12)=[0,0,0,-G,0,0,0,0,0,G,0,0];
   Kuvw(11,1:12)=[0,0,0,0,0,0,0,0,0,0,0,0];
   Kuvw(12,1:12)=[0,0,0,0,0,0,0,0,0,0,0,0];
   % Tranform element matrix to global coordinates
   % Compute transformation matrix
   zeta=Glb2Loc(xio,yio,zio,xjo,yjo,zjo,xko,yko,zko);
   PSI=zeros(12,12);
   PSI(1:3,1:3)=zeta;
   PSI(4:6,4:6)=zeta;
   PSI(7:9,7:9)=zeta;
   PSI(10:12,10:12)=zeta;
   sk=(PSI')*Kuvw*PSI;
end
%**************** End of File ********************************
```

Subroutine to compute finite element mass matrix

```
function
sm=FEmass(type,xio,yio,zio,xjo,yjo,zjo,xko,yko,zko,A,smay,smaz,xpol,rho
)
% This MATLAB subroutine is part of a computer software package for
% the design and analysis of a scaled tailboom structure model.
%
%
% Written by: David E. Heverly II                                  9/1/00
%             Mechanical Engineering Ph.D. Candidate
%             The Pennsylvania State University
%*******************************************************
% Filename = FEmass.m
%*******************************************************
% Form elemental stiffness matrix for the Finite Element Model
```

Subroutine to compute finite element mass matrix

```
%
% Subroutine "Glb2Loc.m" is called to transform from local
% element coordinates to global coordinates
%
%  xio - global X-coordinate of first element node
%  yio - global Y-coordinate of first element node
%  zio - global Z-coordinate of first element node
%  xjo - global X-coordinate of second element node
%  yjo - global Y-coordinate of second element node
%  zjo - global Z-coordinate of second element node
%  xko - global X-coordinate of third element node
%  yko - global Y-coordinate of third element node
%  zko - global Z-coordinate of third element node
%  A - Cross-sectional area
%  smay - 2nd moment of area of the cross section about x-y plane
%  smaz - 2nd moment of area of the cross section about x-z plane
%  xpol - 2nd moment of area of the cross section about y-z plane
%  rho - mass density
%
% Form elemental mass matrix for the Finite Element Model
%
% Four Finite Element Types can be used to construct the model
%
% Type 1: One dimensional Beam Element (2 nodes)
%         degrees-of-freedom: {u,v,w,THETAx,THETAy,THETAz} at each node
%
% Type 2: Two dimensional Triangular Membrane Element (3 nodes)
%         (Plane Stress) degrees-of-freedom: {u,v} at each node
%
% Type 3: One dimensional Rod Element (2 nodes)
%         degrees-of-freedom: {u} at each node
%
% Type 4: One dimensional Discrete Scalar Spring Element (2 nodes)
%         degrees-of-freedom: {u AND/OR theta} at each node
%         Translational stiffness AND/OR Torsional stiffness
%         One-half of concentrated mass value assigned to each node


% Elemental Mass Matrix for type 1 Beam elements
if type == 1
   % Compute element mass matrix
   sm=zeros(12,12); % Initialize element matrix
   xl=sqrt((xjo-xio)^2+(yjo-yio)^2+(zjo-zio)^2);
   ral=rho*A*xl;
   sm(1,1)=(1/3)*ral;
   sm(7,7)=sm(1,1);
   sm(7,1)=(1/6)*ral;
   sm(1,7)=sm(7,1);
   sm(2,2)=((13/35)+6*smaz/(5*A*xl^2))*ral;
   sm(8,8)=sm(2,2);
   sm(6,2)=((11*xl/210)+smaz/(10*A*xl))*ral;
```

Subroutine to compute finite element mass matrix

```
   sm(2,6)=sm(6,2);
   sm(12,8)=-sm(6,2);
   sm(8,12)=sm(12,8);
   sm(8,2)=((9/70)-6*smaz/(5*A*xl^2))*ral;
   sm(2,8)=sm(8,2);
   sm(12,2)=((-13*xl/420)+smaz/(10*A*xl))*ral;
   sm(2,12)=sm(12,2);
   sm(8,6)=-sm(12,2);
   sm(6,8)=sm(8,6);
   sm(3,3)=((13/35)+6*smay/(5*A*xl^2))*ral;
   sm(9,9)=sm(3,3);
   sm(5,3)=((-11*xl/210)-smay/(10*A*xl))*ral;
   sm(3,5)=sm(5,3);
   sm(11,9)=-sm(5,3);
   sm(9,11)=sm(11,9);
   sm(9,3)=((9/70)-6*smay/(5*A*xl^2))*ral;
   sm(3,9)=sm(9,3);
   sm(11,3)=((13*xl/420)-smay/(10*A*xl))*ral;
   sm(3,11)=sm(11,3);
   sm(9,5)=-sm(11,3);
   sm(5,9)=sm(9,5);
   sm(4,4)=(xpol/(3*A))*ral;
   sm(10,10)=sm(4,4);
   sm(10,4)=(xpol/(6*A))*ral;
   sm(4,10)=sm(10,4);
   sm(5,5)=((xl^2/105)+2*smay/(15*A))*ral;
   sm(11,11)=sm(5,5);
   sm(11,5)=((-xl*xl/140)-smay/(30*A))*ral;
   sm(5,11)=sm(11,5);
   sm(6,6)=((xl^2/105)+2*smaz/(15*A))*ral;
   sm(12,12)=sm(6,6);
   sm(12,6)=((-xl*xl/140)-smaz/(30*A))*ral;
   sm(6,12)=sm(12,6);
   % Tranform element matrix to global coordinates
   % Compute transformation matrix
   zeta=Glb2Loc(xio,yio,zio,xjo,yjo,zjo,xko,yko,zko);
   PSI=zeros(12,12);
   PSI(1:3,1:3)=zeta;
   PSI(4:6,4:6)=zeta;
   PSI(7:9,7:9)=zeta;
   PSI(10:12,10:12)=zeta;
   sm=(PSI')*sm*PSI;
end

% Elemental Mass Matrix for type 2 Triangular membrane elements
if type == 2
   % Length of element sides
   L1=sqrt((xjo-xio)^2+(yjo-yio)^2+(zjo-zio)^2);
   L2=sqrt((xko-xjo)^2+(yko-yjo)^2+(zko-zjo)^2);
   L3=sqrt((xko-xio)^2+(yko-yio)^2+(zko-zio)^2);
   theta=acos((L2^2-L1^2-L3^2)/(-2*L1*L3));
```

Subroutine to compute finite element mass matrix

```
   % Element in local (planar) coordinates
   xi=0; yi=0;
   xj=L1; yj=0;
   xk=L3*cos(theta);  yk=L3*sin(theta);
   % Element area
   Ae=0.5*((xj*yk+xi*yj+yi*xk)-(yi*xj+yj*xk+xi*yk));
   % Element consistent mass matrix in local coordinates

Muvw(1:3,1:9)=[2,0,0,1,0,0,1,0,0;0,2,0,0,1,0,0,1,0;0,0,2,0,0,1,0,0,1];

Muvw(4:6,1:9)=[1,0,0,2,0,0,1,0,0;0,1,0,0,2,0,0,1,0;0,0,1,0,0,2,0,0,1];

Muvw(7:9,1:9)=[1,0,0,1,0,0,2,0,0;0,1,0,0,1,0,0,2,0;0,0,1,0,0,1,0,0,2];
   Muvw=((1/12)*rho*Ae*A)*Muvw;
   % Tranform element matrix to global coordinates
   % Compute transformation matrix
   zeta=Glb2Loc(xio,yio,zio,xjo,yjo,zjo,xko,yko,zko);
   PSI=zeros(9,9);
   PSI(1:3,1:3)=zeta;
   PSI(4:6,4:6)=zeta;
   PSI(7:9,7:9)=zeta;
   sm=(PSI')*Muvw*PSI;
end

% Elemental Mass Matrix for type 3 Rod elements
if type == 3
   % Length of element
   L=sqrt((xjo-xio)^2+(yjo-yio)^2+(zjo-zio)^2);
   % Element consistent mass matrix in local coordinates
   Muvw(1:3,1:6)=[2,0,0,1,0,0;0,2,0,0,1,0;0,0,2,0,0,1];
   Muvw(4:6,1:6)=[1,0,0,2,0,0;0,1,0,0,2,0;0,0,1,0,0,2];
   Muvw=((1/6)*rho*A*L)*Muvw;
   % Tranform element matrix to global coordinates
   % Compute transformation matrix
   zeta=Glb2Loc(xio,yio,zio,xjo,yjo,zjo,xko,yko,zko);
   PSI=zeros(6,6);
   PSI(1:3,1:3)=zeta;
   PSI(4:6,4:6)=zeta;
   sm=(PSI')*Muvw*PSI;
end

% Elemental Mass Matrix for type 4 Scalar spring elements
% One-half of concentrated mass value assigned to each node
if type == 4
   % Element consistent mass matrix in local coordinates
   Muvw(1,1:12)=[2,0,0,0,0,0,1,0,0,0,0,0];
   Muvw(2,1:12)=[0,2,0,0,0,0,0,1,0,0,0,0];
   Muvw(3,1:12)=[0,0,2,0,0,0,0,0,1,0,0,0];
   Muvw(4:6,1:12)=zeros(3,12);
   Muvw(7,1:12)=[1,0,0,0,0,0,2,0,0,0,0,0];
   Muvw(8,1:12)=[0,1,0,0,0,0,0,2,0,0,0,0];
```

Subroutine to compute finite element mass matrix

```
   Muvw(9,1:12)=[0,0,1,0,0,0,0,0,2,0,0,0];
   Muvw(10:12,1:12)=zeros(3,12);
   Muvw=((1/6)*rho)*Muvw;
   % Tranform element matrix to global coordinates
   % Compute transformation matrix
   zeta=Glb2Loc(xio,yio,zio,xjo,yjo,zjo,xko,yko,zko);
   PSI=zeros(12,12);
   PSI(1:3,1:3)=zeta;
   PSI(4:6,4:6)=zeta;
   PSI(7:9,7:9)=zeta;
   PSI(10:12,10:12)=zeta;
   sm=(PSI')*Muvw*PSI;
end
%**************** End of File ********************************
```

Subroutine to compute the global to local transformation matirx

```
function zeta=Glb2Loc(xi,yi,zi,xj,yj,zj,xk,yk,zk)
% This MATLAB subroutine is part of a computer software package for
% the design and analysis of a scaled tailboom structure model.
%
%
% Written by: David E. Heverly II                                  9/1/00
%             Mechanical Engineering Ph.D. Candidate
%             The Pennsylvania State University
%*******************************************************
% Filename = Glb2Loc.m
%*******************************************************
% Computation of transformation matrix from global coordinates
% to local element coordinates.
% Given the global coordinates of node "I" ,node "J" & node "K"
% of the element, the nodal coordinate values can be obtained in
% local element coordinates.  {u, v, w}' = [zeta]*{uo, vo, wo}'
%
%  {u, v, w} = displacements in local coor. (tranlations or rotations)
%  {uo, vo, wo} = displacements in global coor. (tranlations or
rotations)
%  [zeta] = 3x3 transformation matrix
%  NOTE: inv([zeta])=[zeta]' ==> {uo, vo, wo}' = [zeta]'*{u, v, w}'
%
%  xi - global X-coordinate of first element node
%  yi - global Y-coordinate of first element node
%  zi - global Z-coordinate of first element node
%  xj - global X-coordinate of second element node
%  yj - global Y-coordinate of second element node
%  zj - global Z-coordinate of second element node
%  xk - global X-coordinate of third element node
%  yk - global Y-coordinate of third element node
```

Subroutine to compute the global to local transformation matirx

```
%  zk - global Z-coordinate of third element node
%  zeta - transformation matrix

% Define local x-y plane vectors V1 & V4
x1=xj-xi;  y1=yj-yi;  z1=zj-zi; % components of V1
x4=xk-xi;  y4=yk-yi;  z4=zk-zi; % components of V4

% Compute local z-axis by cross product of V1 & V4
x3=y1*z4-y4*z1;  % x-comp. of V3
y3=x4*z1-x1*z4;  % y-comp. of V3
z3=x1*y4-x4*y1;  % z-comp. of V3

% Compute local y-axis by cross product of V3 & V1
x2=y3*z1-y1*z3;  % x-comp. of V2
y2=x1*z3-x3*z1;  % y-comp. of V2
z2=x3*y1-x1*y3;  % z-comp. of V2

% Compute vector lengths
V1L=sqrt(x1^2+y1^2+z1^2);
V2L=sqrt(x2^2+y2^2+z2^2);
V3L=sqrt(x3^2+y3^2+z3^2);

% Compute direction cosines for transformation matrix
zeta(1,1)=x1/V1L;  zeta(1,2)=y1/V1L;  zeta(1,3)=z1/V1L;
zeta(2,1)=x2/V2L;  zeta(2,2)=y2/V2L;  zeta(2,3)=z2/V2L;
zeta(3,1)=x3/V3L;  zeta(3,2)=y3/V3L;  zeta(3,3)=z3/V3L;
%**************** End of File ********************************
```

Subroutine to assemble the element matrices into a global matrix

```
function glob=assembl(glob,elem,i,j,k,type);
% This MATLAB subroutine is part of a computer software package for
% the design and analysis of a scaled tailboom structure model.
%
%
% Written by: David E. Heverly II                                  9/1/00
%             Mechanical Engineering Ph.D. Candidate
%             The Pennsylvania State University
%*******************************************************
% Filename = assembl.m
%*******************************************************
% Assembles the global martix from the elemental matrices
%
% glob = global matrix (mass or stiffness)
% elem = element matrix (mass or stiffness)
%
% i = first grid/node point number of the element
% j = second grid/node point number of the element
```

Subroutine to assemble the element matrices into a global matrix

```
% k = third grid/node point number of the element
%
% Four Finite Element Types can be used to construct the model
%
% Type 1: One dimensional Beam Element (2 nodes)
%         degrees-of-freedom: {u,v,w,THETAx,THETAy,THETAz} at each node
%
% Type 2: Two dimensional Triangular Membrane Element (3 nodes)
%         (Plane Stress) degrees-of-freedom: {u,v} at each node
%
% Type 3: One dimensional Rod Element (2 nodes)
%         degrees-of-freedom: {u} at each node
%
% Type 4: One dimensional Discrete Scalar Spring Element (2 nodes)
%         degrees-of-freedom: {u AND/OR theta} at each node
%         Translational stiffness AND/OR Torsional stiffness

% Type 1: Beam elements - 12 global dof
if type==1
   k1=6*(i-1);
   k2=6*(j-1);
   for ii=1:6
     m1=k1+ii;
     m2=k2+ii;
     for jj=1:6
       n1=k1+jj;
       n2=k2+jj;
       glob(m1,n1)=glob(m1,n1)+elem(ii,jj);
       glob(m2,n2)=glob(m2,n2)+elem(6+ii,6+jj);
       glob(m1,n2)=glob(m1,n2)+elem(ii,6+jj);
       glob(m2,n1)=glob(m2,n1)+elem(6+ii,jj);
     end
   end
end

% Type 2: Triangular membrane elements - 9 global dof
if type==2
   k1=6*(i-1);
   k2=6*(j-1);
   k3=6*(k-1);
   for ii=1:3
     m1=k1+ii;
     m2=k2+ii;
     m3=k3+ii;
     for jj=1:3
       n1=k1+jj;
       n2=k2+jj;
       n3=k3+jj;
       glob(m1,n1)=glob(m1,n1)+elem(ii,jj);
       glob(m1,n2)=glob(m1,n2)+elem(ii,jj+3);
       glob(m1,n3)=glob(m1,n3)+elem(ii,jj+6);
```

Subroutine to assemble the element matrices into a global matrix

```
       glob(m2,n1)=glob(m2,n1)+elem(ii+3,jj);
       glob(m2,n2)=glob(m2,n2)+elem(ii+3,jj+3);
       glob(m2,n3)=glob(m2,n3)+elem(ii+3,jj+6);

       glob(m3,n1)=glob(m3,n1)+elem(ii+6,jj);
       glob(m3,n2)=glob(m3,n2)+elem(ii+6,jj+3);
       glob(m3,n3)=glob(m3,n3)+elem(ii+6,jj+6);
     end
   end
end

% Type 3: Rod elements - 6 global dof
if type==3
   k1=6*(i-1);
   k2=6*(j-1);
   for ii=1:3
     m1=k1+ii;
     m2=k2+ii;
     for jj=1:3
       n1=k1+jj;
       n2=k2+jj;
       glob(m1,n1)=glob(m1,n1)+elem(ii,jj);
       glob(m2,n2)=glob(m2,n2)+elem(3+ii,3+jj);
       glob(m1,n2)=glob(m1,n2)+elem(ii,3+jj);
       glob(m2,n1)=glob(m2,n1)+elem(3+ii,jj);
     end
   end
end

% Type 4: Scalar Spring elements - 12 global dof
if type==4
   k1=6*(i-1);
   k2=6*(j-1);
   for ii=1:6
     m1=k1+ii;
     m2=k2+ii;
     for jj=1:6
       n1=k1+jj;
       n2=k2+jj;
       glob(m1,n1)=glob(m1,n1)+elem(ii,jj);
       glob(m2,n2)=glob(m2,n2)+elem(6+ii,6+jj);
       glob(m1,n2)=glob(m1,n2)+elem(ii,6+jj);
       glob(m2,n1)=glob(m2,n1)+elem(6+ii,jj);
     end
   end
end
%***************** End of File *********************************
```

Program to formulate the tailboom FEM model parameters

```
% This MATLAB program is part of a computer software package for
% the design and analysis of a scaled tailboom structure model.
%
%
% Written by: David E. Heverly II                              11/1/00
%             Mechanical Engineering Ph.D. Candidate
%             The Pennsylvania State University
%*********************************************************
% Filename = FEAinput.m
%*********************************************************
% This program creates an input data file for "FEAnalys.m" a Finite
% Element based vibration analysis program of Rigid-jointed Space
Frames.
% This MATLAB m-file must be executed prior to executing "FEAnalys.m"
%
% Four Finite Element Types can be used to construct the model
%
%     Type 1: One dimensional Beam Element (2 nodes)
%              degrees-of-freedom: {u,v,w,THETAx,THETAy,THETAz} at each
node
%
%     Type 2: Two dimensional Triangular Membrane Element (3 nodes)
(Plane Stress)
%              degrees-of-freedom: {u,v} at each node
%
%     Type 3: One dimensional Rod Element (2 nodes)
%              degrees-of-freedom: {u} at each node
%
%     Type 4: One dimensional Discrete Scalar Spring Element (2 nodes)
%              degrees-of-freedom: {u AND/OR theta} at each node
%              Translational stiffness AND/OR Torsional stiffness
between nodes
%*********************************************************


clear    % Clears all variables from computer memory

% General descriptive parameters
%*******************************************************
nj=120;     % Number of joints/nodes
mems=267;   % Number of elements or members
nmatl=10;   % Number of element/material types
nsup=16;    % Number of supported/restrained joints
nconc=3;    % Number of concentrated masses (at joints/nodes)
np=10;      % Number of frequencies desired on output of results
%*******************************************************

%*******************************************************
% Global coordinates of each structural node, followed by the
% global coordinates of the imaginary nodes. Imaginary nodes are
% needed to define the principle "x-y" bending plane of each
```

Program to formulate the tailboom FEM model parameters

```
% Beam Element, which may be an existing node of the structure.
%*******************************************************
x(1)=0.0;          y(1)=7.0;          z(1)=-5.5;     % Root/base end
x(2)=0.0;          y(2)=0.0;          z(2)=-5.5;
x(3)=0.0;          y(3)=-7.0;         z(3)=-5.5;
x(4)=0.0;          y(4)=-7.0;         z(4)=0.0;
x(5)=0.0;          y(5)=-7.0;         z(5)=5.5;
x(6)=0.0;          y(6)=0.0;          z(6)=5.5;
x(7)=0.0;          y(7)=7.0;          z(7)=5.5;
x(8)=0.0;          y(8)=7.0;          z(8)=0.0;          % Root/base end
x(9)=12.0;     y(9)=6.4167;       z(9)=-5.1667;     % 1st frame
x(10)=12.0;    y(10)=0.0;         z(10)=-5.1667;
x(11)=12.0;    y(11)=-6.4167;     z(11)=-5.1667;
x(12)=12.0;    y(12)=-6.4167;     z(12)=0.0;
x(13)=12.0;    y(13)=-6.4167;     z(13)=5.1667;
x(14)=12.0;    y(14)=0.0;         z(14)=5.1667;
x(15)=12.0;    y(15)=6.4167;      z(15)=5.1667;
x(16)=12.0;    y(16)=6.4167;      z(16)=0.0;
x(17)=12.0;    y(17)=4.4167;      z(17)=-3.1667;
x(18)=12.0;    y(18)=-4.4167;     z(18)=-3.1667;
x(19)=12.0;    y(19)=-4.4167;     z(19)=3.1667;
x(20)=12.0;    y(20)=4.4167;      z(20)=3.1667;     % 1st frame
x(21)=14.0;    y(21)=-6.3194;     z(21)=-5.1111;    % Actuator
attachment Right Side Root end
x(22)=14.0;    y(22)=-6.3194;     z(22)=-3.75;
x(23)=14.0;    y(23)=-6.3194;     z(23)=-2.5;
x(24)=14.0;    y(24)=-6.3194;     z(24)=2.5;
x(25)=14.0;    y(25)=-6.3194;     z(25)=3.75;
x(26)=14.0;    y(26)=-6.3194;     z(26)=5.1111;         % Actuator
attachment Right Side Root end
x(27)=14.0;    y(27)=6.3194;      z(27)=5.1111;         % Actuator
attachment Left Side Root end
x(28)=14.0;    y(28)=6.3194;      z(28)=3.75;
x(29)=14.0;    y(29)=6.3194;      z(29)=2.5;
x(30)=14.0;    y(30)=6.3194;      z(30)=-2.5;
x(31)=14.0;    y(31)=6.3194;      z(31)=-3.75;
x(32)=14.0;    y(32)=6.3194;      z(32)=-5.1111;    % Actuator
attachment Left Side Root end
x(33)=21.25;       y(33)=-5.9670;     z(33)=-4.9097;     % Actuator
attachment Right Side Tail end
x(34)=21.25;       y(34)=-5.9670;     z(34)=-3.75;
x(35)=21.25;       y(35)=-5.9670;     z(35)=-2.5;
x(36)=21.25;       y(36)=-5.9670;     z(36)=2.5;
x(37)=21.25;       y(37)=-5.9670;     z(37)=3.75;
x(38)=21.25;       y(38)=-5.9670;     z(38)=4.9097;         % Actuator
attachment Right Side Tail end
x(39)=21.25;       y(39)=5.9670;      z(39)=4.9097;         % Actuator
attachment Left Side Tail end
x(40)=21.25;       y(40)=5.9670;      z(40)=3.75;
x(41)=21.25;       y(41)=5.9670;      z(41)=2.5;
x(42)=21.25;       y(42)=5.9670;      z(42)=-2.5;
```

Program to formulate the tailboom FEM model parameters

```
x(43)=21.25;      y(43)=5.9670;     z(43)=-3.75;
x(44)=21.25;      y(44)=5.9670;     z(44)=-4.9097;    % Actuator
attachment Left Side Tail end
x(45)=24.0;    y(45)=5.8333;        z(45)=-4.8333;    % 2nd frame
x(46)=24.0;    y(46)=0.0;           z(46)=-4.8333;
x(47)=24.0;    y(47)=-5.8333;       z(47)=-4.8333;
x(48)=24.0;    y(48)=-5.8333;       z(48)=0.0;
x(49)=24.0;    y(49)=-5.8333;       z(49)=4.8333;
x(50)=24.0;    y(50)=0.0;           z(50)=4.8333;
x(51)=24.0;    y(51)=5.8333;        z(51)=4.8333;
x(52)=24.0;    y(52)=5.8333;        z(52)=0.0;
x(53)=24.0;    y(53)=3.8333;        z(53)=-2.8333;
x(54)=24.0;    y(54)=-3.8333;       z(54)=-2.8333;
x(55)=24.0;    y(55)=-3.8333;       z(55)=2.8333;
x(56)=24.0;    y(56)=3.8333;        z(56)=2.8333;        % 2nd frame
x(57)=36.0;    y(57)=5.25;          z(57)=-4.5;       % 3rd frame
x(58)=36.0;    y(58)=0.0;           z(58)=-4.5;
x(59)=36.0;    y(59)=-5.25;         z(59)=-4.5;
x(60)=36.0;    y(60)=-5.25;         z(60)=0.0;
x(61)=36.0;    y(61)=-5.25;         z(61)=4.5;
x(62)=36.0;    y(62)=0.0;           z(62)=4.5;
x(63)=36.0;    y(63)=5.25;          z(63)=4.5;
x(64)=36.0;    y(64)=5.25;          z(64)=0.0;
x(65)=36.0;    y(65)=3.25;          z(65)=-2.5;
x(66)=36.0;    y(66)=-3.25;         z(66)=-2.5;
x(67)=36.0;    y(67)=-3.25;         z(67)=2.5;
x(68)=36.0;    y(68)=3.25;          z(68)=2.5;        % 3rd frame
x(69)=48.0;    y(69)=4.6667;        z(69)=-4.1667;    % 4th frame
x(70)=48.0;    y(70)=0.0;           z(70)=-4.1667;
x(71)=48.0;    y(71)=-4.6667;       z(71)=-4.1667;
x(72)=48.0;    y(72)=-4.6667;       z(72)=0.0;
x(73)=48.0;    y(73)=-4.6667;       z(73)=4.1667;
x(74)=48.0;    y(74)=0.0;           z(74)=4.1667;
x(75)=48.0;    y(75)=4.6667;        z(75)=4.1667;
x(76)=48.0;    y(76)=4.6667;        z(76)=0.0;
x(77)=48.0;    y(77)=3.1667;        z(77)=-2.6667;
x(78)=48.0;    y(78)=-3.1667;       z(78)=-2.6667;
x(79)=48.0;    y(79)=-3.1667;       z(79)=2.6667;
x(80)=48.0;    y(80)=3.1667;        z(80)=2.6667;        % 4th frame
x(81)=60.0;    y(81)=4.0833;        z(81)=-3.8333;    % 5th frame
x(82)=60.0;    y(82)=0.0;           z(82)=-3.8333;
x(83)=60.0;    y(83)=-4.0833;       z(83)=-3.8333;
x(84)=60.0;    y(84)=-4.0833;       z(84)=0.0;
x(85)=60.0;    y(85)=-4.0833;       z(85)=3.8333;
x(86)=60.0;    y(86)=0.0;           z(86)=3.8333;
x(87)=60.0;    y(87)=4.0833;        z(87)=3.8333;
x(88)=60.0;    y(88)=4.0833;        z(88)=0.0;
x(89)=60.0;    y(89)=2.5833;        z(89)=-2.3333;
x(90)=60.0;    y(90)=-2.5833;       z(90)=-2.3333;
x(91)=60.0;    y(91)=-2.5833;       z(91)=2.3333;
x(92)=60.0;    y(92)=2.5833;        z(92)=2.333;         % 5th frame
```

Program to formulate the tailboom FEM model parameters

```
x(93)=72.0;       y(93)=3.5;        z(93)=-3.5;       % 6th frame
x(94)=72.0;       y(94)=0.0;        z(94)=-3.5;
x(95)=72.0;       y(95)=-3.5;       z(95)=-3.5;
x(96)=72.0;       y(96)=-3.5;       z(96)=0.0;
x(97)=72.0;       y(97)=-3.5;       z(97)=3.5;
x(98)=72.0;       y(98)=0.0;        z(98)=3.5;
x(99)=72.0;       y(99)=3.5;        z(99)=3.5;
x(100)=72.0;      y(100)=3.5;       z(100)=0.0;
x(101)=72.0;      y(101)=2.0;       z(101)=-2.0;
x(102)=72.0;      y(102)=-2.0;      z(102)=-2.0;
x(103)=72.0;      y(103)=-2.0;      z(103)=2.0;
x(104)=72.0;      y(104)=2.0;       z(104)=2.0;       % 6th frame
x(105)=68.285;    y(105)=0.0;       z(105)=3.6030; % Base of vertical
tail
x(106)=69.359;    y(106)=0.0;       z(106)=6.2069; % Vertical tail
intersection with hoizontal tail
x(107)=75.153;    y(107)=0.0;       z(107)=20.2542;   % Vertica tail
x(108)=80.967;    y(108)=0.0;       z(108)=34.35;     % Top of vertical
tail
x(109)=69.359;    y(109)=-19.456;   z(109)=6.2069; % Horizontal tail
Left end
x(110)=69.359;    y(110)=-9.5;      z(110)=6.2069; % Horizontal tail
x(111)=69.359;    y(111)=9.5;       z(111)=6.2069; % Horizontal tail
x(112)=69.359;    y(112)=19.456;    z(112)=6.2069; % Horizontal tail
Right end
x(113)=-10.0;     y(113)=7.0;       z(113)=-5.5;      % Root/base
support
x(114)=-10.0;     y(114)=0.0;       z(114)=-5.5;
x(115)=-10.0;     y(115)=-7.0;      z(115)=-5.5;
x(116)=-10.0;     y(116)=-7.0;      z(116)=0.0;
x(117)=-10.0;     y(117)=-7.0;      z(117)=5.5;
x(118)=-10.0;     y(118)=0.0;       z(118)=5.5;
x(119)=-10.0;     y(119)=7.0;       z(119)=5.5;
x(120)=-10.0;     y(120)=7.0;       z(120)=0.0;       % Root/base
support
% Imaginary nodes to define bending planes
x(121)=0.0;       y(121)=7.0;       z(121)=-5.5;
x(122)=0.0;       y(122)=-7.0;      z(122)=-5.5;
x(123)=0.0;       y(123)=-7.0;      z(123)=5.5;
x(124)=0.0;       y(124)=7.0;       z(124)=5.5;
x(125)=80.967;    y(125)=90.0;      z(125)=34.35;
x(126)=0.0;       y(126)=0.0;       z(126)=6.2069;
x(127)=60.0;      y(127)=-4.0833;   z(127)=3.8333;
x(128)=60.0;      y(128)=4.0833;    z(128)=3.8333;
x(129)=72.0;      y(129)=3.5;       z(129)=3.5;
x(130)=72.0;      y(130)=-3.5;      z(130)=3.5;
%*********************************************************
%*********************************************************

%*********************************
% Element/Material Type Properties
```

Program to formulate the tailboom FEM model parameters

```
%*********************************************************************
***********
% Skin & frame material - 0.032 inch thick aluminum sheet (Membrane
element)
dens(1)=(0.0979/386.4);% Material density - rhoa [lbf-s^2/in^4]
elast(1)=9.99e6;     % Elastic modulus - E [psi] (Aluminum)
rigd(1)=3.77e6;      % Rigidity modulus - G [psi] (Aluminum)
area(1)=0.032;       % Membrane (sheet metal) thickness [in.]
xin(1)=0;          % Not Used assign zero value
yin(1)=0;          % Not Used assign zero value
zin(1)=0;          % Not Used assign zero value
xjp(1)=0;          % Not Used assign zero value

% Outer Stringer material - (0.75 x 0.75 x 0.125 thick) aluminum angles
(Beam Element)
dens(2)=(0.0979/386.4);% Material density - rhoa [lbf-s^2/in^4]
elast(2)=9.99e6;     % Elastic modulus - E [psi] (Aluminum)
rigd(2)=3.77e6;      % Rigidity modulus - G [psi] (Aluminum)
area(2)=0.17188;     % Cross-sectional area - A [in^2]
xin(2)=0.01732;      % Torsional constant of cross section - J [in^4]
yin(2)=8.6577e-3;    % 2nd moment of area of the cross section about x-
y plane - Iy [in^4]
zin(2)=8.6577e-3;    % 2nd moment of area of the cross section about x-
z plane - Iz [in^4]
xjp(2)=0.01732;      % Polar 2nd moment of area of cross section - Ip
[in^4]

% Inner Stringer Material - (0.125 x 1.0) flat stock aluminum (Beam
Element)
dens(3)=(0.0979/386.4);% Material density - rhoa [lbf-s^2/in^4]
elast(3)=9.99e6;     % Elastic modulus - E [psi] (Aluminum)
rigd(3)=3.77e6;      % Rigidity modulus - G [psi] (Aluminum)
area(3)=0.125;       % Cross-sectional area - A [in^2]
xin(3)=0.01058;      % Torsional constant of cross section - J  [in^4]
yin(3)=1.6276e-4;    % 2nd moment of area of the cross section about x-
y plane - Iy [in^4]
zin(3)=0.01042;      % 2nd moment of area of the cross section about x-
z plane - Iz [in^4]
xjp(3)=0.01058;      % Polar 2nd moment of area of cross section - Ip
[in^4]

% Tail mounting plate - 0.5 inch aluminum plate  (Modeled as 4 Beam
Elements)
dens(4)=(0.0979/386.4);% Material density - rhoa [lbf-s^2/in^4]
elast(4)=9.99e6;     % Elastic modulus - E [psi] (Aluminum)
rigd(4)=3.77e6;      % Rigidity modulus - G [psi] (Aluminum)
area(4)=1.5865;      % Cross-sectional area - A [in^2]
xin(4)=0.4195;       % Torsional constant of cross section - J  [in^4]
yin(4)=0.20976;      % 2nd moment of area of the cross section about x-
y plane - Iy [in^4]
zin(4)=0.20976;      % 2nd moment of area of the cross section about x-
```

Program to formulate the tailboom FEM model parameters

```
z plane - Iz [in^4]
xjp(4)=0.4195;       % Polar 2nd moment of area of cross section - Ip
[in^4]

% Tail section material - (2.0 x 2.0 x 0.125 thick) Square aluminum
tube (Beam Element)
dens(5)=(0.0979/386.4);% Material density - rhoa [lbf-s^2/in^4]
elast(5)=9.99e6;     % Elastic modulus - E [psi] (Aluminum)
rigd(5)=3.77e6;      % Rigidity modulus - G [psi] (Aluminum)
area(5)=0.9375;      % Cross-sectional area - A [in^2]
xin(5)=1.1035;    % Torsional constant of cross section - J  [in^4]
yin(5)=0.5518;    % 2nd moment of area of the cross section about x-y
plane - Iy [in^4]
zin(5)=0.5518;    % 2nd moment of area of the cross section about x-z
plane - Iz [in^4]
xjp(5)=1.1035;    % Polar 2nd moment of area of cross section - Ip
[in^4]

% Tail end plate material - 0.5 inch thick aluminum plate (Membrane
element)
dens(6)=(0.0979/386.4); % Material density - rhoa [lbf-s^2/in^4]
elast(6)=9.99e6;        % Elastic modulus - E [psi] (Aluminum)
rigd(6)=3.77e6;         % Rigidity modulus - G [psi] (Aluminum)
area(6)=0.532;          % Membrane (sheet metal) thickness [in.]
xin(6)=0;            % Not Used assign zero value
yin(6)=0;            % Not Used assign zero value
zin(6)=0;            % Not Used assign zero value
xjp(6)=0;            % Not Used assign zero value

% Piezoceramic Stack actuator properties (Rod Element)
dens(7)=7.0206e-4;   % Material density - rhoa [lbf-s^2/in^4] (PZT)
elast(7)=8.434e6;    % Elastic modulus - E [psi] (stack actuator)
area(7)=0.1963;      % Cross-sectional area - A [in^2]
rigd(7)=0.0;         % Not Used assign zero value
xin(7)=0.0;       % Not Used assign zero value
yin(7)=0.0;       % Not Used assign zero value
zin(7)=0.0;       % Not Used assign zero value
xjp(7)=0.0;       % Not Used assign zero value

% Actuator Precompression rod (Rod Element)  (1/16 in. Dia. mild steel
rod)
dens(8)=0.283/386.4;% Material density - rhoa [lbf-s^2/in^4]  (steel)
elast(8)=10e6;    % Elastic modulus - E [psi]  (mild steel)
area(8)=3.068e-3; % Cross-sectional area - A [in^2]
rigd(8)=0.0;      % Not Used assign zero value
xin(8)=0.0;       % Not Used assign zero value
yin(8)=0.0;       % Not Used assign zero value
zin(8)=0.0;       % Not Used assign zero value
xjp(8)=0.0;       % Not Used assign zero value

% Actuator mounting supports - (1.0 x 1.0 x 0.125 thick) aluminum C-
```

Program to formulate the tailboom FEM model parameters

```
channel (Beam Element)
dens(9)=(0.0979/386.4);% Material density - rhoa [lbf-s^2/in^4]
elast(9)=9.99e6;      % Elastic modulus - E [psi] (Aluminum)
rigd(9)=3.77e6;       % Rigidity modulus - G [psi] (Aluminum)
area(9)=0.3438;       % Cross-sectional area - A [in^2]
%xin(9)=0.08658;      % Torsional constant of cross section - J [in^4]
%yin(9)=0.03401;      % 2nd moment of area of the cross section about x-
y plane - Iy [in^4]
%zin(9)=0.05257;      % 2nd moment of area of the cross section about x-
z plane - Iz [in^4]
%xjp(9)=0.08658;      % Polar 2nd moment of area of cross section - Ip
[in^4]
xin(9)=0.04330;       % Torsional constant of cross section - J [in^4]
yin(9)=0.01701;       % 2nd moment of area of the cross section about x-
y plane - Iy [in^4]
zin(9)=0.02629;       % 2nd moment of area of the cross section about x-
z plane - Iz [in^4]
xjp(9)=0.04330;       % Polar 2nd moment of area of cross section - Ip
[in^4]

% Scalar Spring element properties connecting tailboom to base
structure
dens(10)=0.0;         % Spring element lumped mass[lbf-s^2/in], divided
equally between nodes
elast(10)=1.05e5;     % Translational spring constant [lbf/in]
rigd(10)=0.0;         % Torsional spring constant [in-lbf/rad]
area(10)=0.0;         % Not Used assign zero value
xin(10)=0.0;          % Not Used assign zero value
yin(10)=0.0;          % Not Used assign zero value
zin(10)=0.0;          % Not Used assign zero value
xjp(10)=0.0;          % Not Used assign zero value
%*********************************************************************
***********
%*********************************************************************
***********

%*********************************************************************
***********
%*********************************************************************
***********
% NOTE: The principle "x-y" bending plane (in local element
coordinates)
%       of a Beam Element is defined by the triangular plane formed by
the
%       global "i,j,k" nodes. Node "k" may be an existing node of the
structure
%       or an imaginary node.
%  Element Topology
%   Start  End   Imaginary
%   Node   Node  Node      Element  Material
%     i     j     k        Type     Type
```

Program to formulate the tailboom FEM model parameters

```
Etop=[1     2     10       2        1        % Element 1 Skin
      2     3     10       2        1        % Element 2 Skin
      3     11    10       2        1        % Element 3 Skin
      1     10    9        2        1        % Element 4 Skin
      1     9     122      1        2        % Element 5 BL Stringer
      2     10    121      1        3        % Element 6 BM Stringer
      3     11    121      1        2        % Element 7 BR Stringer
      5     4     12       2        1        % Element 8 Skin
      4     3     12       2        1        % Element 9 Skin
      3     11    12       2        1        % Element 10   Skin
      5     12    13       2        1        % Element 11   Skin
      5     13    124      1        2        % Element 12   TR Stringer
      4     12    123      1        3        % Element 13   MR Stringer
      7     6     14       2        1        % Element 14   Skin
      6     5     14       2        1        % Element 15   Skin
      5     13    14       2        1        % Element 16   Skin
      7     14    15       2        1        % Element 17   Skin
      7     15    123      1        2        % Element 18   TL Stringer
      6     14    123      1        3        % Element 19   TM Stringer
      7     8     16       2        1        % Element 20   Skin
      8     1     16       2        1        % Element 21   Skin
      1     9     16       2        1        % Element 22   Skin
      7     16    15       2        1        % Element 23   Skin
      8     16    124      1        3        % Element 24   ML Stringer
      9     10    46       2        1        % Element 25   *** Skin
      10    11    46       2        1        % Element 26   Skin
      11    47    46       2        1        % Element 27   Skin
      9     46    45       2        1        % Element 28   Skin
      9     32    122      1        2        % Element 29   BL stringer
      32    44    122      3        8        % Element 30   BL
precompression rod
      44    45    122      1        2        % Element 31   BL stringer
      10    46    121      1        3        % Element 32   BM stringer
      11    21    121      1        2        % Element 33   BR stringer
      21    33    121      3        8        % Element 34   BR
precompression rod
      33    47    121      1        2        % Element 35   BR stringer
      13    12    48       2        1        % Element 36   Skin
      12    11    48       2        1        % Element 37   Skin
      11    47    48       2        1        % Element 38   Skin
      13    48    49       2        1        % Element 39   Skin
      13    26    124      1        2        % Element 40   TR stringer
      26    38    124      3        8        % Element 41   TR
precompression rod
      38    49    124      1        2        % Element 42   TR stringer
      26    25    32       1        9        % Element 43 TR actuator
mount, root end
      38    37    44       1        9        % Element 44 TR actuator
mount, tail end
      25    37    28       3        7        % Element 45 TR PZT
Actuator
```

Program to formulate the tailboom FEM model parameters

```
      25    24    32       1        9        % Element 46 TR actuator
mount, root end
      37    36    44       1        9        % Element 47 TR actuator
mount, tail end
      24    23    32       1        9        % Element 48 MR actuator
mount, root end
      36    35    44       1        9        % Element 49 MR actuator
mount, tail end
      23    22    32       1        9        % Element 50 BR actuator
mount, root end
      35    34    44       1        9        % Element 51 BR actuator
mount, tail end
      22    34    31       3        7        % Element 52 BR PZT
Actuator
      22    21    32       1        9        % Element 53 BR actuator
mount, root end
      34    33    44       1        9        % Element 54 BR actuator
mount, tail end
      15    14    50       2        1        % Element 55   Skin
      14    13    50       2        1        % Element 56   Skin
      13    49    50       2        1        % Element 57   Skin
      15    50    51       2        1        % Element 58   Skin
      15    27    123      1        2        % Element 59   TL stringer
      27    39    123      3        8        % Element 60   TL
precompression rod
      39    51    123      1        2        % Element 61   TL stringer
      15    16    52       2        1        % Element 62   Skin
      16    9     52       2        1        % Element 63   Skin
      9     45    52       2        1        % Element 64   Skin
      15    52    51       2        1        % Element 65   Skin
      27    28    21       1        9        % Element 66 TL actuator
mount, root end
      39    40    33       1        9        % Element 67 TL actuator
mount, tail end
      28    40    24       3        7        % Element 68 TL PZT
Actuator
      28    29    21       1        9        % Element 69 TL actuator
mount, root end
      40    41    33       1        9        % Element 70 TL actuator
mount, tail end
      29    30    21       1        9        % Element 71 ML actuator
mount, root end
      41    42    33       1        9        % Element 72 ML actuator
mount, tail end
      30    31    21       1        9        % Element 73 BL actuator
mount, root end
      42    43    33       1        9        % Element 74 BL actuator
mount, tail end
      31    43    22       3        7        % Element 75 BL PZT
Actuator
      31    32    21       1        9        % Element 76 BL actuator
```

Program to formulate the tailboom FEM model parameters

```
mount, root end
      43    44    33       1        9        % Element 77 BL actuator
mount, tail end
      16    52    124      1        3        % Element 78 ML stringer
      12    48    123      1        3        % Element 79 MR stringer
      45    46    58       2        1        % Element 80   *** Skin
      46    47    58       2        1        % Element 81   Skin
      47    59    58       2        1        % Element 82   Skin
      45    58    57       2        1        % Element 83   Skin
      45    57    122      1        2        % Element 84 BL stringer
      46    58    121      1        3        % Element 85 BM Stringer
      47    59    121      1        2        % Element 86 BR stringer
      49    48    60       2        1        % Element 87   Skin
      48    47    60       2        1        % Element 88   Skin
      47    59    60       2        1        % Element 89   Skin
      49    60    61       2        1        % Element 90   Skin
      49    61    124      1        2        % Element 91 TR stringer
      48    60    123      1        3        % Element 92 MR stringer
      51    50    62       2        1        % Element 93   Skin
      50    49    62       2        1        % Element 94   Skin
      49    61    62       2        1        % Element 95   Skin
      51    62    63       2        1        % Element 96   Skin
      51    63    123      1        2        % Element 97 TL stringer
      50    62    123      1        3        % Element 98 TM stringer
      51    52    64       2        1        % Element 99   Skin
      52    45    64       2        1        % Element 100   Skin
      45    57    64       2        1        % Element 101   Skin
      51    64    63       2        1        % Element 102   Skin
      52    64    124      1        3        % Element 103  ML stringer
      57    58    70       2        1        % Element 104   *** Skin
      58    59    70       2        1        % Element 105   Skin
      59    71    70       2        1        % Element 106   Skin
      57    70    69       2        1        % Element 107   Skin
      57    69    122      1        2        % Element 108  BL stringer
      58    70    121      1        3        % Element 109  BM Stringer
      59    71    121      1        2        % Element 110  BR stringer
      61    60    72       2        1        % Element 111   Skin
      60    59    72       2        1        % Element 112   Skin
      59    71    72       2        1        % Element 113   Skin
      61    72    73       2        1        % Element 114   Skin
      61    73    124      1        2        % Element 115  TR stringer
      60    72    123      1        3        % Element 116  MR stringer
      63    62    74       2        1        % Element 117   Skin
      62    61    74       2        1        % Element 118   Skin
      61    73    74       2        1        % Element 119   Skin
      63    74    75       2        1        % Element 120   Skin
      63    75    123      1        2        % Element 121  TL stringer
      62    74    123      1        3        % Element 122  TM stringer
      63    64    76       2        1        % Element 123   Skin
      64    57    76       2        1        % Element 124   Skin
      57    69    76       2        1        % Element 125   Skin
```

Program to formulate the tailboom FEM model parameters

```
63    76    75    2    1    % Element 126   Skin
64    76    124   1    3    % Element 127  ML stringer
69    70    82    2    1    % Element 128   *** Skin
70    71    82    2    1    % Element 129   Skin
71    83    82    2    1    % Element 130   Skin
69    82    81    2    1    % Element 131   Skin
69    81    122   1    2    % Element 132  BL stringer
70    82    121   1    3    % Element 133  BM Stringer
71    83    121   1    2    % Element 134  BR stringer
73    72    84    2    1    % Element 135   Skin
72    71    84    2    1    % Element 136   Skin
71    83    84    2    1    % Element 137   Skin
73    84    85    2    1    % Element 138   Skin
73    85    124   1    2    % Element 139  TR stringer
72    84    123   1    3    % Element 140  MR stringer
75    74    86    2    1    % Element 141   Skin
74    73    86    2    1    % Element 142   Skin
73    85    86    2    1    % Element 143   Skin
75    86    87    2    1    % Element 144   Skin
75    87    123   1    2    % Element 145  TL stringer
74    86    123   1    3    % Element 146  TM stringer
75    76    88    2    1    % Element 147   Skin
76    69    88    2    1    % Element 148   Skin
69    81    88    2    1    % Element 149   Skin
75    88    87    2    1    % Element 150   Skin
76    88    124   1    3    % Element 151  ML stringer
81    82    94    2    1    % Element 152  ***    Skin
82    83    94    2    1    % Element 153   Skin
83    95    94    2    1    % Element 154   Skin
81    94    93    2    1    % Element 155   Skin
81    93    122   1    2    % Element 156  BL stringer
82    94    121   1    3    % Element 157  BM Stringer
83    95    121   1    2    % Element 158  BR stringer
85    84    96    2    1    % Element 159   Skin
84    83    96    2    1    % Element 160   Skin
83    95    96    2    1    % Element 161   Skin
85    96    97    2    1    % Element 162   Skin
85    97    124   1    2    % Element 163  TR stringer
84    96    123   1    3    % Element 164  MR stringer
87    86    98    2    1    % Element 165   Skin
86    85    98    2    1    % Element 166   Skin
85    97    98    2    1    % Element 167   Skin
87    98    99    2    1    % Element 168   Skin
87    99    123   1    2    % Element 169  TL stringer
86    98    123   1    3    % Element 170  TM stringer
87    88    100   2    1    % Element 171   Skin
88    81    100   2    1    % Element 172   Skin
81    93    100   2    1    % Element 173   Skin
87    100   99    2    1    % Element 174   Skin
88    100   124   1    3    % Element 175  ML stringer
87    105   127   1    4    % Element 176  *** Tail
```

Program to formulate the tailboom FEM model parameters

```
mounting plate
      85    105   128      1        4        % Element 177 Tail
mounting plate
      105   97    129      1        4        % Element 178 Tail
mounting plate
      105   99    130      1        4        % Element 179 Tail
mounting plate
      105   106   125      1        5        % Element 180  ***
Vertical tail
      106   107   125      1        5        % Element 181 Vertical
tail
      107   108   125      1        5        % Element 182 Vertical
tail
      109   110   126      1        5        % Element 183 ***
Horizontal tail
      110   106   126      1        5        % Element 184 Horizontal
tail
      106   111   126      1        5        % Element 185 Horizontal
tail
      111   112   126      1        5        % Element 186 Horizontal
tail
      13    12    19       2        1        % Element 187  *** Frame
#1
      12    18    19       2        1        % Element 188 Frame #1
      11    18    12       2        1        % Element 189 Frame #1
      11    10    18       2        1        % Element 190 Frame #1
      10    17    18       2        1        % Element 191 Frame #1
      10    9     17       2        1        % Element 192 Frame #1
      9     16    17       2        1        % Element 193 Frame #1
      16    20    17       2        1        % Element 194 Frame #1
      16    15    20       2        1        % Element 195 Frame #1
      15    14    20       2        1        % Element 196 Frame #1
      14    19    20       2        1        % Element 197 Frame #1
      14    13    19       2        1        % Element 198 Frame #1
      49    48    55       2        1        % Element 199  *** Frame
#2
      48    54    55       2        1        % Element 200 Frame #2
      48    47    54       2        1        % Element 201 Frame #2
      47    46    54       2        1        % Element 202 Frame #2
      46    53    54       2        1        % Element 203 Frame #2
      46    45    53       2        1        % Element 204 Frame #2
      45    52    53       2        1        % Element 205 Frame #2
      52    56    53       2        1        % Element 206 Frame #2
      52    51    56       2        1        % Element 207 Frame #2
      51    50    56       2        1        % Element 208 Frame #2
      50    55    56       2        1        % Element 209 Frame #2
      50    49    55       2        1        % Element 210 Frame #2
      61    60    67       2        1        % Element 211  *** Frame
#3
      60    66    67       2        1        % Element 212 Frame #3
      60    59    66       2        1        % Element 213 Frame #3
```

Program to formulate the tailboom FEM model parameters

```
      59    58    66       2        1        % Element 214 Frame #3
      58    65    66       2        1        % Element 215 Frame #3
      58    57    65       2        1        % Element 216 Frame #3
      57    64    65       2        1        % Element 217 Frame #3
      64    68    65       2        1        % Element 218 Frame #3
      64    63    68       2        1        % Element 219 Frame #3
      63    62    68       2        1        % Element 220 Frame #3
      62    67    68       2        1        % Element 221 Frame #3
      62    61    67       2        1        % Element 222 Frame #3
      73    72    79       2        1        % Element 223  *** Frame
#4
      72    78    79       2        1        % Element 224 Frame #4
      72    71    78       2        1        % Element 225 Frame #4
      71    70    78       2        1        % Element 226 Frame #4
      70    77    78       2        1        % Element 227 Frame #4
      70    69    77       2        1        % Element 228 Frame #4
      69    76    77       2        1        % Element 229 Frame #4
      76    80    77       2        1        % Element 230 Frame #4
      76    75    80       2        1        % Element 231 Frame #4
      75    74    80       2        1        % Element 232 Frame #4
      74    79    80       2        1        % Element 233 Frame #4
      74    73    79       2        1        % Element 234 Frame #4
      85    84    91       2        1        % Element 235  *** Frame
#5
      84    90    91       2        1        % Element 236 Frame #5
      84    83    90       2        1        % Element 237 Frame #5
      83    82    90       2        1        % Element 238 Frame #5
      82    89    90       2        1        % Element 239 Frame #5
      82    81    89       2        1        % Element 240 Frame #5
      81    88    89       2        1        % Element 241 Frame #5
      88    92    89       2        1        % Element 242 Frame #5
      88    87    92       2        1        % Element 243 Frame #5
      87    86    92       2        1        % Element 244 Frame #5
      86    91    92       2        1        % Element 245 Frame #5
      86    85    91       2        1        % Element 246 Frame #5
      97    96    103      2        6        % Element 247  *** Frame
#6
      96    102   103      2        6        % Element 248 Frame #6
      96    95    102      2        6        % Element 249 Frame #6
      95    94    102      2        6        % Element 250 Frame #6
      94    101   102      2        6        % Element 251 Frame #6
      94    93    101      2        6        % Element 252 Frame #6
      93    100   101      2        6        % Element 253 Frame #6
      100   104   101      2        6        % Element 254 Frame #6
      100   99    104      2        6        % Element 255 Frame #6
      99    98    104      2        6        % Element 256 Frame #6
      98    103   104      2        6        % Element 257 Frame #6
      98    97    103      2        6        % Element 258 Frame #6
      14    50    123      1        3        % Element 259   TM
stringer
      1     113   115      4        10       % Element 260 Scalar
```

Program to formulate the tailboom FEM model parameters

```
spring attachement
      2     114   115      4         10       % Element 261 Scalar
spring attachement
      3     115   113      4         10       % Element 262 Scalar
spring attachement
      4     116   120      4         10       % Element 263 Scalar
spring attachement
      5     117   119      4         10       % Element 264 Scalar
spring attachement
      6     118   119      4         10       % Element 265 Scalar
spring attachement
      7     119   117      4         10       % Element 266 Scalar
spring attachement
      8     120   116      4         10];     % Element 267 Scalar
spring attachement
%**************************************************************************
*****
%**************************************************************************
*****

% Constrained Joints/Nodes
% NOTE: 0=No Restraint & 1=Full Restraint of specified d.o.f.
%     Joint #   X-tran  Y-tran  Z-tran  X-rot  Y-rot  Z-rot
Jrest=[  1         0       1       1       1      1      1
         2         0       1       1       1      1      1
         3         0       1       1       1      1      1
         4         0       1       1       1      1      1
         5         0       1       1       1      1      1
         6         0       1       1       1      1      1
         7         0       1       1       1      1      1
         8         0       1       1       1      1      1
         113       1       1       1       1      1      1
         114       1       1       1       1      1      1
         115       1       1       1       1      1      1
         116       1       1       1       1      1      1
         117       1       1       1       1      1      1
         118       1       1       1       1      1      1
         119       1       1       1       1      1      1
         120       1       1       1       1      1      1];

% Concentrated Masses
% Note concentrated masses MUST be located at joints
nposn(1)=643;        % Unconstrained Global dof of U disp. of joint 108
for mass location
xmass(1)=3.559e-2;   % Value of concentrated mass [lbf-s^2/in]
nposn(2)=649;        % Unconstrained Global dof of U disp. of joint 109
for mass location
xmass(2)=1.682e-2;   % Value of concentrated mass [lbf-s^2/in]
nposn(3)=667;        % Unconstrained Global dof of U disp. of joint 112
for mass location
xmass(3)=1.682e-2;   % Value of concentrated mass [lbf-s^2/in]
```

Program to formulate the tailboom FEM model parameters

```
save FEAin  % Saves variables in binary file "FEAin.mat"
            % to be loaded by "FEAnalys.m"
%***************** End of File ********************************
```

Main program to create the FEM finite element model

```
% This MATLAB program is part of a computer software package for
% the design and analysis of a scaled tailboom structure model.
%
%
% Written by: David E. Heverly II                              11/1/00
%             Mechanical Engineering Ph.D. Candidate
%             The Pennsylvania State University
%*********************************************************
% Filename = FEAnalys.m
%*********************************************************
% This a Finite Element based vibration analysis program.
% The input data is created by "FEAinput.m" and loaded by this program.
% The main program calls the following subroutines/function m-files:
%  1.) assembl.m
%  2.) Glb2Loc.m
%  3.) FEstiff.m
%  4.) FEmass.m

%*****************************************************
% Start Main Program
%*****************************************************
clear all         % Clears variables from computer memory
load FEAin        % Loads the binary input data file
dof=6*nj;         % Unrestrained global degrees of freedom

% Initialize Mass & Stiffness Matrices
stiff=zeros(dof,dof);
mass=zeros(dof,dof);

% Loop thru each element: compute element matrices & assemble global
matrices
%************************
for mem=1:mems
 i=Etop(mem,1);
 j=Etop(mem,2);
 k=Etop(mem,3);

 matl=Etop(mem,5);
 E=elast(matl); rho=dens(matl); G=rigd(matl); csa=area(matl);
 TC=xin(matl); smay=yin(matl); smaz=zin(matl); xpol=xjp(matl);
```

Main program to create the FEM finite element model

```
 xi=x(i);  yi=y(i);  zi=z(i);
 xj=x(j);  yj=y(j);  zj=z(j);
 xk=x(k);  yk=y(k);  zk=z(k);


sk=FEstiff(Etop(mem,4),xi,yi,zi,xj,yj,zj,xk,yk,zk,csa,TC,smay,smaz,E,G)
;  % Form elemental Stiffness matrix

sm=FEmass(Etop(mem,4),xi,yi,zi,xj,yj,zj,xk,yk,zk,csa,smay,smaz,xpol,rho
); % Form elemental Mass matrix
 stiff=assembl(stiff,sk,i,j,k,Etop(mem,4));        % Assemble global
stiffness matrix
 mass=assembl(mass,sm,i,j,k,Etop(mem,4));          % Assemble global
mass matrix
end
stiff=(triu(stiff))-(diag(diag(stiff)))+((triu(stiff))');  % Makes
exactly symmetric
mass=(triu(mass))-(diag(diag(mass)))+((triu(mass))');  % Makes exactly
symmetric
%*********************************
disp('Element matrices formed')

% Addition of concentrated translational masses to global mass matrix
%*****************************************************
if nconc>0
 for ii=1:nconc
  n9=nposn(ii);
  mass(n9,n9)=mass(n9,n9)+xmass(ii);
  mass(n9+1,n9+1)=mass(n9+1,n9+1)+xmass(ii);
  mass(n9+2,n9+2)=mass(n9+2,n9+2)+xmass(ii);
 end
end
%*********************************************

% Apply boundary conditions/constraints by deleting rows
% and columns from Unconstrained global matrices.
%*****************************************************
if nsup>0
  for ii=1:nsup
     for jj=1:6
        if Jrest(ii,jj+1)==1
           nn1=6*(Jrest(ii,1)-1)+jj;
           stiff(nn1,1:dof)=zeros(1,dof);
           stiff(1:dof,nn1)=zeros(dof,1);
           mass(nn1,1:dof)=zeros(1,dof);
           mass(1:dof,nn1)=zeros(dof,1);
        end
     end
  end
end
%*********************************
```

Main program to create the FEM finite element model

```
disp('Boundary conditions applied')

% Eliminate zero rows and columns from
% constrained Mass & Stiffness matrices
%************************************
nn1=0;
nn2=0;
for ii=1:dof
   chek=stiff(ii,:)*(stiff(ii,:))';
   if chek<=1e-10
      nn1=nn1+1;
      indx1(nn1)=ii; % Index vector of deleted global dof (zero rows &
columns)
   else
      nn2=nn2+1;
      indx2(nn2)=ii; % Index vector of retained (nonzero) global dof
   end
end
cdof=length(indx2);
for ii=1:cdof
   for jj=1:cdof
      Kg(ii,jj)=stiff(indx2(ii),indx2(jj));
      Mg(ii,jj)=mass(indx2(ii),indx2(jj));
   end
end
%************************************************

%  COMPUTE EIGENVALUES AND EIGENVECTORS
%************************************
nmodes=30;
[evec,eval]=fe_eig((sparse(Mg)),(sparse(Kg)),[3 nmodes 0 0 1e-7]);
for i=1:nmodes
 frq(i)=(eval(i))/(2*pi);  % Natural frequency in Hz
end

% Display natural frequiencies
disp('Frequencies - [Hz]')
for i=1:np
 disp(frq(i))
end
%************************************

% Save data to binary "*.mat" file
save FEAtail91  Kg Mg dof cdof indx1 indx2 eval evec
%**************** End of File ********************************
```

Scaled Tailboom Experiment Equipment List	
Item Description	Quantity
Ling Electronics, Inc., Model LMT-100, Modal Thruster with trunnion base	1
Ling Electronics, Inc., Model STAR 1.0, Amplifier	1
Ling Electronics, Inc., Model CB-1.5, Cooling Blower with 6 ft. hose	1
American Piezo Ceramics, Inc., Model Pst 150/14/100 VS20, Piezoelectric Stack Actuator	4
American Piezo Ceramics, Inc., Model LE 150/200 – 2/2 channel, Actuator Power Supply	2
PCB Piezotronics, Model 481A02, Line-Powered ICP sensor signal conditioner, 16 channel, gain x 1, x 10, x 100	1
PCB Piezotronics, Model 353B01, General purpose ICP accelerometer, quartz shear, 20 mV/g, 1 to 7000 Hz	12
PCB Piezotronics, Model 208C02, Multi-purpose ICP quartz force sensor, +/- 100 lbs, 50 mV/lb	1
PCB Piezotronics, Model 208C04, Multi-purpose ICP quartz force sensor, +/- 500 lbs, 10 mV/lb	2
PCB Piezotronics, 20 ft., 10 ft., & 6 ft. coaxial cables, 10-32 plug to BNC plug, and BNC plug to BNC plug	28
MCM Electronics, Model 24-795, 12 ft. coaxial cable (RG58), BNC plug to BNC plug	15
OMEGA Engineering, Inc., Model SG1-KIT, Complete strain gage application kit	1
OMEGA Engineering, Inc., Model SG-6/120-LY13, Foil strain gages, package of 10	5
DL Instruments, LLC., Model 4302, Dual electronic filter (low pass)	2
Techkor Instrumentation, Model MEPTS-9000, Multichannel universal signal conditioning amplifier, 9000B Wheatstone bridge amp. (strain gage)	1
Gateway, Model P5-150, Desktop personal computer, 150 MHz, 32 MB RAM, Windows 95 OS, MATLAB software, SIMULINK software	1
DSPACE, Inc., Model DS1102 PPC, Controller board, dSPACE Implementation software, Control Desk software	1

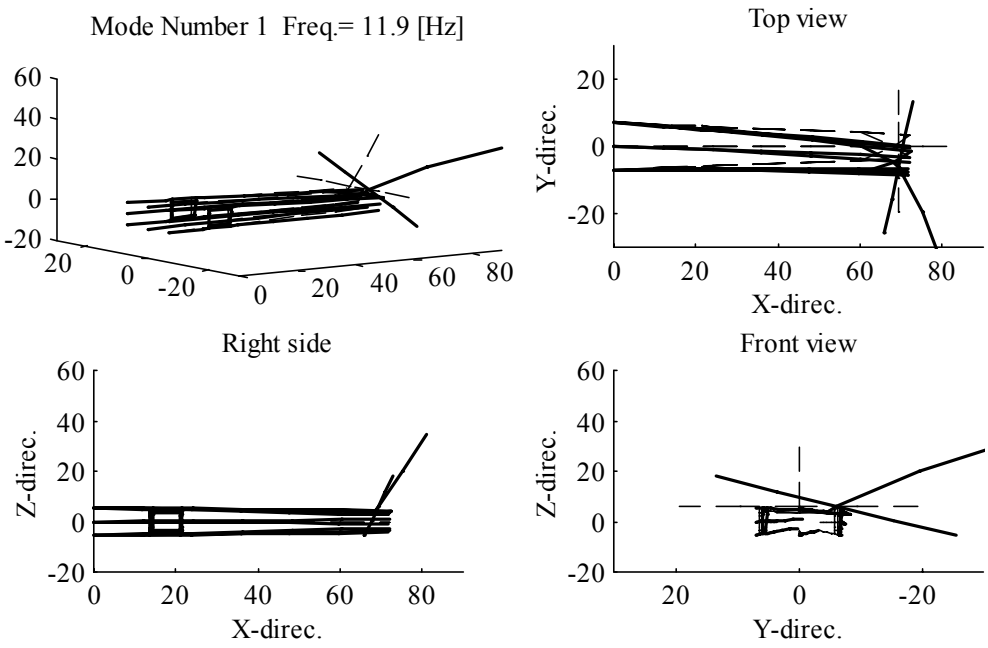

Scaled tailboom Finite Element Model (FEM) mode shape

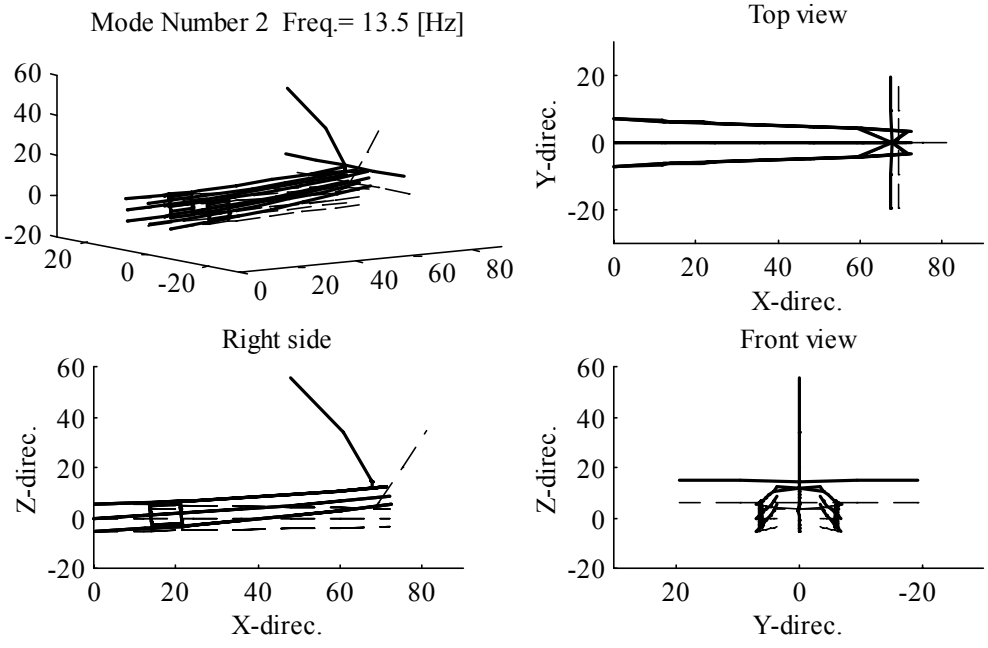

Scaled tailboom Finite Element Model (FEM) mode shape

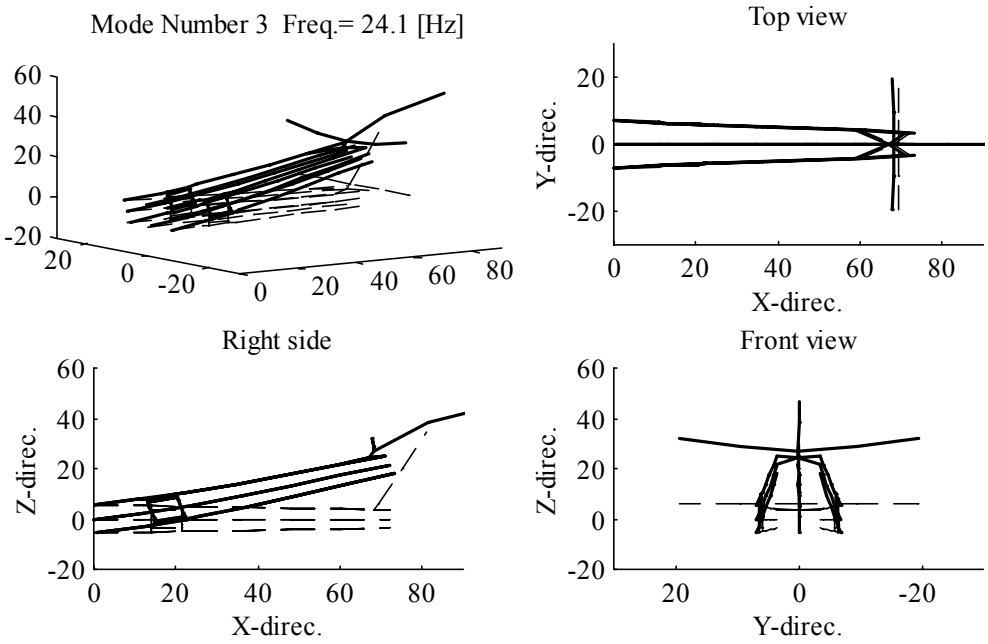

Scaled tailboom Finite Element Model (FEM) mode shape

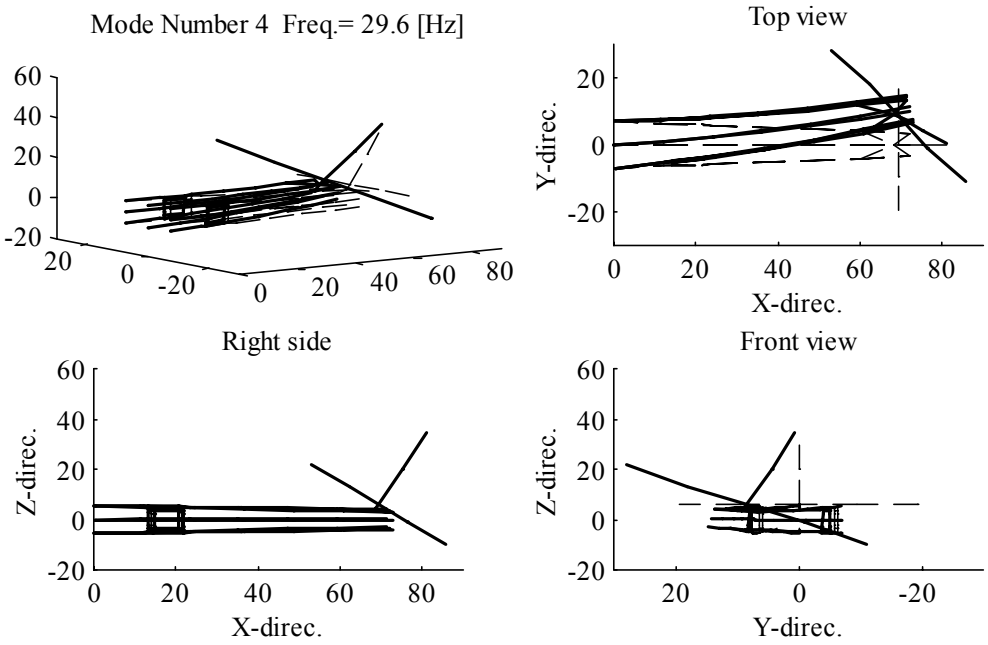

Scaled tailboom Finite Element Model (FEM) mode shape

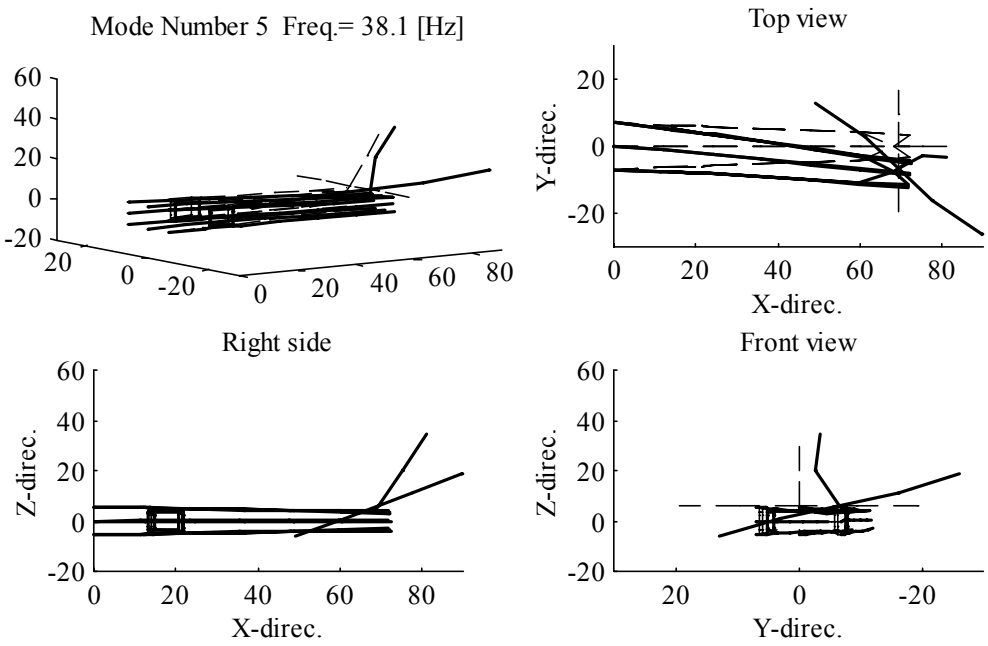

Scaled tailboom Finite Element Model (FEM) mode shape

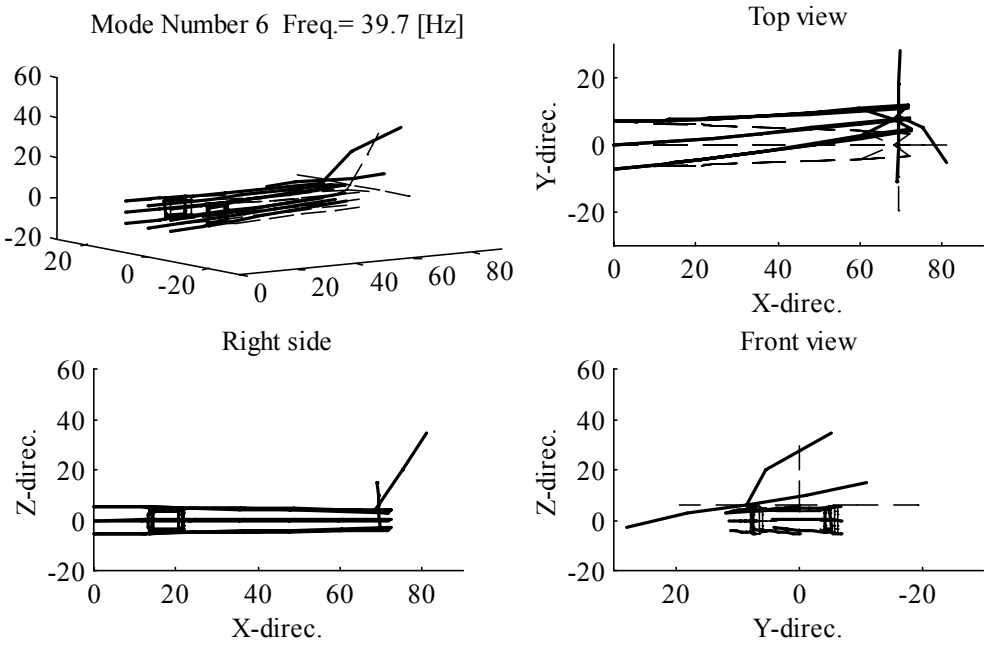

Scaled tailboom Finite Element Model (FEM) mode shape

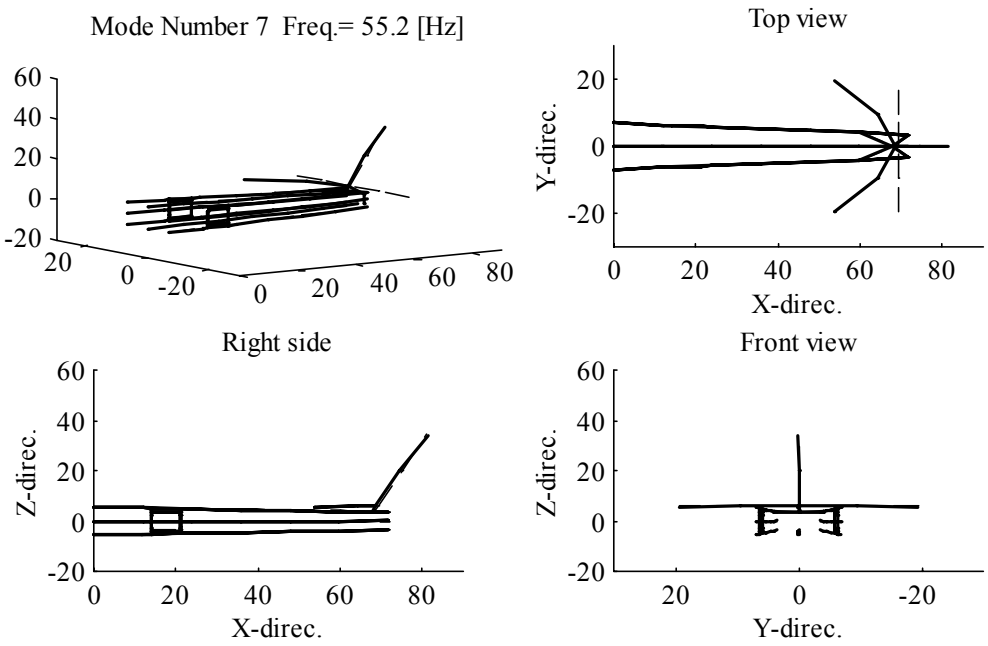

Scaled tailboom Finite Element Model (FEM) mode shape

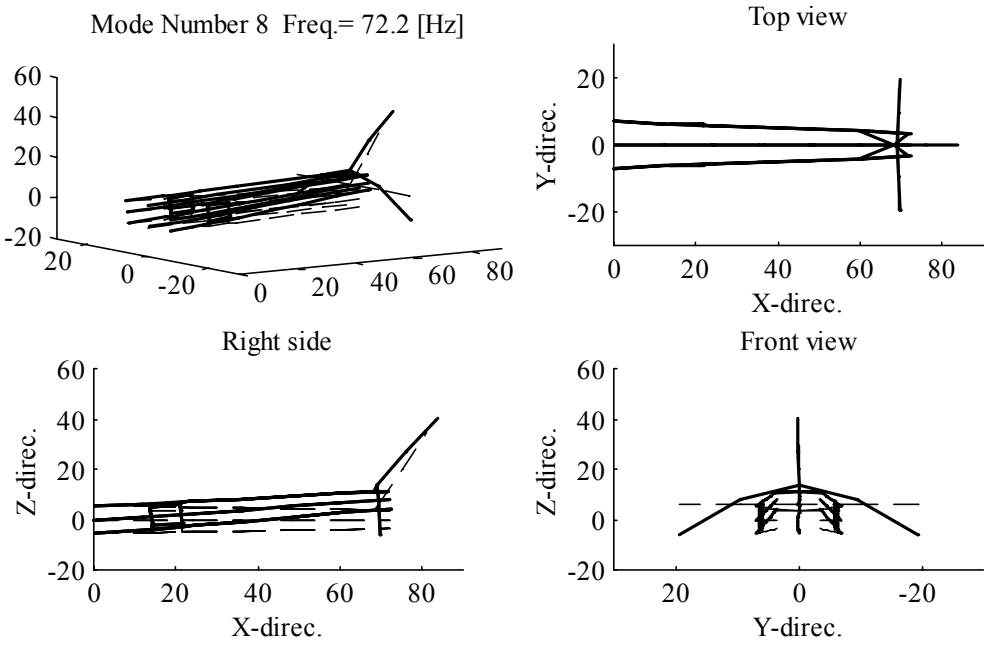

Scaled tailboom Finite Element Model (FEM) mode shape

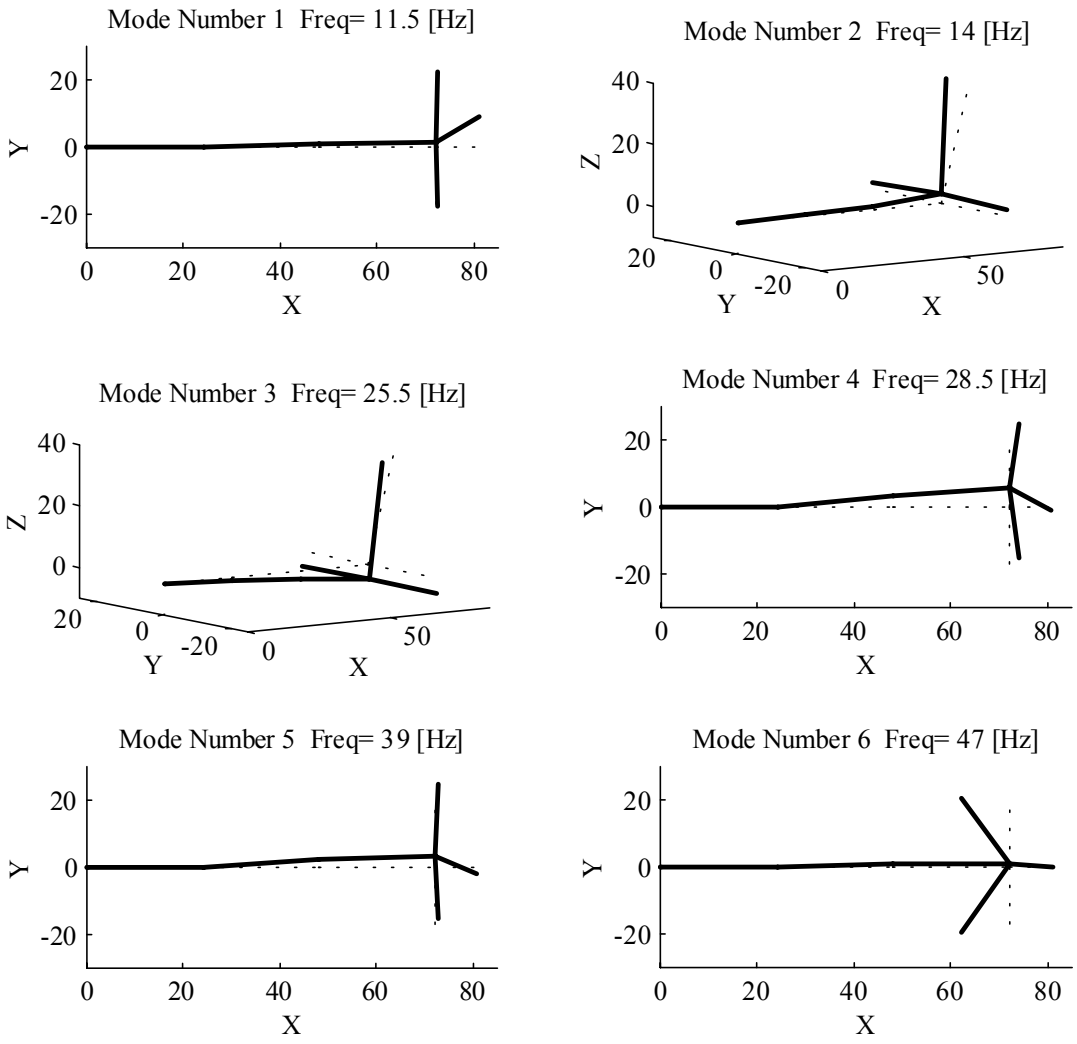

Scaled tailboom model experimental mode shapes

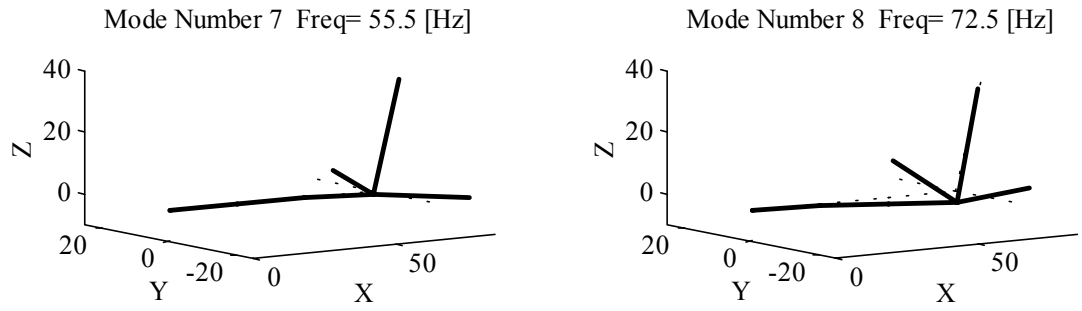

Scaled tailboom model experimental mode shapes

VITA

DAVID E. HEVERLY II

The Pennsylvania State University
University Park, PA 16802

PROFESSIONAL EXPERIENCE

Rotorcraft Center of Excellence and, Structural Dynamics and Controls Laboratory
Pennsylvania State University, University Park - 1996 to 2002:

- ***Graduate Research Assistant*** performing research on the active control of rotorcraft airframe vibrations.
- ***Dissertation:*** Optimal Actuator Placement And Active Structure Design For Control Of Helicopter Airframe Vibrations

Automotive Safety Analysis, Rockville, MD - 1992 to 1996:

- ***Staff Engineer*** performing forensic investigations, accident reconstruction, occupant kinematic analysis, crashworthiness assessments, and expert testimony.

Pennsylvania Transportation Institute
Pennsylvania State University, University Park - 1991 to 1992:

- ***Engineering Associate*** for the bus testing program. Developed testing procedures and implemented improvements to accelerated life testing procedures of mass transit buses. Researched, designed, constructed, and implemented an electronic fuel measuring system for alternative fuels.

Pennsylvania State University, University Park - 1990 to 1991:

- ***Graduate Research Assistant*** for the bus testing program. Developed a technique to correlate the severity of an accelerated life test to the probable service life environment of mass transit buses.
- ***Thesis:*** An Acceleration–Based Correlation For Accelerated Testing Of Heavy Duty Vehicles

CertainTeed Corporation, Blue Bell, PA - 5/90 to 9/90:

- ***Engineering Intern*** for the Insulation Group. Conducted research projects to determine the mechanical properties of fiberglass insulation, and developed a mathematical model to predict the mechanical response of fiberglass insulation to high density packaging. Designed and constructed a device to compress a sample of fiberglass insulation and electronically monitor the long term effects of induced compression.

International Paper Co., Lock Haven, PA - 5/89 to 9/89:

- ***Engineering Intern*** for the Maintenance Department. Responsible for the preparation of proposals for construction projects that included a lubrication storage facility, employee safety equipment, and office renovations. Assisted the preventative maintenance team with the vibration analysis of rotating machinery.

Pennsylvania Department of Transportation - 5/88 to 9/88 and 5/87 to 9/87:

- ***Engineering Intern*** for the Clearfield District. Inspected paving operations to assure that daily highway construction conformed to state specifications.

EDUCATION

- **Ph.D.**, Mechanical Engineering, The Pennsylvania State University, Aug. 2002, GPA = 3.8/4.0
- **M.S.**, Mechanical Engineering, The Pennsylvania State University, Dec. 1991, GPA = 3.9/4.0
- **B.S.**, Mechanical Engineering, The Pennsylvania State University, May 1990, GPA = 3.5/4.0
- **B.A.**, Mathematical Arts and Sciences, Lock Haven University, May 1990, GPA = 3.3/4.0